The Molecular Basis of CRL4 Ubiquitin Ligase Architecture, Targeting and Regulation

Inauguraldissertation

zur

Erlangung der Würde eines Doktors der Philosophie

vorgelegt der

Philosophisch-Naturwissenschaftlichen Fakultät

der Universität Basel

von

Eric Sebastian Fischer

aus Deutschland

Basel, 2013

Genehmigt von der Philosophisch-Naturwissenschaftlichen Fakultät auf Antrag von

Dr. Nicolas Thomä
Prof. Dr. Jeffrey Wade Harper
Prof. Dr. Susan M. Gasser

Basel, den 26.03.2013

Prof. Dr. Jörg Schibler
Dekan

creative commons

Namensnennung-Keine kommerzielle Nutzung-Keine Bearbeitung 2.5 Schweiz

---

Sie dürfen:

das Werk vervielfältigen, verbreiten und öffentlich zugänglich machen

Zu den folgenden Bedingungen:

Namensnennung. Sie müssen den Namen des Autors/Rechteinhabers in der von ihm festgelegten Weise nennen (wodurch aber nicht der Eindruck entstehen darf, Sie oder die Nutzung des Werkes durch Sie würden entlohnt).

Keine kommerzielle Nutzung. Dieses Werk darf nicht für kommerzielle Zwecke verwendet werden.

Keine Bearbeitung. Dieses Werk darf nicht bearbeitet oder in anderer Weise verändert werden.

- Im Falle einer Verbreitung müssen Sie anderen die Lizenzbedingungen, unter welche dieses Werk fällt, mitteilen. Am Einfachsten ist es, einen Link auf diese Seite einzubinden.
- Jede der vorgenannten Bedingungen kann aufgehoben werden, sofern Sie die Einwilligung des Rechteinhabers dazu erhalten.
- Diese Lizenz lässt die Urheberpersönlichkeitsrechte unberührt.

Quelle: http://creativecommons.org/licenses/by-nc-nd/2.5/ch/ Datum: 3.4.2009

Table of Contents

Summary/Abstract

Members of the CUL4-RBX1-DDB1 (CRL4) E3 ubiquitin ligase family regulate multiple cellular processes including development, transcription, and DNA repair. CRL4 type ligases are modularly assembled with specialized substrate receptors (DCAFs), which recruit a specific substrate and thereby confer specificity. Tight regulation of the versatile CRL4 network is crucial to maintain the integrity of important cellular pathways, as deregulation and mutations are often associated with human disease and cancer. A number of regulatory factors for the CRL system have been identified, including the COP9 signalosome (CSN), which has emerged as the major cullin regulator. CSN is a large protease that cleaves the isopeptide bond between a cullin and the ubiquitin-like modifier Nedd8, thereby controlling CRL4 activity.

One of the best characterized DCAFs is the DNA damage binding protein 2 (DDB2), which, as part of the $CRL4^{DDB2}$ ligase, orchestrates the initial steps of nucleotide excision repair (NER). In the first part of my thesis, I applied structural, biochemical and functional methods to elucidate the molecular architecture, targeting, and regulation of this important ligase complex. I demonstrate that $CRL4^{DDB2}$ is recruited to UV-induced lesions in chromatin and provide the structures of the fully assembled CUL4A/B-RBX1-DDB1-DDB2 ligase complexes bound to damaged DNA substrates. These studies reveal the intrinsic mobility of the ligase arm that creates an ubiquitination zone around the substrate binding site. The distance observed between the E2 binding site and the DNA binding site, together with the mobility of the ligase, preclude direct ligase activation through DNA damage binding. Instead, we found that CSN mediates $CRL4^{DDB2}$ inhibition in a CSN5 independent fashion and this inhibition is relieved upon the binding of damaged DNA to the DDB2 receptor. We show that the $CRL4^{CSA}$ ligase, involved in transcription coupled repair, shares common architectural features with $CRL4^{DDB2}$. And that the CSB protein substrate is sufficient to relieve CSN mediated $CRL4^{CSA}$ inhibition. Our data argues in favor of a general mechanism in which $CRL4^{DCAF(WD40)}$ ligases are inhibited by CSN, and in turn,

activation of the ligase is induced by substrate binding to, together with CSN displacement from, the ligase.

The ubiquitin proteasome system (UPS) controls timely degradation of short-lived proteins, including prominent oncogenes and tumor suppressors such as p53, β-catenin or c-myc. Targeting the UPS has emerged as a promising anti-cancer strategy and the FDA approval of *bortezomib* as the "first in class" proteasome inhibitor reflects this. However, global inhibition of the proteasome induces dramatic effects on protein homeostasis and high levels of cell toxicity, promoting efforts to target the UPS upstream of the proteasome, particularly through specific CRLs.

Despite being known to cause multiple birth defects, thalidomide (*contergan*) and its more potent derivative lenalidomide (*revlimid*) are FDA approved and widely used in the treatment of multiple myeloma. While the more recent discovery of the $CRL4^{CRBN}$ ubiquitin ligase as a primary cellular target of thalidomide has been a milestone in understanding thalidomide teratogenicity, a detailed molecular understanding of thalidomide action remains to be elucidated. In the second part of my thesis, I provide the X-ray structure of the DDB1-CRBN heterodimer in complex with the small molecule inhibitors thalidomide, lenalidomide and pomalidomide. The structure provides a molecular rationale for thalidomide action and, for the first time, a structural rationale for specifically targeting a CRL4 E3 ubiquitin ligase.

.

Chapter 1: General Introduction

The spatiotemporally regulated degradation of proteins by posttranslational modification with ubiquitin is an essential and ubiquitous eukaryotic process, discovered in the early 1980s (Ciechanover et al., 1980; Hershko et al., 1980). Ubiquitin emerged as an important posttranslational modification throughout virtually all cellular processes, with the number of ubiquitin conjugating enzymes surpassing the diversity observed for kinases (de Bie and Ciechanover, 2011). Moreover, it has become evident that cellular protein turnover is a wide spread, highly specific and regulated process. Cullin-RING E3 ligase (CRL) form the largest superfamily of ubiquitin E3 ligases and play central roles in virtually all cellular processes, including the early steps of mammalian nucleotide excision repair (NER) (Sugasawa et al., 2005). The enzymatic principles of ubiquitin transfer by Cullin-RING ubiquitin ligases (CRL) are well understood, while a detailed understanding of regulatory mechanisms is still emerging. Regulators of CRL ligases have been discovered and studied, including the COP9 signalosome (CSN), a master regulator of cullins, yet little is known about its ability to differentially regulate the multitude of cullins present in cells.

We studied the detailed molecular architecture of the CUL4A/B-RBX1-DDB1-DDB2 ($CRL4^{DDB2}$) ubiquitin ligase complex examining the molecular basis underlying its targeting to damaged DNA and CSN mediated regulation. We employed structural, biochemical and cellular approaches to elucidate the mechanism of $CRL4^{DDB2}$ activation. We further studied the related $CRL4^{CSA}$ ubiquitin ligase, which binds to a protein substrate instead of DNA, to understand the generality of the observed findings.

Thalidomide, a drug with a long and tragic history, has been identified as targeting the cereblon protein (CRBN), which is part of the $CRL4^{CRBN}$ ubiquitin ligase complex. In the second part of my thesis I worked towards a structural and functional understanding of this “prototype” CRL4 ligase inhibitor.

The following general introduction will provide background information on the ubiquitin proteasome system (UPS) with a focus on cullin-RING ligases. I will also provide an overview of the CRL4 ligase family and finally describe current efforts to modulate the CRL system.

A detailed introduction to the $CRL4^{DDB2}$ and $CRL4^{CSA}$ ligase complexes, their role in nucleotide excision repair (NER) and further roles of CRL4s can be found in **Chapter 2:** *Detecting UV-lesions in the genome: The modular CRL4 ubiquitin ligase does it best* (published manuscript).

The Ubiquitin Proteasome System

The peptide bond as the backbone of proteins is of remarkable stability: the spontaneous hydrolysis of a single bond in a polypeptide chain is anticipated to occur with a half-life of several hundred years under physiological conditions (Wolfenden and Snider, 2001). While, in general, the stability of proteins is desirable, cells need mechanisms for the controlled turnover of proteins to allow regulation, or quality control. This is achieved by proteases, which catalyze the reaction of a nucleophilic attack, where the nucleophile is either a amino acid or a water molecule, on the peptide bond and are rarely energy dependent due to the thermodynamically favorable reaction that they catalyze. Efforts to understand the energy dependence of intracellular proteolysis lead to the discovery of ubiquitin as a 76 amino acid polypeptide that is, via energy dependence, joined to the acceptor lysine of a substrate through an isopeptide bond (Ciehanover et al., 1978; Ciechanover et al., 1980; Hershko et al., 1980; Hershko and Ciechanover, 1998). The transfer of ubiquitin to the substrate, termed ubiquitination or ubiquitylation, occurs as a sequential reaction catalyzed by the ubiquitin activating (E1), the ubiquitin conjugating (E2) and the ubiquitin ligase (E3) enzymes (Hershko et al., 1983), poly-ubiquitination can than lead to recruitment of the 26S proteasome and ATP dependent degradation. Since the first discovery of ubiquitin, it has become evident that proteolysis of cellular proteins is a complex, timed, and tightly regulated process and that the ubiquitin proteasome system (UPS) accounts for the majority of cellular protein turnover. As of today, we know that ubiquitination is not solely a signal for degradation, but also plays important roles in signaling, mediating protein-protein interactions, or as an epigenetic mark. In fact, histone H2A was the first protein discovered to be modified by ubiquitin through an isopeptide bond (Goldknopf et al., 1975), while preceding the groundbreaking discovery of the UPS by Nobel laureates

Aaron Ciechanover, Avram Hershko and Irwin Rose. Moreover, work in the early 1980s on a temperature-sensitive mouse cell line, ts85, provided evidence that the UPS is the principal mechanism for controlled turnover of short-lived proteins (Marunouchi et al., 1980; Ciechanover et al., 1984; Finley et al., 1984), as well providing an initial link to cell cycle control. The role of ubiquitin dependent cyclin turnover, together with numerous other important cellular processes, is now a well-established functional role of the UPS.

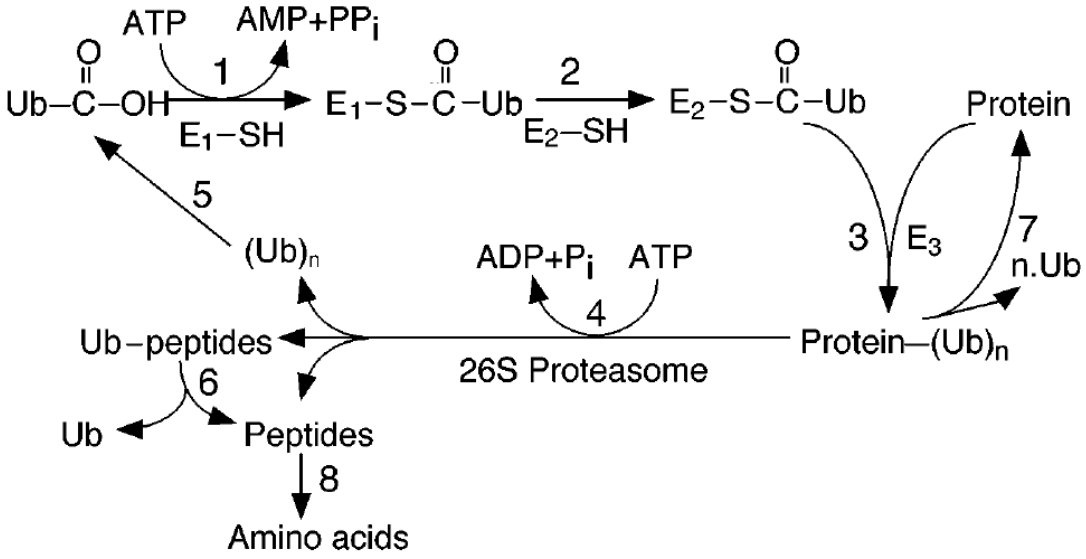

Figure 1.1: **The Ubiquitin Proteasome System:** The cascade of enzymatic reactions in the Ubiquitin Proteasome System (Hershko and Ciechanover, 1998).

Ubiquitin and ubiquitin conjugation: Thioester chemistry

Ubiquitin is one of the most highly conserved eukaryotic proteins, with only three amino acid substitutions from yeast to man (Ozkaynak et al., 1984). Mammals have four genes that encode for the ubiquitin polypeptide, and ubiquitin is either expressed as a precursor of four (Ubb gene) or nine (Ubc gene) ubiquitins in one polypeptide chain in a head-to-tail arrangement, or as a fusion to the ribosomal subunits UB_{L40} and UB_{S27} (Kimura and Tanaka, 2010). Proteolytic cleavage is required to generate functional monomeric ubiquitin with a C-terminal glycine residue that then can be, through the catalytic activity of the E1 enzyme, adenylated, resulting in an acyl-phosphate linkage with AMP (**Figure 1.1**). The ubiquitin-AMP is then attacked by the catalytic cysteine of the E1 enzyme and a thioester linkage is formed between

the E1 Cysteine and the C-terminus of ubiquitin, releasing AMP (Lee and Schindelin, 2008). The thioester-bound ubiquitin is then, by trans-thioesterification, transferred to the catalytic cysteine of an E2 enzyme. The last step of the cascade is catalyzed by an E3 enzyme and transfers the ubiquitin from the E2 cysteine to the ε-amino group of an acceptor lysine in the target protein. The increasing number and specialization of enzymes provides substrate specificity throughout the ubiquitin cascade, the ubiquitin E1s, UBA1 and UBA6, are responsible for ubiquitin activation, tens of E2 enzymes and hundreds of E3's confer substrate specificity. Ubiquitin does not only attach to an acceptor lysine in the target protein, but can also be targeted to one of the seven lysines within another ubiquitin, leading to the formation of a poly-ubiquitin chain. Chain formation can occur as a homogenous chain linked through seven acceptor lysines, while more complex structures such as branched chains and linear chain formation (involving the N-terminus of an acceptor ubiquitin) have also been described (Komander and Rape, 2012). The linkage of a poly-ubiquitin chain determines the fate of the substrate protein: Lys48-linked chains of sufficient length have been associated with proteasomal degradation, while Lys63-linked chains have generally been associated with non-proteasome-related functions, such as protein trafficking or signaling. Less is known about linear chains involved in NF-κB signaling (Walczak et al., 2012), Lys11 linked chains associated with the Anaphase Promoting Complex/Cyclosome (APC/C) (Jin et al., 2008), and much less about other linkages or more complex structures. Despite the formation of poly-ubiquitin chains, mono-ubiquitination occurs at defined acceptor lysines, such as PRC1 mediated ubiquitination of histone H2A (Lys119), and plays important roles throughout cellular processes.

Substrate specificity and chain formation are commonly determined by the nature of the E3 ligase and may be influenced by the E2 conjugating enzyme.

E3 Ligases: Two major families

E3 ligases deliver the substrate lysine at close proximity to the ubiquitin loaded E2, thereby facilitating the transfer of the ubiquitin to the acceptor lysine. E3 ligases do not share a common architecture, but exist as single

proteins or multi-protein complexes; some participate in the ubiquitination reaction by transiently interacting with the ubiquitin, while others never physically interact with ubiquitin. This variety makes it hard to identify ubiquitin E3 ligases based on sequence homology. The precise number of these ligases in humans is still unknown but expected to exceed the roughly 500 protein kinases present in the human genome (Deshaies and Joazeiro, 2009). In the following paragraphs I will provide an overview of the two major ubiquitin E3 ligase families.

HECT E3 ligase

HECT (*Homologues* to *E6AP C-terminus*) domain containing ubiquitin E3s are unique among the ubiquitin ligases, as they involve thioester-intermediates between the catalytic Cysteine of the HECT domain and the C-terminus of ubiquitin prior to transfer to the acceptor lysine (Dye and Schulman, 2007). HECT E3 ligases have evolved to facilitate the formation of poly-ubiquitin chains such as K48-linked (E6AP), and K29-linked (KIAA10), while also directly monoubiquitinating a specific substrate (Rsp5). In mammals, there are roughly 30 HECT domain ubiquitin ligases, and the conserved HECT domain is usually located at the C-terminus, while the N-terminus is commonly involved in substrate binding. The HECT domain itself consists of a bi-loped structure (**Figure 1.2**), where the N-terminal domain contacts the E2, and the C-terminal domain contains the reactive cysteine (Huang et al., 1999). In contrast to the HECT domain E3 ligases, RING domain containing E3 ligases represent the largest family of E3 ligases, and their activity does not involve a direct interaction with ubiquitin.

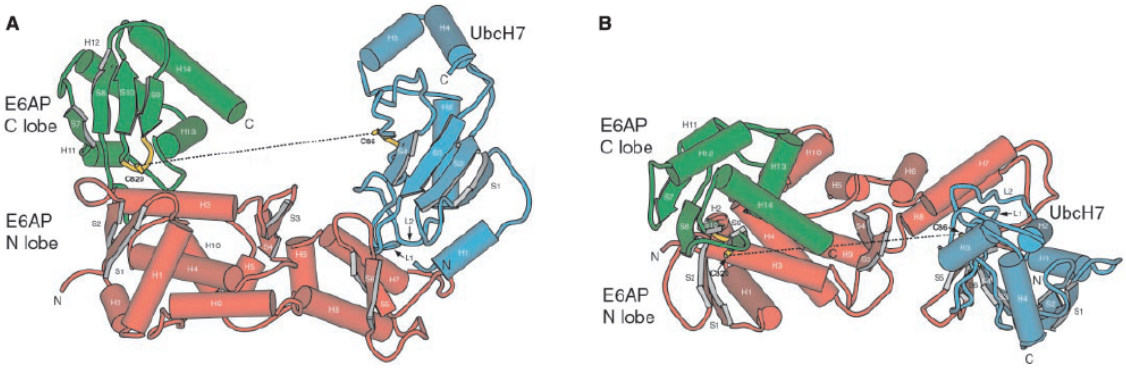

Figure 1.2: **Crystal structure of the HECT E3 ligase E6AP complexed to UbcH7.** (A and B) The C-lobe, depicted in green, and the N-lobe in red, of the HECT E3 ligase (E6AP) in conjunction with the ubiquitin E2 (UbcH7) in blue, all of which form a U-shaped structure. The active site cysteines are depicted in yellow (Huang et al., 200). From a comparison of multiple HECT-containing structures, a hinge point between the C- and N-lope has been anticipated and is thought to position the active site cysteine.

RING type E3 ligases

RING ubiquitin ligases represent the largest family of E3 ligases. Several hundred human genes encode for members of this ligase family (Deshaies and Joazeiro, 2009). The protein Ring1 (Really interesting new gene 1) has been the eponym for the family, and the first to be described as a RING domain containing protein. It then took several years to establish the role of the RING motif as a crucial part of the ubiquitin ligase. Many important concepts of the RING domain function have been established through the discovery and characterization of Rbx1, as ubiquitin ligase activity bearing part of the Skp1-Cullin-F-box (SCF) ubiquitin ligase complex (Kamura et al., 1999; Ohta et al., 1999; Seol et al., 1999; Tan et al., 1999). Moreover, the functional (Joazeiro et al., 1999) as well as structural studies (Zheng et al., 2000) on c-Cbl RING mediated ubiquitin ligase activity deepened the understanding of the RING motif, containing the ubiquitin ligase function. Unlike HECT domain proteins, the ubiquitin ligase activity of RING proteins is comprised of binding to and the activation of an E2 conjugating enzyme without the intermediate transfer of the ubiquitin to the ligase. The canonical RING domain is defined by two zinc ions coordinated by eight conserved cysteine or histidine residues (Dye and Schulman, 2007), while numerous variations exist (Deshaies and Joazeiro, 2009).

RING domain E3 ligases have been implicated in regulating a variety of cellular processes, including cell cycle progression, signal transduction, DNA repair and replication, and even viral infections. RING finger ligases exist as monomeric enzymes that, in the case of c-Cbl with a Src-homology 2 (SH2) domain, bind directly the substrate, and with the RING finger domain the E2 enzyme (Zheng et al., 2000). In contrast, the RING finger proteins can also be part of large multi-protein ubiquitin ligase complexes, such as the 1.5 MDa Anaphase Promoting Complex/Cyclosome (APC/C), where the RING finger protein Apc11 is required for ubiquitin ligase activity (Thornton and Toczyski, 2006). While the work on SCF has significantly contributed to the understanding of RING finger mediated ubiquitination, SCF has also been the founding member for the largest group of ubiquitin ligases: the Cullin-RING ubiquitin ligase (CRL) superfamily.

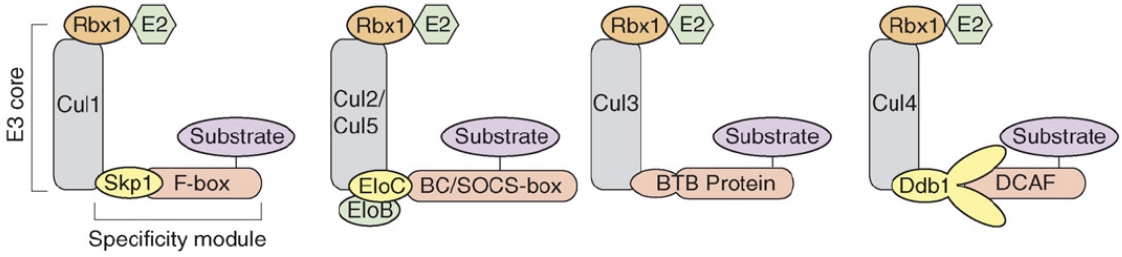

Figure 1.3: **Modular architecture of the cullin-RING ligase family**. Canonical Cullin-RING ligases share a general architecture consisting of the scaffolding Cullin protein (Cul1-5), the small RING finger protein comprising the E2 binding site (Rbx1,2) and either a adaptor protein (Skp1, EloB/C, and DDB1) in conjunction with a substrate receptor (F-box, BC/SOCS-box, and DCAF) or a BTB protein conferring substrate specificity (O'Connel and Harper, 2007).

Cullin-RING Ligases

The superfamily of Cullin-RING ubiquitin ligases (CRL) represents the largest group of E3 ligases (Petroski and Deshaies, 2005), where the highly conserved cullin protein family contributes, as a scaffold protein that binds the small RING finger protein Rbx1 (Kamura et al., 1999; Ohta et al., 1999; Seol et al., 1999; Tan et al., 1999), to the assembly of as many as 400 distinct CRLs. The human genome codes for six canonical cullin proteins, Cul1, Cul2, Cul3, Cul4A, Cul4B, and Cul5 that, in conjunction with the RING finger proteins Rbx1 and Rbx2, provide the backbone for different subfamilies of CRLs, CRL1-5 (**Figure 1.3**). The genes Cul7, PARC, and the Apc2 subunit of

the APC/C share a homology domain with the canonical cullins but differ elsewhere, and are considered atypical cullins (Zachariae et al., 1998; Skaar et al., 2007). The overall assembly of CRLs follows a common scheme; the cullin protein binds with its C-terminus, the RING protein, and with its N-terminus interacts either, as in the case of Cul3, directly with a substrate receptor protein (BTP protein), or for CRL1, 2, 4 and 5, an additional linker protein (Skp1, ElonginB/C or DDB1) connects the cullin with a specific substrate receptor protein. The substrate receptors are diverse and belong to specific families for every cullin: Cul1 associates with F-box proteins (>70 different proteins), Cul2/5 with the BC-box (>50 different proteins), Cul3 with the BTB proteins (>200 different proteins) and Cul4A/B with the DCAF substrate receptor proteins (>30 different proteins) (Jackson and Xiong, 2009). These substrate receptors confer specificity to the CRL and employ various protein-protein interaction domains to specifically bind to a substrate (Schulman et al., 2000; Hao et al., 2007; Scrima et al., 2008; Zhuang et al., 2009). A prerequisite to recognition as a substrate is often a posttranslational modification, such as phosphorylation (Wu et al., 2003), hydroxylation (Min, 2002) or methylation (Lee et al., 2012a).

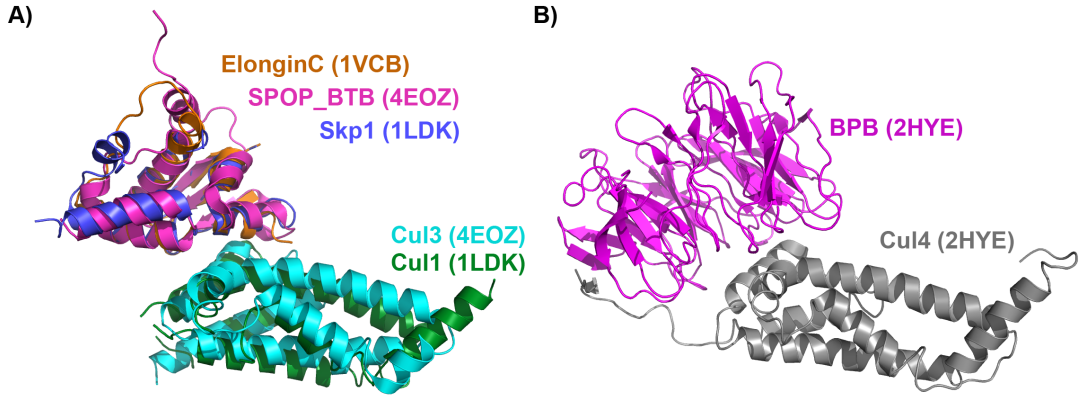

Figure 1.4: **Comparison of Cullin to adaptor binding.** A) overlay of the BTB domain from Elongin C (PDB: 1VCB), SPOP (PDB: 4EOZ) and Skp1 (PDB: 1LDK) colored in orange, magenta and blue, respectively, together with their respective Cul3 (SPOP) and Cul1 (Skp1) cullin colored in cyan and green, respectively. B) The BPB WD40 *β*-propeller domain of DDB1 in magenta, bound to the N-terminal domain of Cul4A in gray (PDB: 2HYE). (Zheng et al., 2002; Angers et al., 2006; Stebbins et al., 1999; Errington et al., 2012).

The structure of the founding member of the CRL superfamily, SCF^{Skp2} (Zheng et al., 2002) established an architectural and assembly logic to be found throughout the CRL family. The cullin forms a rigid arch-shaped scaffold

that, with a globular C-terminal domain, binds to Rbx1, while the elongated helical N-terminal domain binds to the adaptor protein Skp1 (**Figure 1.5**). In the structure of SCF^{Skp2}, Skp1 is bound to the F-box motif of Skp2. Skp2 mediates cell cycle progression by recruiting the Cdk inhibitor p27 for ubiquitination and subsequent degradation. The adaptor protein complex ElonginB/C shares sequence homology with Skp1 and serves as the common adaptor for CRL2 and CRL5 ligase complexes. Crystal structures revealed that Skp1 and ElonginC essentially consist of a *Bric-a-brac, Tramtrack, and Broad complex* (BTB) domain and that the substrate receptor family of BC-box containing proteins is recruited to ElonginB/C, resulting in an overall structural assembly of CRL2/5 ligases similar to that of SCF (Zimmerman et al., 2010). Moreover, the CRL3 subfamily employs BTB family proteins that combine the role of a substrate receptor and adaptor protein but still share a structural homology in the way they interact with Cul3. Characteristic BTB family proteins employ MATH, Kelch or ZnF domains to mediate substrate binding, while dimerization has been observed as a common feature among BTB proteins (Zhuang et al., 2009; Canning et al., 2013). While CRL1, 2, 3 and 5 all employ a BTB fold to mediate the binding of a cullin to the adaptor/substrate receptor complex, the adaptor of the CRL4 family is distinct and structurally unrelated (**Figure 1.4**).

The CUL4 subfamily of CRLs

In contrast to the rather small BTB motif that serves as the common structural entity within the adaptors for CRL1, 2, 3 and 5, CRL4 ligases employ the 127kDa Damaged DNA binding protein 1 (DDB1) as an adaptor to bridge Cul4 and the substrate receptors, so-called DCAFs for *DDB1 and Cul4 associated factors* (Angers et al., 2006) (**Figure 1.4**).

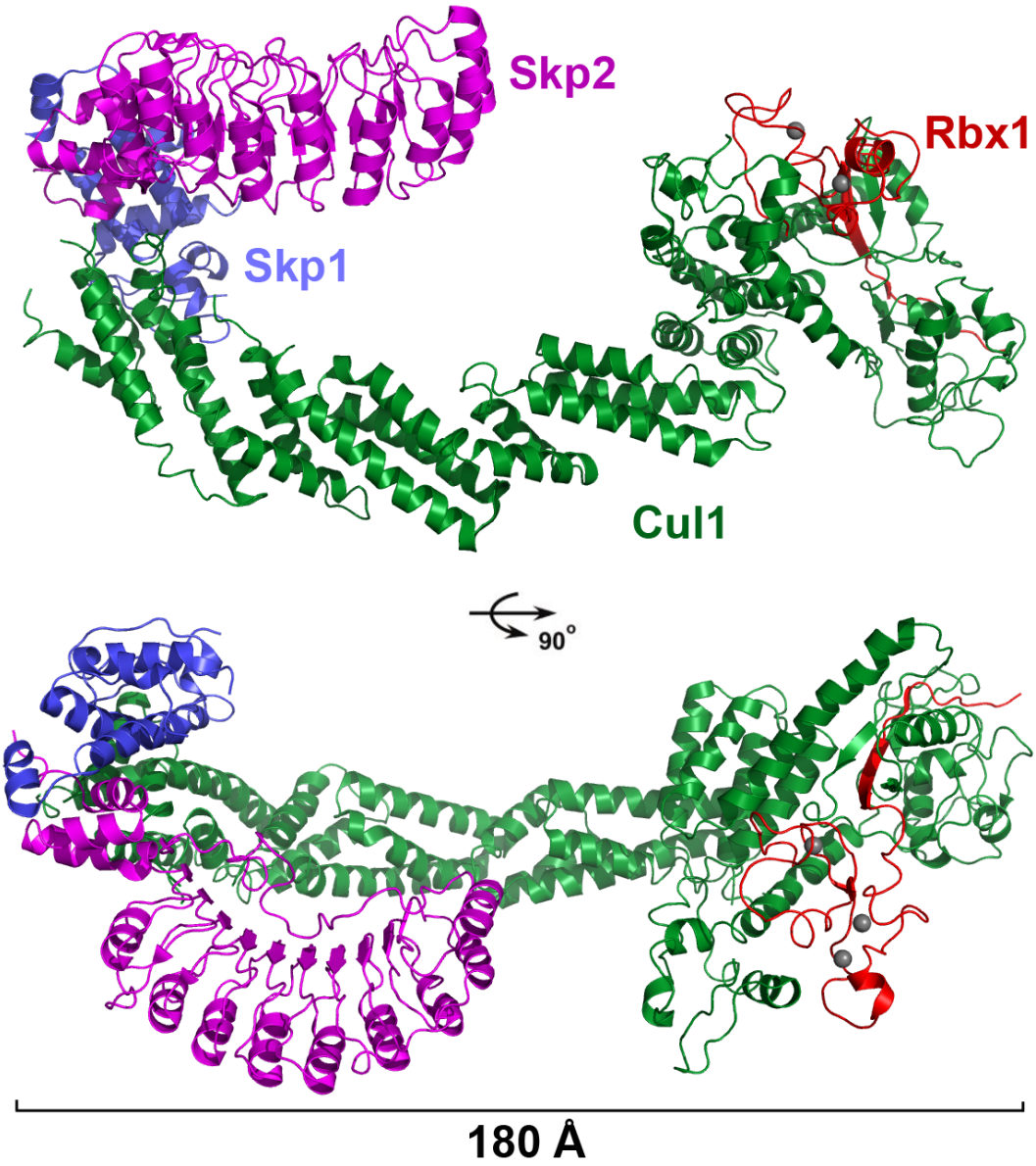

Figure 1.5: Structure of SCF^{Skp2}. A Model of the entire SCF^{Skp2} complex, depicted as ribbon diagram, was generated by superimposing the structures of $SCF^{Fbox(Skp2)}$ (PDB: 1LDK) and Skp1-Skp2 (PDB: 1FQV). Cul1, Rbx1, Skp1 and Skp2 are colored in green, red, blue and magenta, respectively. (Zheng et al., 2000; Schulman et al., 2000).

In addition to endogenous substrate receptors, viral proteins have been shown to bind to a Cul4 ligase and redirect it to degrade targets that would otherwise interfere with viral infection or function (Martin-Lluesma et al., 2008; Sharifi et al., 2012). The V protein of simian virus 5 (SV5v) has been found to recruit STAT proteins to the CRL4 ligase and drive the ubiquitination and degradation of STAT1 (Horvath, 2004), though the structure of the CUL4A-RBX1-DDB1-SV5v complex provided the first insights into the molecular architecture of this CRL family (Angers et al., 2006) (**Figure 1.6**). The adaptor

protein DDB1 comprises three canonical 7-bladed WD40 *β*-propellers in a triangular shape (BPA-BPC), stabilized by a helical C-terminal domain (CTD) (Li et al., 2006). The interaction between Cul4 and DDB1 is mediated by the BPB domain of DDB1 and two N-terminal α-helices of Cul4, corresponding to those used by Cul1 to bind Skp1 (Angers et al., 2006). The NTD and large parts of the CTD of Cul4 resemble the overall structure of Cul1, while the winged-helix B (WHB) domain and the orientation of Rbx1 show structural differences (Zheng et al., 2002; Angers et al., 2006). Despite the lack of sequence or structural similarity between DDB1 and Skp1, the relative arrangement of Rbx1 to the substrate receptor is comparable, positioning Rbx1 and a putative substrate in a similar orientation. Angers et al. further identified a group of putative endogenous CRL4 substrate receptors, including DDB2 and CSA, which are largely characterized by a WD40 *β*-propeller and a DxR motif, and were named DCAF for DDB1 and Cul4 associated factors, further DCAF members were identified through numerous studies (Angers et al., 2006; Bennett et al., 2010; He et al., 2006; Higa et al., 2006; Jin et al., 2006). *In vitro* binding experiments demonstrated that increasing amounts of purified SV5v protein could compete of the binding of an endogenous DCAF protein to DDB1, suggesting a competitive binding mode and similar interfaces used by SV5v and endogenous DCAFs. The structure of the first endogenous DCAF bound to DDB1, the DDB1-DDB2 protein complex (Scrima et al., 2008), detailed for the first time how an endogenous DCAF can bind to the DDB1 protein. Strikingly, it employs a helix-loop-helix motif to bind to the very same binding pocket in the cavity between the BPA and BPC domain of DDB1, as does the helical interacting motif of SV5v. The structure of DDB1-DDB2 further revealed that, in addition to the HLH motif, and similar to SV5v, the DDB2 interaction with DDB1 is mediated through a hydrophobic surface patch (Scrima et al., 2008). Co-crystal structures of DDB1 with interacting peptides of the proteins HBx, WHX, WDTC1, DDB2, WDR21A, WDR22, IQWD1, H326 and WDR40 (Li et al., 2010) revealed that all characterized viral and endogenous DCAFs share a similar helical motif mediating interaction with DDB1. While these findings propose a common architecture (similar to that of DDB2) for DCAFs containing a WD40 *β*-propeller and a preceding helical binding motif, the precise structural constraints and

hallmarks are as yet unresolved. Moreover, prediction of helical motifs has not been possible for all DCAF proteins, and the questions of whether or not non-WD40 DCAFs exist and how they might interact with DDB1 remain unanswered.

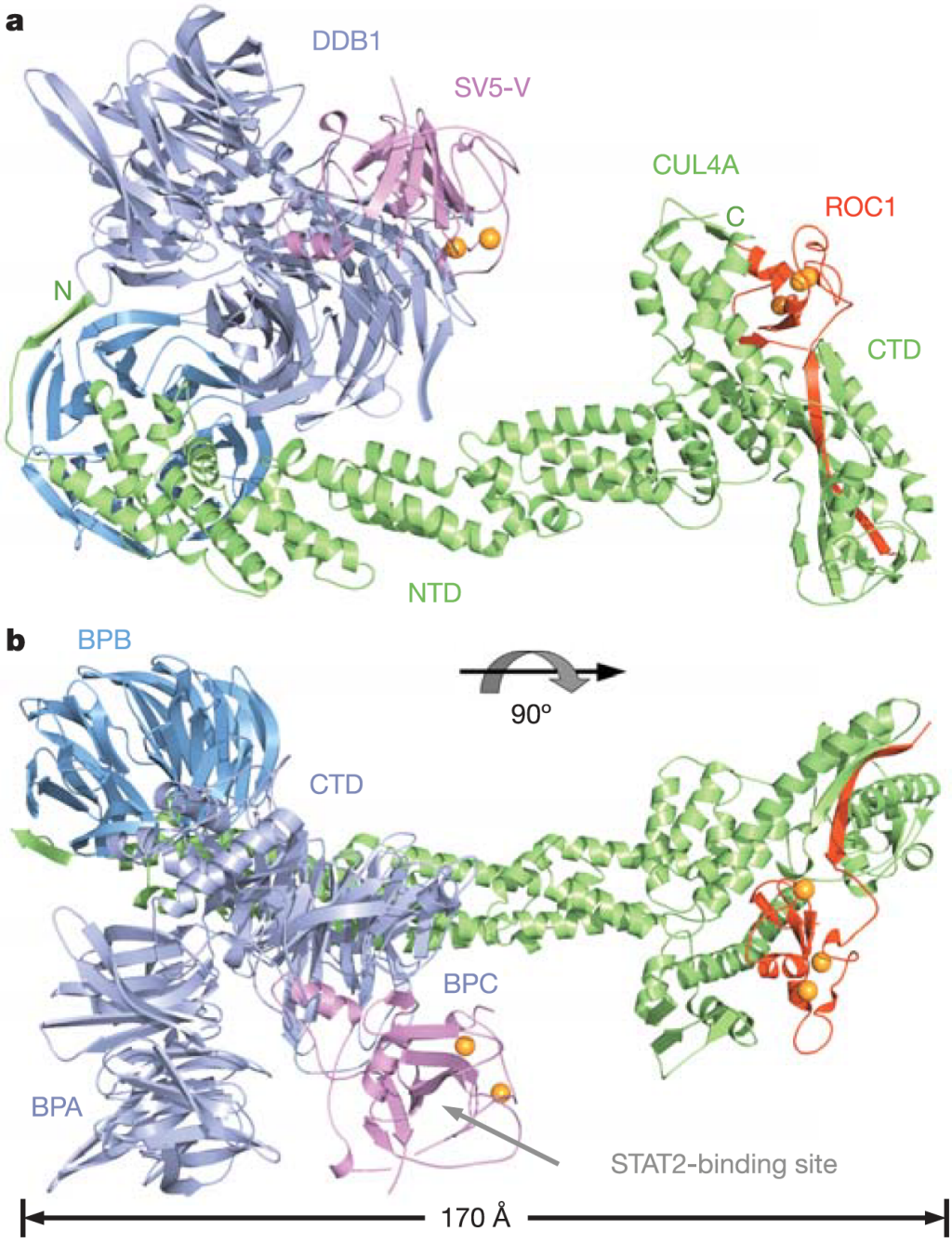

Figure 1.6: **Crystal structure of the CRL4^{SV5v} protein complex. a,b)** Rbx1, Cul4, DDB1 and SV5v are depicted as ribbon diagram in red, green, blue and magenta, respectively. The BPB domain of DDB1 is depicted in blue and the Zn atoms of Rbx1 and SV5v are highlighted as yellow spheres (Angers et al., 2006).

Furthermore, the CRL4 ligase is the only CRL that, in mammals, possesses two isoforms, Cul4A and Cul4B. In contrast to Cul4A, Cul4B has an extended N-terminus (190 amino acids) preceding the cullin homology domain, while the cullin domain shows a sequence identity of 83% over 753 residues. While Cul4A and Cul4B appear to be largely redundant (Liu et al., 2009), Cul4B has been linked to a number of distinct cellular functions and diseases, such as a mild form of X-linked mental retardation (Tarpey et al., 2007), or the degradation of the estrogen receptor (ER-α) (Ohtake et al., 2007). The precise molecular determinants for the specific roles played by Cul4A or Cul4B, as well as the structural homology between the two isoforms, await further investigation.

Despite the fact that only few DCAFs have assigned cellular functions, CRL4 ligases have been associated with a number of important cellular processes. $CRL4^{DDB2}$ and $CRL4^{CSA}$ are associated with the early steps of nucleotide excision repair, as outlined in **Chapter 3**. $CRL4^{Cdt2}$ is an essential CRL4 ligase involved in regulating S/G2 cell cycle transition through timed degradation of the replication licensing factor (Cdt1) (Havens and Walter, 2011). Other targets of $CRL4^{Cdt2}$ include p21 (Abbas et al., 2008; Nishitani et al., 2008) and the histone methyltransferase SET8/Pr-SET7 (Abbas et al., 2010). The VprBP/DCAF1 protein, as part of the $CRL4^{DCAF1}$ ligase complex, has been associated with the tumor suppressor Merlin (Huang and Chen, 2008) and is involved in HIV-1 infection through the Vpr mediated degradation of UNG2 and SAMHD1 (Ahn et al., 2010; 2012). Other putative targets of Cul4 include c-Jun (Wertz et al., 2004), Dacapo/p27Kip1, CyclinE (Higa et al., 2006) or the checkpoint protein CHK1 (Leung-Pineda et al., 2009), although the responsible DCAFs and the underlying mechanisms are unresolved. The prominence of cellular events regulated by CRL ubiquitin ligases requires a tight control of these cellular machines.

Cullin regulation

Instrumental to the regulation of important cellular pathways, cullins themselves are subject to a diversity of regulatory events. A number of proteins and protein complexes have been identified as cullin binding

partners. Upon certain cellular or extracellular signals, such as *UV*-light, low oxygen levels, cell cycle events, or pathogenic infections, CRLs have been shown to be activated or modulated in their activity. In the following paragraphs, I will review the major protein complexes that have been implicated in general cullin regulation. In addition, specific regulators have been associated with an individual or a subset of cullins such as Glomulin (Duda et al., 2012), a protein that binds to Rbx1, occupies the E2 binding site, and has been associated with SCF^{Fbw7} inhibition. Another binding partner that reproducibly co-purifies with certain CRL4 complexes is the small protein DDA1 (DDB1 and DET1 associated factor 1), a protein shown to bind the BPC of DDB1 while its functional role remains elusive (Pick et al., 2007; Olma et al., 2009).

Autocatalytic conjugation of Nedd8 activates the cullin

For the canonical cullins, it has been shown that the autocatalytic conjugation of the ubiquitin-Like Protein (UBL) Nedd8 to a conserved lysine residue in the winged-helix B (WHB) domain of a cullin activates the ligase (Furukawa et al., 2000; Pan et al., 2004). Structural studies (Duda et al., 2008) have revealed that the attachment of Nedd8 induces a conformational change within the globular CTD of the cullin and frees the RING domain of Rbx1 to swing out and adopt multiple conformations. The conformational freedom of Rbx1 leads to increased catalytic activity (Duda et al., 2008; 2011) and is thought to bridge the gap between the E2 binding site and the substrate, observed in the crystal structure of SCF^{Skp2} (Zheng et al., 2002). The fundamental principal of Nedd8 conjugation is similar to the ubiquitin cascade, though it employs the Nedd8 specific E1 enzyme UBA3/NAE1, the E2 enzymes UBE2M (Ubc12), and UBE2F together with the E3 activity of Rbx1 or Rbx2 (Huang et al., 2009). More recently it has been shown that the yeast cullin Cdc53 requires the presence of an additional Nedd8 specific E3, namely the Dcn1 protein in yeast (Scott et al., 2010), which, in conjunction with the E3 activity of the yeast Rbx1 orthologue Hrt1, facilitates efficient neddylation of Cdc53. The extent to which this mechanism is conserved in

mammals and its role among the different cullin families has not been fully resolved.

Nedd8 mediated activation of CRLs is counteracted by the proteolytic cleavage of the Nedd8 modification through a large multi-protein isopeptidase complex, the COP9 signalosome (CSN).

The COP9 Signalosome: Counteracting Cullin activation

The COP9 signalosome (CSN) was originally discovered based on its role in the regulation of photomorphogenesis in the mustard weed *Arabidopsis Thaliana* (Wei and Deng, 1992; Wei et al., 1994; Chamovitz et al., 1996; Kwok et al., 1996). CSN is a large 350 kDa protein complex comprised of subunits csn1 to csn8 (Wei and Deng, 1999) and all or most subunits are conserved from yeast to man. Genetic studies have linked CSN to a variety of cellular processes within a number of model systems, such as photomorphogenesis in *A. Thaliana* (Osterlund et al., 1999), embryonic development in *Drosophila Melanogaster* (Doronkin et al., 2002) or DNA replication in *Schizosaccharomyces pombe* (Mundt et al., 1999; 2002). The discovery that CSN interacts with the cullin-RING ubiquitin ligase complex SCF^{TIR1} (Schwechheimer et al., 2001) and that it promotes cleavage of Nedd8 from the *S. Pombe* Cul1 orthologue, shed light on the biochemical function of CSN (Lyapina, 2001). The CSN5/Jab1 subunit of CSN was subsequently described as a metalloprotease containing a JAMM/MPN+ motif (Cope et al., 2002) and implicated in harboring the catalytic deneddylation activity of CSN. CSN shares significant structural homology with the components of the 19S proteasome lid and the eukaryotic translation initiation factor (eIF3) (Pick et al., 2009). The 19S lid and CSN share a common architecture containing 6 subunits (CSN1, CSN2, CSN3, CSN4, CSN7a/7b and CSN8) that harbor a PCI (Proteasome, COP9 signalosome, Initiation factor) domain at their C-terminus, and 2 subunits (CSN5 and CSN6) containing a MPN (Mpr1-Pad1-N terminal) domain at their N-terminus. The PCI domain is important for the assembly of the CSN complex, whereas the MPN domain with the catalytic JAMM/MPN+ motif in the CSN5 subunit is responsible for metallo-isopeptidase activity (Kapelari et al., 2000; Lyapina, 2001; Cope et al., 2002;

Fang et al., 2008; Sharon et al., 2009). The CSN5 subunit is also present in an isolated free form. The individual CSN5 subunit is catalytically inactive and gets allosterically activated only while embedded in the holocomplex (Cope et al., 2002; Sharon et al., 2009). The JAMM metalloprotease of the proteasome lid subunit Rpn11, in contrast to CSN5, cleaves poly-ubiquitin chains (Verma et al., 2002). CSN is further commonly associated with a conventional deubiquitinating enzyme (DUB) Ubp12 (Groisman et al., 2003; Zhou et al., 2003) that is thought to act in concert with the deneddylation activity of CSN5 to inhibit the ubiquitination activity of CRLs. It has now become widely appreciated that CSN regulates all canonical cullins through the control of neddylation *in vivo*. Despite its role as a negative regulator of CRL activity, functional CSN is also required to sustain CRL function *in vivo* (Schmidt et al., 2009; Wang et al., 2010). Genetic studies demonstrated that the inhibitory role of CSN on CRL activity protects substrate receptors from detrimental autocatalytic ubiquitination (Zhou et al., 2003; He et al., 2005; Wee et al., 2005; Cope and Deshaies, 2006), a potential explanation why CSN would be indispensable for full CRL function.

Though we now understand the biochemical properties of CSN, CSN has been implicated in the regulation of all canonical cullins and this, given that the human genome encodes for hundreds of distinct substrate receptors, raises the question: How can CSN differentially and independently regulate two different CRLs according to a specific stimulus?

CAND1

The CAND1 (Cullin-Associated and Neddylation-Dissociated 1) binds specifically to free cullin-rbx complexes and inhibits neddylation and CRL assembly, thereby keeping the cullin in an inactive form. The structure of CAND1 bound to Cul1-Rbx1 reveals that the heat-repeat protein CAND1 wraps around the cullin, and blocks the N-terminal binding interface for CRL assembly, as well as the neddylation site (Goldenberg et al., 2004). It had been proposed that CAND1 sequesters non-neddylated cullins to prepare them for new CRL assembly in a deneddylation-CAND1-CRL assembly cycle (Schmidt et al., 2009). A recent proteomic study, however, did not further

support a critical role for CAND1 in CRL assembly (Bennett et al., 2010) and further investigation will be required to elucidate the precise role of CAND1 in CRL reorganization and regulation.

Modulating the Ubiquitin Proteasome system with small molecules

The ubiquitin proteasome system (UPS) regulates a wide variety of cellular processes, including protein turnover, DNA damage response, transcription, and cell signaling. Alterations and mutations within the UPS are associated with countless human diseases, such as cancer and neurodegenerative disorders, making the UPS a potential pool for promising drug targets. Within the hierarchical enzymatic cascade of the UPS, a maximum of two E1 enzymes charge several E2 enzymes that, in conjunction with one out of hundreds of E3 ligases, provides substrate specificity (**Figure 1.7**). It is noteworthy that the first successful approach to target the UPS for therapeutic intervention was the proteasome inhibitor *bortezomib* (*Velcade*; Millennium Pharmaceuticals, Cambridge US), which acts the far most downstream in the UPS (Adams, 2004). *Bortezomib* is a peptide boronic acid inhibitor (Adams et al., 1998) of the proteasome and was later approved by the FDA to treat refractory or relapsed multiple myeloma. Although targeting the proteasome lacks any specificity for a specific ubiquitinated substrate, *bortezomib* provides a sufficient therapeutic window together with manageable side effects to be effective in cancer treatment (Aghajanian et al., 2002; Orlowski and Dees, 2003). It is commonly believed that the therapeutic window occurs because heavily dividing tumor cells generate larger amounts of aberrant proteins to be degraded by the UPS and are therefore more susceptible to proteasome inhibition and the resulting change in cellular protein homeostasis (Adams, 2004). Despite the lack in specificity, *bortezomib* has provided clinical proof that targeting the UPS can be a successful approach in treating malignancies and that more specific drugs could ultimately be used to provide promising new medicines. Another compound currently in clinical trials is MLN4924 (Millennium Pharmaceuticals, Cambridge US). MLN4924 targets the Nedd8-specific E1 enzyme NAE1, which controls the activity of the CRL ligase family (Soucy et al., 2009). MLN4924 acts by forming a stable NEDD8-MLN4924

adduct—catalyzed by the UBA3/NAE1 enzyme—that resembles the NEDD8 adenylate but that cannot be further processed by the enzyme. It remains stably bound, thereby inhibiting the E1 (Brownell et al., 2010).

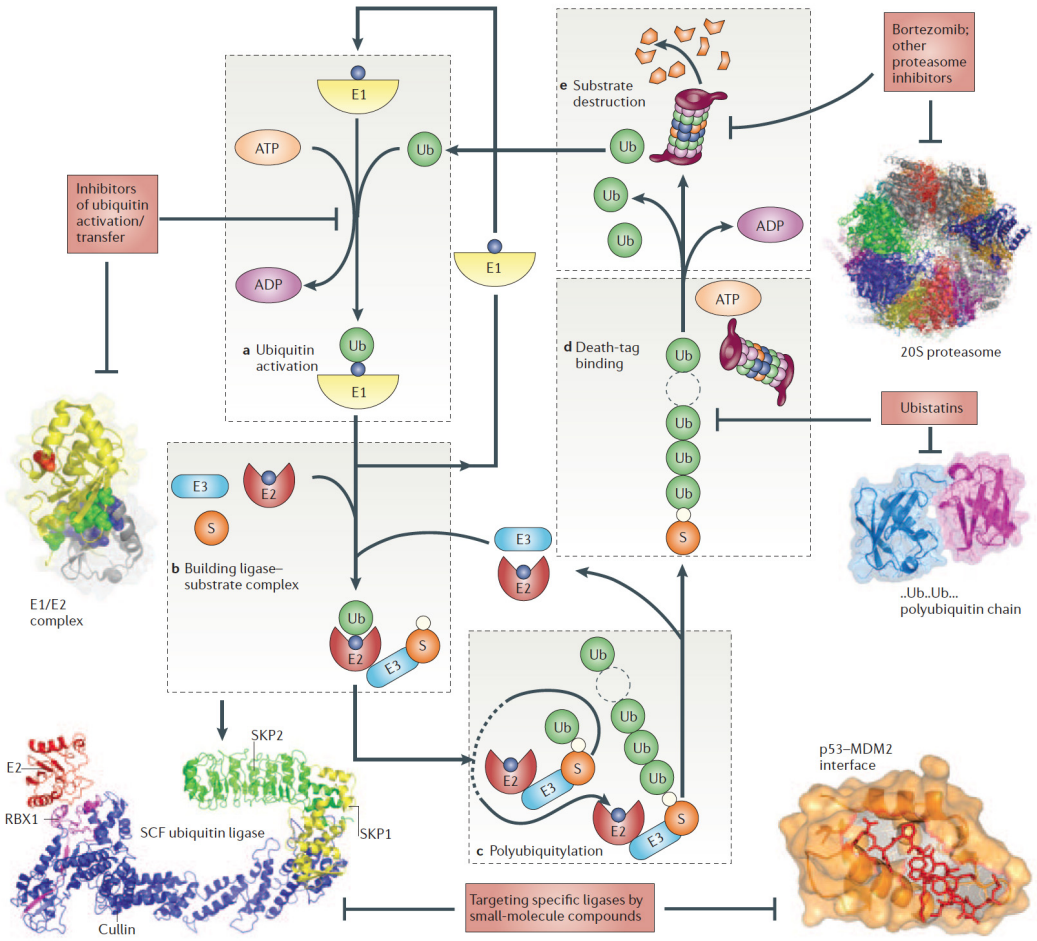

Figure 1.7: Potential drug targets within the Ubiquitin Proteasome System (UPS). (a) Targeting the E1 enzyme will result in pan-UPS inhibition. (b) Targeting the E2 enzyme has been successful in the case of Cdc34 (Ceccarelli et al., 2011) and will provide more specificity then E1 inhibition. To gain true specificity to a certain target pathway or protein, targeting a specific E3 ligase (c) will be required. The final step of the UPS is (d, e) ATP dependent degradation of the poly-ubiquitinated substrate, which is inhibited by the FDA approved small molecule *Bortezomib* (Nalepa et al., 2006).

The nature of the enzymes involved in ubiquitin conjugation represents a challenge for drug development. While the E1 (as well as the proteasome) represents a more conventional enzyme having either an ATP binding pocket, or being a protease-like enzyme to be targeted by small molecules, targeting a specific ubiquitin ligase, such as a CRL, requires the development of protein–protein interaction inhibitors; most of the E3s lack obvious small molecule-binding pockets. Despite these difficulties, efforts to find such small molecules have resulted in a number of compounds targeting specific E3

ligases within the UPS. The protein–protein interaction of the RING finger ubiquitin ligase Mdm2 with p53 (Kussie et al., 1996; Chi et al., 2005), one of the most prominent tumor suppressors, has been one of the first to be successfully targeted by a small molecule. A class of compounds, nutlins (cis-imidazoline-derivatives), was found by screening a chemical compound library for the ability to block the p53-Mdm2 interface (Vassilev et al., 2004). Nutlins have been shown to be competitive inhibitors that bind to the binding groove on Mdm2 and block binding of p53. Recent efforts to target CRL ligases have resulted in tool compounds directed to the yeast CRL ligases SCF^{Cdc4} (Orlicky et al., 2010) and SCF^{Met30} (Aghajan et al., 2010). While these attempts are still far from the clinics, the compound SCF-I2, which inhibits SCF^{Cdc4}, in particular provides proof that it is principally possible to target specific SCF substrate receptors (Orlicky et al., 2010). Interestingly, SCF-I2 does not bind the substrate binding site but rather targets a pocket induced between blades 5 and 6 of the Cdc4 WD40 β-propeller and acts as an allosteric inhibitor of phosphodegron binding.

Another small molecule, thalidomide (*Thalomid*, *Contergan*), was approved by the FDA in 2006 to treat multiple myeloma and leprosy's, and it later turned out to inhibit a specific CRL4 ligase complex.

Thalidomide and derivatives: Specific $CRL4^{CRBN}$ inhibitors?

Thalidomide was developed in the 1950s by the German pharmaceutical company Grünenthal and was first marketed as a mild sedative better known as *Contergan* in Germany. While it was never approved by the FDA as a sedative due to safety concerns, the drug quickly reached over 40 countries. The tragedy commonly associated with thalidomide became apparent in the early 1960s, when thalidomide taken by pregnant women was found to be responsible for multiple and severe birth defects (Knobloch and Rüther, 2008). More than 10,000 children were born with birth defects, such as malformations of the limbs, ears, or internal organs, before the drug was discontinued in 1961. However, studies to unravel the mechanism of teratogenicity continued, and physicians have uncovered several clinical effects such as efficacy in the treatment of leprosy (SHESKIN, 1965),

rheumatoid arthritis (Gutiérrez-Rodríguez, 1984), and chronic graft-versus-host disease (McCarthy et al., 1989; Vogelsang et al., 1992). The discovery that thalidomide inhibits TNF-α production (Sampaio et al., 1991; Makonkawkeyoon et al., 1993) and possesses anti-angiogenic activity (D'Amato et al., 1994) suggested an anti-cancer potential and stimulated research in this direction. Thalidomide was first shown to be effective for the treatment of refractory multiple myeloma (Singhal et al., 1999) and was approved as a treatment by the FDA in 2006. Thalidomide is a derivative of glutamic acid composed of two imide rings: glutarimide and phtalimide. The drug has two isomeric forms, S-thalidomide and R-thalidomide, which rapidly interconvert under physiological conditions (Bosch et al., 2008), and are subject to non-enzymatic and enzymatic breakdown, resulting in numerous metabolites (Ando et al., 2002; Bosch et al., 2008). Advances in the use of thalidomide as an anti-cancer drug have led to the development of new derivatives with the aim of increasing the potency of TNF-α inhibition and making the side effects less severe. This resulted in a class of compounds called immunomodulatory drugs (IMiDs). In particular, lenalidomide (CC-5013, revlimid) and pomalidomide (CC-4047) have proven to be effective in several multiple myeloma, chronic lymphocytic leukemia, non-Hodgkin's leukemia, and solid tumor directed pre-clinical and clinical trials (Bartlett et al., 2004). The FDA has now approved lenalidomide to treat multiple myeloma and 5q-MDS (deletion of chromosome arm 5q associated myelodisplastic syndrome).

Despite the apparent success in clinical use, the precise mode of action associated with thalidomide teratogenicity and anti-cancer potential remains elusive and has led to a variety of proposed models for thalidomide action (Stephens, 1988; Quach et al., 2010). While a majority of the hypotheses lack sufficient experimental support, the oxidative stress hypothesis and the anti-angiogenic hypothesis have gained support as being involved in the teratogenicity of thalidomide, despite the fact that the precise mechanism remains elusive.

Oxidative stress hypothesis

Thalidomide has been shown to induce elevation of reactive oxygen species (ROS) (Wells et al., 1997; Parman et al., 1999), resulting in oxidized DNA and limb malformations in rabbits. It was demonstrated that this is counteracted by phenyl-N-tert-butylnitrone (PNB), a chemical that traps free radicals. Fgf8 and Fgf10 are essential regulators of limb development and their expression is inhibited by thalidomide, which is suppressed by PNB (Hansen et al., 2002; Ito et al., 2011). It was later shown by Knobloch et al. (2007) that thalidomide-induced ROS result in the upregulation of bone morphogenic proteins (BMPs) and programmed cell death. BMPs negatively regulate Fgf, Wnt, and Akt signaling (Ito et al., 2011); Wnt and Akt signaling are important for cell proliferation and survival. This results in a model where thalidomide-induced ROS attenuate the level of BMPs, thereby negatively affecting Fgf, Wnt, and Akt signaling to drive programmed cell death (Ito et al., 2011).

Anti-angiogenesis hypothesis

Following the discovery that thalidomide inhibits Fgf2-induced angiogenesis (D'Amato et al., 1994), the authors hypothesized that the inhibition of angiogenesis caused limb defects by disrupting blood vessel formation crucial to limb development. It was further suggested that the anti-angiogenic properties of thalidomide would cause the downregulation of Fg8/Fgf10 and cell death, in turn causing impaired limb development (Therapontos et al., 2009). However, Ito and colleagues found that in zebrafish, Fgf8 downregulation, together with malformation of the pectoral fins, precedes the formation of blood vessels (Ito et al., 2010). This suggests that, at least in zebrafish, the order of events is different and that additional knowledge of the precise molecular mechanisms underlying anti-angiogenesis is necessary to understand the effect on limb development. A tremendous achievement in understanding thalidomide action came with the discovery of the protein cereblon (CRBN) as a primary cellular target of thalidomide.

CRBN: A primary target of thalidomide

Using a carboxyl-type derivative of thalidomide coupled to magnetic beads (**Figure 1.8**), Ito et al. (2010) were able to identify the protein *cereblon* (CRBN) as direct target of thalidomide. CRBN was readily purified from various human cell lines, including HeLa, 293T, HUVEC, U266, and Jurkat, and was found to be the only direct binding partner of thalidomide under these conditions (Ito et al., 2010). Together with CRBN, the DNA damage binding protein 1 (DDB1) was co-purified, and CRBN turned out to be part of a Cul4-Rbx1-DDB1-CRBN ($CRL4^{CRBN}$) ubiquitin ligase complex. CRBN is a 442 amino acid protein that was originally discovered as being mutated in a mild form of mental retardation (MR) (Higgins et al., 2004). It has been shown that CRBN directly interacts with a large-conductance calcium-activated potassium channel (BK_{Ca}) (Jo et al., 2005) and a voltage-gated chloride channel (Hohberger and Enz, 2009). Moreover, CRBN was found to interact with proteasome subunit beta type 4 (PSMB4) (Lee et al., 2012b) and AMP-activated protein kinase subunit α1 (AMPKα1) (Lee et al., 2011) by yeast two-hybrid screens. However, little is known about the cellular and physiological functions of CRBN, other than that it is a subunit of the $CRL4^{CRBN}$ ubiquitin ligase.

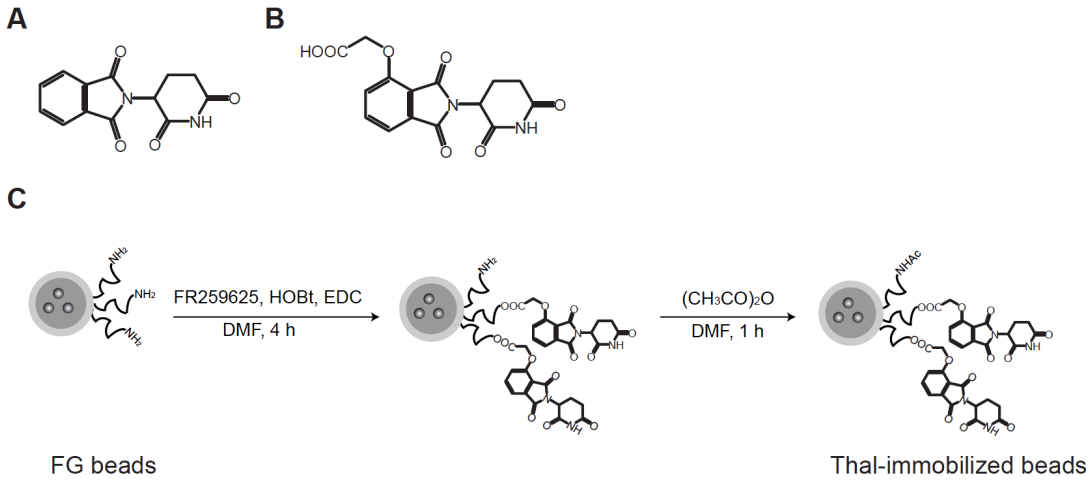

Figure 1.8: Thalidomide coupling on magnetic beads. (A) Chemical structure of thalidomide and (B) thalidomide-derivative to be (C) coupled to FG magnetic beads (Ito et al., 2010).

Following the discovery of CRBN as a direct target of thalidomide, Ito et al. (2010) also found that CRBN is autoubiquitinated *in vivo* and that autoubiquitination is inhibited by thalidomide. In an attempt to validate the role

of CRBN teratogenicity, the authors investigated the effect of thalidomide on the embryonic development of chickens (*Gallus gallus*) and zebrafish (*Danio rerio*). In chicken and zebrafish embryos, limb development and the development of pectoral fins, respectively, was severely impaired upon thalidomide treatment (Ito et al., 2010). The CRBN dependence of this phenotype was further confirmed by the observation that a CRBN mutant deficient in thalidomide binding while maintaining its ability to form a functional ligase ($CRBN_{YW/AA}$) renders embryos expressing this mutant insensitive to thalidomide teratogenicity (Ito et al., 2010). This finding was corroborated by the observation that the knockdown of endogenous CRBN in zebrafish using antisense morpholino oligonucleotides resulted in the malformation of pectoral fins, similar to thalidomide treatment (Ito et al., 2010), and reduction of Fgf8 expression. Similar experiments performed using chicken embryos suggest that the role of CRBN in fin and limb development is conserved (Ito et al., 2010). A potential connection between the previously outlined oxidative stress hypothesis and the role of CRBN is suggested by the common downregulation of Fgf8 and Fgf10. If functional CRBN were required in a pathway controlling levels of ROS, then ROS levels would in turn be elevated in the presence of thalidomide, resulting in reduced levels of Fgf8 and Fgf10. However, there is no experimental evidence of CRBN being involved in the control of reactive oxygen detoxification. Further research about the direct *versus* indirect targets of $CRL4^{CRBN}$ ubiquitination activity will be required to shed light on CRBN functions.

A comprehensive study has also confirmed that CRBN is essential for the anti-myeloma effects of thalidomide, lenalidomide, and pomalidomide (Lopez-Girona et al., 2012). The authors reported that in addition to thalidomide, lenalidomide and pomalidomide also directly interact with CRBN and that CRBN is required for their anti-proliferative potency. Moreover, the acquired resistance of a H929 myeloma cell line to thalidomide treatment has been linked to loss of CRBN expression. Overexpression of functional CRBN, but not $CRBN_{YW/AA}$ mutant protein, in those cells restored thalidomide sensitivity (Lopez-Girona et al., 2012). More detailed structural and functional data on CRBN will be required to decipher IMiD action on this CRL4 ligase complex. Further research about downstream targets would allow a better

understanding of how CRBN is involved in teratogenicity and of the anti-proliferative effects of thalidomide and its derivatives.

Aim of This Thesis

The global branch of mammalian nucleotide excision repair (GGR) has been extensively studied, yet, so far, little is known about the detailed molecular architecture and function of the involved cullin-RING ubiquitin ligase $CRL4^{DDB2}$.

Previous work demonstrated the important role for DDB2 in efficient repair of photo-dimers *in vivo* (Scrima 2008, Nishi 2009). DDB2 is further part of the CUL4-RBX1-DDB1-DDB2 ($CRL4^{DDB2}$) ligase complex (Sugasawa 2005), involved in ubiquitination of XPC, DDB2, histones H3, H4 and H2A (Guerrero-Santoro 2008; Kapetanaki 2006; Wang 2006), and thereby bridging NER to the ubiquitin proteasome system.

A first aim of the present study is to employ structural and functional methodology to elucidate the molecular architecture of the 280kDa $CRL4^{DDB2}$ ligase complex bound to its DNA substrate and to understand its targeting to photo-dimers in chromatin. While $CRL4^{DDB2}$ shows constitutive activity *in vitro*, its ubiquitination activity appears tightly regulated *in vivo*. Characterizing the biochemical and biophysical interplay of $CRL4^{DDB2}$ with the COP9 signalosome (CSN), a master regulator of cullin activity, will address how the ligase complex is activated upon DNA damage recognition.

While $CRL4^{DDB2}$ is a special ligase that recognizes a damaged DNA substrate, rather then a protein substrate, we further set out to characterize CSN mediated CRL4 regulation of other members of the family. Being involved in transcription coupled repair and targeting the CSB protein for ubiquitination, we chose the $CRL4^{CSA}$ ligase to further detail CRL4 regulation.

The cullin family represents the largest subgroup of E3 ubiquitin ligases and is involved in numerous human diseases. Recent advances in the treatment of malignancies using the proteasome inhibitor *velcade/bortezomib* and the Nedd8 E1 inhibitor *MLN4924* shed light on the potential of modulating the ubiquitin proteasome system (UPS) in cancer therapy. The drug *thalidomide (Contergan)*, developed in the 1950's, and its derivative *lenalidomide (Revlimid)* have been FDA approved for treatment of multiple myeloma and a study from Ito and colleagues demonstrated that *thalidomide* binds the protein *cereblon* (CRBN), which is part of the $CRL4^{CRBN}$ ligase

complex. The second aim of the present thesis is, to understand how this small molecule inhibitors target and act on the $CRL4^{CRBN}$ ligase. X-ray crystallography and biochemical methods will be used to elucidate how these inhibitors bind to CRBN and how they modulate the activity of the $CRL4^{CRBN}$ ligase complex.

Chapter 2: The molecular basis of $CRL4^{DDB2/CSA}$ ubiquitin ligase architecture, targeting and activation.

(published manuscript)

Eric S. Fischer[1,8*], Andrea Scrima[1,7*], Kerstin Böhm[1], Syota Matsumoto[2], Gondichatnahalli M. Lingaraju[1], Mahamadou Faty[1], Takeshi Yasuda[3], Simone Cavadini[1], Mitsuo Wakasugi[4], Fumio Hanaoka[5], Shigenori Iwai[6], Heinz Gut[1], Kaoru Sugasawa[2], Nicolas H Thomä[1†]

[1] Friedrich Miescher Institute for Biomedical Research, Maulbeerstrasse 66, CH-4058 Basel, Switzerland
[2] Biosignal Research Center, and Graduate School of Science, Kobe University, 1-1 Rokkodai, Nada-ku, Kobe 657-8501, Japan
[3] National Institute of Radiological Sciences, 4-9-1 Anagawa, Inage-ku, Chiba 263-8555, Japan
[4] Laboratory of Human Molecular Genetics, Graduate School of Natural Science and Technology, Kanazawa University, Kakuma-machi, Kanazawa 920-1192, Japan
[5] Faculty of Science, Gakushuin University, 1-5-1 Meijro, Toshima-ku, Tokyo 171-8588, Japan
[6] Graduate School of Engineering Science, Osaka University, 1-3 Machikaneyama, Toyonaka, Osaka 560-8531 Japan
[7] Present address: Department of Molecular Structural Biology, Helmholtz-Centre for Infection Research, Inhoffenstrasse 7, D-38124 Braunschweig, Germany
[8] Universität Basel, Petersplatz 10, CH-4003 Basel, Switzerland

Cell *2011, Volume 147, pg 1024-1039*

Summary: The DDB1-CUL4-RBX1 (CRL4) ubiquitin ligase family regulates a diverse set of cellular pathways through dedicated substrate receptors (DCAFs). The DCAF DDB2 detects UV-induced pyrimidine dimers in the genome and facilitates nucleotide excision repair. We provide the molecular basis for DDB2 receptor-mediated cyclobutane pyrimidine dimer recognition in chromatin. The structures of the fully assembled DDB1-DDB2-CUL4A/B-RBX1 ($CRL4^{DDB2}$) ligases reveal that the mobility of the ligase arm creates a defined ubiquitination zone around the damage, which precludes direct ligase activation by DNA lesions. Instead, the COP9 signalosome (CSN) mediates the $CRL4^{DDB2}$ inhibition in a CSN5 independent, non-enzymatic, fashion. In turn, CSN inhibition is relieved upon DNA damage binding to the DDB2 module within CSN-$CRL4^{DDB2}$. The Cockayne syndrome A DCAF complex crystal structure shows that $CRL4^{DCAF(WD40)}$ ligases share common architectural features. Our data support a general mechanism of ligase activation, which is induced by CSN displacement from $CRL4^{DCAF}$ on substrate binding to the DCAF.

author contributions: ESF designed and performed the experiments in figures 3, 4, 5, 7, S2, S3, S4 and S5. AS designed and performed the experiments in figures 1, 2 and S1. KB, AS and EF designed and performed the experiments in figures 6, S6 and S7. SM designed and performed the experiments in figures 5a-c. GML purified and provided recombinant COP9 signalosome. MF purified the CAND1-CUL4B protein for crystallization. TY designed and performed the experiments in figures 2b-e. SC analyzed CRL4-CSN complexes by EM. MW tested DDB1 mutants for complementation in Chicken DT40 cells. FM contributed to the design of experiments in figures 2b-e. SI provided synthetic DNA oligos containing *6-4PP* or *CPD* lesions. HG helped with data collection and structure determination. KS designed the experiments in figures 2b-e and 5a-c, NHT designed the experiments and wrote the manuscript together with ESF, AS and KB.

The molecular basis of CRL4$^{DDB2/CSA}$ ubiquitin ligase architecture, targeting, and activation

Eric S. Fischer1,8*, Andrea Scrima1,7*, Kerstin Böhm1, Syota Matsumoto2, Gondichatnahalli M. Lingaraju1, Mahamadou Faty1, Takeshi Yasuda3, Simone Cavadini1, Mitsuo Wakasugi4, Fumio Hanaoka5, Shigenori Iwai6, Heinz Gut1, Kaoru Sugasawa2, Nicolas H Thomä1†

1 Friedrich Miescher Institute for Biomedical Research, Maulbeerstrasse 66, CH-4058 Basel, Switzerland
2 Biosignal Research Center, and Graduate School of Science, Kobe University, 1-1 Rokkodai, Nada-ku, Kobe 657-8501, Japan
3 National Institute of Radiological Sciences, 4-9-1 Anagawa, Inage-ku, Chiba 263-8555, Japan
4 Laboratory of Human Molecular Genetics, Graduate School of Natural Science and Technology, Kanazawa University, Kakuma-machi, Kanazawa 920-1192, Japan
5 Faculty of Science, Gakushuin University, 1-5-1 Meijro, Toshima-ku, Tokyo 171-8588, Japan
6 Graduate School of Engineering Science, Osaka University, 1-3 Machikaneyama, Toyonaka, Osaka 560-8531 Japan
7 Present address: Department of Molecular Structural Biology, Helmholtz-Centre for Infection Research, Inhoffenstrasse 7, D-38124 Braunschweig, Germany
8 Universität Basel, Petersplatz 10, CH-4003 Basel, Switzerland

† to whom correspondence should be addressed: nicolas.thoma@fmi.ch

* both authors have contributed equally

Keywords: Xeroderma pigmentosum, Cockayne syndrome, CSA, DDB2, CRL4, CSN, COP9, CDT2, CSB, DCAF1, cullin, chromatin and damage repair.

Summary

The DDB1-CUL4-RBX1 (CRL4) ubiquitin ligase family regulates a diverse set of cellular pathways through dedicated substrate receptors (DCAFs). The DCAF DDB2 detects UV-induced pyrimidine dimers in the genome and facilitates nucleotide excision repair. We provide the molecular basis for DDB2 receptor-mediated cyclobutane pyrimidine dimer recognition in chromatin. The structures of the fully assembled DDB1-DDB2-CUL4A/B-RBX1 ($CRL4^{DDB2}$) ligases reveal that the mobility of the ligase arm creates a defined ubiquitination zone around the damage, which precludes direct ligase activation by DNA lesions. Instead, the COP9 signalosome (CSN) mediates the CRL4DDB2 inhibition in a CSN5 independent, non-enzymatic, fashion. In turn, CSN inhibition is relieved upon DNA damage binding to the DDB2 module within CSN-$CRL4^{DDB2}$. The Cockayne syndrome A DCAF complex crystal structure shows that $CRL4^{DCAF(WD40)}$ ligases share common architectural features. Our data support a general mechanism of ligase activation, which is induced by CSN displacement from $CRL4^{DCAF}$ on substrate binding to the DCAF.

Introduction

The evolutionarily conserved CUL4 E3 ligase family, in concert with its DDB1 adaptor, regulates a diverse set of cellular processes including development, transcription, replication and DNA repair (Jackson and Xiong, 2009). Specificity is conferred by a set of more than 50 WD40 containing substrate receptors, also referred to as DCAFs (DDB1 CUL4 Associated Factors) (Angers et al., 2006; Bennett et al., 2010; He et al., 2006; Higa et al., 2006; Jin et al., 2006). A large fraction of these targeting modules is directed towards chromatin-associated proteins. One of the best characterized substrate receptors is the damaged DNA binding protein 2 (DDB2), which binds to UV-induced DNA pyrimidine dimers. The DDB2 receptor is part of the DDB1-DDB2-CUL4-RBX1 E3 ligase complex ($CRL4^{DDB2}$) (Scrima et al., 2011). This bi-functional damage detection and ubiquitin ligase complex serves in the repair of UV-induced DNA lesions in chromatin.

Exposure of the genomic DNA to ultraviolet light (UV) results in the formation of covalent crosslinks between neighboring pyrimidine nucleotides. These pyrimidine dimers, if left unrepaired, stall transcription by RNA polymerase II (RNAPII). Unrepaired lesions require error-prone translesion polymerases in S phase (Friedberg, 2001), which potentially introduce oncogenic mutations. Cyclobutane pyrimidine dimers (CPD) and (6-4) pyrimidine-pyrimidone photoproducts (6-4PP) are the two major photo lesions, accounting for approximately 75 % and 25 % of genomic UV-lesions, respectively (Mitchell et al., 1989). Compared to 6-4PP, CPDs cause relatively minor thermodynamic duplex destabilization (Jing et al., 1998), and are found frequently obscured by organization into nucleosomes (Gale and Smerdon, 1988). These biophysical and cellular properties render CPDs the most difficult photo-lesion to detect. CPDs are thereby highly mutagenic and major facilitators of skin carcinogenesis (Hoeijmakers, 2009).

The mammalian global genome repair branch of nucleotide excision repair (NER) surveys the genome for lesions and actively repairs pyrimidine dimers (Aboussekhra et al., 1995). NER thereby functions as a central pathway in safeguarding metazoan cells against sun-induced skin carcinogenesis. XPC-RAD23-Centrin2 acts as a lesion surveillance complex, recruiting the core NER machinery to damaged sites (Volker et al., 2001). Assembly of the NER complex results in rapid damage excision and repair synthesis, with repair generally proceeding in a fast and error free fashion. While XPC is required for global genome NER, it has little or no affinity for CPD lesions, and does not recognize 6-4PP in the context of chromatin (Batty et al., 2000; Sugasawa et al., 2001; Yasuda et al., 2005). Recently, XPC recruitment to chromatin was shown to be facilitated by the DDB1-DDB2 (UV-DDB) complex (Nishi et al., 2009). In the absence of DDB2, XPC remains localized to 6-4PP and to a lesser extent to CPDs, albeit with substantially delayed kinetics (Sugasawa, 2010). The precise mechanism of XPC recruitment to sites of UV damage, in the absence of DDB2 is unclear. DDB2 binds to CPD and 6-4PP pyrimidine dimers with the highest reported affinity and specificity of all metazoan damage recognition factors (Payne and Chu, 1994; Wittschieben et al., 2005). Mutations in DDB2 give rise to XP complementation group E (Tang and Chu, 2002). In DDB2-deficient XPE cells, CPD repair is largely abolished, while 6-

4PP repair is affected to a lesser extent (Hwang et al., 1998; Moser et al., 2005; Tang et al., 2000). The structural basis of 6-4PP recognition by DDB1-DDB2 is known (Scrima et al., 2008) but it is currently unclear how DDB2 recognizes CPD lesions, which are chemically distinct from the 6-4PP and frequently encapsulated in nucleosomes (Gale and Smerdon, 1988).

DDB1-DDB2 appears constitutively bound to CUL4 which targets XPC and DDB2 for ubiquitination (Sugasawa et al., 2005). In addition, histones H2A, H3 and H4 surrounding the lesion are ubiquitinated in a UV-dependent fashion (Guerrero-Santoro et al., 2008; Kapetanaki et al., 2006; Wang et al., 2006). DDB2 autoubiquitination leads to the loss of DNA damage binding and rapid DDB2 degradation (Sugasawa et al., 2005). XPC ubiquitination, in contrast, retains the complex at the site of UV damage without immediate proteasomal degradation. The differential response of XPC and DDB2 upon ubiquitination has been linked to a ubiquitin-dependent damage handover from $CRL4^{DDB2}$ to XPC (Sugasawa et al., 2005). $CRL4^{DDB2}$ is found in complex with the COP9 signalosome (CSN) (Hannss and Dubiel, 2011). CSN is an 8-subunit isopeptidase complex, which via the proteolytic activity of its CSN5 subunit removes the ubiquitin-like NEDD8 from cullins. NEDD8 is considered as an activator and its removal renders the ligase complex inactive (Furukawa et al., 2000). Recruitment of $CRL4^{DDB2}$ to sites of DNA damage in chromatin appears to correlate with CSN release (Groisman et al., 2003; Takedachi et al., 2010). The molecular mechanism triggering CRL4DDB2 activation in response to damage binding is currently unresolved.

While the DDB2 substrate receptor recruits $CRL4^{DDB2}$ to DNA damage, other CRL4 substrate receptors are recruited by protein epitopes. Prominent examples include DCAF1, CDT2 and the Cockayne syndrome A (CSA) protein (Lee and Zhou, 2007). All CRL4 substrate receptors are linked to CUL4 through the DDB1 adaptor. CSA is functionally unrelated to DDB2 and serves in the transcription coupled branch of NER. $CRL4^{CSA}$ is recruited to sites of CSB and stalled RNA polymerase II, where it facilitates DNA repair and the subsequent transcription restart (Tornaletti, 2009). Reported $CRL4^{CSA}$ ubiquitination targets include the Cockayne syndrome B protein (CSB), a SWI/SNF ATPase (Troelstra et al., 1992). $CRL4^{DDB2}$ and $CRL4^{CSA}$, as well as other cullin-RING type ligases are inhibited by CSN (Bennett et al., 2010). It is

currently unclear how CSN inhibition is retained at the majority of cellular cullin ligase complexes, while CSN specifically dissociates from those ligases that undergo activation in response to a given stimulus (i.e.: CSN mediated dissociation and activation of $CRL4^{DDB2}$ and $CRL4^{CSA}$ in response to UV).

Here we provide the molecular basis for $CRL4^{DDB2}$ recruitment to CPD lesions in chromatin, and characterize how the damage recognition process results in ubiquitin ligase activation, a process mediated by CSN. We present the structure of the DDB1-CSA complex, which in conjunction with biochemical data presented argues in favor of conserved architectural and regulatory principles amongst CRL4 ligases.

Results

CPD recognition by DDB2 involves β-hairpin insertion and lesion flipping

The DDB2 damage detection module has previously been postulated to undergo conformational changes upon binding of a pyrimidine dimer resulting in $CRL4^{DDB2}$ activation in vivo (Takedachi et al., 2010). We therefore focused on the structure of the DDB1-DDB2 complex bound to CPD-containing duplexes, its physiological substrate. DDB1-DDB2 has the highest reported affinity for CPD lesions among metazoan damage recognition factors. Its absolute affinity, however, was not sufficient to allow successful crystallization in the presence of CPD duplexes. We then engineered DDB1-DDB2 crystal contacts disfavoring crystallization of the DNA-free (apo) state, biasing crystallization towards CPD co-complexes. This was done by mutating DDB1 contacts that occur only in the apo-DDB1-DDB2 crystal lattice, as DDB1 is not involved in DNA binding (Figure S1). This approach led to the structures of DDB1-DDB2 bound to four different cis-syn CPD-containing DNA duplexes, observed in different space groups and crystal packing arrangements (Figure 1; Figure S1). Due to the overall structural similarity among these DNA co-complex structures, the discussion focuses on the 3.0 Å resolution structure of DDB1-DDB2 bound to a 13mer duplex having a 5' overhang on both strands (CPD#1).

Consistent with the DDB1-DDB2 6-4PP complex (Scrima et al., 2008), the CPD-containing duplex is exclusively held by the DDB2 WD40 propeller. The DNA traverses the central cavity of the WD40 propeller along the axis defined

by DDB2 blades 7 and 4, pointing away from DDB1 (Figure 1). A DDB2 β-hairpin, comprising Phe371, Gln372 and His373 is inserted into the minor groove of the duplex at the site of the CPD. Insertion of this damage-recognition finger (Scrima et al., 2008) proceeds with duplex unwinding of ~12.6° (Figure S1d), widening of the minor groove to ~18 Å (Table S2) and extrusion of the CPD into an extra-helical, flipped out conformation. The observed kink angle of the cis-syn CPD DNA in the highest resolution CPD complex is ~45°.

The DDB2 binding interface is specifically tailored towards CPD recognition

The 6-4PP structure previously revealed few contacts between DDB2 and the extruded 6-4PP (Scrima et al., 2008). The 6-4PP has the pyrimidine-pyrimidone rings angled at ~90° and can therefore not fully engage the DDB2 damage recognition pocket (Figure 1c and d). The boat-shaped cis-syn CPD, in contrast, provides a high degree of surface complementarity through packing with its hydrophobic carbons (at C5 and C6 positions) against the hydrophobic core of the DDB2 pocket (Figure 1). This interaction is stabilized by DDB2 residues Trp239, Ile213, Gly192 and the Cα of Arg214. The four hydrophilic carbonyl groups of the CPD (at the C2/C4 positions), located on the opposing face, are solvent exposed and contact water molecules. The carboxylic group of Asp237 contacts the D+2 pyrimidine nitrogen at N3. The overall arrangement results in a larger contact area of 327 Å2 for the CPD moiety versus 265 Å2 for the 6-4PP.

Comparison with existing structures of protein-free CPD duplexes indicated that the DNA conformation seen in the DDB2-CPD complex (Figure 1) closely resembles previously observed protein-free cis-syn CPD duplexes (Figure S1). DDB2, through its pyrimidine dimer binding pocket and overall DNA shape complementarity thereby specifically supports CPD recognition.

The DDB1-DDB2 complex does not change its conformation in response to damage binding

The DDB2 6-4PP, THF (Scrima et al., 2008) and CPD structures illustrate that the DNA is intrinsically flexible and can adapt to DDB2 despite differences in the DNA sequence (see Figure S1). The plasticity of the DNA is

contrasted with the rigidity of DDB2. In all DNA bound and DNA free structures available, DDB2 including its ß-hairpin does not change its conformation. Thus, DDB2 serves as a rigid damage recognition unit. As a consequence DDB2 binding to its physiological CPD substrate does not trigger conformational changes that could serve as the signal in ligase activation (see below).

DDB2 mediated detection of CPD lesions in chromatin

The DDB2 DNA binding interface has previously been proposed to allow readout of lesions embedded in nucleosomes (Scrima et al., 2008). This is of notable biological importance, as the majority of CPDs appear encapsulated in nucleosomes (Gale and Smerdon, 1988). The DNA curvature observed when bound to DDB2 matches the nucleosomal curvature (Scrima et al., 2008) which was proposed to facilitate pyrimidine dimer readout through the minor groove. In order to test whether the DDB2 interface is compatible with nucleosomal damage detection, damage-containing nucleosomes were initially prepared by UV irradiation of DNA prior to the assembly of core particles (Supplemental experimental procedures). Electrophoretic mobility shift assays (EMSA) (Supplemental experimental procedures) demonstrated that DDB1-DDB2 is able to specifically recognize irradiated, linker free, mononucleosomes (Figure 2a). We subsequently prepared nucleosomes containing a chemically synthesized 6-4PP or CPD lesion (Figure 2b and c). Driven by nucleosome positioning sequence consisting of alternating A/T- and G/C-rich regions, these lesions were located at the sites where the minor groove is oriented away from the surface of the histone octamer (Yasuda et al., 2005). DDB1-DDB2 recognizes a single 6-4PP embedded in the nucleosome (Figure 2b lanes 10-12) and comparable binding can be observed in the presence of the equal amount of 6-4PP-containing naked DNA (Figure 2b, lanes 13-16). Binding was also detected for the CPD-containing nucleosomes (Figure 2c). CPD nucleosome binding was weaker than that of the 6-4PP (Figure 2d and e), in line with its intrinsically lower helix destabilization (Jin et al., 1998). Binding of CPD-containing nucleosomes was comparable, however, with DDB2 affinities observed for naked CPD-containing DNA. The DDB2 DNA binding interface in addition to being

optimized for CPD recognition, also confers compatibility for detecting CPDs and 6-4PPs in nucleosomes.

Measurements of cellular diffusion rates identified the $CRL4^{DDB2}$ complex as the functional macromolecular entity in DDB2 mediated DNA damage recognition (Luijsterburg et al., 2007). We therefore examined binding of the fully assembled $CRL4^{DDB2}$ complex to irradiated nucleosomes (Figure 2f). Analogous to our findings with DDB1-DDB2, we observed that the $CRL4^{DDB2}$ complex is able to specifically recognize lesions in nucleosomes, suggesting that the presence of CUL4 is compatible with damage recognition in chromatin. In an effort to understand the interplay between damage binding and ligase activation, we subsequently focused on the structure of the $CRL4^{DDB2}$ complex bound to damaged DNA duplexes.

Structures of DDB1-DDB2-CUL4A/B-RBX1 bound to damage-containing duplexes

We first determined the structure of DDB1-DDB2-CUL4A-RBX1 ($CRL4A^{DDB2}$) bound to a 12 bp DNA duplex containing a tetrahydrofuran (THF) lesion, a well characterized DDB2 substrate (Wittschieben et al., 2005). The structure of this 290 kDa nucleoprotein complex was refined by rigid body refinement to 5.9 Å resolution with an Rwork of 26.9 % (Rfree of 27 %) as outlined in Supplemental experimental procedures. Fragments from previously available high resolution structures of CUL4A (Angers et al., 2006), DDB1, DDB2 and DNA (Scrima et al., 2008) were positioned using iterative cycles of molecular replacement searches (Supplemental experimental procedures). The location of these individual rigid bodies was validated with anomalous dispersion methods using a selenomethionine (SeMet) labeled $CRL4A^{DDB2}$ complex. Phases derived from molecular replacement were used for calculation of anomalous difference Fourier electron density maps, which allowed identification of peaks for 50 % of the 55 expected Se at 3.0 σ (90 % at 2.0 σ). All peaks were located within 5 Å of their predicted position (Figure S2d). Calculation of composite omit maps with CNS (Brunger et al., 1998) further corroborated the correct placement of the different domains of the large complex (Figure S2c). Well defined 2mFobs-DFcalc density was observed for CUL4A, DDB1 (BPB, BPC&BPA), DDB2 (helix-loop-helix motif

and WD40 propeller) and the 24 nucleotides of the DNA duplex. While density was present for the segment of RBX1 residues 19–39 that integrates into the CUL4A C-terminal β-sandwich (Angers et al., 2006), no density was observed for the remainder.

Figure 3 shows the structure of $CRL4A^{DDB2}$ complex bound to a damage-containing duplex. $CRL4A^{DDB2}$ assumes an overall U-shaped assembly, with two extended arms of nearly equal length. The thicker arm is contributed by DDB1-DDB2 (extreme dimensions 75 Å x 45 Å), while the thinner arm comprises CUL4A (75 Å x 23 Å). The connection between them is made by the N-terminus of CUL4A (aa 39–96) in conjunction with the DDB1-BPB domain (Angers et al., 2006). The DDB1-DDB2 and CUL4A extended arms are angled at about 50°. The overall complex assumes an approximately square arrangement (160 Å x 140 Å). The largely helical CUL4A fold is attached exclusively to the BPB WD40 propeller of DDB1 (Figure 3). The observed distances between the CUL4A arm and the remainder of the DDB1 (BPC+BPA) propellers are generally more than 15-20 Å. The distance between CUL4A and the DNA duplex is around 50 Å. This arrangement excludes specific interactions between CUL4A and the DNA, or CUL4A and the BPA and BPC propellers of DDB1 (Figure 3).

The CUL4A and CUL4B ligases are structurally indistinguishable

Since human cells possess two CUL4 isoforms, CUL4A and CUL4B (Jackson and Xiong, 2009) with DDB1-DDB2 reported to exist in complex with both of them (Groisman et al., 2003; Wang et al., 2006), we determined the crystal structure of CUL4B-RBX1 bound to DDB1-DDB2 in the presence of a second 12 bp THF containing duplex DNA (7.4 Å resolution). While the cullin fold of CUL4B (aa 192–913) has high sequence identity to CUL4A (84 % over 722 residues), the CUL4B N-terminus is unique to CUL4B. CUL4B 1–191 aa N-terminus was predicted to be mostly unstructured and was removed prior to co-expression of the CRL4DDB2 complex.

In the absence of known structures of CUL4B, we first determined the structure of CUL4B (in complex with CAND1) at 3.8Å resolution (Supplemental experimental procedures). Analysis of CUL4A and CUL4B folds revealed superimposable structures (rmsd of 1.54 Å over 677 residues)

rendering the two homologues structurally indistinguishable (see Figure 4c and Figure S3 for the mapping of CUL4B mutations resulting in X-linked mental retardation).

The CUL4 E3 ligase freely rotates around a rotation axis defined by DDB1 and the damage

The structure of the DDB1-DDB2-CUL4B-RBX1 ($CRL4B^{DDB2}$) complex was solved following a similar strategy, as outlined for $CRL4A^{DDB2}$ (Supplemental experimental procedures). The overall architecture of the two $CRL4B^{DDB2}$ complexes, observed in the asymmetric unit was comparable with $CRL4A^{DDB2}$ (Figure 4). Clear density for RBX1, again was only visible for 19–39 aa in both molecules of $CRL4B^{DDB2}$. Comparison of the $CRL4A^{DDB2}$ with the two $CRL4B^{DDB2}$ molecules revealed the DDB1-BPB domain in three different rotational states. As the BPB domain is the anchor point of the CUL4 ligase, its mobility directly translates into the mobility of the entire ligase arm. Within the three molecules observed in our study (Figure 4a and b), CUL4 rotates around 60° along an axis defined by the damage and DDB1 (BPB propeller) (Figure 4). Minimal distances observed between CUL4B and DNA, and between CUL4B and DDB1 (BPC), for the two CUL4B molecules were between 25–35 Å and 5–27 Å, respectively. The cullin fold with its kink of ~80° between cullin repeats 1 and 2 is shaped to allow rotation over BPC blades 2 and 3 towards the DDB1 C-terminus without steric clashes with DDB1 (Figure 4).

The DDB1 BPB domain mobility structurally insulates the CUL4 ligase from the DDB2 module

Examination of the 11 available medium/high resolution DDB1 molecules obtained in crystallographic studies (Angers et al., 2006; Li et al., 2006; Li et al., 2010; Scrima et al., 2008) suggest a total BPB domain rotation range of at least 150° (Figure 4d). Analysis of the expected energetics of rotation, as calculated by differences in solvation energy for the individual DDB1 (BPB) vs. DDB1 (BPC-BPA) interfaces (Krissinel and Henrick, 2007) predicts that the observed rotations are iso-energetic (Figure 4e). As a consequence, $CRL4^{DDB2}$ is expected to rotate up to 150° establishing a ubiquitination zone

restricted to 60–80 Å, Upon modification with the small ubiquitin-like modifier NEDD8 and resultant release of RBX1, the ubiquitination zone increases to 30-110 Å (Duda et al., 2008) (Figure 4d).

The overall modular architecture of $CRL4^{DDB2}$ implies that CUL4 cannot be directly activated through conformational changes induced by DDB2 damage binding. The mobility of the ligase arm further insulates CUL4 from DDB2. Activation of the ligase in response to DNA damage therefore requires additional factors. We next focused on known regulators and their role in $CRL4^{DDB2}$ regulation.

The DDB2-N-terminus is autoubiquitinated and regulates DDB2 levels after UV irradiation

The $CRL4^{DDB2}$ complex, in vivo, undergoes DDB2 autoubiquitination and degradation following UV irradiation. In contrast, the recombinant $CRL4^{DDB2}$ complex undergoes DDB2 autoubiquitination irrespective of the presence and absence of DNA damage. The DDB2 subunit has previously been shown to undergo polyubiquitination at multiple sites (Sugasawa et al., 2005). Using mass spectrometry, in conjunction with a ubiquitin variant lacking lysine residues required for polyubiquitination, we identified the human DDB2 Lys residues 5, 11, 35, 40 and 151 as the main targets for $CRL4^{DDB2}$ autoubiquitination in vitro (Figure S4a to d). The majority of these sites (Lys5, 11, 35 and 40) are located within the unstructured DDB2 N-terminus. When determining the human DDB1-DDB2 complex structure DDB2 aa 1–59 were absent from the electron density maps, and were removed for subsequent structural studies. In vitro, deletion of the DDB2 N-terminus, 1–40 aa ($DDB2_{\Delta N}$), ablated the majority of ubiquitin acceptor sites (Figure 5a). On the basis of random-polymer-theory (Creighton, 1992) the very N-terminus of DDB2 is estimated to have a root-mean-square distance of about 90 Å from the beginning of the DDB2 structure (aa 1-66). The DDB2 N-terminus is thereby located on the edge of the active ubiquitination zone of the ligase.

Next, we assessed the effect of these lysine residues in cells, in response to UV damage. A normal human fibroblast cell line, WI38 VA13, was used to stably express HA-tagged wild type DDB2 or a construct in which 7 N-terminal lysines (at positions 4, 5, 11, 22, 35, 36, and 40) were mutated to arginines

($DDB2_{7KR}$). $DDB2_{7KR}$ remained associated with DDB1 and CUL4 in a manner identical to that seen for wild type DDB2 (Figure 5b). After blocking translation by cycloheximide treatment and UV irradiation, $DDB2_{7KR}$ showed remarkable stability compared to the wild type DDB2; cellular wild type DDB2 levels mostly disappeared 1 h after UV, whereas $DDB2_{7KR}$ levels remained unchanged for 5 h (Figure 5c). Differences in total levels of wild type DDB2 and $DDB2_{7KR}$ are visible as early as 30min post UV, at a time when CSN has previously been shown to dissociate from the complex (Groisman et al., 2003). Wild type and $DDB2_{7KR}$ were not degraded in response to UV in the presence of MG132, an inhibitor of the proteasome (Rapić-Otrin et al., 2002) (Figure 5c). The lysine residues at the DDB2 N-terminus (aa 5-40), which are targeted by $CRL4^{DDB2}$ for autoubiquitination in vitro, hence regulate the overall cellular concentration of DDB2 in response to UV.

The COP9 signalosome mediates activation between DDB2 and the ubiquitin ligase

DDB2 is autoubiquitinated by $CRL4^{DDB2}$ in cis irrespective of the presence or absence of DNA damage in vitro. In vivo, however, DDB2 ubiquitination and degradation proceeds in a DNA damage specific fashion. CSN has been implicated in CUL4 inhibition through deneddylation, and is known to dynamically associate with $CRL4^{DDB2}$ complexes (Groisman et al., 2003). Dissociation of the CSN from $CRL4^{DDB2}$ had previously been observed in the presence of nucleosomes (Takedachi et al., 2010). We first examined the effect of CSN on $CRL4^{DDB2}$ autoubiquitination. DDB2, within the $CRL4^{DDB2}$ complex, was readily ubiquitinated in the presence of an E1 (UBA1) and E2 (UbcH5A), as previously observed (Sugasawa et al., 2005). DDB2 autoubiquitination, however, was severely inhibited in the presence of CSN (Figure 5d, lanes 4 and 6). The inhibitory effect of CSN was observed in the presence of wild type CSN5, or using a CSN5 catalytic mutant deficient in deneddylation (CSN_{ASM}). We then carried out ubiquitination reactions in the presence of irradiated DNA plasmids. Under these conditions CSN, or CSN_{ASM}, no longer protected DDB2 from undergoing autoubiquitination (Figure 5d, lanes 5 and 7). We then examined the DNA specificity of activation. Short duplexes between 15 and 24bp in length containing either

THF, 6-4PP or CPD (Figure 5e) were sufficient to overcome CSN inhibition and triggered DDB2 autoubiquitination. Duplexes containing undamaged DNA, on the other hand, did not relieve protection (Figure 5e, lane 6). Analogously, a DDB2 mutant defective in damage DNA binding $DDB2_{K244E}$ (Wittschieben et al., 2005) was unable to relieve CSN inhibition (Figure 5f). EMSA and equilibrium size exclusion chromatography indicated that $CRL4^{DDB2}$ dissociated from the CSN-$CRL4^{DDB2}$ in the presence of small damage-containing DNA duplexes (Figure S5). We thereby conclude that substrate binding to the DDB2 subunit of $CRL4^{DDB2}$ triggers CSN release, relieves inhibition and results in an active ligase complex. The DDB2 N-terminus subsequently becomes subjected to $CRL4^{DDB2}$ autoubiquitination, which triggers cellular DDB2 degradation in response to UV irradiation.

Previous studies reported a deubiquitination (DUB) enzyme, UBP12, associated with CSN preparation immunopurified from human cells (Zhou et al., 2003). Our recombinant CSN, overexpressed and purified to homogeneity from insect cells (Enchev et al., 2010) (Figure S4) did not show any discernable deubiquitination activity, in the presence or absence of damaged DNA (Figure S4). In addition, while UBP12 DUB activity was previously shown to be inhibited by ubiquitin-aldehyde (Zhou et al., 2003), we observed no such effect on DNA mediated $CRL4^{DDB2}$ activation in the presence of 3.9 μM ubiquitin-aldehyde (Figure 5e, lanes 1 and 2), a concentration that was sufficient to inhibit a control DUB added to the reaction (Figure S5d). The CSN inhibitory properties observed in vitro are therefore intrinsic to the complex and not due to CSN5 mediated deneddylation, or CSN-associated DUB activity.

In a minimal, recombinant system we have fully reconstituted DNA damage-dependent activation of $CRL4^{DDB2}$ mediated by CSN (see Figure S5 for mapping of CSN subunits required for protection/release). While the $CRL4^{DDB2}$ complex, as depicted in Figure 3 and 4, is active in the presence of E1 and E2 conjugating enzymes, its activity is inhibited by CSN. The presence of UV damaged DNA serves to relieve CSN inhibition providing a mechanism for DNA-dependent activation of the $CRL4^{DDB2}$ ligase.

The CSA DDB1 complex reveals a common architecture of the DDB1-DCAF family

DDB2 is a member of the large family of DCAFs, functioning as a DNA damage specific receptor recruiting $CRL4^{DDB2}$ to pyrimidine dimer sites. Additional DCAFs have been described, the majority of which serve as substrate receptors to CRL4 ubiquitin ligases. These receptors likely do not bind DNA, but rather recognize proteins. In the $CRL4^{DDB2}$ structures, DDB2 emerges as modular unit insulated from the CUL4 ligase. The absence of specific interactions between DDB2 and CUL4 would principally allow exchange of DDB2 for other WD40 containing substrate adaptors. We thus focused on the DDB1-CSA-CUL4-RBX1 ($CRL4^{CSA}$) ligase, seemingly unrelated to DDB2 besides the WD40 repeat in its protein sequence, which functions in the transcription-coupled repair (TCR) branch of NER (Fousteri and Mullenders, 2008).

Cockayne syndrome (CS) is a rare congenital disease exhibiting defects in the TCR branch of NER. The stalling of RNAPII observed in the presence of damaged nucleotides tightens the interaction between the RNAPII and the Cockayne syndrome B (CSB) SWI/SNF ATPase. The complex of RNAPII and CSB in turn is a prerequisite for the arrival of the Cockayne syndrome A protein complex ($CRL4^{CSA}$) (Fousteri et al., 2006). Both CSA and CSB are required for successful repair and transcription restart. $CRL4^{CSA}$ has been implicated in the ubiquitination and subsequent degradation of CSB in a UV-dependent fashion (Groisman et al., 2006).

We have determined the structure of the human DDB1-CSA complex at 3.3 Å resolution (Figure 6). The structure was solved by molecular replacement as outlined in Supplemental experimental procedures. CSA comprises a seven-bladed WD40 propeller (aa 30–365) that attaches to DDB1 through a helix-loop-helix motif (aa 1–29). The CSA helix-loop-helix motif (HLH-box) and the WD40 propeller were well ordered, whereas no interpretable electron density was found for the C-terminus of CSA (aa 364 to 396) and the C-terminal affinity tag. Irrespective of the limited (20 %) sequence identity between DDB2 and CSA, the DDB1-CSA and DDB1-DDB2 complexes show high overall structural similarity (backbone rmsd of 3.4 Å for 355 CSA/DDB2 residues).

The location of CSA patient mutations are indicated in Figure 6b. We note that CSA mutations resulting in milder forms of CS type III (and UV sensitive syndrome $UV^{S}S$) are point mutations expected to cause only limited structural damage. Mutations giving rise to the more severe forms, CS type I and II are point mutations, deletions and premature chain termination mutations expected to severely compromise the CSA structure (see Table S6 for detailed analysis of CSA patient mutations and discussion of structure & phenotype correlations).

The CSA-DDB1 interaction is mediated through the HLH-BOX

DDB1 comprises three WD40 domains (BPA, BPB and BPC) and a C-terminal α-helical domain (CTD). We found that CSA binds to DDB1 with an N-terminal HLH-box segment formed by aa 1–29 (Figure 6a and d). The HLH-box localizes to a cleft between the DDB1 propellers BPA and BPC. The two parallel HLH-box helices, α1 and α2, pack against each other. The HLH-box interaction surface with DDB1 encompasses the outer surface of α1 and the N-terminal tip of α2 (aa 16–20). The majority of CSA α1 interactions with DDB1 are hydrophobic (CSA Met1, Leu5), or contact DDB1 through H-bonds (CSA Ser6, Arg8, Gln9). While α1 is buried deeply in the BPC DDB1 propeller, α2 is further detached from DDB1 pointing towards the DDB1 (BPA) propeller. CSA α2, contacts DDB1 largely through H-bonds and long-range salt bridges comprising CSA α2 residues Arg17 and Arg20, respectively.

Analysis of helix-loop-helix motifs identified in other WD40 containing DCAFs

The unexpected structural similarity between DDB2 and CSA prompted us to reinvestigate whether the majority of WD40 containing DCAFs bind DDB1 in a similar fashion. In proteomic studies approximately 50 WD40-containing DCAFs proteins were identified as putative substrate receptors (Angers et al., 2006; Bennett et al., 2010; He et al., 2006; Higa et al., 2006; Jin et al., 2006). Out of the 18 WD40 containing DCAFs, identified in at least two proteomic studies, 13 contained an HLH-box (Figure S6a). In addition to the conserved α1 helix (Fukumoto et al., 2008; Li et al., 2010) (Figure 6d to g), we now also detect conservation for helix α2. The beginning of α2 (residues +1 to +3) is composed of small and hydrophilic side chains, followed by large hydrophobic

residues (Phe, Leu and Tyr) at the +4 position, which pack against α1 (Figure 6c). A large, often polar, residue is found in the +6 position interacting with DDB1 (BPA). The length of the loop between α1 and α2 appears non-conserved and varies between 2 and 7 residues.

Based on these sequence signatures, we identify DDB1-(WD40) DCAF family members CDT2, DCAF1, WDR21, WDR23, WDR40, WDR22, WDR32, and PHIP among others (Figure S6) as having a HLH-box predicted to bind DDB1 in a manner similar to DDB2 and CSA. The resultant $CRL4^{DCAF(WD40)}$ complexes are expected to strongly resemble CRL4DDB2 sharing principle properties such as ligase mobility (see Figure S6c for a model of $CRL4^{CSA}$).

We then tested the functional interplay between $CRL4^{CSA}$ and CSN in vitro. We observed that CSA is also autoubiquitinated in vitro (Figure 7a, lane 2) and that CSA autoubiquitination is in turn inhibited by the addition of CSN (or CSN_{ASM}) (Figure 7a, lane 3 and 5). Providing the $CRL4^{CSA}$ substrate CSB relieved CSN inhibition, and led to ubiquitination of CSB and CSA (Figure 7a, lanes 4, 6 and 7 and Figure 7b). In a fully recombinant in vitro system, damage DNA binding to $CRL4^{DDB2}$, as well as CSB binding to $CRL4^{CSA}$, displaces CSN resulting in activation of the CRL4 ligase complex.

The overall functional and regulatory constraints following from the $CRL4^{DDB2}$ (and $CRL4^{CSA}$) architectures thus likely extend to other members of the $CRL4^{DCAF}$ family.

Discussion

The molecular basis of targeting, recruitment and activation of the $CRL4^{DDB2}$ ligase in chromatin

On the basis of our findings, we propose the following working model for $CRL4^{DDB2}$ recruitment and activation in response to UV damage (Figure 7c): In the absence of DNA damage, nuclear $CRL4^{DDB2}$ is complexed to CSN in a non-chromatin-bound form (Groisman et al., 2003). Following UV damage, $CRL4^{DDB2}$-CSN is recruited to DNA by its ability to interrogate nucleosomes for the presence of 6-4PP and CPD lesions (Figure 2). $CRL4^{DDB2}$ is structurally optimized for recognition of CPDs, which due to their small intrinsic helix destabilization frequently escapes detection by other damage surveillance factors (Figure 1). XPC-RAD23, alone, has no significant affinity

for CPD and is unable to detect 6-4PP lesions in chromatin (Yasuda et al., 2005). Yet XPC is essential for efficient NER repair. The ability of $CRL4^{DDB2}$ to recognize 6-4PPs, and particularly CPDs, embedded in nucleosomes provides a pathway to recruit XPC to lesions in chromatin and activate the ligase thus facilitating NER (Sugasawa, 2006). We find that DNA damage binding to DDB2 directly displaces CSN from $CRL4^{DDB2}$ resulting in ligase activation (Figure 5). Active CRL4DDB2 targets histones, XPC and possibly additional proteins located within ~100 Å around the lesion for ubiquitination. The release of CSN additionally allows $CRL4^{DDB2}$ to autoubiquitinate its DDB2 subunit on the N-terminus (Figure 4). This results in degradation of DDB2 and may function as a timing device delimiting $CRL4^{DDB2}$ activity following UV. A $CRL4^{DDB2}$ variant defective in DNA binding, as seen in patient XP82TO, retains CSN binding and in vivo does not undergo autoubiquitination and degradation following UV (Rapid-Otrin et al., 2002; Wittschieben et al., 2005; Matsunda et al., 2005; Takedachi et al., 2010) (Figure 5f).

The architecture of the $CRL4^{DCAF}$ family

The $CRL4^{DDB2}$ ligase is perceived to be a special case, as it recognizes a non-protein substrate. The ligand, in this case DNA, is atypically not the target for ubiquitination, but rather proteins in its proximity are the entities ubiquitinated. In order to examine how other $CRL4^{DCAF}$ complexes, structurally and functionally, relate to $CRL4^{DDB2}$, we determined the structure of the DDB1-CSA complex. The DDB1-CSA complex, which was shown to bind a protein epitope rather than damaged DNA (Groisman et al., 2006) revealed a surprising overall architectural similarity to the DDB1-DDB2 complex. We find that CSN mediated inhibition of $CRL4^{CSA}$ is released through addition of CSB, similar to what has been observed for $CRL4^{DDB2}$. In vivo, the disappearance of CSN from the $CRL4^{CSA}$ complex (ca. 4h post UV) coincides with ubiquitination and disappearance of CSB (Groisman et al., 2006). Structure-based sequence analysis identified a common HLH motif within the WD40-DCAF family expected to link other WD40 containing DCAFs to DDB1 in a manner similar to that of CSA and DDB2. At present, we can not exclude that alternative DCAF binding modes exist, or that access of the DCAF HLH-box to DDB1 is subject to regulation. Our results demonstrate that

$CRL4^{DDB2}$, $CRL4^{CSA}$ and with it the majority of $CRL4^{DCAF/WD40}$ complexes are predicted, to share a common architectural scaffold. These CRL4 ligases are expected to exhibit mobility, and hence, absence of direct crosstalk between the DCAF substrate receptor and the ubiquitin ligase, requiring CSN to mediate activation.

Substrate dependent crosstalk between CRL4 complexes and the COP9 signalosome

CSN is a key regulator of cullin-RING ligase activity. The involvement of CSN in ligase regulation poses the following question: how is a specific ligase regulated by CSN, without affecting the remainder of cullin-RING ligases. We find that the association and inhibition of $CRL4^{DDB2}$ by CSN is relieved upon DNA damage binding to the WD40 propeller of DDB2 (Figure 5). A similar behavior is seen for $CRL4^{CSA}$ where CSB binding displaces CSN (Figure 7a and b). Indeed, we observe in $CRL4^{DDB2}$-CSN negative stained EM single particle reconstructions that the DDB2 subunit is held in close proximity to CSN (data not shown). Other structurally related $CRL4^{DCAF}$ complexes are thus expected to bind CSN in a similar fashion. This strongly suggests that CSN release and subsequent activation of $CRL4^{DCAF}$ complexes are simply triggered by substrate binding to the DCAF within the $CRL4^{DCAF}$-CSN complex.

Protection of substrate receptors by CSN has previously been described for the CRL1 and CRL3 families in vivo (Bornstein et al., 2006; Schmidt et al., 2009; Zhou et al., 2003) and likely extends to the CRL4 family (Bennett et al., 2010). The protective effect of CSN on DDB2 autoubiquitination observed in this study is independent of deubiquitinating enzymes, and does not require CSN5 mediated deneddylation (see Figure S5 for CSN subunits required for inhibition). Similar properties have been observed for the CSN-$CRL4^{CSA}$ interplay, although the cellular role of CSA autoubiquitination is unclear at present. In vivo. (i) the intrinsic CSN deneddylase activity, (ii) CSN-associated deubiquitinases and (iii) the non-enzymatic CSN inhibition observed are all expected to act in concert inhibiting CRL4 in the absence of an activating cue. Further work is needed to define the relative contribution of these three strategies (i-iii) to CSN mediated inhibition in vivo. However, all three levels of

inhibition are simultaneously relieved once DDB2 (CSA) contacts DNA damage (CSB), as the direct contact between receptor and substrate results in CSN dissociation and loss of receptor protection. In light of the conserved architecture of the majority of $CRL4^{DCAF(WD40)}$ complexes this provides a general mechanism for regulating the CRL4 CSN interplay.

Acknowledgement

This work was supported by the Novartis Research Foundation and grants to N.H.T from the European Research Council (ERC-2010-StG 260481-MoBa-CS), OnocSuisse (OCS-02365-02-2009) and the Swiss National Foundation (31003A_120205). An SNF Ambizione Grant (A.S.), an EMBO STF (E.S.F.), and Presidential Postdoc Fellowship (G.M.L.). K.S. was supported by Grants-in-Aid from the Ministry of Education, Culture, Sports, Science and Technology of Japan and by the Takeda Science Foundation. We thank Susan Gasser, Dirk Schübeler, Lukas Leder, Martin Renatus and Philip Jeffrey for help and discussion. We are grateful to Daniel Hess and Dominique Klein (FMI protein analysis facility) for carrying out the mass-spectrometric analysis. Part of this work was performed at the Swiss Light Source at the Paul Scherrer Institut, Villigen, Switzerland.

Experimental Procedures

Protein expression and purification: All proteins used for structure determination were cloned into pFastBac Dual vectors (Invitrogen) and expressed and purified from High Five cells (Invitrogen) as outlined in Scrima et al., 2008 (see also Supplemental experimental procedures). Purified recombinant CSB protein was provided as a kind gift from Regina Groisman. Enzymes for neddylation such as NAE1/UBA3 and UbcH12, as well as NEDD8, were purified as N-terminal His6 fusion proteins from Escherichia coli (Duda et al., 2008). hsUBA1, hsUbcH5A, hsUbcH5B, hsUbiquitin and hsUbiquitin-K0 were purchased from Boston Biochem.

Oligonucleotides used in this study: Single stranded DNA oligonucleotides and oligonucleotides containing tetrahydrofuran (THF) lesion were purchased from Sigma Aldrich. Oligonucleotides containing the cis-syn CPD were synthesized using phosphor-amidite building blocks (Glenn Research, USA). Sequences of oligonucleotides used are provided in the Tables S4 and S5.

Crystallization & Structure solution: Crystallization conditions as well as data collection and refinement statistics are given in Table S1.

Cellular assays: HA-tagged DDB2 (wild type or mutant) was stably overexpressed in a normal human fibroblast cell line, WI38 VA13, by using the pIREShyg vector. The transformed cells were exposed to UVC (10 J/m2) and incubated for various times. Whole cell extracts were prepared and analyzed by immunoblotting.

In vitro ubiquitination assays: Assays for autoubiquitination were carried out as described in Sugasawa, 2006. Antibodies used include α-hsDDB2 (AF3297, R&D Biosystems), α-XPC (Sugasawa et al., 2005), α-CSA (GTX100145, GeneTex), α-CSB (SC10458, Santa Cruz) and horseradish peroxidase (HRP)-conjugated secondary antibodies against Goat IgG (R&D Biosystems) and rabbit IgG (GeneTex).

Accession Numbers

CPD#1(pdb:4A08), CPD#2(pdb:4A09), CPD#3(pdb:4A0A), CPD#4(pdb: 4A0B), CAND1-CUL4B(pdb:4A0C), CRL4ADDB2-DNA(pdb:4A0K), CRL4BDDB2-DNA(pdb:4A0L), DDB1-CSA(pdb:4A11)

References

Aboussekhra, A., Biggerstaff, M., Shivji, M.K., Vilpo, J.A., Moncollin, V., Podust, V.N., Protić, M., Hübscher, U., Egly, J.M., and Wood, R.D. (1995).

Mammalian DNA nucleotide excision repair reconstituted with purified protein components. Cell 80, 859-868.

Angers, S., Li, T., Yi, X., MacCoss, M.J., Moon, R.T., and Zheng, N. (2006). Molecular architecture and assembly of the DDB1-CUL4A ubiquitin ligase machinery. Nature 443, 590-593.

Batty, D., Rapic Otrin, V., Levine, A., and Wood, R. (2000). Stable binding of human XPC complex to irradiated DNA confers strong discrimination for damaged sites. J Mol Biol 300, 275-290.

Bennett, E.J., Rush, J., Gygi, S.P., and Harper, J.W. (2010). Dynamics of cullin-RING ubiquitin ligase network revealed by systematic quantitative proteomics. Cell 143, 951-965.

Bornstein, G., Ganoth, D., and Hershko, A. (2006). Regulation of neddylation and deneddylation of cullin1 in SCFSkp2 ubiquitin ligase by F-box protein and substrate. Proc Natl Acad Sci U S A 103, 11515-11520.

Brunger, A., Adams, P., Clore, G., DeLano, W., Gros, P., Grosse-Kunstleve, R., Jiang, J., Kuszewski, J., Nilges, M., Pannu, N., et al. (1998). Crystallography & NMR system: A new software suite for macromolecular structure determination. Acta Crystallogr D Biol Crystallogr 54, 905-921.

Creighton, T.E. (1992). Proteins: Structures and Molecular Properties, second edition edn (W. H. Freeman and Company).

Duan, M.-R., and Smerdon, M.J. (2010). UV damage in DNA promotes nucleosome unwrapping. J Biol Chem 285, 26295-26303.

Duda, D., Borg, L., Scott, D., Hunt, H., Hammel, M., and Schulman, B. (2008). Structural insights into NEDD8 activation of cullin-RING ligases: conformational control of conjugation. Cell 134, 995-1006.

Enchev, R.I., Schreiber, A., Beuron, F., and Morris, E.P. (2010). Structural insights into the COP9 signalosome and its common architecture with the 26S proteasome lid and eIF3. Structure 18, 518-527.

Fousteri, M., and Mullenders, L.H.F. (2008). Transcription-coupled nucleotide excision repair in mammalian cells: molecular mechanisms and biological effects. Cell research 18, 73-84.

Fousteri, M., Vermeulen, W., van Zeeland, A.A., and Mullenders, L.H. (2006). Cockayne syndrome A and B proteins differentially regulate recruitment of

chromatin remodeling and repair factors to stalled RNA polymerase II in vivo. Mol Cell 23, 471-482.

Friedberg, E.C. (2001). How nucleotide excision repair protects against cancer. Nat Rev Cancer 1, 22-33.

Fukumoto, Y., Dohmae, N., and Hanaoka, F. (2008). Schizosaccharomyces pombe Ddb1 recruits substrate-specific adaptor proteins through a novel protein motif, the DDB-box. Mol Cell Biol 28, 6746-6756.

Furukawa, M., Zhang, Y., McCarville, J., Ohta, T., and Xiong, Y. (2000). The CUL1 C-terminal sequence and ROC1 are required for efficient nuclear accumulation, NEDD8 modification, and ubiquitin ligase activity of CUL1. Mol Cell Biol 20, 8185-8197.

Gale, J.M., and Smerdon, M.J. (1988). Photofootprint of nucleosome core DNA in intact chromatin having different structural states. J Mol Biol 204, 949-958.

Groisman, R., Kuraoka, I., Chevallier, O., Gaye, N., Magnaldo, T., Tanaka, K., Kisselev, A.F., Harel-Bellan, A., and Nakatani, Y. (2006). CSA-dependent degradation of CSB by the ubiquitin-proteasome pathway establishes a link between complementation factors of the Cockayne syndrome. Genes Dev 20, 1429-1434.

Groisman, R., Polanowska, J., Kuraoka, I., Sawada, J., Saijo, M., Drapkin, R., Kisselev, A., Tanaka, K., and Nakatani, Y. (2003). The ubiquitin ligase activity in the DDB2 and CSA complexes is differentially regulated by the COP9 signalosome in response to DNA damage. Cell 113, 357-367.

Guerrero-Santoro, J., Kapetanaki, M., Hsieh, C., Gorbachinsky, I., Levine, A., and Rapic-Otrin, V. (2008). The cullin 4B-based UV-damaged DNA-binding protein ligase binds to UV-damaged chromatin and ubiquitinates histone H2A. Cancer Res 68, 5014-5022.

Hannss, R., and Dubiel, W. (2011). COP9 signalosome function in the DDR. FEBS Lett.

He, Y., McCall, C., Hu, J., Zeng, Y., and Xiong, Y. (2006). DDB1 functions as a linker to recruit receptor WD40 proteins to CUL4-ROC1 ubiquitin ligases. Genes Dev 20, 2949-2954.

Higa, L., Wu, M., Ye, T., Kobayashi, R., Sun, H., and Zhang, H. (2006). CUL4-DDB1 ubiquitin ligase interacts with multiple WD40-repeat proteins and regulates histone methylation. Nat Cell Biol 8, 1277-1283.

Hoeijmakers, J.H.J. (2009). DNA damage, aging, and cancer. N Engl J Med 361, 1475-1485.

Hwang, B.J., Toering, S., Francke, U., and Chu, G. (1998). p48 Activates a UV-damaged-DNA binding factor and is defective in xeroderma pigmentosum group E cells that lack binding activity. Mol Cell Biol 18, 4391-4399.

Jackson, S., and Xiong, Y. (2009). CRL4s: the CUL4-RING E3 ubiquitin ligases. Trends Biochem Sci 34, 562-570.

Jin, J., Arias, E., Chen, J., Harper, J., and Walter, J. (2006). A family of diverse Cul4-Ddb1-interacting proteins includes Cdt2, which is required for S phase destruction of the replication factor Cdt1. Mol Cell 23, 709-721.

Jing, Y., Kao, J.F., and Taylor, J.S. (1998). Thermodynamic and base-pairing studies of matched and mismatched DNA dodecamer duplexes containing cis-syn, (6-4) and Dewar photoproducts of TT. Nucleic Acids Res 26, 3845-3853.

Kapetanaki, M.G., Guerrero-Santoro, J., Bisi, D.C., Hsieh, C.L., Rapić-Otrin, V., and Levine, A.S. (2006). The DDB1-CUL4ADDB2 ubiquitin ligase is deficient in xeroderma pigmentosum group E and targets histone H2A at UV-damaged DNA sites. Proc Natl Acad Sci U S A 103, 2588-2593.

Krissinel, E., and Henrick, K. (2007). Inference of macromolecular assemblies from crystalline state. J Mol Biol 372, 774-797.

Lee, J., and Zhou, P. (2007). DCAFs, the missing link of the CUL4-DDB1 ubiquitin ligase. Mol Cell 26, 775-780.

Li, T., Chen, X., Garbutt, K.C., Zhou, P., and Zheng, N. (2006). Structure of DDB1 in complex with a paramyxovirus V protein: viral hijack of a propeller cluster in ubiquitin ligase. Cell 124, 105-117.

Li, T., Robert, E.I., van Breugel, P.C., Strubin, M., and Zheng, N. (2010). A promiscuous alpha-helical motif anchors viral hijackers and substrate receptors to the CUL4-DDB1 ubiquitin ligase machinery. Nat Struct Mol Biol 17, 105-111.

Luijsterburg, M.S., Goedhart, J., Moser, J., Kool, H., Geverts, B., Houtsmuller, A.B., Mullenders, L.H.F., Vermeulen, W., and van Driel, R. (2007). Dynamic in

vivo interaction of DDB2 E3 ubiquitin ligase with UV-damaged DNA is independent of damage-recognition protein XPC. Journal of Cell Science 120, 2706-2716.

Mitchell, D.L., Adair, G.M., and Nairn, R.S. (1989). Inhibition of transient gene expression in Chinese hamster ovary cells by triplet-sensitized UV-B irradiation of transfected DNA. Photochem Photobiol 50, 639-646.

Moser, J., Volker, M., Kool, H., Alekseev, S., Vrieling, H., Yasui, A., van Zeeland, A., and Mullenders, L. (2005). The UV-damaged DNA binding protein mediates efficient targeting of the nucleotide excision repair complex to UV-induced photo lesions. DNA Repair (Amst) 4, 571-582.

Nishi, R., Alekseev, S., Dinant, C., Hoogstraten, D., Houtsmuller, A.B., Hoeijmakers, J.H., Vermeulen, W., Hanaoka, F., and Sugasawa, K. (2009). UV-DDB-dependent regulation of nucleotide excision repair kinetics in living cells. DNA Repair (Amst) 8, 767-776.

Payne, A., and Chu, G. (1994). Xeroderma pigmentosum group E binding factor recognizes a broad spectrum of DNA damage. Mutat Res 310, 89-102.

Rapić-Otrin, V., McLenigan, M.P., Bisi, D.C., Gonzalez, M., and Levine, A.S. (2002). Sequential binding of UV DNA damage binding factor and degradation of the p48 subunit as early events after UV irradiation. Nucleic Acids Res 30, 2588-2598.

Schmidt, M.W., McQuary, P.R., Wee, S., Hofmann, K., and Wolf, D.A. (2009). F-box-directed CRL complex assembly and regulation by the CSN and CAND1. Mol Cell 35, 586-597.

Scrima, A., Fischer, E.S., Lingaraju, G.M., Böhm, K., Cavadini, S., and Thomä, N.H. (2011). Detecting UV-lesions in the genome: The modular CRL4 ubiquitin ligase does it best! FEBS letters.

Scrima, A., Konícková, R., Czyzewski, B.K., Kawasaki, Y., Jeffrey, P.D., Groisman, R., Nakatani, Y., Iwai, S., Pavletich, N.P., and Thomä, N.H. (2008). Structural basis of UV DNA-damage recognition by the DDB1-DDB2 complex. Cell 135, 1213-1223.

Sugasawa, K. (2006). UV-induced ubiquitylation of XPC complex, the UV-DDB-ubiquitin ligase complex, and DNA repair. J Mol Histol 37, 189-202.

Sugasawa, K. (2010). Regulation of damage recognition in mammalian global genomic nucleotide excision repair. Mutat Res 685, 29-37.

Sugasawa, K., Okamoto, T., Shimizu, Y., Masutani, C., Iwai, S., and Hanaoka, F. (2001). A multistep damage recognition mechanism for global genomic nucleotide excision repair. Genes Dev 15, 507-521.

Sugasawa, K., Okuda, Y., Saijo, M., Nishi, R., Matsuda, N., Chu, G., Mori, T., Iwai, S., Tanaka, K., Tanaka, K., et al. (2005). UV-Induced Ubiquitylation of XPC Protein Mediated by UV-DDB-Ubiquitin Ligase Complex. Cell 121, 387-400.

Takedachi, A., Saijo, M., and Tanaka, K. (2010). DDB2 complex-mediated ubiquitylation around DNA damage is oppositely regulated by XPC and Ku and contributes to the recruitment of XPA. Mol Cell Biol 30, 2708-2723.

Tang, J., and Chu, G. (2002). Xeroderma pigmentosum complementation group E and UV-damaged DNA-binding protein. DNA repair 1, 601-616.

Tang, J.Y., Hwang, B.J., Ford, J.M., Hanawalt, P.C., and Chu, G. (2000). Xeroderma pigmentosum p48 gene enhances global genomic repair and suppresses UV-induced mutagenesis. Mol Cell 5, 737-744.

Tornaletti, S. (2009). DNA repair in mammalian cells: Transcription-coupled DNA repair: directing your effort where it's most needed. Cell Mol Life Sci 66, 1010-1020.

Troelstra, C., van Gool, A., de Wit, J., Vermeulen, W., Bootsma, D., and Hoeijmakers, J.H. (1992). ERCC6, a member of a subfamily of putative helicases, is involved in Cockayne's syndrome and preferential repair of active genes. Cell 71, 939-953.

Volker, M., Mone, M., Karmakar, P., van Hoffen, A., Schul, W., Vermeulen, W., Hoeijmakers, J., van Driel, R., van Zeeland, A., and Mullenders, L. (2001). Sequential assembly of the nucleotide excision repair factors in vivo. Mol Cell 8, 213-224.

Wang, H., Zhai, L., Xu, J., Joo, H., Jackson, S., Erdjument-Bromage, H., Tempst, P., Xiong, Y., and Zhang, Y. (2006). Histone H3 and H4 ubiquitylation by the CUL4-DDB-ROC1 ubiquitin ligase facilitates cellular response to DNA damage. Mol Cell 22, 383-394.

Wittschieben, B., Iwai, S., and Wood, R. (2005). DDB1-DDB2 (xeroderma pigmentosum group E) protein complex recognizes a cyclobutane pyrimidine dimer, mismatches, apurinic/apyrimidinic sites, and compound lesions in DNA. J Biol Chem 280, 39982-39989.

Yasuda, T., Sugasawa, K., Shimizu, Y., Iwai, S., Shiomi, T., and Hanaoka, F. (2005). Nucleosomal structure of undamaged DNA regions suppresses the non-specific DNA binding of the XPC complex. DNA repair 4, 389-395.
Zhou, C., Wee, S., Rhee, E., Naumann, M., Dubiel, W., and Wolf, D.A. (2003). Fission yeast COP9/signalosome suppresses cullin activity through recruitment of the deubiquitylating enzyme Ubp12p. Mol Cell 11, 927-938.

Figure Legends:

Figure 1: DDB1-DDB2 in complex with CPD-containing duplexes

(A) Cartoon representation of DDB1-DDB2-CPD. DDB2, green; DDB1 (BPA), red; (BPB), magenta; (BPC), yellow; DDB1-CTD, gray and the DNA in black and gray for the damaged and undamaged strand respectively, with CPD shown in red. The DDB2 residues involved in DNA binding are shown as close-up. (B) Schematic representation of DNA-protein interactions. (C and D) Close-up view of the CPD/6-4PP fit to the hydrophobic binding pocket. (D) Close-up of the bound CPD lesion, demonstrating that the DDB2 binding pocket preferentially accommodates the CPD. See also Figure S1, Tables S2 and S3.

Figure 2: DDB2 is able to recognize 6-4PP and CPDs embedded in nucleosomes

(A) EMSA of the DDB1-DDB2 complex binding to UV-damaged nucleosome core particles (NCP), indicated amounts of DDB1-DDB2 were incubated with UV-damaged or undamaged mononucleosomes. (B) EMSA analysis of DDB1-DDB2 binding to nucleosomes containing a specific 6-4PP lesion, indicated amounts of DDB1-DDB2 were incubated with 0.2 fmol of naked DNA (lanes 1-6), mononucleosomes (lanes 7-12) or both (lanes 13-16). The non-damaged DNA control is shown as indicated. (C) As in (B) using CPD containing nucleosomes. (D) and (E) Quantitative analysis of DDB1-DDB2 binding to free lesion containing DNA or lesion embedded in the nucleosomes 6-4PP (B) or CPD (C). (F) EMSA analysis of DDB1-DDB2 and $CRL4A^{DDB2}$ complex binding to UV-damaged mononucleosomes.

Figure 3: The structure of the CRL4A^{DDB2} complex bound to THF containing duplex

Cartoon representation of the CRL4A^{DDB2} complex structure: DDB2, green; DDB1 (BPA), red; (BPB), magenta; (BPC), orange, DDB1-CTD, gray; CUL4A, cullin repeat domains (CRD1-3) and C-terminal domain (CTD) depicted in gray to black; RBX1 in cyan. The DNA is shown in black and orange for the undamaged and damaged strand respectively. DDB1 and DDB2 are shown as surface in the bottom panel. See also Figure S2.

Figure 4: The structures of CRL4B^{DDB2} bound to DNA damage: rotational mobility of the ligase

(A, B) Overlay of the three experimental CUL4 orientations indicating the rotational mobility of CUL4 (in gray) respective to DDB2 (depicted as surface in green) and the bound DNA substrate (depicted in orange and black). (C) Overlay of medium to high resolution CUL4A and CUL4B structures and schematic representation of domain boundaries. (D) Model of CRL4DDB2 with the CUL4 arm depicted in the most distal DDB1-BPB orientations and the resultant ubiquitination hot zone indicated in light orange and gray. (E) Table of available medium to high resolution DDB1 structures with the corresponding orientation of CUL4 and predicted ePISA solvation energies of DDB1 (BPB) to DDB1 (BPA/BPC) interactions. See also Figure S3.

Figure 5: CSN dependent regulation of CRL4^{DDB2} mediated ubiquitination of the DDB2 N-terminus regulates degradation following UV exposure

(A) In vitro ubiquitination assays using K-less ubiquitin and the CRL4A^{DDB2} complex containing either full-length DDB2 (DDB2-FL) or DDB2-ΔN. The reaction mixture was subjected to immunoblot analysis with indicated antibodies. (B) HA-tagged DDB2-FL or DDB2-7KR was stably overexpressed in a normal human fibroblast cell line. Extracts from these cells as well as the parental cell line (indicated by -) were subjected to immunoprecipitation with anti-HA antibody and immunoblot analysis with indicated antibodies. One percent each of the input extracts (I) and unbound fractions (U) were analyzed in parallel. (C) The cell line stably expressing HA-DDB2-FL or HA-DDB2-7KR

was exposed to UV irradiation 2 h after treatment with 1 mM cycloheximide (CHX) in the presence or absence of 5 μM MG132. Cells were further incubated for various times in the presence of CHX (± MG132) and whole cell extracts were subjected to immunoblotting using indicated antibodies. (D) In vitro ubiquitination assays were performed with wild type $CRL4A^{DDB2}$ complex and analyzed by DDB2 immunoblot. Wild type CSN complex (lane 4) or a complex containing a CSN5 active site mutant (lane 5) significantly inhibited the autoubiquitination of DDB2. This inhibition was relieved by the addition of UV-irradiated DNA to the reaction (lanes 5 and 7). (E) Small oligonucleotides containing an THF abasic site mimic (lane 3), CPD lesion (lane 4) or 6-4PP lesion (lane 5) were sufficient to relieve the inhibition, whereas an undamaged oligonucleotide of similar length did not affect the inhibition (lane 6). Ubiquitin-aldehyde had no effect on the reaction (lane 1 and 2). (F) In vitro ubiquitination assays were performed with $CRL4A^{DDB2}$ complex harboring the K244E DDB2 patient mutation. In contrast to wt DDB2, the inhibition by CSN_{ASM} was not relieved upon damaged DNA addition (lane 4). See also Figure S4, S5 and Table S5.

Figure 6:The structure of DDB1-CSA suggests a shared architecture of $CRL4^{DCAF}$ complexes

(A) Overall structure of the DDB1-CSA complex. CSA: blue, DDB1 (BPA): red, (BPB): magenta, (BPC): yellow, DDB1-CTD: gray. Schematic overview of the CSA organization. (B) CSA mutations linked to different phenotypes of Cockayne syndrome (white: CSI, red: CSIII/UVSS). (C) HMM based sequence logo and corresponding secondary structure of the helix-loop-helix box (see Figure S6a for full alignment). (D) Superposition using DDB1-BPA/BPC results in a similar orientation of CSA (blue) and DDB2 (green) showing the common architecture of the complexes. Close-up view of the helix-loop-helix motif in hsCSA (E), drDDB2 (F) and hsDDB2 (G), respectively. Residues belonging to the conserved motif are indicated. See also Figure S6, S7 and Table S6.

Figure 7: Model for $CRL4^{DDB2}$ ligase activation and release of CSN upon damage binding

(A) In vitro ubiquitination assays were performed with $CRL4A^{CSA}$ complex and analyzed by CSA immunoblot. Wild type COP9 signalosome (CSN) complex (lane 3) or a complex containing a CSN5 active site mutant (lane 5) significantly inhibited DDB2 autoubiquitination. This inhibition was relieved by the addition of CSB to the reaction (lanes 4, 6 and 7). Unspecific cross-reactivity of the anti-CSA antibody is indicated with a red asterisk. CSB immunoblotting demonstrated that the CSB substrate is also ubiquitinated in this reaction (B). (C) In complex with CSN, $CRL4^{DDB2}$ is held in a ubiquitin ligase inactive state. UV irradiation induces lesion formation in chromatin and recruitment of the $CRL4^{DDB2}$-CSN complex to the site of damage. It is currently not clear if DDB2 binds on the nucleosome, or to a looped off intermediate (Duan and Smerdon, 2010). Binding to chromatin/nucleosome results in steric displacement of CSN (involving CSN subunits 1,2,3,4 & 6) and ligase activation. This in turn allows for ubiquitination of diverse substrates within the zone of ubiquitination including histones, XPC and DDB2.

Figure 1

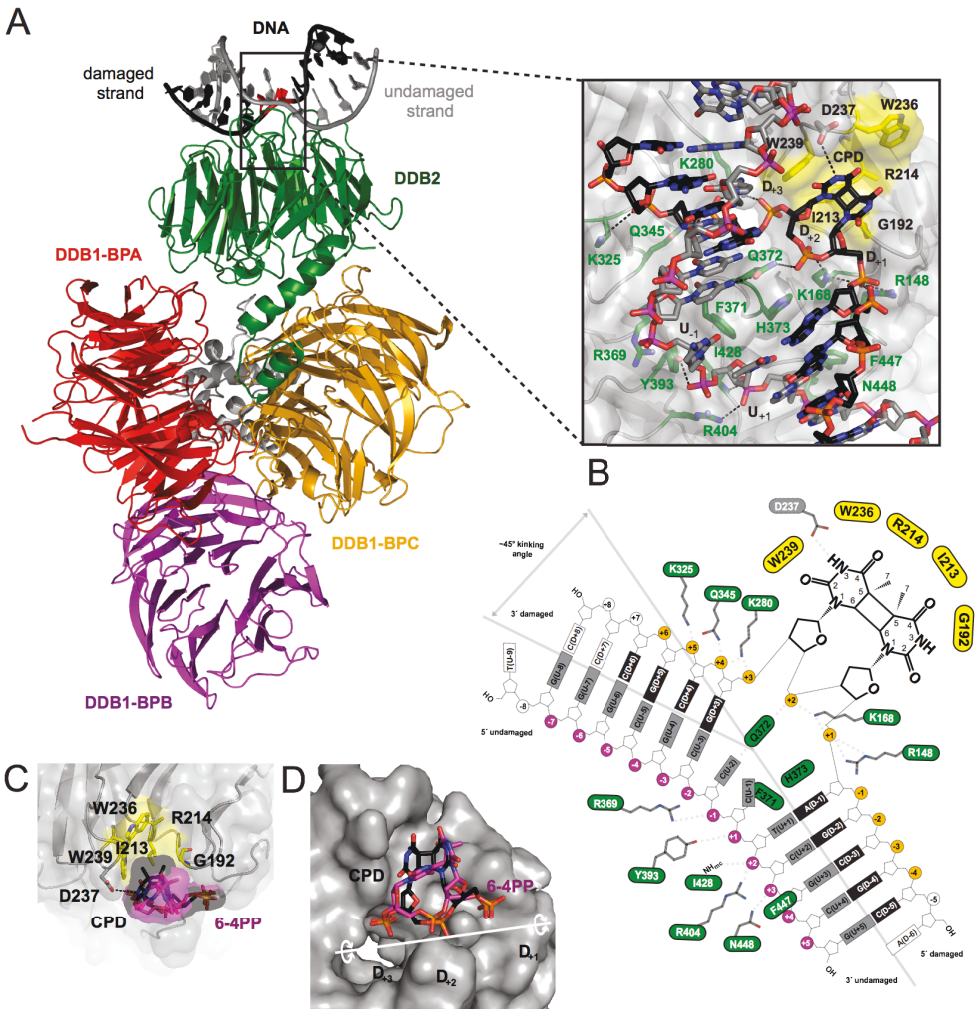
A
DNA
damaged strand
undamaged strand
DDB2
DDB1-BPA
DDB1-BPC
DDB1-BPB
D237
W236
W239
CPD
K280
R214
I213
G192
Q345
K325
Q372
R148
K168
F371
H373
R369
I428
F447
Y393
N448
R404
B
C
W236
R214
W239
I213
G192
D237
CPD
6-4PP
D
CPD
6-4PP

Figure 2

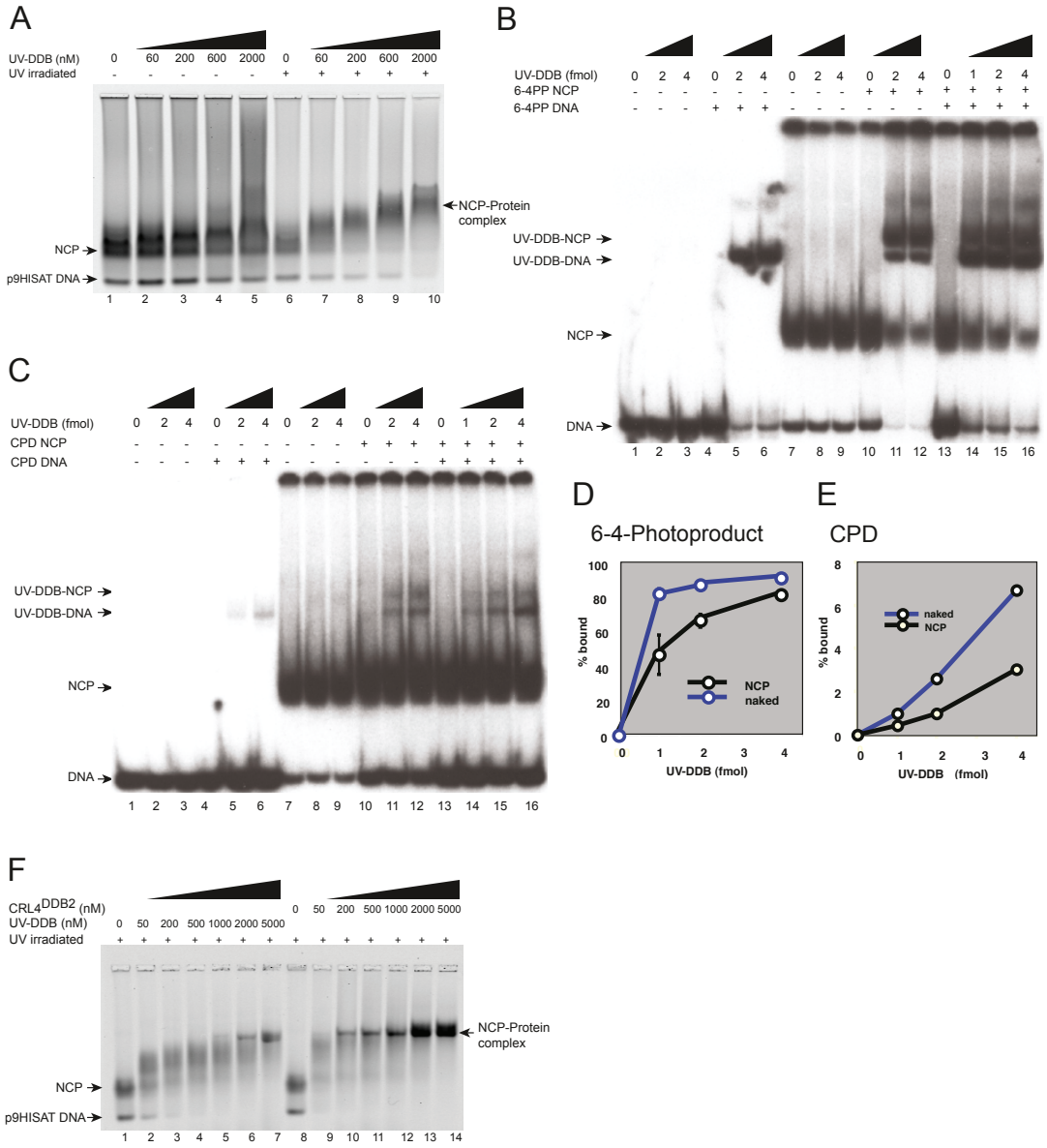
A
UV-DDB (nM) 0 60 200 600 2000 0 60 200 600 2000
UV irradiated - - - - - + + + + +
NCP-Protein complex
NCP
p9HISAT DNA
1 2 3 4 5 6 7 8 9 10
B
UV-DDB (fmol) 0 2 4 0 2 4 0 2 4 0 2 4 0 1 2 4
6-4PP NCP - - - - - - - - - + + + + + + +
6-4PP DNA - - - + + + - - - - - - + + + +
UV-DDB-NCP
UV-DDB-DNA
NCP
DNA
1 2 3 4 5 6 7 8 9 10 11 12 13 14 15 16
C
UV-DDB (fmol) 0 2 4 0 2 4 0 2 4 0 2 4 0 1 2 4
CPD NCP - - - - - - - - - + + + + + + +
CPD DNA - - - + + + - - - - - - + + + +
UV-DDB-NCP
UV-DDB-DNA
NCP
DNA
1 2 3 4 5 6 7 8 9 10 11 12 13 14 15 16
D
6-4-Photoproduct
% bound
NCP
naked
UV-DDB (fmol)
E
CPD
% bound
naked
NCP
UV-DDB (fmol)
F
CRL4DDB2 (nM) 0 50 200 500 1000 2000 5000
UV-DDB (nM) 0 50 200 500 1000 2000 5000
UV irradiated + + + + + + + + + + + + + +
NCP-Protein complex
NCP
p9HISAT DNA
1 2 3 4 5 6 7 8 9 10 11 12 13 14

Figure 3

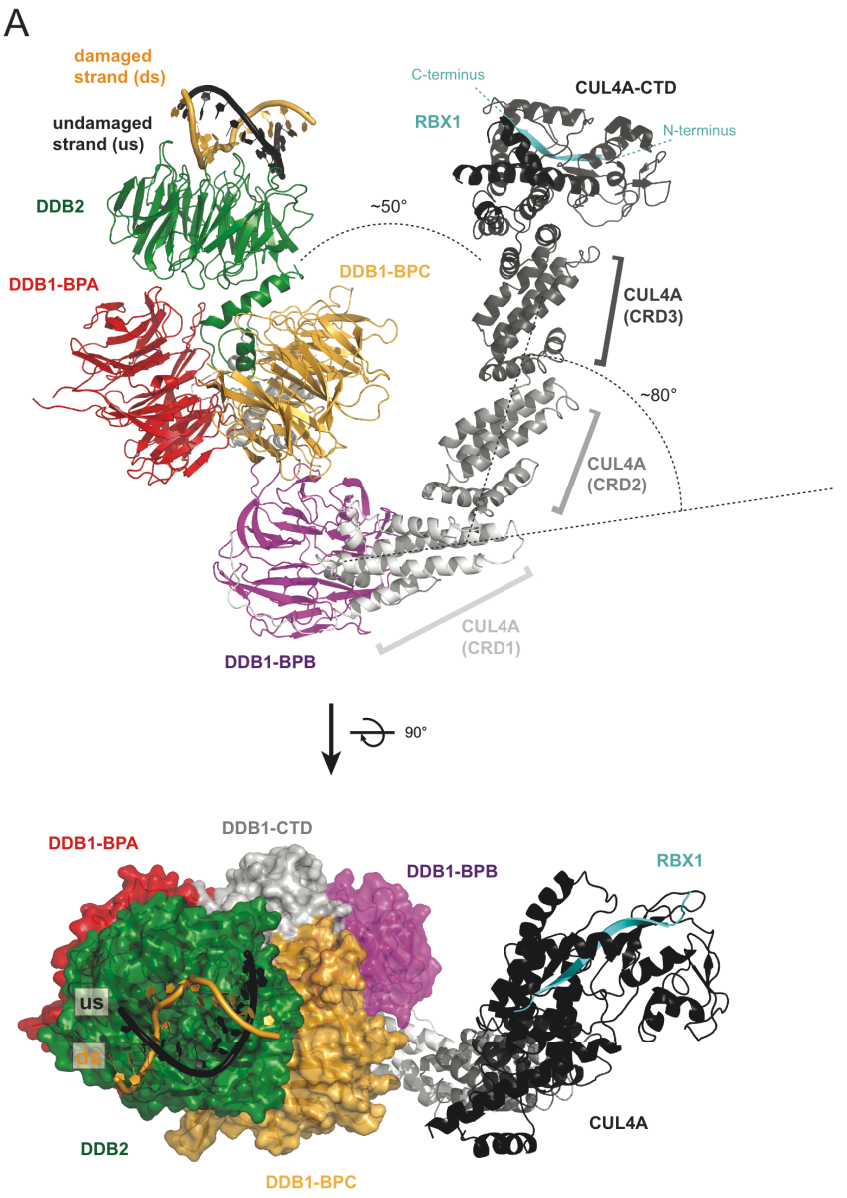
A
damaged strand (ds)
undamaged strand (us)
DDB2
DDB1-BPA
DDB1-BPC
DDB1-BPB
C-terminus
CUL4A-CTD
RBX1
N-terminus
~50°
CUL4A (CRD3)
~80°
CUL4A (CRD2)
CUL4A (CRD1)
90°
DDB1-CTD
DDB1-BPA
DDB1-BPB
RBX1
us
ds
CUL4A
DDB2
DDB1-BPC

Figure 4

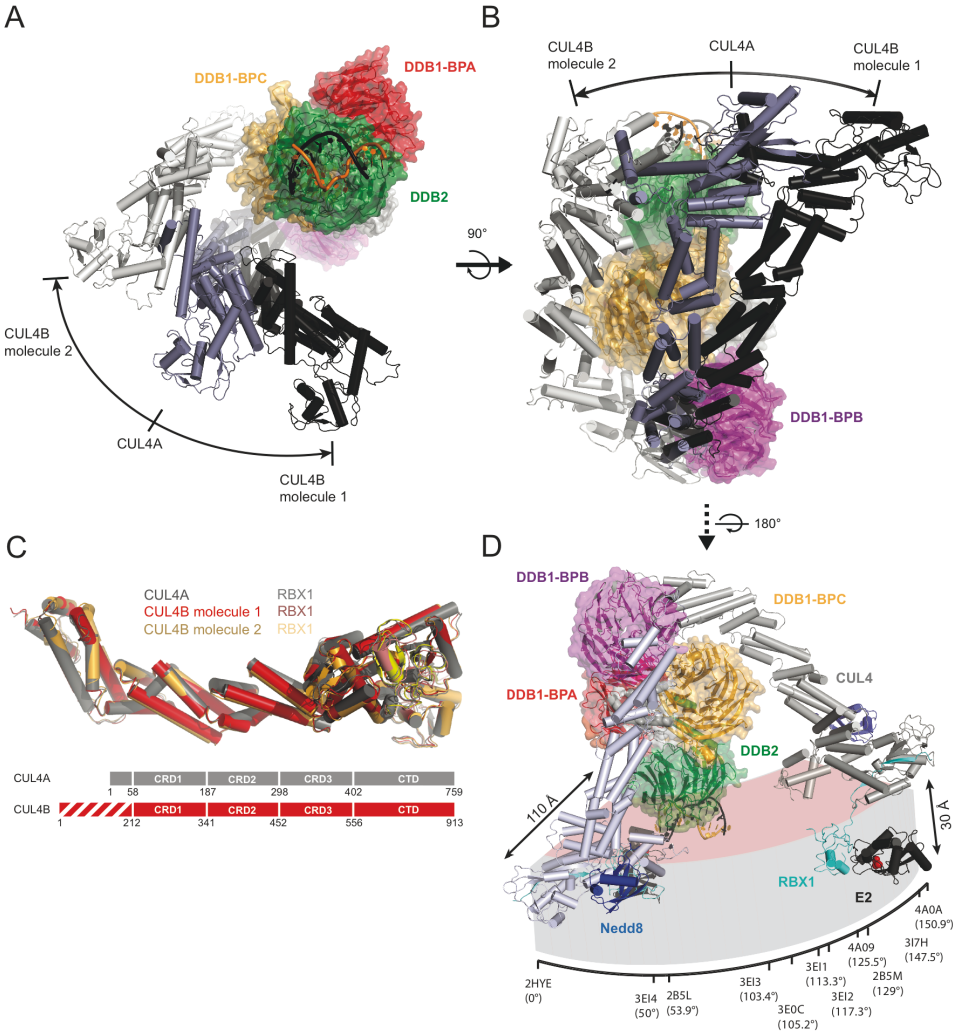

E

PDB	angle	ΔG (kcal/mol)
2HYE	0.0°	-1.3
3EI4 (mol1, 2, 3)	50.0°	-3.2
2B5L	53.9°	-2.3
3EI3	103.4°	0.0
3EOC	105.2°	-3.1
3EI1	113.3°	3.7
3EI2	117.3°	3.7
4A09	125.5°	1.5
2B5M	129.0°	4.7
3I7H	147.5°	0.9
4A0A	150.9°	3.2

Figure 5

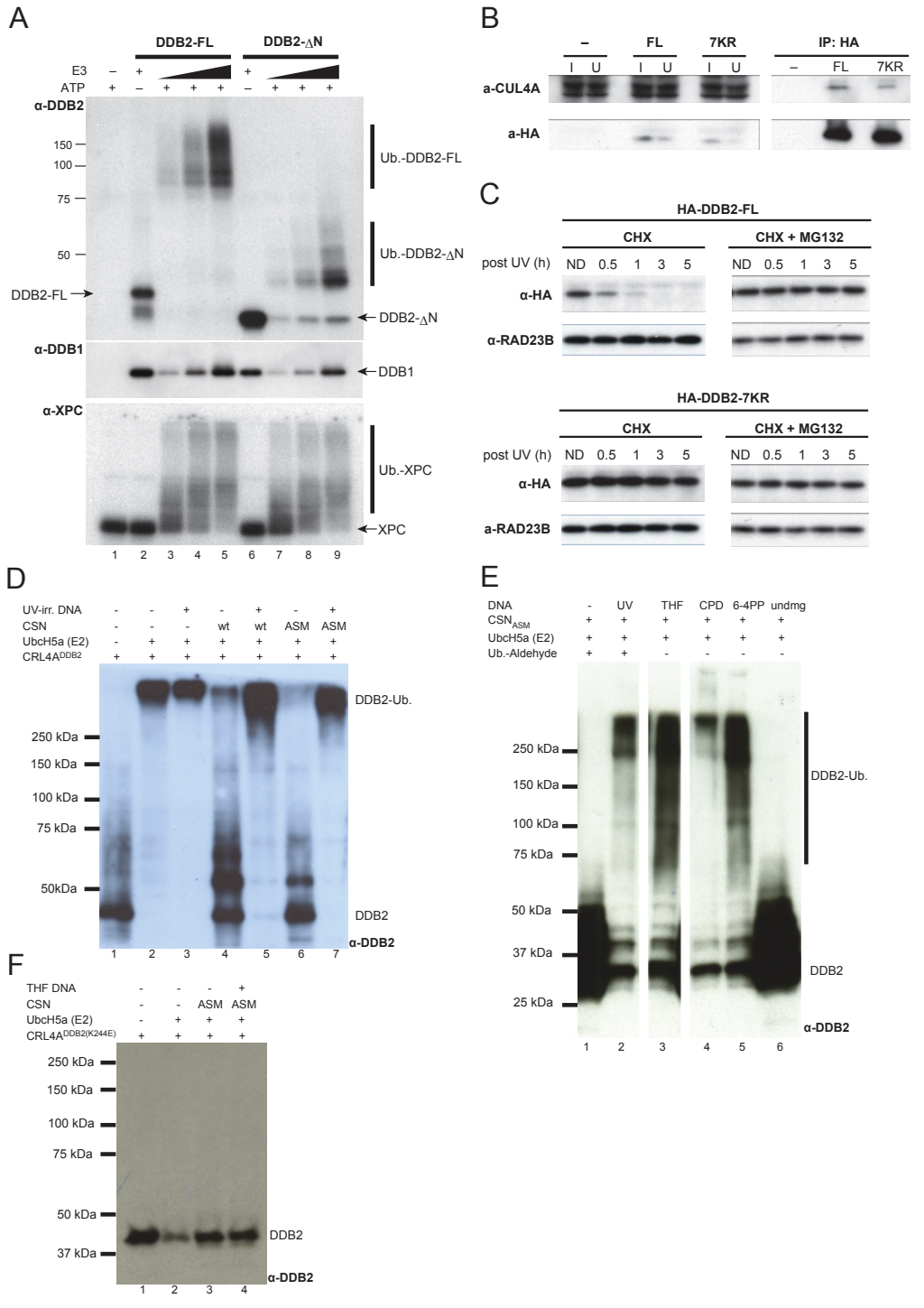
A
DDB2-FL
DDB2-ΔN
E3
ATP
α-DDB2
150
100
75
50
Ub.-DDB2-FL
Ub.-DDB2-ΔN
DDB2-FL
DDB2-ΔN
α-DDB1
DDB1
α-XPC
Ub.-XPC
XPC
1 2 3 4 5 6 7 8 9
B
–
FL
7KR
IP: HA
I U I U I U
– FL 7KR
a-CUL4A
a-HA
C
HA-DDB2-FL
CHX
CHX + MG132
post UV (h)
ND 0.5 1 3 5
α-HA
α-RAD23B
HA-DDB2-7KR
CHX
CHX + MG132
post UV (h)
ND 0.5 1 3 5
α-HA
a-RAD23B
D
UV-irr. DNA
CSN
UbcH5a (E2)
CRL4A^DDB2
wt wt ASM ASM
DDB2-Ub.
250 kDa
150 kDa
100 kDa
75 kDa
50kDa
DDB2
α-DDB2
1 2 3 4 5 6 7
E
DNA
CSN_ASM
UbcH5a (E2)
Ub.-Aldehyde
UV THF CPD 6-4PP undmg
250 kDa
150 kDa
100 kDa
75 kDa
50 kDa
37 kDa
25 kDa
DDB2-Ub.
DDB2
α-DDB2
1 2 3 4 5 6
F
THF DNA
CSN
UbcH5a (E2)
CRL4A^DDB2(K244E)
ASM ASM
250 kDa
150 kDa
100 kDa
75 kDa
50 kDa
37 kDa
DDB2
α-DDB2
1 2 3 4

Figure 6

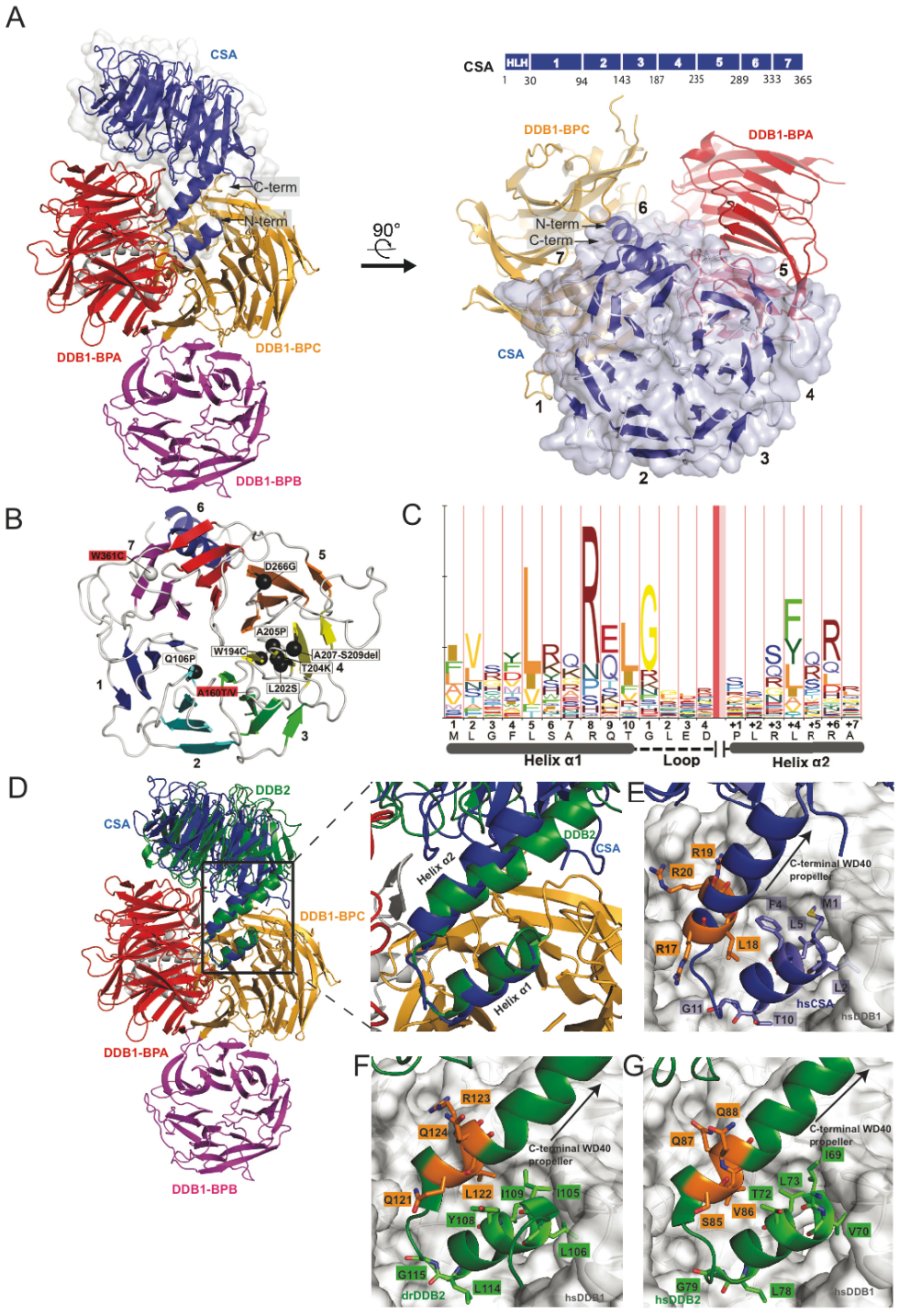
A
CSA
C-term
N-term
DDB1-BPA
DDB1-BPC
DDB1-BPB
90°
CSA
HLH
1
2
3
4
5
6
7
1
30
94
143
187
235
289
333
365
DDB1-BPC
DDB1-BPA
N-term
C-term
CSA
B
W361C
D266G
A205P
W194C
A207-S209del
T204K
Q106P
L202S
A160T/V
C
Helix α1
Loop
Helix α2
D
DDB2
CSA
DDB1-BPC
DDB1-BPA
DDB1-BPB
Helix α2
Helix α1
E
R19
R20
C-terminal WD40 propeller
F4
M1
L5
R17
L18
G11
T10
hsCSA
hsDDB1
F
R123
Q124
C-terminal WD40 propeller
Q121
L122
I109
I105
Y108
L106
G115
L114
drDDB2
hsDDB1
G
Q88
Q87
C-terminal WD40 propeller
I69
L73
T72
V86
S85
V70
G79
L78
hsDDB2
hsDDB1

Figure 7

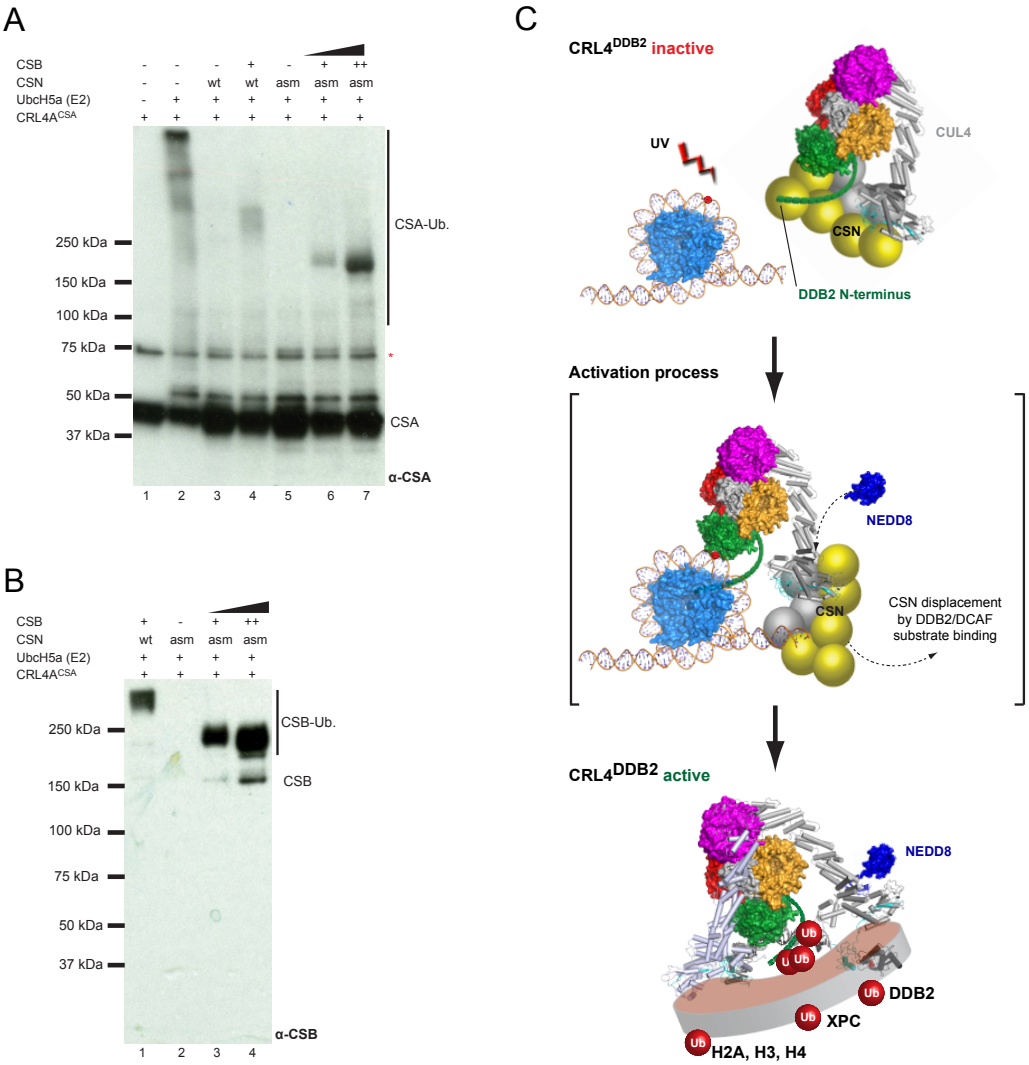
A
CSB - - - + - + ++
CSN - - wt wt asm asm asm
UbcH5a (E2) - + + + + + +
CRL4A^CSA + + + + + + +
250 kDa
150 kDa
100 kDa
75 kDa
50 kDa
37 kDa
CSA-Ub.
CSA
α-CSA
1 2 3 4 5 6 7
B
CSB + - + ++
CSN wt asm asm asm
UbcH5a (E2) + + + +
CRL4A^CSA + + + +
250 kDa
150 kDa
100 kDa
75 kDa
50 kDa
37 kDa
CSB-Ub.
CSB
α-CSB
1 2 3 4
C
CRL4^DDB2 inactive
UV
CUL4
CSN
DDB2 N-terminus
Activation process
NEDD8
CSN
CSN displacement by DDB2/DCAF substrate binding
CRL4^DDB2 active
NEDD8
Ub
DDB2
XPC
H2A, H3, H4

Supplemental Information:

The molecular basis of CRL4$^{DDB2/CSA}$ ubiquitin ligase architecture, targeting and activation

Eric S. Fischer[1,8*], Andrea Scrima[1,7*], Kerstin Böhm[1], Syota Matsumoto[2], Gondichatnahalli M. Lingaraju[1], Mahamadou Faty[1], Takeshi Yasuda[3], Simone Cavadini[1], Mitsuo Wakasugi[4], Fumio Hanaoka[5], Shigenori Iwai[6], Heinz Gut[1], Kaoru Sugasawa[2], Nicolas H Thomä[1†]

[1] Friedrich Miescher Institute for Biomedical Research, Maulbeerstrasse 66, CH-4058 Basel, Switzerland

[2] Biosignal Research Center, and Graduate School of Science, Kobe University, 1-1 Rokkodai, Nada-ku, Kobe 657-8501, Japan

[3] National Institute of Radiological Sciences, 4-9-1 Anagawa, Inage-ku, Chiba 263-8555, Japan

[4] Laboratory of Human Molecular Genetics, Graduate School of Natural Science and Technology, Kanazawa University, Kakuma-machi, Kanazawa 920-1192, Japan

[5] Faculty of Science, Gakushuin University, 1-5-1 Meijro, Toshima-ku, Tokyo 171-8588, Japan

[6] Graduate School of Engineering Science, Osaka University, 1-3 Machikaneyama, Toyonaka, Osaka 560-8531, Japan

[7] Present address: Department of Molecular Structural Biology, Helmholtz-Centre for Infection Research , Inhoffenstrasse 7, D-38124 Braunschweig, German

[8] Universität Basel, Petersplatz 10, CH-4003 Basel, Switzerland

† to whom correspondence should be addressed: nicolas.thoma@fmi.ch

* both authors have contributed equally

Supplemental Information Inventory

Figure S1: hsDDB1-drDDB2 CPD structures. Related to Figure 1

(A, B) Surface mutations were introduced in DDB1 in an attempt to favor CPD bound DDB1-DDB2 crystallization, relative to the apo-form. As DDB1 does not contact the DNA within the DDB1-DDB2 complex (Scrima et al., 2008) mutants were introduced to interfere with crystal-packing of symmetry related DDB1 molecules (marked DDB1*) in the apo-form. These mutations did not affect the DDB1-DDB2 or DDB2-DNA interfaces. The following mutations of DDB1 residues were expressed and purified based on analysis of the DNA free (pdb: 3EI3) versus the 6-4PP bound DDB1-DDB2 complex (pdb: 3EI1): E127K, E127S, Q174A, A175D, E194A, S196A. E224K, E224S and E127K/E224K (**Supplemental Figure S1a and b**). DDB1 mutants E194A, E224K and E224S each resulted in diffraction grade CPD co-crystals.

(C) Overlay of CPD2, CPD4 and 6-4PP (3EI1) focusing on the lesion and opposing bases. The DNA path around the lesions is largely anchored through contacts between the phosphate moieties and DDB2 residues Lys280 (binding duplex base: D_{+3} & D_{+4}), Lys168 (D_{+1} & D_{+2}), Gln372 (D_{+2}), Arg148 (D_{+1}), Arg404 (U_{+2}), Tyr393 (U_{+1}) and Arg369 (U_{-1}). While the 6-4PP and CPD containing duplexes are characterized by different orientations of their ribose moieties and nucleotide ring systems, their phosphate groups (positions D_{+1},D_{+2},D_{+3}) (**Figure 1**) are indistinguishable within experimental error. This is made possible through compensatory rotations around the phosphate backbone torsions linking bases D_{-1}/D_{+1} and D_{+2}/D_{+3} (**Figure S1d**). Difference in the sequence such as a pyrimidine/purine at the U_{-1} location, the major nucleotide enabling kinking of the undamaged strand, are compensated through rolling the base in/out of the duplex respectively through the 3' and 5' phosphate torsions (**Supplementary Figure S1c**). The phosphate backbone thereby serves as molecular pivot points buffering difference in DNA sequence and conformation. The plasticity of the DNA renders DDB2 a DNA sequence-independent recognition module, able to accommodate different pyrimidine dimer lesions, while being optimized for detecting CPD pyrimidine dimers.

(D) Close-up view of the CPD lesion obtained in the four structures with $2mF_{obs}$-DF_{calc} contoured at 1σ. A total of four structures of hsDDB1-drDDB2 bound to four different CPD containing oligonucleotides (see Table S1, **Figure S1d**) were determined (with CPD #4 containing two molecules/asymmetric unit (ASU)). The five

molecules crystallized in different space groups with different packing arrangements. The DDB1 (BPB) domain was found to be mobile, and fully disordered in CPD#3. DDB1 (BPA+BPC) and DDB2 observed in the four structures share an overall rmsd of 0.98 Å (CPD #1 as reference, vs. CPD #2, CPD #3, CPD #4_Mol1, CPD #4_Mol2). Overlay of the individual DNA structures using the 7 bp stretch in direct contact with DDB2 (damaged bases: D_{-3} to D_{+4} and undamaged bases: U_{-4} to U_{+3}) resulted in an average rmsd of 1.36 Å, or 0.95 Å, using all atoms or the phosphate atom backbone, respectively. The residues outside the 7 bp core (especially 3' of the CPD) show larger deviations due to lattice contacts and local unwinding. The DNA is exclusively bound by DDB2 at the narrow end of the WD40 propeller (**Figure 1a**) where it adopts two B-type stretches spanning 5 bp and 4 bp (**Supplemental Figure S1e**), on the 5' and 3' end of the di-nucleotide damage respectively. Three arginine and three lysine residues (Arg148, Arg369, Arg404, Lys168, Lys280 and Lys325) were found contacting the phosphate backbone. Lys168, in particular, compensates the local phosphate backbone negative charge directly at the lesion, where the phosphate-phosphate distance (D_{+1} to D_{+2}) is reduced from about 7 Å (B-DNA) to 5.9 Å (**Supplemental Table S3)**.

(E) Schematic representation of the DNA conformation based on 3DNA analysis (Lu and Olson, 2008).

(F) Overlay of the CPD duplex obtained from the CPD1 crystal and the X-ray crystallographic structure of a free CPD containing oligonucleotide (1N4A), aligned using 4 bp of B-type DNA 5' to the CPD lesion. The structures of 6-4PP containing DNA duplexes in solution showed no similarity with the DDB2-bound duplexes (Scrima et al., 2008), whereas the CPD conformation observed in the presence of DDB2 closely resembles two protein-free CPD duplex structures previously described by Park et al., 2002. The CPD, like other DNA lesions, confers flexibility onto the duplex (Yang, 2008). The protein-free DNA structures thereby, depict one intermediate out of the populated solution ensemble, which is expected to become rigidified upon protein binding. The two cis-syn CPD structures, and that observed in the presence of DDB2, share a comparable kink towards the major groove (CPD_{DDB2}:~45°; CPD_{free}:~30°), similar helix unwinding (CPD_{DDB2}:~12.6°; CPD_{free}:~9.3°) and widened minor grooves (CPD_{DDB2}:18 Å; CPD_{free}:13 Å) resulting in an overall rmsd of 1.92 Å over 8 bp (see **Supplementary Information 1**).

(G) CPD containing DNA duplexes bound to DDB2, Photolyase (1TEZ) and T4 EndonucleaseV (1VAS). Proteins are shown as surface in gray and the DNA as cartoon with the CPD highlighted as sticks (black). The approximate helical bend is indicated (Mees et al., 2004; Vassylyev et al., 1995).

(H) Overlay of the DNA overall conformations of an 31 bp THF, 16bp THF (3EI2), 6-4PP (3EI1) and CPD (CPD1) with DDB2 depicted as surface in gray.

Figure S2: CRL4A^{DDB2} structure bound to a THF containing duplex. Related to Figure 3

(A) Cartoon representation of the CRL4A^{DDB2} complex, $2mF_{obs}$-DF_{calc} electron density (contoured at 1.0 σ) is shown in blue.

(B) Ribbon representation of the SeMet labeled CRL4A^{DDB2} complex highlighting predicted Se positions as green balls. Anomalous difference map contoured at 3.0 σ is shown in blue.

(C) Cartoon representation of the CRL4A^{DDB2} complex, composite omit electron density (contoured at 0.8 σ) is shown in blue.

(D) Summary of observed peaks in the anomalous difference map for the CRL4A^{DDB2} complex.

(E, F and G) SDS-PAGE analysis of CRL4A^{DDB2} complexes used in this study.

(H) Surface representation of the DDB1-BPB domain and close-up of the linker region as cartoon between DDB1-(BPA, BPC) and DDB1-(BPB) domains (residues 384-399 and 702-719) of three different DDB1 conformations (pdb: 2HYE, 2B5L and 3EI1 (Angers et al., 2006; Li et al., 2006; Scrima et al., 2008)) and DDB1-BPB domain of 2B5L in light blue shown as surface.

Figure S3: The CRL4B^{DDB2}-THF and CAND1-CUL4B structures. Related to Figure 4

(A, B) Cartoon representation of the CRL4B^{DDB2} complex structure with CUL4B in gray, RBX1 in cyan, DDB1-BPA in red, DDB1-BPB in magenta, DDB1-BPC in orange, DDB2 in green, and the DNA depicted in black and orange for the undamaged and damaged strand respectively. Molecule 1 **(A)** and molecule 2 **(B)** are shown with the corresponding composite omit electron density (contoured at 0.8

σ) in blue or the $2mF_{obs}$-DF_{calc} electron density (contoured at 1.0 σ) for molecule 1 **(C)** and molecule 2 **(D)** in blue.

(E) Cartoon representation of the CAND1-CUL4B structure with CAND1 depicted in cyan, blue and purple and CUL4B in gray to black. The overall complex of CAND1 and CUL4B resembles the previously determined structure of CAND1-CUL1 (Goldenberg et al., 2004). CAND1 and CUL4B/CUL1 are arranged in a head-to-tail fashion, with CAND1 adopting a sinuous super-helical structure wrapping around the cullin fold (**Supplemental Figure S3e**). The two CAND1/CUL4B complex molecules observed exhibit the following minor rigid body movements: (*i*) a ~2-3° hinge motion in the N-terminal domain of CUL4B (residues 210-379: preceding cullin repeat 2) coupled to a ~3-4° rotation of the CAND1 C-terminal (arm residues 791-1216); (*ii*) a rotation of RBX1 and the CUL4 CTD (residues 637-913) ~1-2.5° in conjunction with the CAND1 N-terminus (residues 4-408) (**Supplemental Figure S3e**). The two CAND1 hinge-points (residues 408 and 791) are preceded by an unstructured loop region, which likely facilitates the movement around the hinge (**Supplemental Figure S3f**).

The structures of both CUL4B molecules superimpose well with CUL4A (rmsd of 1.54 Å over 677 residues). Together with the more than 84 % identity (93 % similarity) between CUL4A and CUL4B (residues 192-913) we conclude that both CUL4 type cullins share identical overall structures and exhibit limited flexibility in the N- & C-terminal domains.

CAND1 bound CUL4B aligns with CAND1 bound CUL1 with an rmsd of 3.1 Å. The main differences among the two cullin folds originated from the orientations of the cullin NTD and CTD domains (see above and Angers et al., 2006). Comparison of the CUL1, 4A and 4B molecules further supports the notion of a small degree of flexibility within these domains (Angers et al., 2006). While relatively small differences are detected within the CUL4A/4B branch, more pronounced differences are observed between CUL1 and CUL4A/B (**Supplemental Figure S3g)**.

Between the CAND1-CUL1 and the two CAND1-CUL4B structures, similar patches on CAND1 and CUL4B/CUL1 are being used for cullin binding. Conserved C-terminal cullin epitopes located on CUL1/4 helix 23 & 29 are recognized through conserved interactions with the CAND1 (**Supplemental Figure S3e**). Additional sites of interaction with CUL1/CUL4B cluster in the CAND1 N-terminal (residues 1-208,

HEAT repeat helices B1-B5), the C-terminal region (residues 704-1190, HEAT repeat helices B20-B22, B24-27) and the beta-hairpin element (residues 1062-1077). The less conserved central region of CAND1 (residues 209-703), however, only displays few cullin interaction sites (B11-B12, B16-18). While similar residues are buried in the two CAND1/CUL4B molecules, detailed hydrogen-bonding and salt bridge interaction are often formed in a manner involving neighboring residues N_{+1}/N_{-1}.

(F) Superposition of the CAND1 originating from CAND1/CUL1 structure (1U6G (Goldenberg et al., 2004)) and from the CAND1/CUL4B structure.

(G) Superposition of CUL1 originating from CAND1/CUL1 (1U6G) with CUL4B from the CAND1/CUL4B structure. Significant differences between CUL4 and CUL1 are observed in loop regions CUL4B:509-515 (CUL1: 355-362) and CUL4:277-284 (CUL1: 109-114). Both these loops constitute substantial interaction surfaces for the cullin and CAND1 and push the cullin in a slightly different conformation. These conformational changes in the cullin are being compensated through expansion/compaction of the CAND1 super-helical U-shaped conformation. The overall surface area buried in both proteins upon complex formation is comparable CAND1-CUL4B (7327.6 $Å^2$) and CAND1-CUL1 (6683.7 $Å^2$).

Positional cloning coupled to large scale sequencing efforts revealed multiple mutations in the CUL4B gene implicated in X-linked mental retardation (XLMR) (Tarpey et al., 2007). In addition to missense mutations, and the presence of premature stop codons, a functional CUL4B null patient suffering from XLMR has been described (Isidor et al., 2010). Patients show clinical symptoms of mental retardation in conjunction with growth retardation, gait ataxia, tremor, hypogonadism and gynecomastia (reviewed in Kerzendorfer et al., 2011). The XLMR syndrome patients, defective in CUL4B, show very little clinical similarity with those patients defective in NER, such as Xeroderma pigmentosum (XP) and Cockayne syndrome (CS). The structures of CUL4A and the corresponding cullin moiety of CUL4B (residues 192-913) are indistinguishable. In agreement with the structural resemblance, we did not observe significant differences in the activity in vitro, and observed that both CUL4A and CUL4B bound to DDB1 with comparable affinity upon co-expression (data not shown). The structure of CUL4B now provides a molecular rationale for mapping of patients mutations:

Premature termination mutations: The premature termination mutations (p.308X, p.337X, p.388X, p.806X, p.836X) lead all to CUL4B C-terminus truncations, resulting in loss of RBX1 binding. The absence of RBX1 in turn, removes the docking site of the ubiquitin E2 enzyme, rendering the CUL4B E3 ligase inactive. In cases where such CUL4B mutant proteins are produced (see for example Kerzendorfer et al., 2010), they are expected to function as dominant negatives competing with the access of active CUL4 ligases to DDB1.

Point mutations: p.T213I is located near the interface between CUL4B and DDB1 in a partially solvent exposed region. Mutation of Thr231 into a hydrophobic Ile is expected to influence the conformation of helix (H1), which directly mediates DDB1 attachment. Two further point mutations have been described: R572C is located in close proximity to CAND1 binding. V745A is located in proximity to the RBX1. Both mutations are, however, structurally conservative and their mutagenic mode of action remains unclear.

Figure S4: The DDB2 N-terminus as target for autoubiquitination. Related to Figure 5

(A) SDS-PAGE analysis of in vitro ubiquitinated $CRL4A^{DDB2}$ for analysis by mass spectrometry, sample positions are indicated by 1, 2 and 3.

(B) Ubiquitin acceptor lysines mapped by LC-MS/MS with corresponding peptide sequence and experimental data.

(C, D) Two representative MS/MS spectra for peptides harboring ubiquitin receptor Lys K40 and K11, corresponding fragmentation for b, b++, y and y++ ions is shown.

(E) SDS-PAGE analysis of proteins used for crystallization and assays.

(F, G) SDS-PAGE analysis of CUL4A autoubiquitination in the presence and absence of CSN or CSN_{ASM}, and SDS-PAGE analysis of the deubiquitination activity of CSN towards CUL4 **(G).** Autoubiquitination (**Supplementary Figure S4f**) and neddylation (data not shown) of CUL4A within the $CRL4^{DDB2}$ complex was unaffected by the presence or absence of the CSN_{ASM} (**Supplementary Figure S4f, lanes 1 and 4**). We further observed that active CSN could remove ubiquitin attached to the neddylation site of CUL4 (**Supplementary Figure S4g, lane 1**) as identified by mass spectrometry (data not shown). However, CSN was unable to remove ubiquitin from

DDB2 or CSA (**Supplementary Figure S4h and i**). In addition, the deubiquitination of CUL4-ubiquitin was dependant on CSN5, as no such activity was observed with CSN_{ASM} (**Supplementary Figure S4g, lane 2**).

(H, I) Ubiquitinated CSA **(H)** or DDB2 **(I)** has been incubated with CSN prior to immunoblotting in order to investigate potential deubiquitination activity of CSN, no such activity could be observed.

Figure S5: CSN mediates activation between DDB2 and the ubiquitin ligase. Related to Figure 5

(A, B) Inhibition and DNA-dependent relieve of DDB2 autoubiquitination by CSN complexes carrying an active site mutation (CSN_{ASM}, inactive isopeptidase) lacking either the CSN5 subunit or the CSN5 and CSN7 subunit (A), or the CSN8 (B).

(C) Additional CSN subcomplexes lacking the indicated subunits were tested for proficiency in DDB2 protection. We set out to define which CSN subunits are required to confer DNA damage mediated DDB2 protection by CSN. For that purpose we purified a number of CSN complexes (see **Supplementary Experimental Procedures)** using a single subunit bearing an N-terminal Strep-II tag. Complexes purified include CSN1*2345678, $CSN1*2345_{ASM}678$, CSN12346*78, CSN12346*8, CSN123*678, CSN123*68, CSN1238*, CSN123*, CSN1*2 (***** asterisk denotes the subunit carrying the tag) all of which were subjected to in vitro autoubiquitination and protection assays. We observed that CSN 5, 7 and 8 are dispensable to provide DDB2 protection against CUL4-mediated DDB2 autoubiquitination with complexes lacking these subunits also being as proficient in DNA damage dependent loss of DDB2 autoubiquitination protection (**Supplementary Figure S5a and b**). Complexes lacking either CSN4, or CSN6 did no longer protect DDB2 from CUL4 mediated autoubiquitination. Subunits CSN1, 2 and 3 were required for the structural integrity of the complex and could not be deleted in the context of the 8 subunit CSN complex. An isolated CSN 1, 2 and 3 complex, however, did not provide protection. Based on these findings CSN protection appears to be mediated by CSN 4 & 6, with CSN1, 2 and 3 playing possible scaffolding roles that by itself are not sufficient to stabilize the complex.

(D) Inhibition and DNA-dependent release of DDB2 autoubiquitination by CSN_{ASM} in the presence of recombinant Usp2 counteracting DDB2 autoubiquitination (lane 2) and with Usp2 inhibited by Ub.-Aldehyde (lane 3).

(E, F) Cy5 fluorescence **(E)** or Alexa488 fluorescence **(F)** scan of a native PAGE EMSA titrating CSN_{ASM} into a DNA(THF)-$CRL4A^{DDB2}$-Nedd8 (species I, V) complex. Upon increasing CSN concentration the level of free DNA (species IV) increases and the DNA free CSN- $CRL4A^{DDB2}$-NEDD8 complex can be observed in the pocket of the gel. We carried out Electrophoretic mobility shift assays (EMSA) to examine the effect of damaged DNA duplex addition on the CSN-$CRL4A^{DDB2}$ complex: The complex of $CRL4A^{DDB2}$-NEDD8 and a 15 bp THF containing duplex was preformed and then subjected to increasing amounts of CSN (**Supplementary Figure S5e-f**). In order to follow the fate of individual components we used a synthetic THF oligonucleotide carrying a Cy5 label on the opposing strand, in combination with an Alexa488 labeled $CRL4A^{DDB2}$-NEDD8 complex. Titrations were performed with a CSN complex harboring a CSN5 mutant (CSN_{ASM}), which is defective in CSN5 mediated cullin deneddylation. All complexes are expressed in High Five insect cells (Enchev et al., 2010). Addition of CSN_{ASM} resulted in the dissociation of the $CRL4A^{DDB2}$-DNA complex (**Supplementary Figure S5e and f,** lane 5-8, species I and V) giving rise to free DNA (**Supplementary Figure S5e,** species IV), $CRL4A^{DDB2}$-NEDD8 bound CSN_{ASM} complex (**Supplementary Figure S5f** in the gel loading pockets) and a protein bound DNA^{THF} species (**Supplementary Figure S5e,** species II & III). Species II & III did not show an Alexa488 signal, arguing that they are free of CUL4-NEDD8, likely consisting of DDB2 bound DNA^{THF}. Importantly, no significant accumulation of novel species was observed containing both CUL4-NEDD8 (Alexa488 channel) and DNA (Cy5 channel) (compare **Supplementary Figure S5e & f**, lanes 6-8). The DNA observed upon addition of CSN, in turn, likely originates from the displacement of DNA from the free $CRL4^{DDB2}$-NEDD8-DNA complex resulting in CSN-$CRL4^{DDB2}$-NEDD8 (**Supplementary Figure S5f).** These findings are consistent with DNA mediated dissociation of $CRL4^{DDB2}$-CSN.

(G and H) SEC-MALS analysis of a CSN-$CRL4A^{DDB2}$-Nedd8 complex in the absence **(G)** or presence **(H)** of a 24bp oligonucleotide harboring a THF site. We subsequently tested the effect of DNA^{THF} on CSN-$CRL4A^{DDB2}$-NEDD8 using size exclusion chromatography. We found that $CRL4A^{DDB2}$-NEDD8 showed tight binding to CSN_{ASM} under these conditions (see **Supplementary Figure S5g**). However, no binding of $CRL4^{DDB2}$ to CSN was detected in the absence of neddylation such binding between CSN and $CRL4A^{DDB2}$ was only detectable in pulldown assays, data not shown. We carried out gelfiltration experiments using 42 µM $CRL4A^{DDB2}$-NEDD8 mixed with 30.45 µM CSN_{ASM} in the presence, or absence of 200 µM 24 bp DNA^{THF}

(**Supplementary Figure S5g and h**). The average molecular weight of the CSN-CRL4A^{DDB2}-NEDD8 peak, in the absence of DNA^{THF} determined by multi-angle light-scattering (MALS) was 519 kDa (9.39 ml). The apparent molecular weight decreased to 467 kDa (9.47 ml) in the presence of DNA^{THF}. DNA^{THF} binding analogously resulted in earlier elution of CRL4A^{DDB2}, 10.64 ml (264 kDa) compared to 10.85 ml (255 kDa) in the absence of nucleic acid. The loss in apparent molecular weight of the CSN containing peak, and concomitant gain in retention time for the CRL4A^{DDB2} is consistent with partial dissociation of the CSN-CRL4^{DDB2}-NEDD8 complex. Due to the peak overlap of CSN, CSN-CRL4^{DDB2}-NEDD8 and CRL4^{DDB2}-NEDD8-DNA^{THF} containing species, different peaks and molecular weights could not be fully deconvoluted. **(I)** SEC-MALS analysis of the CSN$_{ASM}$ complex.

Figure S6: Structure of the Cockayne Syndrome A protein (CSA) bound to DDB1. Related to Figure 6

(A) Helix-loop-helix motif in DCAFs: Sequence alignment of 77 sequences N-terminal of WD40 propellers of DCAFs by T-COFFEE (Notredame et al., 2000).

(B) Surface conservation of CSA: Identical, strongly similar and weakly similar residues as shown in the sequence alignment are highlighted in red, orange and yellow, respectively.

(C) Model of CRL4^{CSA} complex based on two orientations of the DDB1-BPB domain.

(D) Mapping of interaction sites using StrepII-tagged CSA and His-tagged DDB1-BPB or DDB-BPA/BPC in pulldown experiments.

(E) SDS-PAGE analysis of the DDB1-CSA complex used for crystallization.

Figure S7: Multiple sequence alignment of CSA. Related to Figure 6

Sequence alignment and secondary structure assignment of CSA. Sequences were aligned with ClustalW (Larkin et al., 2007). Conservation score and secondary structure elements are given below and on top of the sequences, respectively (Caffrey et al., 2007).

Table S1: Crystallographic data and refinement statistics. Related to Experimental Procedures

Data collection	***hsDDB1-drDDB2 CPD #1***	***hsDDB1-drDDB2 CPD #2***	***hsDDB1-drDDB2 CPD #3***	***hsDDB1-drDDB2 CPD #4***	***CRL4A^{DDB2}***	***SeMet-CRL4A^{DDB2} #522***	***SeMet-CRL4A^{DDB2} #566***	***SeMet-CRL4A^{DDB2} #523***	***CAND1-CUL4B***	***CRL4B^{DDB2}***	***DDB1-CSA***
Beamline	SLS X10SA	SLS X10SA	SLS X06DA	SLS X10SA	SLS X10SA	SLS X06DA	SLS X06DA	SLS X06DA	SLS X10SA	SLS X06DA	SLS X06DA/X10SA
Wavelength (**Å**)	1.0000	1.0000	1.0000	1.0000	1.0000	0.9600	0.9600	0.9600	1.0000	1.0015	1.0000
Space Group	$P2_12_12_1$	$P2_12_12_1$	$C222_1$	$P22_12_1$	$C2$	$C2$	$C2$	$C2$	$P2_1$	$P2_1$	$P3_221$
Cell parameters											
a, b, c (Å)	114.37, 116.70, 137.58	111.65, 122.94, 154,20	155.64, 227.14, 114.32	113.10, 145.90, 224.44	210.65, 78.02, 276.62	212.20, 77.40, 275.20	215.00, 77.70, 277.30	212.70, 77.20, 275.80	77.09, 152.36, 263.01	130.80, 155.84, 255.39	138.33, 138.33, 244.97
α, β, γ (deg)	90, 90, 90	90, 90, 90	90, 90, 90	90, 90, 90	90, 108.5, 90	90, 108, 90	90, 108.7, 90	90, 108.1, 90	90, 89.4, 90	90, 94.2, 90	90, 90, 120
Resolution (Å)	50.0-3.0 (3.1-3.0)	50.0-3.1 (3.2-3.1)	50.0-3.6 (3.7-3.6)	50.0-3.8 (3.9-3.8)	20.0-5.9 (6.08-5.93)	50-5.9 (6.11-5.90)	30.0-7.0 (7.25-7.00)	40.0-6.5 (6.73-6.50)	50.0-3.8 (3.9-3.8)	30.0-7.4 (7.59-7.40)	50-3.3 (3.39-3..31)
Completeness (%)	99.4 (100.0)	99.8 (99.6)	99.4 (99.2)	99.7 (99.7)	98.5 (99.9)	73.2 (35.0)	81.5 (39.1)	85.1 (39.2)	99.7 (99.8)	97.5 (99.1)	92.4 (78.4)
Unique reflections	37332 (3465)	39092 (3471)	23751 (1834)	37310 (2758)	11289 (823)	8396 (392)	5674 (264)	7329 (326)	59850 (4435)	13547 (1013)	38124 (2352)
Redundancy	6.3 (6.3)	7.3 (7.6)	5.3 (5.4)	7.4 (7.6)	4.9 (5.3)	3.0 (2.0)	6.5 (4.8)	6.8 (3.2)	3.8 (3.8)	3.7 (3.7)	2.2 (1.9)
R_{sym} (%)	11.6 (58.7)	12.9 (57.7)	23.3 (57.2)	14.3 (62.1)	13.9 (55.3)	8.3 (36.9)	13.3 (41.9)	7.3 (41.0)	9.2 (51.1)	9.0 (62.2)	10.4 (43.1)
I/σI	14.2 (4.1)	16.0 (4.5)	8.7 (3.4)	11.9 (3.2)	8.07 (2.41)	19.9 (2.0)	20 (2.5)	24.4 (2.1)	10.2 (2.8)	10.2 (2.3)	7.0 (2.0)
Refinement											
PDB code	4A08	4A09	4A0A	4A0B	4A0K				4A0C	4A0L	4A11
R_{work}/R_{free}	23.4/29.4	24.5/30.7	26.7/34.7	24.3/31.9	26.9/27.0				23.8/31.8	31.8/32.0	17.6/23.3
Reflections (working set)	35444	37137	22561	35416	11036				56857	13523	38079
Reflections (test set)	1866	1955	1188	1864	552				2993	1352	1908
Number of Atoms											
Protein	11369	11497	9007	22823	17402				30818	34587	11081
DNA	495	607	648	1135	483				0	966	0
Water	16	22	0	0	0				0	0	0
Ligand	26	1	1	0	0				6	0	0
R.m.s. deviations											
Bond lengths (Å)	0.006	0.006	0.007	0.007	*				0.007	*	0.009
Bond Angles (deg)	1.085	0.988	1.076	1.123	*				1.139	*	1.342
Ramachandran											
favoured	94.7	93.7	91.4	90.3	*				88.5	*	95.9
disallowed	0.4	0.3	0.3	0.9	*				1.5	*	0
Avg. B-factor (Å^2)	48.7	56.7	73.5	126.5	299.0				128.6	253.6	84.2
Crystallization											
Reservoir	100 mM MES, 25 mM NaOH, 18% PEG 350MME	100 mM MES, 15 mM NaOH, 21% PEG 200	100 mM MES, 28 mM NaOH, 16% PEG 350MME	100 mM MES, 15 mM NaOH, 18% PEG 350MME	100 mM Tris-HCl pH 8.3, 33% PEG 200	100 mM Tris-HCl pH 7.9, 35% PEG 200	100 mM Tris-HCl pH 8.5, 29% PEG 200	100 mM Tris-HCl pH 8.5, 31% PEG 200	100 mM MES pH6.3, 30% PEG200, 2% PEG 8000	100 mM MES pH 6.2, 3.1% PEG 6000, 4% ethyleneglycol	1.4-1.58 M $NaKPO_4$, 0.1 M NaMalonate, 0-0.1 M Li_2SO_4
Protein	DDB1-E194A/DDB2	DDB1-E194A/DDDB2	DDB1-E224K/DDB2	DDB1-E224S/DDB2	DDB1/DDB2/ CUL4A/RBX1	DDB1/DDB2/ CUL4A/RBX1	DDB1/DDB2/ CUL4A/RBX1	DDB1/DDB2/ CUL4A/RBX1	CAND1/CUL4B/ RBX1	DDB1/DDB2/ CUL4B/RBX1	DDB1/CSA
Concentration (mg/ml)	9	9	10	9	16	12	12	12	12	20	5 - 10
Cryoprotectant	100 mM MES, 35 mM NaOH, 35% PEG 350MME, 20mM CaAcetate	100 mM MES, 15 mM NaOH, 35% PEG 200, 20mM CaAcetate	Paratone N	100 mM MES, 35 mM NaOH, 35% PEG350MME, 20mM CaAcetate	Reservoir	Reservoir	Reservoir	Reservoir	Reservoir	100 mM MES pH 6.5, 5% PEG 6000, 30% ethyleneglycol	2M NaMalonate, 0.1M Tris-HCl pH 8.0

Values in parentheses are for the highest resolution shell

[a] $R_{work} = \frac{\sum_{hkl}||F_{obs}|-|F_{calc}||}{\sum_{hkl}|F_{obs}|}$; [b] R_{free} is the same as R_{work}, but calculated on the reflections set aside from refinement.

* Subunits from high resolution search models (2HYE, 3EI2 and 4A0C) have been placed by molecular replacement and were rigid body refined.

Table S2: Minor/major groove width for CPD#1. Related to Figure 1

Major groove		**Minor groove**	
Base (D→U+m; m=4)	Width (Å)	Base (D→U+m; m=-3)	Width (Å)
C(D-5)→T(U+1)	17.07	**G(D-2) →G(U+5)**	14.70
G(D-4) →C(U-1)	19.76	**A(D-1) →C(U+4)**	15.34
C(D-3) →C(U-2)	18.51	**CPD(D+1)**	14.76
G(D-2) →C(U-3)	18.35	**→G(U+3)**	15.21
A(D-1) →G(U-4)	17.69	**CPD(D+2)**	18.18
CPD(D+1) →C(U-5)	20.02	**→C(U+2)**	14.81
	16.18	**G(D+3) →T(U+1)**	12.89
CPD(D+2) →G(U-6)	11.78	**C(D+4) →C(U-1)**	14.18
	16.60	**G(D+5) →C(U-2)**	
G(D+3) →G(U-7)		**C(D+6) →C(U-3)**	
C(D+4) →G(U-8)			

Table S3: Phosphate-Phosphate distance for CPD#1. Related to Figure 1

Damaged Strand	**PP-distance (Å)**	**PP-distance (Å)**	**Undamaged strand**
D-5 ←→D-4	6.42	6.63	**U+5**
D-4 ←→D-3	6.24	6.98	**←→U+4**
D-3 ←→D-2	6.66	6.22	**U+4**
D-2 ←→D-1	6.51	6.99	**←→U+3**
D-1 ←→D+1	6.18	6.93	**U+3**
D+1 ←→D+2	5.90 ←	5.95	**←→U+2**
D+2 ←→D+3	K168	6.58	**U+2**
D+3 ←→D+4	5.99	7.00	**←→U+1**
D+4 ←→D+5	6.00 ←	6.72	**U+1 ←→U-1**
D+5 ←→D+6	K280	6.83	**U-1 ←→U-2**
	6.87	5.58	**U-2 ←→U-3**
	6.35	7.58	**U-3 ←→U-4**
			U-4 ←→U-5
			U-5 ←→U-6
			U-6 ←→U-7
			U-7 ←→U-8

Table S4: Oligonucleotides used for crystallization. Related to Experimental Procedures

DDB1/DDB2-CPD #1	damaged strand	5'-ACGCGA(CPD)GCGCCC-3
	undamaged strand	5'-TGGGCGCCCTCGCG-3'
DDB1/DDB2-CPD #2	damaged strand	5'-GGTGAAA(CPD)AGCAGG -3'
	undamaged strand	5'-CCTGCTCCTTTCACCC-3'
DDB1/DDB2-CPD #3	damaged strand	5'-GGGTGAAT(CPD)AGCAGG-3'
	undamaged strand	5'-CCTGCTCCATTCACCC-3'
DDB1/DDB2-CPD #4	damaged strand	5'- GGGTGAAT(CPD)AGCAGG -3
	undamaged strand	5'-CCTGCTCCATTCACCC-3'
$CRL4A^{DDB2}$-THF	damaged strand:	5'-GCTACT(THF)ACGCA-3
	undamaged strand:	5'-TGCGTAAGTAGC-3'
$CRL4A^{DDB2}$ (1x C3)	linked strand	5'-TGCGTAAGTAGCT(C3)CGATCT(THF)ACGGAA-3'
	complementary 1	5'-TCCGTAAGATCG-3'
	complementary 2	5'-GCTACT(THF)ACGCAA-3'
$CRL4A^{DDB2}$ (2x C3)	linked strand	5'-TGCGTAAGTAGCT(C3)(C3)CGATCT(THF)ACGGAA-3'
	complementary 1	5'-TCCGTAAGATCG-3'
	complementary 2	5'-GCTACT(THF)ACGCAA-3'

Table S5: Oligonucleotides used for EMSA and biochemical assays. Related to Figure 5

15bp DNA^{THF}-Cy5	damaged strand	5'-AAATGAAT(THF)AAGCAGG-3
	undamaged strand	5'-(Cy5)CCTGCTTTATTCATTT-3'
15bp DNA^{THF}	damaged strand	5'-AAATGAAT(THF)AAGCAGG-3
	undamaged strand	5'-CCTGCTTTATTCATTT-3'
15bp DNA	undamaged strand	5'-AAATGAATAAAGCAGG-3
	undamaged strand	5'-CCTGCTTTATTCATTT-3'
24bp DNA^{THF}	damaged strand	5'-GTCCTGAATGAAT(THF)ACGCAA -3'
	undamaged strand	5'-TTGCGTAATTCATTCAGGAC -3'
21bp DNA$^{6\text{-}4PP}$	damaged strand	5'-TTTCCTAGACT(6-4PP)GCCCAATTA -3
	undamaged strand	5'-ATAATTGGGCAAAGTCTAGGAA -3'
16bp DNA^{CPD}	damaged strand	5'- GGGTGAAT(CPD)AGCAGG -3
	undamaged strand	5'-CCTGCTCCATTCACCC-3'

Table S6: Reported CSA mutations in Cockayne Syndrome patients. Related to Figure 6

Mutations	*Patient*	*CS class*	*Location*	*Expected Effect*
Q106P	*CS2SE*	*CS I*	*Blade 1 – hydrophobic core, pointing into the central cavity of the WD40 propeller*	*Integrity of the fold: impaired DDB1 & substrate binding*
A160T	*CS852VI*	*CS III*	*Blade 3 – hydrophobic core of the blade*	*Minor effect on the fold affecting DDB1 binding and possibly substrate binding*
A160V	*CS3BE*	*CS I*	*Blade 3 – hydrophobic core of the blade*	*Minor effect on the fold affecting DDB1 binding and possibly substrate binding*
W194C	*CS655VI*	*CS I*	*Blade 4 – hydrophobic cavity that appears no longer filled by the W > S mutations*	*Integrity of the fold: impaired DDB1 & substrate binding*
L202S	*08STR3*	*CS I*	*Blade 4 – hydrophobic cavity, in which a more polar residues is positioned*	*Integrity of the fold: impaired DDB1 & substrate binding*
T204K	*4_1, 4_2*	*CS I*	*Blade 4 – hydrogen bonds with Trp214, His185 and Lys212. The T > K mutation would be expected to result in significant steric clashes*	*integrity of the fold: impaired DDB1 & substrate binding*
A205P	*AGO7075*	*CS I*	*Blade 4 – hydrophobic core of the propeller. The A > P mutations likely interferes with the β-sheet conformation , due to disallowed Ramachandran space*	*Integrity of the fold: impaired DDB1 & substrate binding. Lack of DDB1 binding has been demonstrated*
D266G	*CS861VI, 08STR2, 08STR2_2, 3_1, 3_2*	*CS I*	*Blade 5 – tight turn (Asp is the canonical WD40 residues in this position). The change to Gly is conservative, however, and expected to have mostly local effects*	*Likely interfering with substrate binding on the narrow side of the WD40 propeller*
Deletion A207-S209	*CS794VI*	*CS I*	*Blade: truncates the loop between strands B and C. Effect is expected to be local*	*Likely interfering with substrate binding on the narrow side of the WD40 propeller*
W361C	*UV^{S}SVI*	*UV^{S}S*	*Blade 7: Cys mutations results in the hydrophobic cavity not being properly filled. Conservative mutation, however, expected to cause only limited damage*	*Mildly interfering with the integrity of the WD40 fold: impaired DDB1 & substrate binding*

Mutations of CSA were identified in 41 CS patients: 8 different point mutations, 8 frameshift mutations, 4 deletions and 3 stop codon insertions have been described (Laugel et al., 2010). CS has been classified into three different sub-groups according to the severity and onset of the disease: the most severe form (class 1) has an onset in utero (COFS) or during the first years of life; (class 2) manifests itself in the early teens, while class 3 becomes apparent after the second or third decade of life. The least severe phenotype is observed in UV sensitivity syndrome (UV^{S}S), which is also associated with mutations in CSA (Laugel et al., 2010) and comes with no obvious developmental phenotype, unlike classes I, II and III.

On the basis of the structure, there are three conceivable ways to impair CSA function: (*i*) point mutations in the structured HLH-WD40 domain abolishing DDB1 binding, which has been directly observed in the A205P mutation (Jin et al., 2006); (*ii*) mutations preventing substrate binding on the narrow face of the WD40 propeller; (*iii*) and those interfering with the overall

fold expected to affect both substrate binding and DDB1 binding as well as protein stability.

Genotype/Phenotype correlations: The structure now provides a molecular rationale for the observed Cockayne patient mutations. Deletions of the N-terminus, residues Δ2-4 or Δ2-7 are expected to impair CSA binding to DDB1. Premature chain termination mutants, as seen in patients, on the other hand are expected to give rise to misfolded CSA WD40 domains, which likely retain binding to DDB1, but are expected to be defective in substrate binding. The majority of point mutations concerns the hydrophobic core of the WD40 propeller and likely exerts their mutagenic effect through WD40 folding mutations. Out of eight point mutations, four (and a short deletion) are clustered in blade 4 (**Figure 6b**). The four residues are closely spaced occupying position CSA 194, 202, 204 and 205. As this blade is not obviously involved in DDB1 interactions, we propose that blade 4 is selected for in patient derived mutations due to its involvement in substrate binding. On the basis of the patterns of conserved hydrophobic residues (Tyr/Phe100 & Phe120) present in all CSA orthologues (**Supplementary Figure S6a and S7**), combined with the patient mutations assigned to blade 4, we speculate that the CSA substrate might be bound crossing blade 4/5 & blade 2.

It is frequently stated that no genotype/phenotype correlation exists for patients suffering from CS. Such relationship is principally complicated by the fact that both alleles have to be defective or absent for the carrier to develop the disease. Analyzing the patient mutations we note, however, that point mutations, deletions and frame-shifts give rise to CS type I and II. The mutations leading to the milder form of CS type III and UV^{S}S, on the other hand, are point mutations. Mutations A160T (CS III) and W361C (UV^{S}S), both are predicted to cause only limited damage to the propeller. We therefore predict that CSA mutations in type III comprise largely those point mutations that only cause limited, localized damage to CSA integrity.

The three WD40 propellers of DDB1 provide several potential binding sites for DCAFs. For initial mapping of the interacting surfaces of CSA/DDB1 StrepII-tagged CSA was co-expressed with His_6-tagged DDB1(ΔBPB) and DDB1-BPB (BPB only). DDB1(ΔBPB) did co-purify with CSA, while DDB1-

BPB was not able to bind (**Supplementary Figure S6d**). Further a C-terminal truncated CSA (1-367) did co-purify with DDB1 similar to full-length CSA. We therefore observed no evidence for the involvement of the DDB1-BPB domain in CSA binding. This is in agreement with earlier co-precipitation studies (Jin et al., 2006): the mutation of a single residue (W953A) on the top face of BPC (facing towards the bottom of BPA) of DDB1 resulted in significant reduced binding of CSA. In the CSA-DDB1 structure W953 of DDB1 is involved in stacking interaction with R19 of CSA.

The binding mode of CSA with the HLH motif in a cleft formed by BPA and BPC of DDB1 was independent confirmed by an additional crystal structure obtained at lower resolution (6.0 Å) from crystals in a different space group (I23, a=b=c=279.06 Å). The $P3_221$ crystal form was also obtained with a C-terminally truncated CSA (1-367). Here, as well as in the high resolution structure (main text) clear electron density for the HLH motif of CSA was observed after a molecular replacement with DDB1 (BPA+BPC, BPB).

Supplemental Experimental Procedures

Protein expression and purification

hsDDB1 (aa 1-1140) and drDDB2 (aa 94-457) co-complexes were expressed and purified as described in Scrima et al., 2008. DDB1-mutants were generated using the PIPE mutagenesis protocol (Klock and Lesley, 2009). The $CRL4A^{DDB2}$ complex was expressed and purified using baculoviruses for hsDDB1 (aa 1-1140), drDDB2 (aa 94-457), hsCUL4A (aa 38-759), mmRBX1 (aa 12-108) as N-terminal His_6 fusion proteins in Hi-5 insect cells (Scrima et al., 2008). Cells were lysed by sonication (in 50 mM Tris pH 8.0, 200 mM NaCl, 5 mM β-ME, 0.1 % Triton X-100, 1 mM PMSF and 1 tablet of complete protease inhibitor cocktail Roche Applied Science). Following high-speed centrifugation, the supernatant was passed over Ni-NTA affinity resin, target protein complex was eluted and subjected to Poros50HQ ion exchange chromatography. Purification was completed with size exclusion chromatography using a 26/60 Superdex S200 column (GE Healthcare) in 50 mM HEPES pH 7.4, 200 mM NaCl and 2 mM DTT. $CRL4B^{DDB2}$ (His_6-TEV-CUL4B aa 192-913) complex purification was performed similar to that of $CUL4A^{DDB2}$, with the exception that $CRL4B^{DDB2}$ was subjected to overnight 1 % proteolytic cleavage using TEV protease following affinity purification. N-terminally StrepII-tagged hsCAND1 (aa 1-1230) and His_6-tagged hsCUL4B (aa 192-913)/mmRBX1 (aa 12-108) was co-expressed and Ni-NTA affinity purified, followed by size exclusion chromatography in 50 mM HEPES pH 7.4, 200mM NaCl and 5 mM DTT. C-terminally StrepII-tagged hsCSA (aa 1-396) and His_6-tagged hsDDB1 (aa 1-1140) was co-expressed and StrepII affinity purified followed by ion exchange and size exclusion chromatography (see above). $CRL4A^{DDB2(K244E)}$ complex was purified from Hi-5 insect cells as described in Sugasawa et al., 2006.

Recombinant hsCSB was overexpressed in Hi-5 insect cells and purified as N-terminal His_6 fusion protein as described for DDB1-DDB2 (Scrima et al., 2008). Untagged recombinant hsCSB overexpressed and purified from insect cells was provided as a kind gift from Regina Groisman. While the untagged hsCSB was ubiquitinated in our in vitro assay, ubiquitination could not be observed with N-terminal tagged hsCSB.

The purified complexes were concentrated as indicated in **Supplemental Table S1**, flash frozen in liquid nitrogen and stored at -80°C.

Crystallization

Crystals of the DDB1/drDDB2–DNA (CPD #1, #2, #3, #4), CRL4A^{DDB2}-DNA, CRL4B^{DDB2}-DNA and CAND1/CUL4B complexes were grown at 20 °C–24 °C using the hanging drop diffusion method. In protein-DNA complexes typically a 1.20-1.35 molar excess of DNA was added to the protein solution and incubated on ice for 20 minutes prior to crystallization by mixing the protein solution in a 1:1 ratio with reservoir solution (**Supplemental Table S1**). Crystals of the DDB1-CSA complex were grown using the sitting drop vapor diffusion method at 20 °C. Drops contained 5-10 mg/ml protein complex and reservoir solution containing 1.4-1.58 M $KNaPO_4$, 0.1 M Na Malonate and 0-0.1 M Li_2SO_4 at a 1:1 ratio.

Crystals were transferred into cryo-solution prior to flash-freezing or were directly flash frozen in liquid nitrogen for data collection (**Supplemental Table S1**). Data sets were collected at the Swiss Light Source, Paul Scherrer Institut, Villigen, Switzerland, and processed with XDS (Kabsch, 1993). For DDB1-CSA three datasets from three crystals were merged to give a complete dataset to a resolution of 3.3 Å.

The CRL4A^{DDB2}-DNA complex revealed packing of the DNA duplex within the crystal lattice in a head-to-tail fashion to a symmetry related CRL4A^{DDB2} molecule. In an effort to improve crystal-packing, we covalently linked the two DNA molecules mimicking a continuous DNA duplex connecting the two symmetry related molecules. For this approach we used one, two and three flexible methyl group linkers introduced to connect the 3' end of one undamaged strand to the 5' end of the damaged strand. The sequence of the linked damaged strand was slightly modified to prevent self-annealing (**Supplementary Table S4**). A number of these DNA constructs resulted in crystals that, however, resulted at best in diffraction quality and resolution equal to the parental crystal form (CRL4^{DDB2}-THF, see below). The nominally highest resolution data set was collected using CRL4A^{DDB2}-THF.

Oligonucleotides used for crystallization

CPD containing single stranded DNA oligonucleotides were synthesized as described in (Iwai et al., 1996) using cis-syn thymine dimer phosphoramidite building blocks (Glenn Reasearch, USA). Complementary oligonucleotides and oligonucleotides harboring a THF abasic site mimic were synthesized by Sigma-Aldrich and purified on a Microsorb 300-5 PureDNA HPLC column (Varian, Inc., USA). Oligonucleotides were annealed in 10 mM HEPES pH 7.4; 50 mM NaCl and subsequently stored at −20 °C. Unmodified and modified oligonucleotides used for biochemistry were also ordered from Sigma-Aldrich and HPLC purified by the manufacturer. For a list of oligunucleotides used in crystallization see Supplementary Table S4 and S5 for oligonucleotides used in biochemical assays.

Structure determination and model building

Structures of DDB1-drDDB2-DNA complexes were solved by molecular replacement using DDB1 (BPA+BPC), DDB1 (BPB) and DDB2 (all taken from pdb: 3EI1) as search models for Phaser (McCoy et al., 2007).

The structure of CAND1/CUL4B was determined by molecular replacement using the CAND1 model taken from the previously determined structure of CUL1-CAND1 (1U6G). For the search, CAND1 was split into an N-terminal (aa 4-849) and a C-terminal (aa 850-1216) model. An initial homology model for CUL4B (aa 210-913)/RBX1 (aa 19-108) was generated using MODELLER (Eswar et al., 2006). The models were used in successive molecular replacement rounds in Phaser (McCoy et al., 2007).

The $CRL4A^{DDB2}$ complex structure was determined by sequential domain placement in step-wise molecular replacement searches. CUL4A attached to the BPB domain of DDB1 (obtained from pdb: 2HYE) was successfully located using Phaser (McCoy et al., 2007). The solution was fixed and DDB1 (BPC+BPA) (obtained from pdb: 3EI2) was located using Molrep (Vagin and Teplyakov, 1997), followed by localization of DDB2-DNA (pdb: 3EI2). The unbiased molecular replacement search reassembled the linker between the DDB1 (BPB) and DDB1 (BPA+BPC) domains, resembling the interface previously observed in DDB1 structures.

The $CRL4B^{DDB2}$ complex structure was determined by molecular replacement with Molrep (Vagin and Teplyakov, 1997) using a strategy similar to that outlined for $CRL4A^{DDB2}$. A search model of CUL4B (obtained from the previously solved CUL4B/CAND1 complex structure) was used instead of CUL4A and allowed us to locate the two molecules in the ASU. The two CUL4B molecules were subsequently fixed and additional rounds of molecular replacement allowed the placement of DDB1 (BPA+BPC) (obtained from pdb: 3EI2) and DDB2-DNA (obtained from pdb: 3EI2).

The structure of DDB1-CSA was determined by molecular replacement using Phaser (McCoy et al., 2007). As search models DDB1 (BPA& BPC, BPB from pdb: 3EI1) and a homology model of the WD40 propeller of CSA (Kelley and Sternberg, 2009) were used. Phases calculated from the placement of DDB1 provided clear electron density for the HLH motif of CSA.

Rigid body refinement for $CRL4A^{DDB2}$-DNA and $CRL4B^{DDB2}$-DNA was carried out with Phenix (Adams et al., 2010). DDB1-DDB2-DNA, CAND1/CUL4B and DDB1-CSA structures were refined using Refmac5 (Murshudov et al., 1997) with additional rounds of refinement in Phenix and Buster used for DDB1-CSA (Adams et al., 2010; Bricogne et al., 2010). Manual model building was performed using Coot (Emsley and Cowtan, 2004). The final models were verified using composite omit maps as implemented in CNS (Brunger et al., 1998). Figures were generated in the PyMol package (DeLano Scientific; http://www.pymol.org).

Experimental Structure validation

The CUL4A-RBX1-DDB1-DDB2 complex was expressed in High Five insect cells in the presence of seleno-methionine (SeMet) substituted minimal medium (see Cronin et al., 2007 for detailed procedures). The SeMet labeled protein crystallized under conditions similar to that of the native protein. The resulting crystals belonged to space group C2 sharing identical cell parameters to that of the unmodified complex (**Supplemental Table S1**). Single anomalous dispersion (SAD) datasets, with resolutions ranging between 5.9 Å and 8 Å, were recorded at beam-line X06DA (Swiss Light Source, PSI), which was equipped with a Mar225CCD detector. Data was acquired in an inverse beam setup with alternating 1° wedges spaced 180°

apart in order to minimize loss of anomalous signal due to radiation damage. Reflections were indexed, scaled and integrated using the HKL2000 package (Otwinowski and Minor, 1997). The structures were solved by molecular replacement with Phaser (McCoy et al., 2007). Anomalous difference maps were calculated using FFT from the CCP4 package (Collaborative Computational Project, 1994) and averaged in Coot (Emsley and Cowtan, 2004). Within in the averaged anomalous difference maps (3.0 σ), 50 % of the $CRL4A^{DDB2}$ methionine positions could be located at their predicted position (see **Supplemental Figure S2b and d)**. Additional support for the domain placement was obtained using composite omit maps (**Supplemental Figure S2c**).

Attempts to validate the $CRL4B^{DDB2}$ structure through Se-Met data collection were unsuccessful due to the inability to grow crystals despite extensive trials. The $CRL4B^{DDB2}$ crystal form required TEV cleavage, Se-Met labeled CRL4B complex, however, is rendered largely insoluble following TEV cleavage. The $CRL4B^{DDB2}$ structure was validated by composite omit maps as implemented in CNS (Brunger et al., 1996). **Supplemental Figure S3a and b** show the validation of the individual rigid bodies used in refinement: DDB1(BPA+BPC), DDB1(BPB), CUL4B, DNA, RBX1.

Reconstitution of irradiated mononucleosomes

Mononucleosomes were reconstituted as described (Luger et al., 1997) using 134 bp p9HISAT-DNA (Losa et al., 1990) and recombinantly expressed and purified histones (H2A, H2B, H3 from X. tropicalis*;* H4 from S. cerevisiae*)*. For UV-damaged nucleosomes, DNA was irradiated prior to reconstitution with 2000 J/m^2 at 254 nm in a Stratalinker UV Crosslinker 2400. Mononucleosome reconstitution and protein binding were analyzed on native 0.7 % agarose run in 0.2x TB buffer at 100 V for 120 min at 4 °C. Detection was performed with a Typhoon Imager (Amersham) using tracer amounts of Cy5-labeled DNA.

Electrophoretic mobility shift assays

EMSA, employing native agarose or polyacrylamide gels, were used to analyze nucleosomes and perform binding studies. Non-denaturing poly-

acrylamide gels (15x25 cm) were poured (5 % acrylamide/Bis-acrylamide 29/1; 0.5x TBE; 0.1 % APS; 60 µl TEMED) and pre-run for 1 h with 150 V at 4 °C in 0.5x TBE. Samples were mixed 1:2 with 2x EMSA-buffer (10 mM Triethanolamine pH 7.4; 50 mM NaCl, 1 mM DTT, 100 µg/ml BSA). Native 0.7 % agarose gels were run in 0.2x TB buffer at 100 V for 120 min at 4°C. Detection of fluorescently labeled oligonucleoteides and proteins was carried out on a Typhoon Imager (Amersham).

DDB1-DDB2 and CRL4^{DDB2} binding to UV irradiated nucleosomes

For the analysis of UV-DDB binding to non-irradiated and irradiated nucleosome core particles (NCP) (**Figure 2a**) approximately 70 nM NCP were mixed with increasing amounts of UV-DDB and 500 ng dI/dC competitor DNA in EMSA-buffer and incubated for 20 min on ice prior to the analysis by EMSA. Analysis of CRL4^{DDB2} binding to irradiated NCP (**Figure 2f**) was performed under similar conditions with 50 nM NCP and increasing amounts of protein (no competitor) in EMSA-buffer.

Reconstitution of NCPs containing a positioned 6-4PP or CPD and EMSAs to analyze DDB1-DDB2 binding were performed essentially as described previously (Yasuda et al., 2005). Binding reactions were carried out in 15 µl including 0.2 fmol ^{32}P-labeled NCP and/or naked DNA and the indicated amounts of DDB1-DDB2. A 5% non-denaturing polyacrylamide gel was used for electrophoresis.

In vitro ubiquitination assays and CSN protection assay

In vitro ubiquitination assays were performed as previously described (Sugasawa, 2006) with 40 nM E1 (UBA1, Boston Biochem), 1.89 µM E2 (UbcH5A or UbcH5B, Boston Biochem), 20 nM CRL4^{DDB2} complex or CRL4^{DDB2}-NEDD8 (data not shown), 40 µM ubiquitin (Boston Biochem) or 10 µM K_0-ubiquitin (Boston Biochem). The reaction was incubated for 30 min at 30 °C and subsequently analyzed by SDS-PAGE coupled to immunoblotting. To assess the protection of DDB2 by CSN, an ubiquitin reaction mixture lacking the E2 was pre-incubated with the corresponding CSN complex for 15 min on ice, the assay was subsequently initiated by E2 addition. Loss of protection of DDB2 autoubiquitination was tested by adding 1.5 µM of the

appropriate DNA oligonucleotide followed by 30 min incubation at 30 °C. To exclude the presence of contamination through DNA activated deubiquitinating enzymes (DUB), we performed control assays in the presence of 3.9 µM ubiquitin-aldehyde, a potent DUB inhibitor (**Figure 5e, lanes 1-2**) (Melandri et al., 1996; Zhou et al., 2003). We further spiked the reaction with recombinant Usp2 and tested the potential of ubiquitin-aldehyde to inhibit DUB activity, as expected, DDB2 autoubiquitination was only observed in the presence of ubiquitin-aldehyde (**Supplementary Figure S5d**). In vitro ubiquitination assays with $CRL4^{CSA}$/CSB were carried out under similar experimental conditions with 70nM $CRL4^{CSA}$ and between 100nM and 1uM CSB to test the relieve of CSN inhibition.

To further exclude potential deubiquitination activity of our CSN preparations, ubiquitinated $CRL4^{DDB2}$ or $CRL4^{CSA}$ complexes were incubated with active CSN and subjected to immunoblot (**Supplementary Figure S4h and i**). No deubiquitinating activity could be observed.

Neddylation of $CRL4^{DDB2}$ and labeling with Alexa488

In vitro neddylation of $CRL4^{DDB2}$ complexes was carried out as previously described (Duda et al., 2008) followed by purification of neddylated complexes by size exclusion chromatography. In order to fluorescently label the NEDD8, a thiol-reactive Alexa488-maleimide (Invitrogen) was conjugated to a Nedd8(M1C) mutant according to the manufacturer's instructions with TCEP as reductive agent and the Alexa488-NEDD8 conjugate was purified by size exclusion chromatography after addition of glutathione to absorb free reactive species. The Alexa488-NEDD8 was then conjugated to $CRL4A^{DDB2}$ complex by in vitro neddylation (Duda et al., 2008) with subsequent purification by size exclusion chromatography.

Mapping of Ubiquitin sites by LC-MS/MS

The $CRL4A^{DDB2}$ complex was subjected to in vitro autoubiquitination, and subsequently analyzed by SDS-PAGE (**Supplementary Figure S4a**). Several DDB2 bands were excised from the gel, subjected to tryptic digest and analyzed by NanoLC-MS/MS with a 1200 HPLC (Agilent) connected to a LTQ

Orbitrap Velos (Thremo Scientific). The ubiquitinated peptides were identified with Mascot searching Swiss-Prot 2010_09 (Perkins et al., 1999)

and manually validated. Peptide fragmentation and spectras are shown for two representative peptides harboring the ubiquitin acceptor lysines K11 and K40 (**Figure S4c and d**).

SEC-MALS

To determine the average mass of protein complexes, size exclusion chromatography (SEC) using a Superdex 200 10/300 column (GE Healthcare) was coupled to multi angle light scattering (MALS) using an Optilab T-rEX refractive index detector and a miniDAWN TREOS 3 angle MALS detector (Wyatt Technology). The runs were done in 50 mM HEPES pH7.4, 200 mM NaCl and 1mM DTT and 50 µl sample volume were injected.

Supplemental References

Adams, P.D., Afonine, P.V., Bunkoczi, G., Chen, V.B., Davis, I.W., Echols, N., Headd, J.J., Hung, L.W., Kapral, G.J., Grosse-Kunstleve, R.W.*, et al.* (2010). PHENIX: a comprehensive Python-based system for macromolecular structure solution. Acta Crystallogr D Biol Crystallogr *66*, 213-221.

Angers, S., Li, T., Yi, X., MacCoss, M.J., Moon, R.T., and Zheng, N. (2006). Molecular architecture and assembly of the DDB1-CUL4A ubiquitin ligase machinery. Nature *443*, 590-593.

Bricogne, G., Blanc, E., Brandl, M., C., F., Keller, P., Paciorek, P., Roversi, P., Sharff, A., Smart, O., Vonrhein, C.*, et al.* (2010). BUSTER version 2.9. Cambridge, United Kingdom: Global Phasing Ltd.

Brunger, A., Adams, P., Clore, G., DeLano, W., Gros, P., Grosse-Kunstleve, R., Jiang, J., Kuszewski, J., Nilges, M., Pannu, N.*, et al.* (1998). Crystallography & NMR system: A new software suite for macromolecular structure determination. Acta Crystallographica Section D-Biological Crystallography *54*, 905-921.

Collaborative Computational Project, N. (1994). The CCP4 suite: programs for protein crystallography. Acta Crystallographica Section D-Biological Crystallography *50*, 760-763.

Cronin, C.N., Lim, K.B., and Rogers, J. (2007). Production of selenomethionyl-derivatized proteins in baculovirus-infected insect cells. Protein Sci *16*, 2023-2029.

Duda, D., Borg, L., Scott, D., Hunt, H., Hammel, M., and Schulman, B. (2008). Structural insights into NEDD8 activation of cullin-RING ligases: conformational control of conjugation. Cell *134*, 995-1006.

Emsley, P., and Cowtan, K. (2004). Coot: model-building tools for molecular graphics. Acta Crystallographica Section D-Biological Crystallography *60*, 2126-2132.

Enchev, R.I., Schreiber, A., Beuron, F., and Morris, E.P. (2010). Structural insights into the COP9 signalosome and its common architecture with the 26S proteasome lid and eIF3. Structure *18*, 518-527.

Eswar, N., Webb, B., Marti-Renom, M.A., Madhusudhan, M.S., Eramian, D., Shen, M.Y., Pieper, U., and Sali, A. (2006). Comparative protein structure modeling using Modeller. Curr Protoc Bioinformatics *Chapter 5*, Unit 5 6.

Goldenberg, S.J., Cascio, T.C., Shumway, S.D., Garbutt, K.C., Liu, J., Xiong, Y., and Zheng, N. (2004). Structure of the Cand1-Cul1-Roc1 complex reveals regulatory mechanisms for the assembly of the multisubunit cullin-dependent ubiquitin ligases. Cell *119*, 517-528.

Isidor, B., Pichon, O., Baron, S., David, A., and Le Caignec, C. (2010). Deletion of the CUL4B gene in a boy with mental retardation, minor facial anomalies, short stature, hypogonadism, and ataxia. Am J Med Genet A *152A*, 175-180.

Iwai, S., Shimizu, M., Kamiya, H., and Ohtsuka, E. (1996). Synthesis of a phosphoramidite coupling unit of the pyrimidine (6-4) pyrimidone photoproduct and its incorporation into oligodeoxynucleotides. Journal of the American Chemical Society *118*, 7642-7643.

Jin, J., Arias, E., Chen, J., Harper, J., and Walter, J. (2006). A family of diverse Cul4-Ddb1-interacting proteins includes Cdt2, which is required for S phase destruction of the replication factor Cdt1. Molecular cell *23*, 709-721.

Kabsch, W. (1993). Automatic Processing of Rotation Diffraction Data from Crystals of Initially Unknown Symmetry and Cell Constants. Journal of Applied Crystallography *26*, 795-800.

Kelley, L.A., and Sternberg, M.J. (2009). Protein structure prediction on the Web: a case study using the Phyre server. Nat Protoc *4*, 363-371.

Kerzendorfer, C., Hart, L., Colnaghi, R., Carpenter, G., Alcantara, D., Outwin, E., Carr, A.M., and O'Driscoll, M. (2011). CUL4B-deficiency in humans: Understanding the clinical consequences of impaired Cullin 4-RING E3 ubiquitin ligase function. Mechanisms of ageing and development.

Kerzendorfer, C., Whibley, A., Carpenter, G., Outwin, E., Chiang, S.-C., Turner, G., Schwartz, C., El-Khamisy, S., Raymond, F.L., and O'Driscoll, M. (2010). Mutations in Cullin 4B result in a human syndrome associated with increased camptothecin-induced topoisomerase I-dependent DNA breaks. Human molecular genetics *19*, 1324-1334.

Klock, H.E., and Lesley, S.A. (2009). The Polymerase Incomplete Primer Extension (PIPE) method applied to high-throughput cloning and site-directed mutagenesis. Methods in molecular biology (Clifton, NJ) *498*, 91-103.

Larkin, M.A., Blackshields, G., Brown, N.P., Chenna, R., McGettigan, P.A., McWilliam, H., Valentin, F., Wallace, I.M., Wilm, A., Lopez, R.*, et al.* (2007). Clustal W and Clustal X version 2.0. Bioinformatics *23*, 2947-2948.

Laugel, V., Dalloz, C., Durand, M., Sauvanaud, F., Kristensen, U., Vincent, M.C., Pasquier, L., Odent, S., Cormier-Daire, V., Gener, B.*, et al.* (2010). Mutation update for the CSB/ERCC6 and CSA/ERCC8 genes involved in Cockayne syndrome. Hum Mutat *31*, 113-126.

Li, T., Chen, X., Garbutt, K.C., Zhou, P., and Zheng, N. (2006). Structure of DDB1 in complex with a paramyxovirus V protein: viral hijack of a propeller cluster in ubiquitin ligase. Cell *124*, 105-117.

Losa, R., Omari, S., and Thoma, F. (1990). Poly(dA).poly(dT) rich sequences are not sufficient to exclude nucleosome formation in a constitutive yeast promoter. Nucleic Acids Res *18*, 3495-3502.

Lu, X., and Olson, W. (2008). 3DNA: a versatile, integrated software system for the analysis, rebuilding and visualization of three-dimensional nucleic-acid structures. Nat Protoc *3*, 1213-1227.

Luger, K., Rechsteiner, T.J., Flaus, A.J., Waye, M.M., and Richmond, T.J. (1997). Characterization of nucleosome core particles containing histone proteins made in bacteria. J Mol Biol *272*, 301-311.

McCoy, A., Grosse-Kunstleve, R., Adams, P., Winn, M., Storoni, L., and Read, R. (2007). Phaser crystallographic software. Journal of Applied Crystallography *40*, 658-674.

Mees, A., Klar, T., Gnau, P., Hennecke, U., Eker, A.P.M., Carell, T., and Essen, L.-O. (2004). Crystal structure of a photolyase bound to a CPD-like DNA lesion after in situ repair. Science (New York, NY) *306*, 1789-1793.

Melandri, F., Grenier, L., Plamondon, L., Huskey, W.P., and Stein, R.L. (1996). Kinetic studies on the inhibition of isopeptidase T by ubiquitin aldehyde. Biochemistry *35*, 12893-12900.

Murshudov, G., Vagin, A., and Dodson, E. (1997). Refinement of macromolecular structures by the maximum-likelihood method. Acta Crystallographica Section D-Biological Crystallography *53*, 240-255.

Notredame, C., Higgins, D., and Heringa, J. (2000). T-Coffee: A novel method for fast and accurate multiple sequence alignment. Journal of molecular biology *302*, 205-217.

Otwinowski, Z., and Minor, W. (1997). Processing of X-ray diffraction data collected in oscillation mode. Macromolecular Crystallography, Pt A *276*, 307-326.

Perkins, D.N., Pappin, D.J., Creasy, D.M., and Cottrell, J.S. (1999). Probability-based protein identification by searching sequence databases using mass spectrometry data. Electrophoresis *20*, 3551-3567.

Scrima, A., Konícková, R., Czyzewski, B.K., Kawasaki, Y., Jeffrey, P.D., Groisman, R., Nakatani, Y., Iwai, S., Pavletich, N.P., and Thomä, N.H. (2008). Structural basis of UV DNA-damage recognition by the DDB1-DDB2 complex. Cell *135*, 1213-1223.

Sugasawa, K. (2006). The xeroderma pigmentosum group C protein complex and ultraviolet-damaged DNA-binding protein: functional assays for damage recognition factors involved in global genome repair. Methods Enzymol *408*, 171-188.

Tarpey, P.S., Raymond, F.L., O'Meara, S., Edkins, S., Teague, J., Butler, A., Dicks, E., Stevens, C., Tofts, C., Avis, T.*, et al.* (2007). Mutations in CUL4B, which encodes a ubiquitin E3 ligase subunit, cause an X-linked mental retardation syndrome associated with aggressive outbursts, seizures, relative macrocephaly, central obesity, hypogonadism, pes cavus, and tremor. Am J Hum Genet *80*, 345-352.

Vagin, A., and Teplyakov, A. (1997). MOLREP: an automated program for molecular replacement. Journal of Applied Crystallography.

Vassylyev, D.G., Kashiwagi, T., Mikami, Y., Ariyoshi, M., Iwai, S., Ohtsuka, E., and Morikawa, K. (1995). Atomic model of a pyrimidine dimer excision repair enzyme complexed with a DNA substrate: structural basis for damaged DNA recognition. Cell *83*, 773-782.

Yang, W. (2008). Structure and mechanism for DNA lesion recognition. Cell Res *18*, 184-197.

Yasuda, T., Sugasawa, K., Shimizu, Y., Iwai, S., Shiomi, T., and Hanaoka, F. (2005). Nucleosomal structure of undamaged DNA regions suppresses the non-specific DNA binding of the XPC complex. DNA repair *4*, 389-395.

Zhou, C., Wee, S., Rhee, E., Naumann, M., Dubiel, W., and Wolf, D.A. (2003). Fission yeast COP9/signalosome suppresses cullin activity through recruitment of the deubiquitylating enzyme Ubp12p. Molecular cell *11*, 927-938.

Figure S1

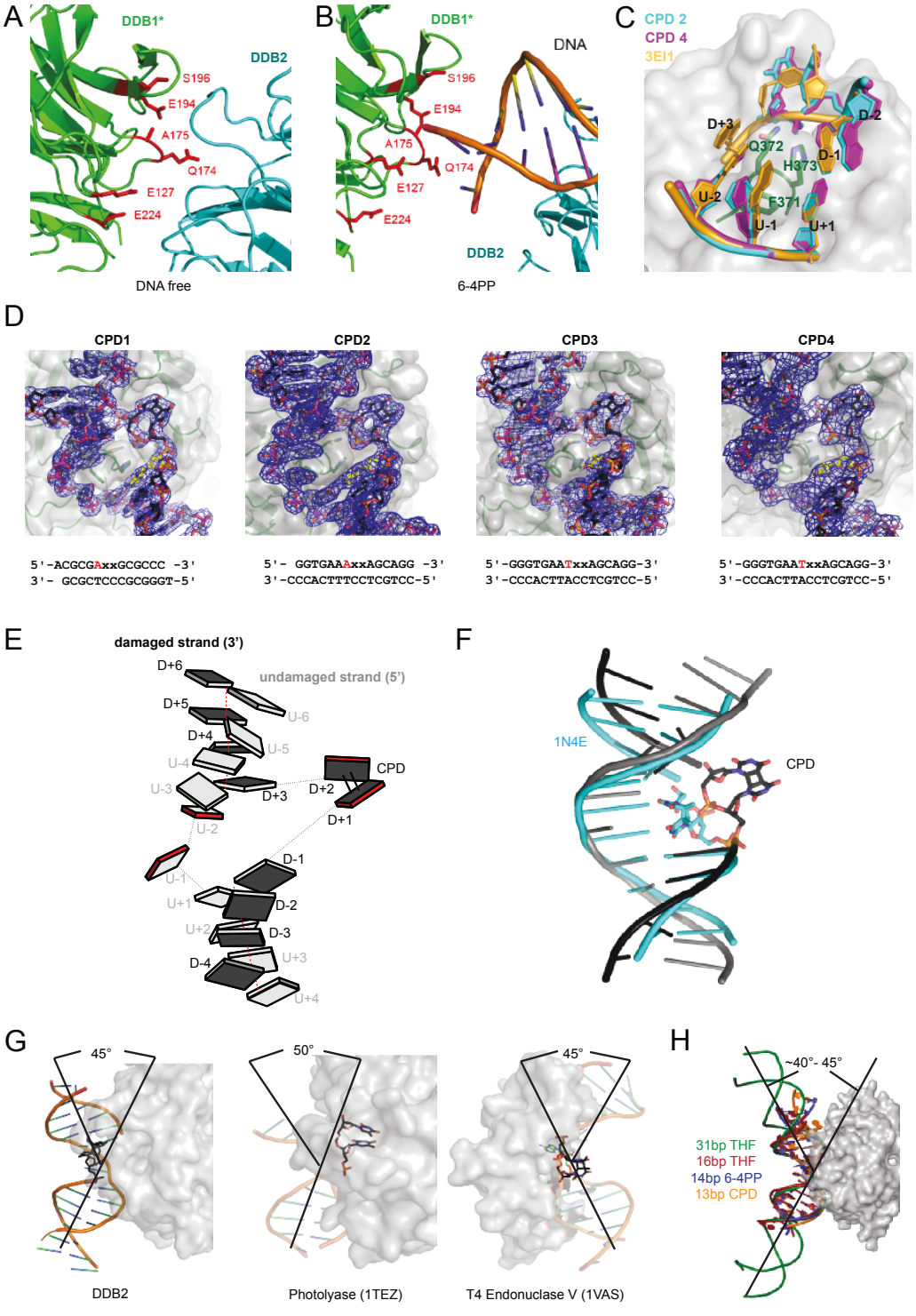
A
DDB1*
DDB2
S196
E194
A175
Q174
E127
E224
DNA free
B
DDB1*
DNA
S196
E194
A175
Q174
E127
E224
DDB2
6-4PP
C
CPD 2
CPD 4
3EI1
D+3
D-2
Q372
H373
D-1
U-2
F371
U-1
U+1
D
CPD1
CPD2
CPD3
CPD4
5'-ACGCGAxxGCGCCC -3'
3'- GCGCTCCCGCGGGT-5'
5'- GGTGAAAxxAGCAGG -3'
3'-CCCACTTTCCTCGTCC-5'
5'-GGGTGAATxxAGCAGG-3'
3'-CCCACTTACCTCGTCC-5'
5'-GGGTGAATxxAGCAGG-3'
3'-CCCACTTACCTCGTCC-5'
E
damaged strand (3')
undamaged strand (5')
D+6
D+5
D+4
D+3
D+2
D+1
D-1
D-2
D-3
D-4
U-6
U-5
U-4
U-3
U-2
U-1
U+1
U+2
U+3
U+4
CPD
F
1N4E
CPD
G
45°
50°
45°
DDB2
Photolyase (1TEZ)
T4 Endonuclase V (1VAS)
H
~40°- 45°
31bp THF
16bp THF
14bp 6-4PP
13bp CPD

Figure S2

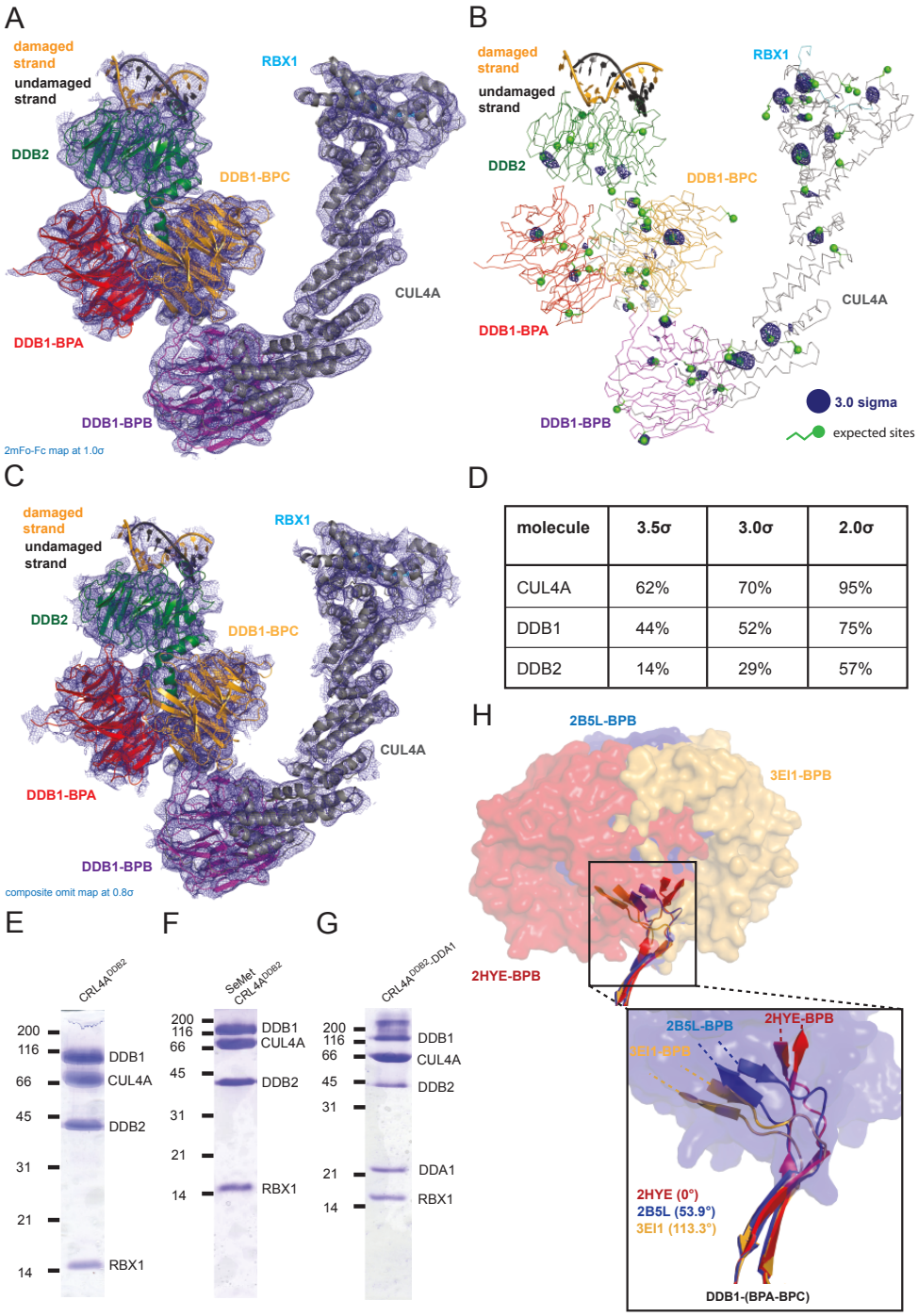

molecule	3.5σ	3.0σ	2.0σ
CUL4A	62%	70%	95%
DDB1	44%	52%	75%
DDB2	14%	29%	57%

Figure S3

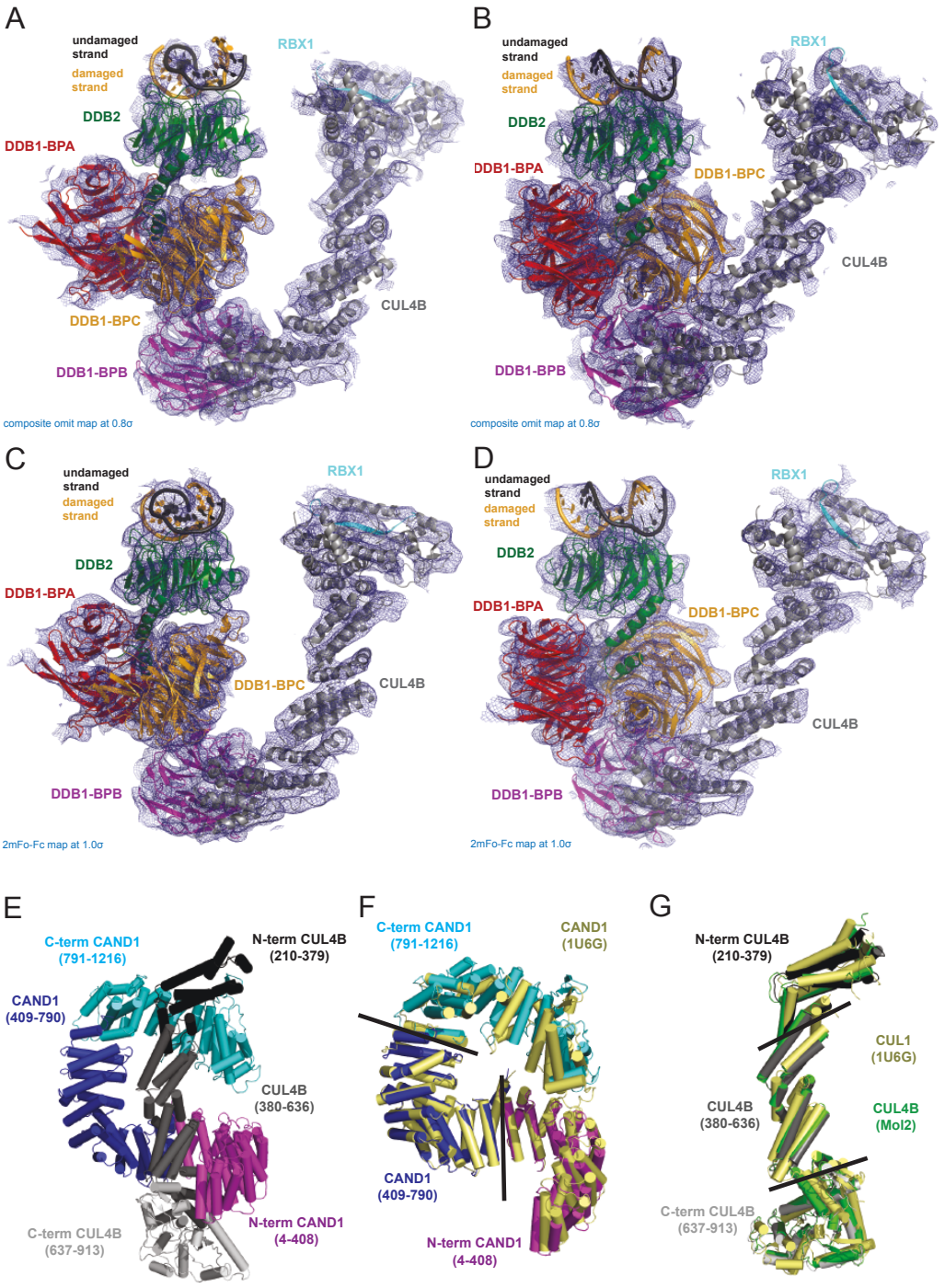
A
undamaged strand
damaged strand
DDB2
DDB1-BPA
RBX1
CUL4B
DDB1-BPC
DDB1-BPB
composite omit map at 0.8σ
B
undamaged strand
damaged strand
DDB2
DDB1-BPA
RBX1
DDB1-BPC
CUL4B
DDB1-BPB
composite omit map at 0.8σ
C
undamaged strand
damaged strand
DDB2
DDB1-BPA
RBX1
DDB1-BPC
CUL4B
DDB1-BPB
2mFo-Fc map at 1.0σ
D
undamaged strand
damaged strand
DDB2
DDB1-BPA
RBX1
DDB1-BPC
CUL4B
DDB1-BPB
2mFo-Fc map at 1.0σ
E
C-term CAND1 (791-1216)
N-term CUL4B (210-379)
CAND1 (409-790)
CUL4B (380-636)
N-term CAND1 (4-408)
C-term CUL4B (637-913)
F
C-term CAND1 (791-1216)
CAND1 (1U6G)
CAND1 (409-790)
N-term CAND1 (4-408)
G
N-term CUL4B (210-379)
CUL1 (1U6G)
CUL4B (380-636)
CUL4B (Mol2)
C-term CUL4B (637-913)

Figure S4

A

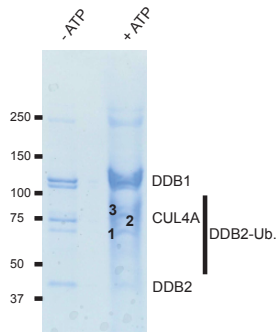

B

Ub. site	MS peptide hsDDB2 sequence	Mr (obs)	Mr (calc)	Δppm	Ions score	conserved
K5	K. KRPETQKTSEIVLRPR. N	2165.2006	2165.2029	-1	17	++
K11	K. RPETQKTSEIVLRPR.N	1923.0617	1923.0650	-2	47	+
K35	R. SPLELEPEAKK. L	1353.7141	1353.7139	0	52	+++
K40	K. LCAKGSGPSR. R	1145.5615	1145.5611	0	40	+
K151	K. DKPTFIKGIGAGGSITGLK. F	1973.0937	1973.0946	0	15	++

C

K40
ms2 573.78 2+

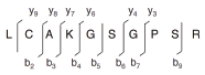

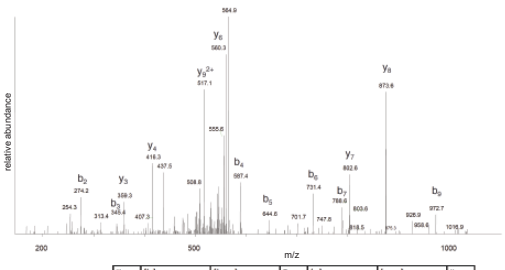

#	(b)	(b++)	Seq.	(y)	(y++)	#
1	114.0913	57.5493	L			10
2	274.1220	137.5646	C	1033.4844	517.2458	9
3	345.1591	173.0832	A	873.4537	437.2305	8
4	587.2970	294.1521	K	802.4166	401.7119	7
5	644.3185	322.6629	G	560.2787	280.6430	6
6	731.3505	366.1789	S	503.2572	252.1323	5
7	788.3719	394.6896	G	416.2252	208.6162	4
8	885.4247	443.2160	P	359.2037	180.1055	3
9	972.4567	486.7320	S	262.1510	131.5791	2
10			R	175.1190	88.0631	1

D

K11
ms2 642.36 3+

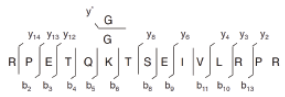

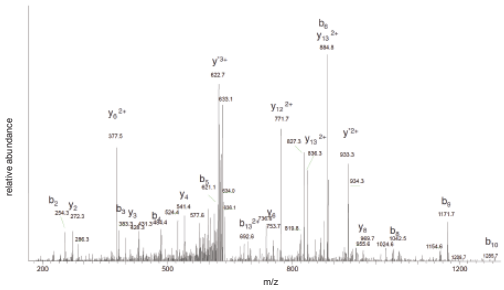

#	(b)	(b++)	Seq.	(y)	(y++)	#
1	157.1084	79.0578	R			15
2	254.1612	127.5842	P	1767.9712	884.4892	14
3	383.2037	192.1055	E	1670.9184	835.9628	13
4	484.2514	242.6293	T	1541.8758	771.4415	12
5	612.3100	306.6586	Q	1440.8281	720.9177	11
6	854.4479	427.7276	K	1312.7696	656.8884	10
7	955.4956	478.2514	T	1070.6317	535.8195	9
8	1042.5276	521.7674	S	969.5840	485.2956	8
9	1171.5702	586.2887	E	882.5520	441.7796	7
10	1284.6543	642.8308	I	753.5094	377.2583	6
11	1383.7227	692.3650	V	640.4253	320.7163	5
12	1496.8067	748.9070	L	541.3569	271.1821	4
13	1652.9078	826.9576	R	428.2728	214.6401	3
14	1749.9606	875.4839	P	272.1717	136.5895	2
15			R	175.1190	88.0631	1

E

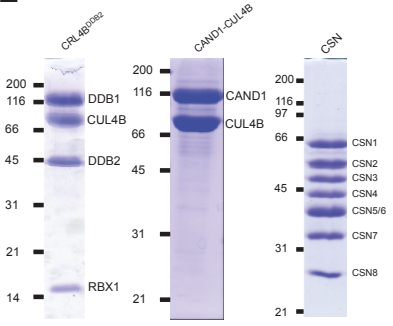

F

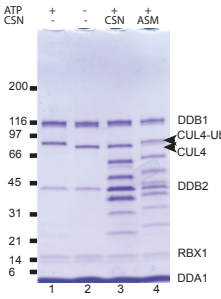

G

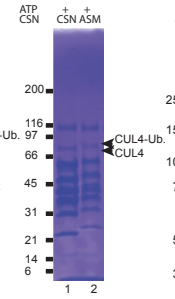

H

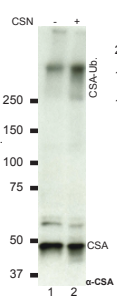

I

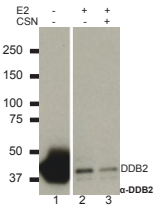

Figure S5

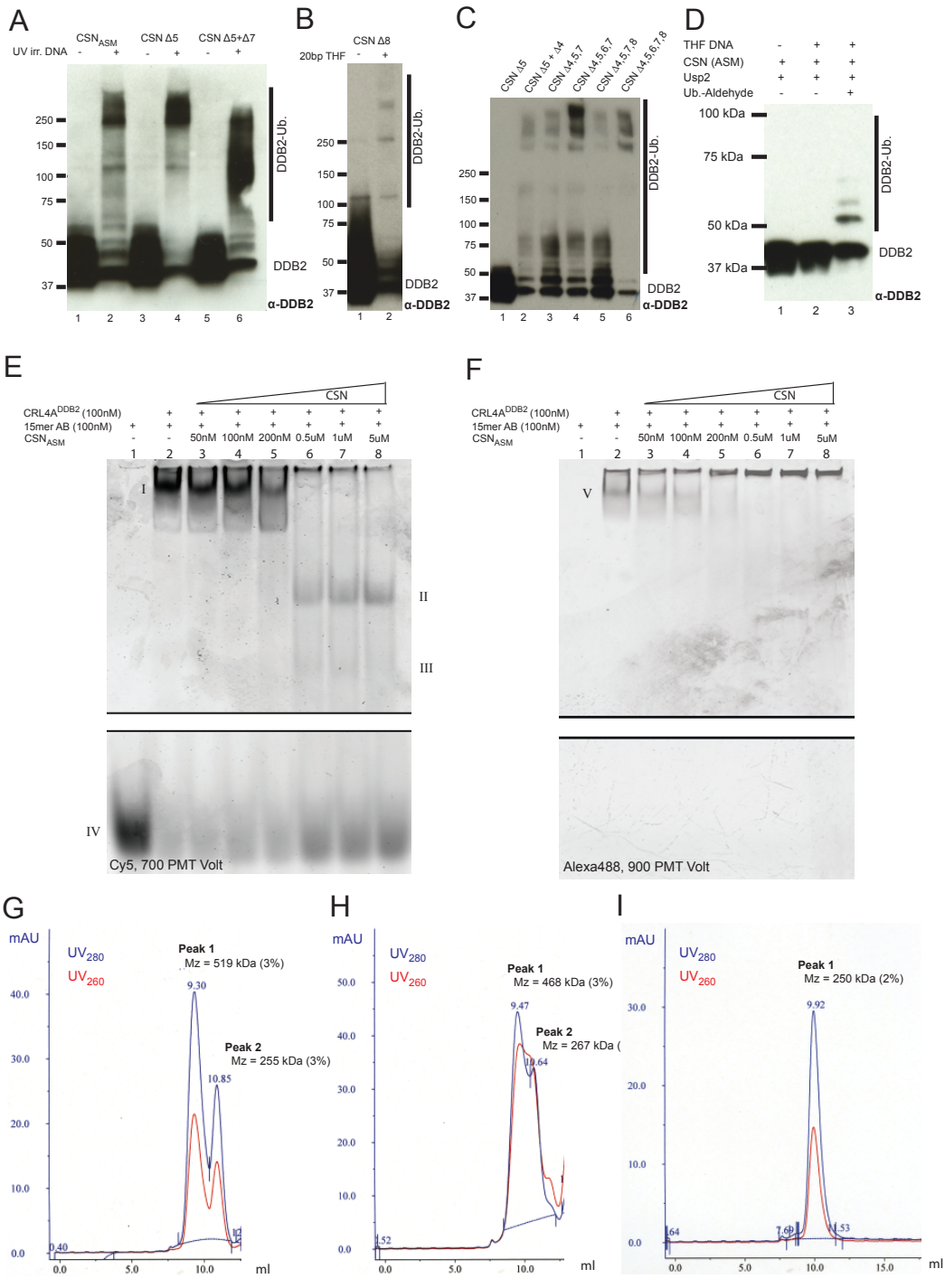
A
CSN_ASM
CSN Δ5
CSN Δ5+Δ7
UV irr. DNA
DDB2-Ub.
DDB2
α-DDB2
B
CSN Δ8
20bp THF
C
CSN Δ5
CSN Δ5 + Δ4
CSN Δ4,5,7
CSN Δ4,5,6,7
CSN Δ4,5,7,8
CSN Δ4,5,6,7,8
D
THF DNA
CSN (ASM)
Usp2
Ub.-Aldehyde
100 kDa
75 kDa
50 kDa
37 kDa
E
CRL4A^DDB2 (100nM)
15mer AB (100nM)
CSN_ASM
CSN
50nM 100nM 200nM 0.5uM 1uM 5uM
I
II
III
IV
Cy5, 700 PMT Volt
F
V
Alexa488, 900 PMT Volt
G
mAU
UV280
UV260
Peak 1
Mz = 519 kDa (3%)
Peak 2
Mz = 255 kDa (3%)
ml
H
Peak 1
Mz = 468 kDa (3%)
Peak 2
Mz = 267 kDa (
I
Peak 1
Mz = 250 kDa (2%)

Figure S6

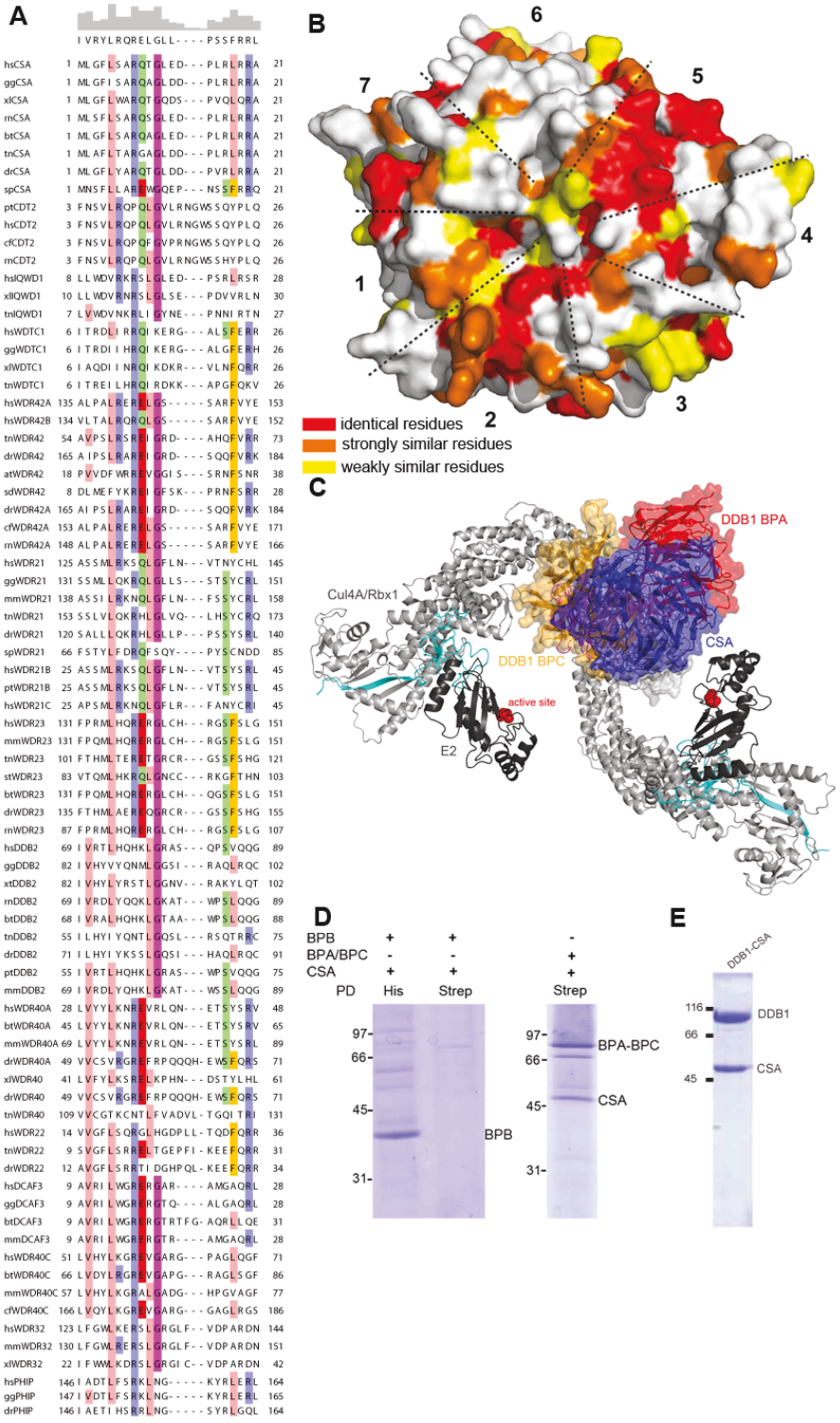
A
B
6
7
5
4
1
2
3
identical residues
strongly similar residues
weakly similar residues
C
DDB1 BPA
Cul4A/Rbx1
CSA
DDB1 BPC
active site
E2
D
BPB
BPA/BPC
CSA
PD
His
Strep
Strep
97-
66-
45-
31-
BPB
BPA-BPC
CSA
E
DDB1-CSA
116
66
45
DDB1
CSA

Figure S7

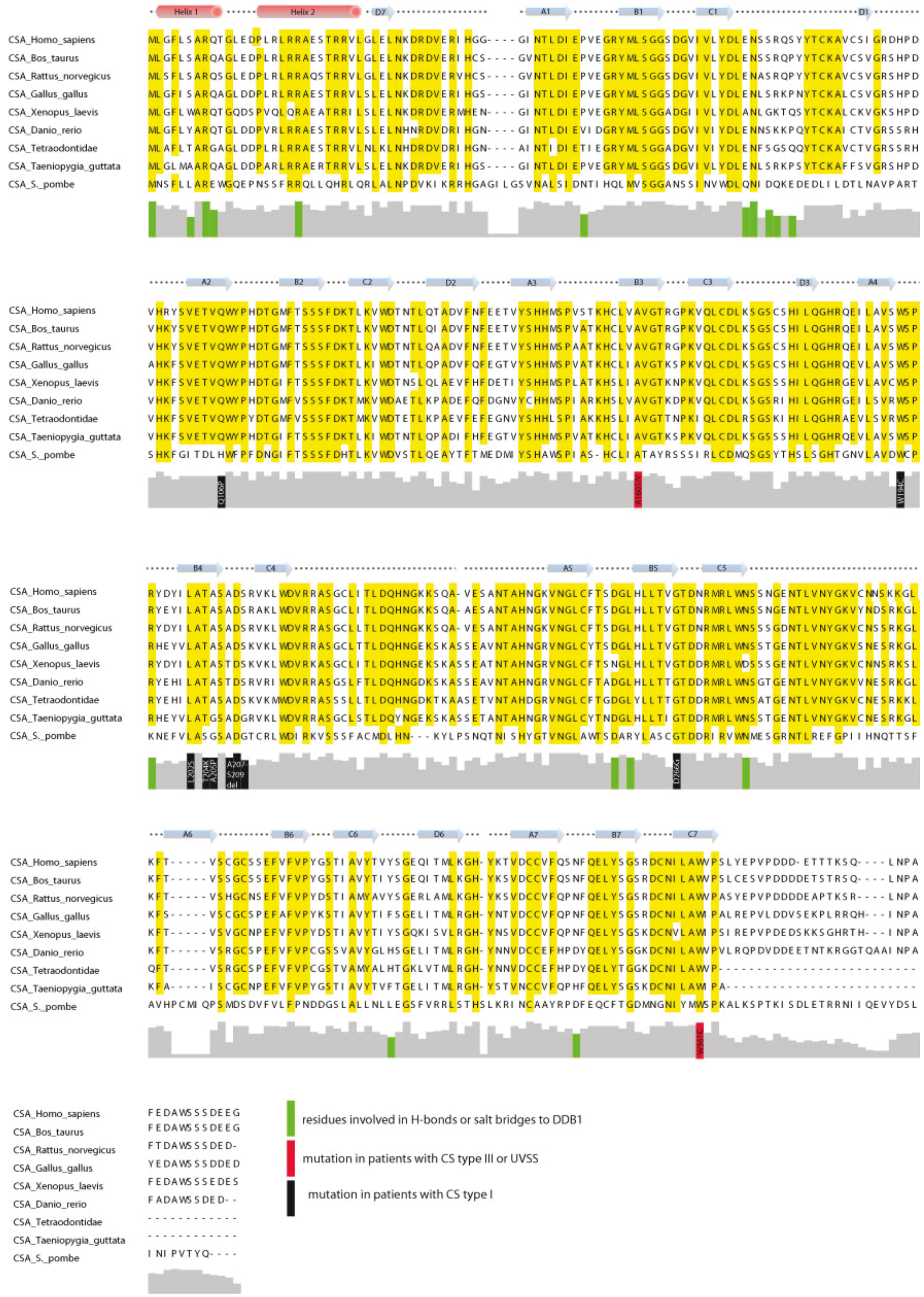
CSA_Homo_sapiens
CSA_Bos_taurus
CSA_Rattus_norvegicus
CSA_Gallus_gallus
CSA_Xenopus_laevis
CSA_Danio_rerio
CSA_Tetraodontidae
CSA_Taeniopygia_guttata
CSA_S._pombe
residues involved in H-bonds or salt bridges to DDB1
mutation in patients with CS type III or UVSS
mutation in patients with CS type I

Chapter 3: Detecting UV-lesions in the genome: The modular CRL4 ubiquitin ligase does it best!

(published manuscript).

Andrea Scrima[1], Eric S. Fischer[1,2], Gondichatnahalli M. Lingaraju[1], Kerstin Böhm[1], Simone Cavadini[1], Nicolas H. Thomä[1]*

[1] Friedrich Miescher Institute for Biomedical Research, Maulbeerstrasse 66, CH-4058 Basel, Switzerland
[2] Universität Basel, Petersplatz 10, CH-4003 Basel, Switzerland
*corresponding author

FEBS Letter *2011 Sep 16, Volume 585(18), pg. 2818-2825*

Summary

The DDB1-DDB2-CUL4-RBX1 complex serves as the primary detection device for UV-induced lesions in the genome. It simultaneously functions as a CUL4 type E3 ubiquitin ligase. We review the current understanding of this dual function ubiquitin ligase and damage detection complex. The DDB2 damage binding module is merely one of a large family of possible DDB1-CUL4 associated factors (DCAF), most of which are substrate receptors for other DDB1-CUL4 complexes. DDB2 and the Cockayne syndrome A protein (CSA) function in nucleotide excision repair, whereas the remaining receptors operate in a wide range of other biological pathways. We will examine the modular architecture of DDB1-CUL4 in complex with DDB2, CSA and CDT2 focusing on shared architectural, targeting and regulatory principles.

author contributions: AS, ESF, GML, KB, SM and NHT wrote the manuscript. AS designed the figures.

Detecting UV-lesions in the genome: The modular CRL4 ubiquitin ligase does it best!

Andrea Scrima, Eric S. Fischer, Gondichatnahalli M. Lingaraju, Kerstin Böhm, Simone Cavadini, Nicolas H. Thomä*

*Corresponding author

Friedrich Miescher Institute for Biomedical Research, Maulbeerstrasse 66, CH-4058 Basel, Switzerland.

Abstract:

The DDB1-DDB2-CUL4-RBX1 complex serves as the primary detection device for UV-induced lesions in the genome. It simultaneously functions as a CUL4 type E3 ubiquitin ligase. We review the current understanding of this dual function ubiquitin ligase and damage detection complex. The DDB2 damage binding module is merely one of a large family of possible DDB1-CUL4 associated factors (DCAF), most of which are substrate receptors for other DDB1-CUL4 complexes. DDB2 and the Cockayne syndrome A protein (CSA) function in nucleotide excision repair, whereas the remaining receptors operate in a wide range of other biological pathways. We will examine the modular architecture of DDB1-CUL4 in complex with DDB2, CSA and CDT2 focusing on shared architectural, targeting and regulatory principles.

Key words: Genome stability, CUL4, CDT2, DDB2 and CSA

Repair of UV-induced DNA lesions is facilitated by CUL4 type E3 ubiquitin transferases

The nucleotide excision repair (NER) pathway safeguards the genome against bulky DNA adducts and UV-light induced pyrimidine dimers [1-4]. If left unrepaired, these lesions interfere with the progression of transcription [5] and replication [6], requiring extensive post replicative repair. It only very recently emerged that NER requires targeted ubiquitination events in vivo [7]. The two major CUL4 E3 ubiquitin ligase substrate receptors in NER are the Cockayne syndrome protein A (CSA) and the damage DNA binding protein 2 (DDB2), both of which are connected to the ligase through the DDB1 adaptor subunit. Proteomic studies have revealed that the remainder of the CUL4-DDB1 RING LIGASE (CRL4) family comprises more than fifty different substrate receptor complexes. Additionally, two closely related CUL4 human paralogs, CUL4A and CUL4B have been identified which differ mainly in a large N-terminal extension present only in CUL4B [8]. By examining three of the best characterized CRL4 ubiquitin E3 ligases, all of which function in the UV-response to damage ($CRL4^{DDB2}$, $CRL4^{CSA}$ and $CRL4^{CDT2}$), we will highlight common architectural principles and detail our current understanding of CRL4 targeting and regulation.

Nucleotide Excision Repair, an overview

NER consists of two branches that differ in the mechanism of lesion detection: in transcription coupled repair (TCR) damaged DNA bases initiate NER through RNA polymerase II stalling [9, 10]; in global genome repair (GGR) the non-transcribed genome is continuously interrogated for DNA damage through specialized surveillance protein complexes including XPC-HR23B [11, 12] and DDB1-DDB2 [2]. TCR and GGR are thought to ultimately converge into a common pathway comprising: (i) local scanning for the lesion and duplex unwinding by the 10 subunit TFIIH complex [7, 13], (ii) 5' incision through the XPF-ERCC1 endonuclease [14], (iii) initiation of DNA gap re-synthesis and 3' incision catalysed by XPG, (iv) removal of a 24-32 bp damage-containing oligonucleotide, (v) and nick ligation. Overall more than 30 polypeptides are involved in this process resulting in error free repair [15]. NER generally proceeds in a rapid fashion and does not interfere with cell

cycle progression. Checkpoint activation is typically only triggered once the damage is considered too extensive to be repaired [16]. Mutations in NER components result in a number of rare autosomal recessive diseases including Xeroderma pigmentosum (XP), Cockayne syndrome (CS & XP-CS), UV-sensitive syndrome (UVSS) and Trichothiodystrophie (TTD) [3, 9, 17, 18]. These types of DNA repair defects are frequently associated with various forms of UV-sensitivity, neurological and development complications, and in case of XP pronounced skin cancer predisposition.

First responders: the $CRL4^{DDB2}$ ligase in pyrimidine dimer detection in vivo.

UV-light transforms adjacent pyrimidine bases into covalent photo-dimers. The majority of these cross-links are cyclobutane pyrimidine dimers (CPD), and to a lesser extent 6-4 pyrimidine-pyrimidone photoproducts (6-4PP) [19, 20]. Detecting pyrimidine dimers within a large genome poses an exquisite challenge. The DDB1-DDB2 complex plays an important role in the initial pyrimidine dimer recognition in vivo [21-25]. Within the DDB1-DDB2 complex, the DDB2 subunit is found mutated in patients belonging to Xeroderma pigmentosum complementation group E (XP-E) [26]. Cells lacking DDB2 are substantially impaired in the repair of CPDs [27-29]. Recent X-ray crystallographic studies provided the molecular mechanism of high affinity and specificity 6-4PP recognition by DDB1-DDB2 (Figure 1) [30]. DDB1-DDB2 largely comprises four WD40 propeller domains. The 127 kDa DDB1 protein contains three WD40-domains (BPA, BPB & BPC) [31]. The sides of the DDB1-BPA and BPC propeller domains are facing each other at an angle of ~60° and form the binding cavity for DDB2 [30]. DDB2 binding to DDB1 is mediated by the N-terminal helix-loop-helix motif preceding the DDB2 WD40 propeller [30, 32]. The DDB1-DDB2 complex binds damage-containing DNA duplexes exclusively through the DDB2 WD40 propeller domain. The DDB1-BPB domain, which is located on the opposing face of the DDB1-DDB2 module, provides the attachment site for the cullin4 ubiquitin ligase subunit [33] (Figure 1). In vivo, DDB1-DDB2 exists in complex with both CUL4A-RBX1 and CUL4B-RBX1 paralogs [34-37]. Architecturally, DDB1 acts as an adaptor linking the E3 ubiquitin ligase (CUL4) to the UV-damage detection module

(DDB2). The protein complex specialised for the recognition of pyrimidine dimers in human cells thus doubles as an E3 ubiquitin ligase complex.

The mechanism of pyrimidine dimer recognition: Showing DNA damage the damage recognition finger

DDB2 utilizes a conserved tri-peptide Phe-Gln-His (FQH) hairpin to interrogate the duplex for damage. This hairpin forms a surprisingly rigid unit that inserts into the minor groove, at the lesion, in a finger like fashion. Concomitant with insertion of the damage recognition finger, the lesion is flipped out and stabilised in a hydrophobic pocket present at the DDB2 surface (Figure 1). This pocket serves to restrict the size of the modification accommodated, biasing DDB2 towards photo-dimer recognition and preventing larger base adducts from being bound. Co-crystallisation of DDB1-DDB2 with a single-nucleotide abasic site (AP) lesion, embedded in a duplex, revealed an almost identical dual base pair flip of the abasic site and the adjacent 3´ undamaged base. This is surprising, as unlike in the case of 6-4PP, only one base is damaged in the AP containing duplex. The damage recognition finger, which spans exactly two nucleotides, therefore inherently triggers a di-nucleotide flip upon insertion. This flip is independent of whether the adjacent 3' base is modified or not [30]. Contrary to the common notion, it was concluded that DDB2 does not appear to recognize the 'helix distortion of the lesions' per se, as the DDB2 bound DNA conformation differs significantly from those of damaged duplexes free in solution. DDB2 rather tests whether the damage recognition 'finger' can be inserted into the duplex, assessing the DNA conformation around the damage, and examines whether the DNA can fit to the rigid DDB2 binding 'mold'. The structural basis of high affinity CPD recognition, the biological role of the DDB2 in which it excels above all other known human damage detection factors, currently remains elusive.

UV-lesion detection in chromatin: the missing link

The challenging task of detecting UV-lesions within vast genomes is further compounded by the presence of chromatin. In chromatin, the DNA is wrapped around an octamer of core histones, with additional linker histones implicated in further compaction. In vivo, the position of the photo-dimers respective to

the nucleosome core particle depends on the kind of lesion present: the strongly duplex distorting 6-4PP is found randomly localized in nucleosomes and linkers [38], while the highly mutagenic and difficult to detect CPD clusters are found in surface exposed regions of nucleosome [39]. How then are these lesions detected and repaired within nucleosomes? While the global genome repair branch of NER can be effectively reconstituted on naked DNA, the presence of nucleosomes was clearly inhibitory for repair in vitro [40]. NER inhibition occurred on multiple levels including damage recognition [41, 42]. Nucleosome remodeling complexes can function as a principal means to remove nucleosomes, providing NER with a DNA substrate that more closely resembles the naked DNA. Several chromatin remodeling complexes have been implicated in NER. Cells in which chromatin remodelers Ino80 [43] and SWI/SNF (Brg1) [44, 45] have been deleted become UV-sensitive. While remodelers offer a potential solution to facilitate downstream repair processes, they are unlikely to provide a means to directly find the damage. How then is damage being read out in chromatin? Recent studies focusing on nucleosome dynamics in the presence and absence of damage indicated that the DNA around the octamer core unwraps leaving proteins sufficient time (and room) to gain access to the lesion [46, 47]. In vivo, DDB2 localizes to chromatin in a UV-dependent manner [48, 49] and remains associated with mono-nucleosomes upon treatment with micrococcal nuclease [35]. DDB1-DDB2 is therefore a likely candidate for recognizing pyrimidine dimers embedded in nucleosome core particles. The direct interactions between NER damage detection factors including DDB1-DDB2, XPC/Rad4 and chromatin remodelers has been described [43, 45, 50] offering a principal means to recruit remodelers and facilitate NER in an otherwise repressive chromatin environment.

DDB1-DDB2 mediated histone ubiquitination surrounding the sites of damage

Additional evidence implicating DDB1-DDB2-CUL4-RBX1 ($CRL4^{DDB2}$) in damage recognition in chromatin came from studies reporting $CRL4^{DDB2}$ dependent ubiquitination of histones H2A, H3 and H4 in response to UV irradiation [51-53]. This histone ubiquitination response appeared to be largely

mono-ubiquitination. In vitro, CUL4 mediated ubiquitination gives rise to poly-ubiquitin chains. Whether a deubiquitination enzyme, a specific E2 transferase, or a regulatory protein serves to restrict the extent of ubiquitination in vivo, is currently not known. $CRL4^{DDB2}$ mediated ubiquitination of histones is likely to be local and restricted to the immediate ~100Å vicinity of the lesion [30, 54]. In vitro histone ubiquitination by $CRL4^{DDB2}$ altered the stability of the nucleosome core driving partial histone eviction [53]. Histone ubiquitination with concomitant destabilisation of neighboring nucleosomes thus offers an additional mechanism to evict histones and drive assembly of the NER machinery in a chromatin environment (Figure 2) [30, 55]. Mono-ubiquitination of histones could, in addition, function as a recruitment signal for additional auxiliary repair factors (see below).

Ubiquitination overseeing damage handover from DDB2 to XPC

$CRL4^{DDB2}$ ubiquitination has been implicated in resolving one of the central conundrums of NER damage recognition [25]: while DDB1-DDB2 has the highest affinity for UV-induced photo-dimers in vitro, and appears to be the first protein complex at the lesion in vivo [23, 24, 41], it is dispensable in vitro [15]. XPC, in contrast binds 6-4PP with two orders of magnitude lower affinity than DDB2 [25, 56, 57] and has no discernable affinity for CPD, yet is essential for NER both in vitro and in cells. As DDB1-DDB2 is required for efficient XPC recruitment to chromatin [23], the question arises as to how damage is handed over from DDB2 to XPC. Recent work demonstrated that CRL4DDB2 targets XPC, as well as DDB2 for ubiquitination in a UV-dependent fashion [25]. Poly-ubiquitination of DDB2 ablates DNA binding by DDB1-DDB2 and results in proteasome mediated DDB2 degradation [58, 59]. Poly-ubiquitination of XPC, on the other hand, does not appear to affect DNA damage binding [25] and XPC is protected from immediate proteasomal degradation, likely through association with HR23 [60-62]. This and further studies [63] place DDB1-DDB2 in the recruitment of XPC to the sites of damage in chromatin, with a subsequent handover of the lesion from DDB2 to XPC in an ubiquitin dependent manner [7, 30]. XPC thereby emerges as an indispensable core component of NER, which in vivo does, however, require

assistance from DDB1-DDB2 in finding specific lesions. The exact molecular nature of the damage handover complex from DDB2 to XPC remains elusive. The damage probing hairpin of both DDB2 (hsDDB2: 334FQH336) and XPC (hsXPC: 799FHGGYS804) cannot simultaneously engage with the lesion damage due to large steric clashes [30, 64]. Three, mutually non-exclusive possibilities for such a handover complex have been considered: (i) XPC binding, via the TGD domain, to the undamaged duplex 3´of the lesion with DDB2 engaging the pyrimidine dimer; (ii) XPC attaching to DDB2 through protein-protein interaction [25], and (iii) in a more indirect fashion XPC recruitment by ubiquitination (for example of the histone or DDB2) as the HR23 subunit also carries a UBA domain [65]. In particular in the latter mechanism $CRL4^{DDB2}$ could recruit XPC to lesions such as CPDs, for which XPC has no measurable affinity by itself, yet is required for repair in vivo. Interpretation of the role of CRL4 mediated ubiquitination in NER has been complicated [66], also by the finding that mice carrying a Cul4a deletion in skin cells are less likely to develop UV-induced skin cancers [67]. As CUL4A is involved in many different cellular pathway regulated in response to UV, such as the CRL4CDT2-p21 controlled by UV cell cycle checkpoint, it is currently unclear which CRL4 adaptor is responsible for the mouse cancer phenotype.

A related DDB1-CSA-CUL4 ligase in Cockayne syndrome

A general feature of DDB1-CUL4 cullin E3 ligases is their modularity (Figure 1). Largely through proteomic studies a number of DDB1-CUL4 associated proteins have been identified [68]. The family of these proteins is known as DCAFs (DDB1-CUL4-associated-factor) [33], DWD-proteins (DDB1-binding and WD40-repeat) [69] or CDW-proteins (CUL4- and DDB1-associated WDR proteins) [70]. These DCAFs fall in two potential categories: substrate receptors recruiting CRL4 complexes and regulators of CUL4 function. DDB2 thereby is one out of more than fifty possible substrate receptors described. DDB2 recruits the ligase to sites of damages, whereas the majority of these CUL4-DDB1 ligase receptors, including CSA [71], are likely to recognize protein epitopes, or posttranslational modifications of

proteins. In a ‘plug and play’ fashion these receptors can be exchanged, customizing CRL4 substrate specificity to different pathways (Figure 1).

The role of the Cockayne syndrome A protein (CSA) in transcription coupled repair.

We will first examine the Cockayne syndrome A $CRL4^{CSA}$ ligase complex involved in transcription coupled repair of damages located on the actively transcribed strand [4, 9, 72-74]. Cockayne syndrome is a rare autosomal disease with mutations in two proteins CSA [75] and CSB [76]. The hallmarks of Cockayne syndrome include developmental defects, photosensitivity, premature aging and mental retardation [3, 77]. While CSA is integrated in a CRL4CSA ubiquitin ligase complex [35], CSB functions as SWI/SNF chromatin remodeler [78]. CSA and CSB both appear intertwined with the general transcription machinery [13]. Mutations in CSA and CSB are indistinguishable on the patient level arguing for a common pathway. Upon RNA polymerase II (RNAPII) stalling, both CSA and CSB are required for repair and transcription restart. CSB has been implicated in the remodeling of stalled RNAPII complexes to which it binds tightly in the presence of damage [79, 80]. CSA is translocated to the nucleus, in a CSB-dependent manner, and co-localises with CSB at sites of stalled RNAPII [81]. Arrival of CSA is required for recruitment of HMGN1 (high mobility group nucleosome-binding domain-containing protein 1), XAB2 (XPA-binding protein 2) and transcript elongation factor TFIIS [82].

Five lines of evidence suggest the involvement of the ubiquitin proteasome system in TCR: (i) CSA is constitutively found in complex with DDB1 and CUL4 [35], (ii) ubiquitination of CSB was observed under high UV conditions, with proteasome dependent CSB degradation during later stages of TCR [71], (iii) UV-dependent CSB degradation is absent in cells lacking CSA but can be restored by exogenous CSA, and (iv) the DDB1-CSA-CUL4A ligase was capable of CSB ubiquitination in vitro; (v) finally, CSB has a ubiquitin binding (UBA) domain which was found essential for CSB function in TCR [83]. The structure and architecture of the CRL4CSA complex is currently unknown. The current data is consistent with CSB functioning as a $CRL4^{CSA}$ recruitment and ubiquitination substrate [71]. Other, as yet

unidentified targets cannot be ruled out at present, however. While the $CRL4^{DDB2}$ and $CRL4^{CSA}$ ligase complexes differ substantially in respect to their function, there are interesting mechanistic parallels: the respective main targets of $CRL4^{DDB2}$ and $CRL4^{CSA}$, XPC-HR23 and CSB both carry UBA domains believed to play important regulatory roles in NER. What these UBA domains recognize and what functional consequences UBA target binding has, remains an active area of research.

The role of DDB1-CDT2-CUL4 in genomic stability and beyond

DDB1-CDT2-CUL4 ($CRL4^{CDT2}$), a third essential CUL4 ligase, oversees the S/G2 cell cycle transitions through degradation of the replication licensing factor CDT1 [84-86]. Additional human targets include the cell cycle regulator p21 [87, 88] and the histone methyltransferase SET8/Pr-SET7 [89-92]. Degradation of these substrates proceeds in a DNA replication and UV-dependent manner. In S. pombe $CRL4^{Cdt2}$ has been implicated in the ubiquitination of Spd1, a ribonucleotide reductase inhibitor [93] and Epe1 [94], which assists in the sculpting of heterochromatic boundaries. In most cases examined, CDT2 has been shown to interact with its substrates through a conserved, PIP (PCNA-interacting peptide) box containing degron motif in a manner dependent on the proliferation cell nuclear antigen (PCNA) [86, 95-100]. The requirement of two polypeptides (PCNA + PIP containing target) for substrate recognition is intriguing, and might suggest that CDT2 uses PCNA as an additional level of proofreading in proper substrate selection.

CSN functions as a master regulator of cullin type E3 ligases

The COP9 signalosome (CSN) has been reported to play a central role in the regulation of all cullin E3 ligases (Figure 2) [35, 101]. Similar to other cullin-RING E3 ligases [102], the CUL4 E3 ligase is activated through attachment of NEDD8, a small ubiquitin-like modifier [35, 54]. The removal of NEDD8 from cullins is catalysed through the metallo-isopeptidase activity of the COP9 signalosome (CSN) [103, 104]. CSN is an eight subunit, ~350 kDa protein complex conserved in all eukaryotes [35, 105-107]. CSN shares significant sequence and structural homology with the components of the 19S

proteosome lid. The first three-dimensional EM structure of the CSN complex at 25 Å resolution shows a central cleft along with two CSN segments corresponding to CSN1/2/3/8 and CSN4/5/6/7 [108-110]. The exact mode of cullin binding to CSN is currently not known.

CSN a master regulator of ubiquitin ligase, challenges for regulation.

Detailed understanding of CSN regulation is complicated by the observed discrepancies between biochemical and genetic properties of the complex. Gene deletion studies, for example, demonstrated that S. pombe csn1- and csn2- strains are sensitive to UV and ionizing radiation, along with a slow DNA replication phenotype [111, 112]. The catalytic csn5 deletion mutant, in contrast, did not display this pronounced phenotype [111], suggesting that the CSN function extends beyond catalytic cullin de-neddylation through the CSN5 isopeptidase. Intriguingly, despite being a master regulator of all cullins, CSN appears nevertheless able to differentially regulate CRL4 ligases in response to a common stimulus, such as UV: in the absence of UV-damage, CSN is associated with the un-neddylated $CRL4^{DDB2}$ and $CRL4^{CSA}$ complexes. Upon UV-damage, CSN dissociates from $CRL4^{DDB2}$ [35, 49] allowing its neddylation. At later time points, CSN de-neddylates and re-associates with the $CRL4^{DDB2}$ complex [113]. In TCR, on the other hand, $CRL4^{CSA}$ complexed to CSN rapidly locates to the damage site upon UV irradiation [35], and only dissociates at a much later time point. The PCNA-dependent ubiquitin-mediated proteolysis of CDT1 by $CRL4^{CDT2}$ for example also proceeds in response to UV, similarly mediated by CSN [100, 114]. The open question currently is whether CSN can selectively regulate defined CRL4-substrate receptor complexes in response to a given stimulus, while not interfering with the remainder of cullin-CSN complexes, and if so how it does achieve this kind of mechanistic specificity? Specialized CSN release CRL4 factors may exist regulating CSN release in response to cellular signals [49].

General principles of DDB1-DCAF-CUL4 architecture and regulation

What general architectural, targeting and regulatory principles can we deduce from these CRL4 complexes?

1. Architecture

All structurally characterized DDB1-DCAF complexes [32] utilize a helical motif in binding DDB1. This motif structurally resembles DDB2 helix1. Helix1 equivalents, although only moderately conserved, have been identified in the protein sequence of several DCAF proteins and are referred to as DDB-box (devoted to DDB1 binding) [115]. A number of WD40 containing DCAFs, however, do not appear to contain recognizable helical domains. It is currently unclear if those helices simply escape detection or whether fundamentally different DDB1 binding modes exist (Figure 1). When comparing different proteomic studies identifying DCAFs a common set of about 10 to 20 WD40 containing DCAFs have been consistently identified in most studies [33, 68-70, 99, 116], most of those appear to have helical motifs that could be used for DDB1 binding. Currently, there is no direct evidence for DDB1 binding mediated by WDXR motifs equivalent to the WDXR motif present in DDB2, which, as seen in the DDB1-DDB2 structure, is not part of the DDB1 interface or the DNA binding interface [30]. Yet mutation of the WDXR motif (R273H) in DDB2 gives rise to a mutant protein that is no longer able to bind to DNA damage, likely due to local unfolding of the propeller [57]. By analogy, it should thus be considered that mutation of the corresponding WDXR in other DCAFs could also indirectly ablate DDB1 binding through interference with WD40 folding, leaving the possibility that WDXR is not necessarily part of the DDB1-DCAF interface. Additional DDB1-DCAF structures are required to resolve this issue.

2. WD40 containing and non-WD40 containing DCAFs

The majority of DCAFs comprise WD40 propeller domains. We propose that those DCAFs who have helical elements preceding the WD40 propeller bind DDB1 in a manner resembling the DDB1-DDB2 complex. Other proteins have been classified as DCAFs that do not contain WD40 propeller domains. They often do have helical elements, nevertheless, and likely bind DDB1 using those motifs (Figure 1). Their mode of DDB1 attachment is likely to be equivalent to that seen in the SV5V-DDB1 [31] and DDB2 (helix1)-DDB1 structures.

3. Substrate recognition and ubiquitination

In case of WD40 containing DCAFs, the WD40 propeller is used for recruiting the CRL4 complex to the ubiquitination target. The ligand binding site of this WD40 propeller is expected to be located at the narrow face of the WD40 propeller cone, pointing away from DDB1 [30] (Figure 1). This ligand, which recruits the CRL4 complex via the WD40 of the substrate receptor, however, does not necessarily have to be the target that undergoes ubiquitination (see DDB2). As the ligase is able to span distances up to 100Å, the recruiting ligand and the ubiquitination target might therefore also be separate proteins/ligands (Figure 2).

4. Regulation

As outlined above, the CRL4 family is likely to be under the control of the signalosome (Figure 2). Substrate binding to the WD40 DCAF could also be regulated through posttranslational modification, as is commonly observed in the CUL1 family of targets [117]. For example, substrates might require phosphorylation prior to $CRL4^{DCAF}$ binding [118], with phosphorylation being the key determinant for binding/regulation. As is already evident in case of $CRL4^{CDT2}$, more complicated substrate binding schemes appear in operation, ensuring tight regulation of the ligase function. Additionally, a number of DDB1 binding proteins have been identified, for example DET1 [119] and DDA1 [116], which might have a regulatory role rather than serving as a substrate receptor.

Within the large CUL4 family [36], the $CRL4^{DDB2}$ ligase is currently the best understood representative in respect to its structure, function and regulation. While DDB2 recognizes damaged DNA as a recruiting substrate, the majority of the remaining receptors likely recognizes protein epitopes (or posttranslational modification thereof). More work will be needed to define what these epitopes are and how ubiquitination is regulated in these $CRL4^{DCAF}$ ligases. Furthermore, we will need to understand the functional role of the plethora of DDB1-CUL4 associated factors, which do not function as substrate receptors. Understanding CRL4 targeting and regulation is expected to significantly improve our understanding of the various biological pathways these proteins operate in.

Acknowledgements:

A.S. was supported by an EMBO LTF and Ambizione by the Swiss National Science Foundation. Work in the laboratory is supported by the Novartis Research Foundation, an ERC young investigator grant and grants by the Swiss National Science Foundation and OncoSuisse.

References:

1. Bergink S, Jaspers NGJ & Vermeulen W (2007) Regulation of UV-induced DNA damage response by ubiquitylation. DNA Repair (Amst) 6, 1231-1242.

2. Wittschieben B & Wood R (2003) DDB complexities. DNA Repair (Amst) 2, 1065-1069.

3. Hoeijmakers JH (2009) DNA damage, aging, and cancer. N Engl J Med 361, 1475-1485.

4. Friedberg EC (2001) How nucleotide excision repair protects against cancer. Nat Rev Cancer 1, 22-33.

5. Brueckner F, Hennecke U, Carell T & Cramer P (2007) CPD damage recognition by transcribing RNA polymerase II. Science 315, 859-862.

6. Lopes M, Foiani M & Sogo JM (2006) Multiple mechanisms control chromosome integrity after replication fork uncoupling and restart at irreparable UV lesions. Molecular Cell 21, 15-27.

7. Sugasawa K (2010) Regulation of damage recognition in mammalian global genomic nucleotide excision repair. Mutat Res, 685(1-2):29-37.

8. Kerzendorfer C, Hart L, Colnaghi R, Carpenter G, Alcantara D, Outwin E, Carr AM & O'Driscoll M (2011) CUL4B-deficiency in humans: Understanding the clinical consequences of impaired Cullin 4-RING E3 ubiquitin ligase function. Mech Ageing Dev, in press

9. Hanawalt PC & Spivak G (2008) Transcription-coupled DNA repair: two decades of progress and surprises. Nat Rev Mol Cell Biol 9, 958-970.

10. Fousteri M & Mullenders LHF (2008) Transcription-coupled nucleotide excision repair in mammalian cells: molecular mechanisms and biological effects. Cell Res 18, 73-84.

11. Sugasawa K (2008) XPC: its product and biological roles. Adv Exp Med Biol 637, 47-56.
12. Clement FC, Camenisch U, Fei J, Kaczmarek N, Mathieu N & Naegeli H (2010) Dynamic two-stage mechanism of versatile DNA damage recognition by xeroderma pigmentosum group C protein. Mutat Res 685, 21-28.
13. Lainé J-P & Egly J-M (2006) When transcription and repair meet: a complex system. Trends Genet 22, 430-436.
14. Staresincic L, Fagbemi AF, Enzlin JH, Gourdin AM, Wijgers N, Dunand-Sauthier I, Giglia-Mari G, Clarkson SG, Vermeulen W & Schärer OD (2009) Coordination of dual incision and repair synthesis in human nucleotide excision repair. EMBO J 28, 1111-1120.
15. Aboussekhra A, Biggerstaff M, Shivji MK, Vilpo JA, Moncollin V, Podust VN, Protić M, Hübscher U, Egly JM & Wood RD (1995) Mammalian DNA nucleotide excision repair reconstituted with purified protein components. Cell 80, 859-868.
16. Giannattasio M, Follonier C, Tourrière H, Puddu F, Lazzaro F, Pasero P, Lopes M, Plevani P & Muzi-Falconi M (2010) Exo1 competes with repair synthesis, converts NER intermediates to long ssDNA gaps, and promotes checkpoint activation. Molecular Cell 40, 50-62.
17. Rapić-Otrin V, Navazza V, Nardo T, Botta E, McLenigan M, Bisi DC, Levine AS & Stefanini M (2003) True XP group E patients have a defective UV-damaged DNA binding protein complex and mutations in DDB2 which reveal the functional domains of its p48 product. Hum Mol Genet 12, 1507-1522.
18. Gillet LCJ & Schärer OD (2006) Molecular mechanisms of mammalian global genome nucleotide excision repair. Chem Rev 106, 253-276.
19. Ravanat JL, Douki T & Cadet J (2001) Direct and indirect effects of UV radiation on DNA and its components. J Photochem Photobiol B, Biol 63, 88-102.
20. Cadet J, Voituriez L, Grand A, Hruska FE, Vigny P & Kan LS (1985) Recent aspects of the photochemistry of nucleic acids and related model compounds. Biochimie 67, 277-292.

21. Chu G & Chang E (1988) Xeroderma pigmentosum group E cells lack a nuclear factor that binds to damaged DNA. Science 242, 564-567.
22. Keeney S, Chang GJ & Linn S (1993) Characterization of a human DNA damage binding protein implicated in xeroderma pigmentosum E. J Biol Chem 268, 21293-21300.
23. Fitch M, Nakajima S, Yasui A & Ford J (2003) In vivo recruitment of XPC to UV-induced cyclobutane pyrimidine dimers by the DDB2 gene product. J Biol Chem 278, 46906-46910.
24. Moser J, Volker M, Kool H, Alekseev S, Vrieling H, Yasui A, van Zeeland A & Mullenders L (2005) The UV-damaged DNA binding protein mediates efficient targeting of the nucleotide excision repair complex to UV-induced photo lesions. DNA Repair (Amst) 4, 571-582.
25. Sugasawa K, Okuda Y, Saijo M, Nishi R, Matsuda N, Chu G, Mori T, Iwai S, Tanaka K, Tanaka K, et al. (2005) UV-induced ubiquitylation of XPC protein mediated by UV-DDB-ubiquitin ligase complex. Cell 121, 387-400.
26. Tang J & Chu G (2002) Xeroderma pigmentosum complementation group E and UV-damaged DNA-binding protein. DNA Repair (Amst) 1, 601-616.
27. Hwang BJ, Ford JM, Hanawalt PC & Chu G (1999) Expression of the p48 xeroderma pigmentosum gene is p53-dependent and is involved in global genomic repair. Proc Natl Acad Sci USA 96, 424-428.
28. Bohr VA, Smith CA, Okumoto DS & Hanawalt PC (1985) DNA repair in an active gene: removal of pyrimidine dimers from the DHFR gene of CHO cells is much more efficient than in the genome overall. Cell 40, 359-369.
29. Tang JY, Hwang BJ, Ford JM, Hanawalt PC & Chu G (2000) Xeroderma pigmentosum p48 gene enhances global genomic repair and suppresses UV-induced mutagenesis. Mol Cell 5, 737-744.
30. Scrima A, Konickova R, Czyzewski BK, Kawasaki Y, Jeffrey PD, Groisman R, Nakatani Y, Iwai S, Pavletich NP & Thoma NH (2008) Structural Basis of UV DNA-Damage Recognition by the DDB1-DDB2 Complex. Cell 135, 1213-1223.
31. Li T, Chen X, Garbutt KC, Zhou P & Zheng N (2006) Structure of DDB1 in complex with a paramyxovirus V protein: viral hijack of a propeller cluster in ubiquitin ligase. Cell 124, 105-117.

32. Li T, Robert EI, van Breugel PC, Strubin M & Zheng N (2010) A promiscuous alpha-helical motif anchors viral hijackers and substrate receptors to the CUL4-DDB1 ubiquitin ligase machinery. Nat Struct Mol Biol 17, 105-111.

33. Angers S, Li T, Yi X, MacCoss MJ, Moon RT & Zheng N (2006) Molecular architecture and assembly of the DDB1-CUL4A ubiquitin ligase machinery. Nature 443, 590-593.

34. Alekseev S, Luijsterburg MS, Pines A, Geverts B, Mari PO, Giglia-Mari G, Lans H, Houtsmuller AB, Mullenders LH, Hoeijmakers JH, et al. (2008) Cellular concentrations of DDB2 regulate dynamic binding of DDB1 at UV-induced DNA damage. Mol Cell Biol 28, 7402-7413.

35. Groisman R, Polanowska J, Kuraoka I, Sawada J, Saijo M, Drapkin R, Kisselev A, Tanaka K & Nakatani Y (2003) The ubiquitin ligase activity in the DDB2 and CSA complexes is differentially regulated by the COP9 signalosome in response to DNA damage. Cell 113, 357-367.

36. Jackson S & Xiong Y (2009) CRL4s: the CUL4-RING E3 ubiquitin ligases. Trends Biochem Sci 34, 562-570.

37. Shiyanov P, Nag A & Raychaudhuri P (1999) Cullin 4A associates with the UV-damaged DNA-binding protein DDB. J Biol Chem 274, 35309-35312.

38. Gale JM & Smerdon MJ (1990) UV induced (6-4) photoproducts are distributed differently than cyclobutane dimers in nucleosomes. Photochem Photobiol 51, 411-417.

39. Gale JM, Nissen KA & Smerdon MJ (1987) UV-induced formation of pyrimidine dimers in nucleosome core DNA is strongly modulated with a period of 10.3 bases. Proc Natl Acad Sci USA 84, 6644-6648.

40. Gong F, Kwon Y & Smerdon MJ (2005) Nucleotide excision repair in chromatin and the right of entry. DNA Repair (Amst) 4, 884-896.

41. Yasuda T, Sugasawa K, Shimizu Y, Iwai S, Shiomi T & Hanaoka F (2005) Nucleosomal structure of undamaged DNA regions suppresses the non-specific DNA binding of the XPC complex. DNA Repair (Amst) 4, 389-395.

42. Thoma F (2005) Repair of UV lesions in nucleosomes--intrinsic properties and remodeling. DNA Repair (Amst) 4, 855-869.

43. Jiang Y, Wang X, Bao S, Guo R, Johnson DG, Shen X & Li L (2010) INO80 chromatin remodeling complex promotes the removal of UV lesions by the nucleotide excision repair pathway. Proc Natl Acad Sci U S A 107, 17274-17279.

44. Zhang L, Zhang Q, Jones K, Patel M & Gong F (2009) The chromatin remodeling factor BRG1 stimulates nucleotide excision repair by facilitating recruitment of XPC to sites of DNA damage. Cell Cycle 8(23), 3953-3959.

45. Zhao Q, Wang QE, Ray A, Wani G, Han C, Milum K & Wani AA (2009) Modulation of nucleotide excision repair by mammalian SWI/SNF chromatin-remodeling complex. J Biol Chem 284, 30424-30432.

46. Duan M-R & Smerdon MJ (2010) UV damage in DNA promotes nucleosome unwrapping. The Journal of biological chemistry 285, 26295-26303.

47. Li G, Levitus M, Bustamante C & Widom J (2005) Rapid spontaneous accessibility of nucleosomal DNA. Nat Struct Mol Biol 12, 46-53.

48. Otrin VR, McLenigan M, Takao M, Levine AS & Protic M (1997) Translocation of a UV-damaged DNA binding protein into a tight association with chromatin after treatment of mammalian cells with UV light. J Cell Sci 110 (Pt 10), 1159-1168.

49. Takedachi A, Saijo M & Tanaka K (2010) DDB2 complex-mediated ubiquitylation around DNA damage is oppositely regulated by XPC and Ku and contributes to the recruitment of XPA. Mol Cell Biol 30, 2708-2723.

50. Gong F, Fahy D & Smerdon MJ (2006) Rad4-Rad23 interaction with SWI/SNF links ATP-dependent chromatin remodeling with nucleotide excision repair. Nat Struct Mol Biol 13, 902-907.

51. Guerrero-Santoro J, Kapetanaki M, Hsieh C, Gorbachinsky I, Levine A & Rapic-Otrin V (2008) The cullin 4B-based UV-damaged DNA-binding protein ligase binds to UV-damaged chromatin and ubiquitinates histone H2A. Cancer Res 68, 5014-5022.

52. Kapetanaki MG, Guerrero-Santoro J, Bisi DC, Hsieh CL, Rapić-Otrin V & Levine AS (2006) The DDB1-CUL4ADDB2 ubiquitin ligase is deficient in xeroderma pigmentosum group E and targets histone H2A at UV-damaged DNA sites. Proc Natl Acad Sci USA 103, 2588-2593.

53. Wang H, Zhai L, Xu J, Joo H, Jackson S, Erdjument-Bromage H, Tempst P, Xiong Y & Zhang Y (2006) Histone H3 and H4 ubiquitylation by the CUL4-DDB-ROC1 ubiquitin ligase facilitates cellular response to DNA damage. Mol Cell 22, 383-394.
54. Duda D, Borg L, Scott D, Hunt H, Hammel M & Schulman B (2008) Structural insights into NEDD8 activation of cullin-RING ligases: conformational control of conjugation. Cell 134, 995-1006.
55. Sugasawa K (2009) UV-DDB: a molecular machine linking DNA repair with ubiquitination. DNA Repair (Amst) 8, 969-972.
56. Batty D, Rapic'-Otrin V, Levine A & Wood R (2000) Stable binding of human XPC complex to irradiated DNA confers strong discrimination for damaged sites. J Mol Biol 300, 275-290.
57. Wittschieben B, Iwai S & Wood R (2005) DDB1-DDB2 (xeroderma pigmentosum group E) protein complex recognizes a cyclobutane pyrimidine dimer, mismatches, apurinic/apyrimidinic sites, and compound lesions in DNA. J Biol Chem 280, 39982-39989.
58. Chen X, Zhang Y, Douglas L & Zhou P (2001) UV-damaged DNA-binding proteins are targets of CUL-4A-mediated ubiquitination and degradation. The Journal of biological chemistry 276, 48175-48182.
59. Nag A, Bondar T, Shiv S & Raychaudhuri P (2001) The xeroderma pigmentosum group E gene product DDB2 is a specific target of cullin 4A in mammalian cells. Mol Cell Biol 21, 6738-6747.
60. Ortolan TG, Chen L, Tongaonkar P & Madura K (2004) Rad23 stabilizes Rad4 from degradation by the Ub/proteasome pathway. Nucleic Acids Res 32, 6490-6500.
61. Schauber C, Chen L, Tongaonkar P, Vega I, Lambertson D, Potts W & Madura K (1998) Rad23 links DNA repair to the ubiquitin/proteasome pathway. Nature 391, 715-718.
62. Heessen S, Masucci MG & Dantuma NP (2005) The UBA2 domain functions as an intrinsic stabilization signal that protects Rad23 from proteasomal degradation. Molecular Cell 18, 225-235.
63. Nishi R, Alekseev S, Dinant C, Hoogstraten D, Houtsmuller A, Hoeijmakers J, Vermeulen W, Hanaoka F & Sugasawa K (2009) UV-DDB-

dependent regulation of nucleotide excision repair kinetics in living cells. DNA Repair (Amst), 8(6):767-76.

64. Min J & Pavletich N (2007) Recognition of DNA damage by the Rad4 nucleotide excision repair protein. Nature 449, 570-575.

65. Ryu K-S, Lee K-J, Bae S-H, Kim B-K, Kim K-A & Choi B-S (2003) Binding surface mapping of intra- and interdomain interactions among hHR23B, ubiquitin, and poly-ubiquitin binding site 2 of S5a. The Journal of biological chemistry 278, 36621-36627.

66. Chen X, Zhang J, Lee J, Lin PS, Ford JM, Zheng N & Zhou P (2006) A kinase-independent function of c-Abl in promoting proteolytic destruction of damaged DNA binding proteins. Mol Cell 22, 489-499.

67. Liu L, Lee S, Zhang J, Peters SB, Hannah J, Zhang Y, Yin Y, Koff A, Ma L & Zhou P (2009) CUL4A abrogation augments DNA damage response and protection against skin carcinogenesis. Mol Cell 34, 451-460.

68. Bennett EJ, Rush J, Gygi SP & Harper JW (2010) Dynamics of cullin-RING ubiquitin ligase network revealed by systematic quantitative proteomics. Cell 143, 951-965.

69. He YJ, McCall CM, Hu J, Zeng Y & Xiong Y (2006) DDB1 functions as a linker to recruit receptor WD40 proteins to CUL4-ROC1 ubiquitin ligases. Genes Dev 20, 2949-2954.

70. Higa LA, Wu M, Ye T, Kobayashi R, Sun H & Zhang H (2006) CUL4-DDB1 ubiquitin ligase interacts with multiple WD40-repeat proteins and regulates histone methylation. Nat Cell Biol 8, 1277-1283.

71. Groisman R, Kuraoka I, Chevallier O, Gaye N, Magnaldo T, Tanaka K, Kisselev AF, Harel-Bellan A & Nakatani Y (2006) CSA-dependent degradation of CSB by the ubiquitin-proteasome pathway establishes a link between complementation factors of the Cockayne syndrome. Genes Dev 20, 1429-1434.

72. Svejstrup JQ (2007) Contending with transcriptional arrest during RNAPII transcript elongation. Trends Biochem Sci 32, 165-171.

73. van Hoffen A, Natarajan AT, Mayne LV, van Zeeland AA, Mullenders LH & Venema J (1993) Deficient repair of the transcribed strand of active genes in Cockayne's syndrome cells. Nucleic Acids Res 21, 5890-5895.

74. Venema J, Mullenders LH, Natarajan AT, van Zeeland AA & Mayne LV (1990) The genetic defect in Cockayne syndrome is associated with a defect in repair of UV-induced DNA damage in transcriptionally active DNA. Proc Natl Acad Sci U S A 87, 4707-4711.

75. Henning KA, Li L, Iyer N, McDaniel LD, Reagan MS, Legerski R, Schultz RA, Stefanini M, Lehmann AR, Mayne LV, et al. (1995) The Cockayne syndrome group A gene encodes a WD repeat protein that interacts with CSB protein and a subunit of RNA polymerase II TFIIH. Cell 82, 555-564.

76. Troelstra C, van Gool A, de Wit J, Vermeulen W, Bootsma D & Hoeijmakers JH (1992) ERCC6, a member of a subfamily of putative helicases, is involved in Cockayne's syndrome and preferential repair of active genes. Cell 71, 939-953.

77. Cleaver JE, Lam ET & Revet I (2009) Disorders of nucleotide excision repair: the genetic and molecular basis of heterogeneity. Nat Rev Genet 10, 756-768.

78. Troelstra C, Odijk H, de Wit J, Westerveld A, Thompson LH, Bootsma D & Hoeijmakers JH (1990) Molecular cloning of the human DNA excision repair gene ERCC-6. Mol Cell Biol 10, 5806-5813.

79. van Gool AJ, Citterio E, Rademakers S, van Os R, Vermeulen W, Constantinou A, Egly JM, Bootsma D & Hoeijmakers JH (1997) The Cockayne syndrome B protein, involved in transcription-coupled DNA repair, resides in an RNA polymerase II-containing complex. EMBO J 16, 5955-5965.

80. Citterio E, Van Den Boom V, Schnitzler G, Kanaar R, Bonte E, Kingston RE, Hoeijmakers JH & Vermeulen W (2000) ATP-dependent chromatin remodeling by the Cockayne syndrome B DNA repair-transcription-coupling factor. Mol Cell Biol 20, 7643-7653.

81. Kamiuchi S, Saijo M, Citterio E, de Jager M, Hoeijmakers JH & Tanaka K (2002) Translocation of Cockayne syndrome group A protein to the nuclear matrix: possible relevance to transcription-coupled DNA repair. Proc Natl Acad Sci U S A 99, 201-206.

82. Fousteri M, Vermeulen W, van Zeeland AA & Mullenders LH (2006) Cockayne syndrome A and B proteins differentially regulate recruitment of chromatin remodeling and repair factors to stalled RNA polymerase II in vivo. Mol Cell 23, 471-482.

83. Anindya R, Mari PO, Kristensen U, Kool H, Giglia-Mari G, Mullenders LH, Fousteri M, Vermeulen W, Egly JM & Svejstrup JQ (2010) A ubiquitin-binding domain in Cockayne syndrome B required for transcription-coupled nucleotide excision repair. Mol Cell 38, 637-648.
84. Arias EE & Walter JC (2005) Replication-dependent destruction of Cdt1 limits DNA replication to a single round per cell cycle in Xenopus egg extracts. Genes Dev 19, 114-126.
85. Zhong W, Feng H, Santiago FE & Kipreos ET (2003) CUL-4 ubiquitin ligase maintains genome stability by restraining DNA-replication licensing. Nature 423, 885-889.
86. Nishitani H, Sugimoto N, Roukos V, Nakanishi Y, Saijo M, Obuse C, Tsurimoto T, Nakayama KI, Nakayama K, Fujita M, et al. (2006) Two E3 ubiquitin ligases, SCF-Skp2 and DDB1-Cul4, target human Cdt1 for proteolysis. EMBO J 25, 1126-1136.
87. Nishitani H, Shiomi Y, Iida H, Michishita M, Takami T & Tsurimoto T (2008) CDK inhibitor p21 is degraded by a proliferating cell nuclear antigen-coupled Cul4-DDB1Cdt2 pathway during S phase and after UV irradiation. The Journal of biological chemistry 283, 29045-29052.
88. Abbas T, Sivaprasad U, Terai K, Amador V, Pagano M & Dutta A (2008) PCNA-dependent regulation of p21 ubiquitylation and degradation via the CRL4Cdt2 ubiquitin ligase complex. Genes Dev 22, 2496-2506.
89. Abbas T, Shibata E, Park J, Jha S, Karnani N & Dutta A (2010) CRL4(Cdt2) regulates cell proliferation and histone gene expression by targeting PR-Set7/Set8 for degradation. Molecular Cell 40, 9-21.
90. Centore RC, Havens CG, Manning AL, Li J-M, Flynn RL, Tse A, Jin J, Dyson NJ, Walter JC & Zou L (2010) CRL4(Cdt2)-mediated destruction of the histone methyltransferase Set8 prevents premature chromatin compaction in S phase. Molecular Cell 40, 22-33.
91. Oda H, Hübner MR, Beck DB, Vermeulen M, Hurwitz J, Spector DL & Reinberg D (2010) Regulation of the histone H4 monomethylase PR-Set7 by CRL4(Cdt2)-mediated PCNA-dependent degradation during DNA damage. Molecular Cell 40, 364-376.
92. Jørgensen S, Eskildsen M, Fugger K, Hansen L, Larsen MSY, Kousholt AN, Syljuåsen RG, Trelle MB, Jensen ON, Helin K, et al. (2011)

SET8 is degraded via PCNA-coupled CRL4(CDT2) ubiquitylation in S phase and after UV irradiation. J Cell Biol 192, 43-54.

93. Liu C, Poitelea M, Watson A, Yoshida SH, Shimoda C, Holmberg C, Nielsen O & Carr AM (2005) Transactivation of Schizosaccharomyces pombe cdt2+ stimulates a Pcu4-Ddb1-CSN ubiquitin ligase. EMBO J 24, 3940-3951.

94. Braun S, Garcia JF, Rowley M, Rougemaille M, Shankar S & Madhani HD (2011) The Cul4-Ddb1(Cdt)² ubiquitin ligase inhibits invasion of a boundary-associated antisilencing factor into heterochromatin. Cell 144, 41-54.

95. Arias EE & Walter JC (2006) PCNA functions as a molecular platform to trigger Cdt1 destruction and prevent re-replication. Nat Cell Biol 8, 84-90.

96. Senga T, Sivaprasad U, Zhu W, Park JH, Arias EE, Walter JC & Dutta A (2006) PCNA is a cofactor for Cdt1 degradation by CUL4/DDB1-mediated N-terminal ubiquitination. J Biol Chem 281, 6246-6252.

97. Havens CG & Walter JC (2009) Docking of a specialized PIP Box onto chromatin-bound PCNA creates a degron for the ubiquitin ligase CRL4Cdt2. Molecular Cell 35, 93-104.

98. Hu J & Xiong Y (2006) An evolutionarily conserved function of proliferating cell nuclear antigen for Cdt1 degradation by the Cul4-Ddb1 ubiquitin ligase in response to DNA damage. J Biol Chem 281, 3753-3756.

99. Jin J, Arias EE, Chen J, Harper JW & Walter JC (2006) A family of diverse Cul4-Ddb1-interacting proteins includes Cdt2, which is required for S phase destruction of the replication factor Cdt1. Mol Cell 23, 709-721.

100. Higa LA, Banks D, Wu M, Kobayashi R, Sun H & Zhang H (2006) L2DTL/CDT2 interacts with the CUL4/DDB1 complex and PCNA and regulates CDT1 proteolysis in response to DNA damage. Cell Cycle 5, 1675-1680.

101. Hotton SK & Callis J (2008) Regulation of cullin RING ligases. Annual review of plant biology 59, 467-489.

102. Chiba T & Tanaka K (2004) Cullin-based ubiquitin ligase and its control by NEDD8-conjugating system. Curr Protein Pept Sci 5, 177-184.

103. Cope GA, Suh GS, Aravind L, Schwarz SE, Zipursky SL, Koonin EV & Deshaies RJ (2002) Role of predicted metalloprotease motif of Jab1/Csn5 in cleavage of Nedd8 from Cul1. Science 298, 608-611.

104. Lyapina S, Cope G, Shevchenko A, Serino G, Tsuge T, Zhou C, Wolf DA, Wei N, Shevchenko A & Deshaies RJ (2001) Promotion of NEDD-CUL1 conjugate cleavage by COP9 signalosome. Science 292, 1382-1385.
105. Wei N, Serino G & Deng XW (2008) The COP9 signalosome: more than a protease. Trends Biochem Sci 33, 592-600.
106. Pintard L, Kurz T, Glaser S, Willis JH, Peter M & Bowerman B (2003) Neddylation and deneddylation of CUL-3 is required to target MEI-1/Katanin for degradation at the meiosis-to-mitosis transition in C. elegans. Curr Biol 13, 911-921.
107. Schwechheimer C & Deng XW (2001) COP9 signalosome revisited: a novel mediator of protein degradation. Trends Cell Biol 11, 420-426.
108. Kapelari B, Bech-Otschir D, Hegerl R, Schade R, Dumdey R & Dubiel W (2000) Electron microscopy and subunit-subunit interaction studies reveal a first architecture of COP9 signalosome. J Mol Biol 300, 1169-1178.
109. Enchev RI, Schreiber A, Beuron F & Morris EP (2010) Structural insights into the COP9 signalosome and its common architecture with the 26S proteasome lid and eIF3. Structure 18, 518-527.
110. Sharon M, Mao H, Boeri Erba E, Stephens E, Zheng N & Robinson CV (2009) Symmetrical modularity of the COP9 signalosome complex suggests its multifunctionality. Structure 17, 31-40.
111. Mundt KE, Liu C & Carr AM (2002) Deletion mutants in COP9/signalosome subunits in fission yeast Schizosaccharomyces pombe display distinct phenotypes. Molecular biology of the cell 13, 493-502.
112. Mundt KE, Porte J, Murray JM, Brikos C, Christensen PU, Caspari T, Hagan IM, Millar JB, Simanis V, Hofmann K, et al. (1999) The COP9/signalosome complex is conserved in fission yeast and has a role in S phase. Current biology : CB 9, 1427-1430.
113. Luijsterburg MS, Goedhart J, Moser J, Kool H, Geverts B, Houtsmuller AB, Mullenders LHF, Vermeulen W & van Driel R (2007) Dynamic in vivo interaction of DDB2 E3 ubiquitin ligase with UV-damaged DNA is independent of damage-recognition protein XPC. J Cell Sci 120, 2706-2716.
114. Higa LA, Mihaylov IS, Banks DP, Zheng J & Zhang H (2003) Radiation-mediated proteolysis of CDT1 by CUL4-ROC1 and CSN complexes constitutes a new checkpoint. Nat Cell Biol 5, 1008-1015.

115. Fukumoto Y, Dohmae N & Hanaoka F (2008) Schizosaccharomyces pombe Ddb1 recruits substrate-specific adaptor proteins through a novel protein motif, the DDB-box. Mol Cell Biol 28, 6746-6756.
116. Olma MH, Roy M, Le Bihan T, Sumara I, Maerki S, Larsen B, Quadroni M, Peter M, Tyers M & Pintard L (2009) An interaction network of the mammalian COP9 signalosome identifies Dda1 as a core subunit of multiple Cul4-based E3 ligases. J Cell Sci 122, 1035-1044.
117. Duda DM, Scott DC, Calabrese MF, Zimmerman ES, Zheng N & Schulman BA (2011) Structural regulation of cullin-RING ubiquitin ligase complexes. Curr Opin Struct Biol. 21(2):257-264.
118. Choe KP, Przybysz AJ & Strange K (2009) The WD40 repeat protein WDR-23 functions with the CUL4/DDB1 ubiquitin ligase to regulate nuclear abundance and activity of SKN-1 in Caenorhabditis elegans. Mol Cell Biol 29, 2704-2715.
119. Wertz IE, O'Rourke KM, Zhang Z, Dornan D, Arnott D, Deshaies RJ & Dixit VM (2004) Human De-etiolated-1 regulates c-Jun by assembling a CUL4A ubiquitin ligase. Science 303, 1371-1374.

Figure legend:

Figure 1: Modular architecture of CRL4^{DCAF} complexes

Tentative model of the CRL4^{DDB2} complex by overlaying the DDB1-DDB2 complex bound to a 6-4 PP containing oligonucleotide [30] and the DDB1-CUL4/RBX1 complex [33], assuming no overall conformational changes. The architecture of DDB1-DDB2 serves as a structural archetype for complex formation between WD40-type DCAF receptor proteins and DDB1. The overall assembly of CRL4^{DCAF} complexes and putative modes of association of (I) helix-containing WD40-type DCAF receptors (as seen in DDB1-DDB2), (II) hypothetical assembly of non-helix WD40 DCAFs and (III) non-WD40 DCAFs (as seen in DDB1-SV5V) are depicted.

Inlet panel: Structural details of UV-lesion recognition. The DDB2 (green) FQH-hairpin 'finger' (yellow) inserts into the damaged DNA duplex (grey and black) and concomitantly extrudes the 6-4 PP lesion (red) into a hydrophobic surface pocket.

Figure 2: Regulation of CRL4^{DCAF} complexes

a) DDB2 specific NER pathway: (1) Recruitment of inactive CSN-CRL4^{DDB2} to the nucleosome embedded lesion. (2) Ubiquitin ligase activation by CSN release and CUL4 neddylation; subsequent ubiquitination of nearby proteins, including DDB2 auto-ubiquitination, XPC and histones. (3) Ubiquitination induced eviction of the histone octamer facilitating recruitment of the NER-repairosome and initiation of damage repair. Proteasomal degradation of ubiquitinated DDB2 is implicated in CRL4DDB2 release and damage handover to downstream NER factors.

b) General model for CRL4^{DCAF} regulation: (1) Recruitment of inactive CSN-CRL4^{DCAF} through DCAF receptor proteins. (2) Release of CSN with subsequent CUL4 neddylation and ligase activation resulting in substrate ubiquitination. (3) Pathway specific induction of coordinated cellular events, such as proteasomal degradation of the substrate protein, relocalisation or recruitment of interaction partners.

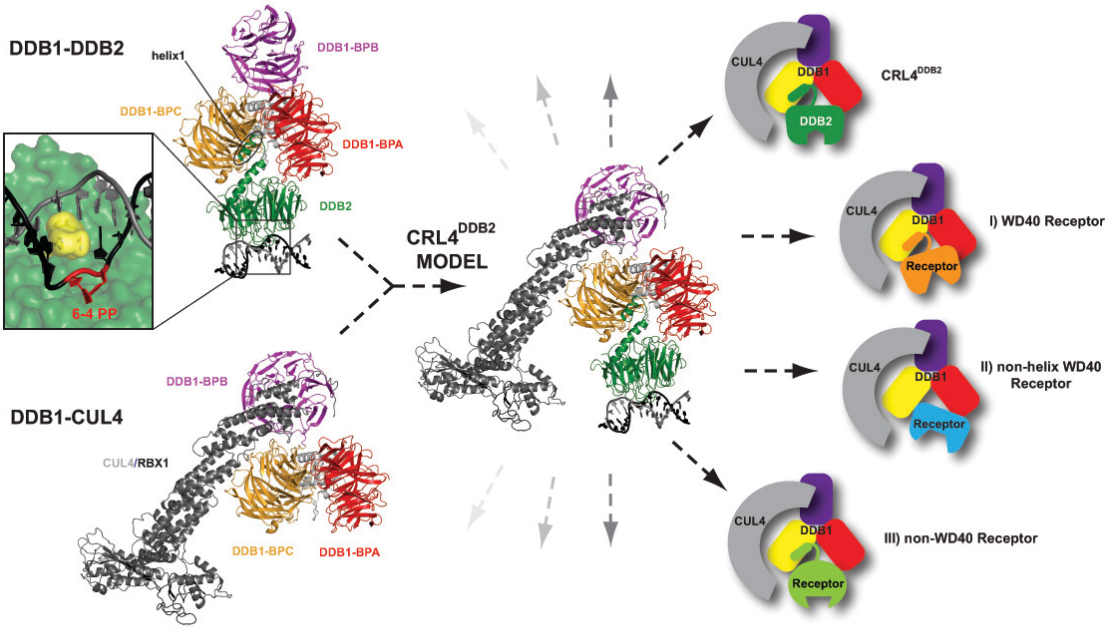
DDB1-DDB2
helix1
DDB1-BPB
DDB1-BPC
DDB1-BPA
DDB2
6-4 PP
DDB1-CUL4
DDB1-BPB
CUL4/RBX1
DDB1-BPC
DDB1-BPA
CRL4DDB2
MODEL
CUL4
DDB1
DDB2
CRL4DDB2
CUL4
DDB1
Receptor
I) WD40 Receptor
CUL4
DDB1
Receptor
II) non-helix WD40
Receptor
CUL4
DDB1
Receptor
III) non-WD40 Receptor

Figure 1

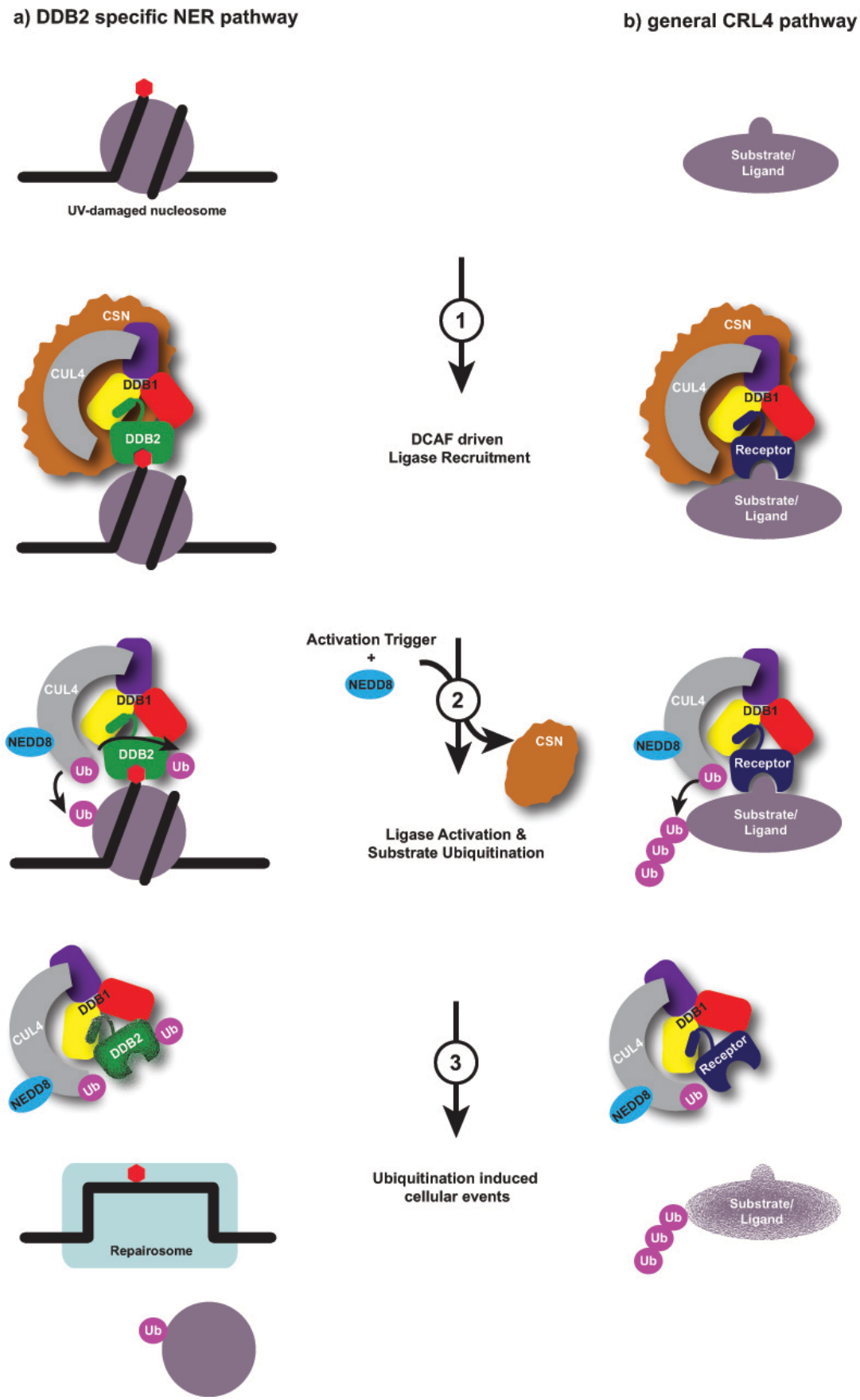
a) DDB2 specific NER pathway
b) general CRL4 pathway
UV-damaged nucleosome
Substrate/
Ligand
CSN
CUL4
DDB1
DDB2
1
DCAF driven
Ligase Recruitment
CSN
CUL4
DDB1
Receptor
Substrate/
Ligand
CUL4
DDB1
NEDD8
DDB2
Ub
Ub
Ub
Activation Trigger
+
NEDD8
2
CSN
Ligase Activation &
Substrate Ubiquitination
CUL4
DDB1
NEDD8
Receptor
Ub
Substrate/
Ligand
Ub
Ub
Ub
CUL4
DDB1
DDB2
Ub
NEDD8
Ub
3
Ubiquitination induced
cellular events
CUL4
DDB1
Receptor
NEDD8
Ub
Repairosome
Substrate/
Ligand
Ub
Ub
Ub
Ub

Figure 2

Chapter 4: Structural basis of $CRL4^{CRBN}$ inhibition by Thalidomide and its derivatives

Materials and methods

Cloning and protein expression

Homo sapiens DDB1 (residues 1-1140) (Scrima et al., 2008) and *gallus gallus* CRBN (residues 1-445) were cloned into pAC derived vectors (BD biosciences PharMingen, San Jose, CA USA) and recombinant baculoviruses were prepared according to the manufacturers protocol. Proteins were expressed as N-terminal His_6 (DDB1) and N-terminal StrepII (CRBN) tagged fusion proteins in Hi-Five insect cells (Invitrogen).

For purification, cells were resuspended in lysis buffer (50mM Tris-HCl pH8.0, 200mM NaCl, 0.1% Triton X-100, 5mM TCEP (*tris*(2-carboxyethyl)phosphine), 1mM PMSF and 1 tablet/100ml Sigma protease inhibitor cocktail) and lysed by sonification. The lysate was clarified by ultracentrifugation and proteins were then purified using *Strep-Tactin* affinity purification. Proteins were further purified by anion exchange chromatography (Poros 50HQ) using a 0-800mM NaCl gradient. Size exclusion chromatography (SEC) (HiLoad 16/60 Superdex 200; GE Healthcare) in 50mM HEPES pH 7.4, 200mM NaCl and 0.25mM TCEP yielded protein without visible contamination (coomasie stained SDS-PAGE). The purified protein was concentrated using “Amicon Ultra” spin concentration devices, flash frozen in liquid nitrogen and stored at -80°C until further use.

Compounds, enzymes and antibodies used

(S)-Thalidomide, (R)-Thalidomide and lenalidomide (*revlimid*) used for crystallization were kind gifts from NIBR Cambridge (USA). (S)-Thalidomide for biochemistry was purchased from Sigma Aldrich (USA) (T150-100MG) and lenalidomide (S1029) for biochemistry and pomalidomide (S1567) for

crystallization and biochemistry were purchased from Selleckchem (USA). All compounds were dissolved in DMSO at various concentrations.

Ubiquitin activating enzyme E1 (UBA1), ubiquitin conjugating enzyme E2 (UbcH5a, UbcH5b), ubiquitin and “K-0 ubiquitin” were purchased from Boston Biochem (USA). Anti-Flag M2 Antibody was provided by the lab of S. Gasser (Friedrich Miescher Institute, Basel, Switzerland) and initially purchased from Sigma Aldrich. Horseradish peroxidase (HRP)-conjugated secondary antibodies against mouse IgG were purchased from Abcam (ab6728).

Crystallization of hsDDB1-ggCRBN

Protein-thalidomide/lenalidomide co-crystals were obtained by mixing of thalidomide or lenalidomide with purified hsDDB1-ggCRBN protein complex in a 2-3:1 molar ratio. Initial screening was carried out using a phoenix liquid handling robot (Art Robbins, CA, USA) using commercially available screens (Hampton, USA; Quiagen, DE), initial hits were refined in a 24 well hanging drop vapour diffusion setup by mixing 1µl of protein solution with 1µl of reservoir solution (100mM Na-Cacodylate, 80mM NaH_2PO_4, 120mM K_2HPO_4, 700mM-1200mM tri-NaCitrate). Diffraction grade hsDDB1-ggCRBN-pomalidomide co-crystals were obtained under similar conditions.

Data collection was carried out at beamlines X10SA and X06DA of the Swiss Light Source (Paul Scherrer Institute, Villigen, Switzerland) with a Pilatus 2M or Pilatus 6M detector, respectively. Collected data sets were processed using XDS (Kabsch, 1993).

Structure solution and Model building

The crystals contained one molecule in the asymmetric unit (AU). The structure was solved by molecular replacement using Phaser (Mccoy et al., 2007) with the BPA/BPC/CTD of DDB1 (3EI1) as search model. The BPA/BPC/CTD domains of DDB1 were fixed and the BPB domain searched with Molrep (Vagin and Teplyakov, 1997). Rigid body refinement on DDB1 domains was done with Phenix (Adams et al., 2010).

De novo model building for the CRBN subunit was carried out with Coot (Emsley and Cowtan, 2004), all structures were refined using phenix.refine

(Adams et al., 2010) and Buster (Smart et al., 2012). Figures were generated with PyMol (DeLano Scientific, http://www.pymol.org).

In vitro ubiquitination assays

In vitro ubiquitination assays and CSN protection assays were carried out as described in Fischer et al., 2011. Final enzyme concentrations in the reaction mix were 15-20 µM ubiquitin, 0.04 µM E1, 0.07 µM $CRL4^{CRBN}$ complex, 1 µM E2 (UbcH5a or UbcH5b) in 1x Ubiquitin Assay Buffer (Sugasawa, 2006). CSN concentrations user for $CRL4^{CRBN}$ inhibition varied between 100nM-400nM as indicated in **Figure 4.3**.

Data collection	***hsDDB1-ggCRBN Thalidomide***	***hsDDB1-ggCRBN Lenalidomide***	***hsDDB1-ggCRBN Pomalidomide***
Beamline	SLS X06DA	SLS X10SA	SLS X10SA
Wavelength **(Å)**	0.9999	1.0000	1.0000
Space Group	$P3_221$	$P3_221$	$P3_221$
Cell parameters			
a, b, c (Å)	172.27, 172.27, 140.16	172.27, 172.27, 139.90	170.89, 170.89, 138.58
α, β, γ (deg)	90, 90, 120	90, 90, 120	90, 90, 120
Resolution (Å)	30.0-3.07 (3.15-3.07)	30.0-3.16 (3.24-3.16)	50.0-3.70 (3.92-3.70)
Completeness (%)	99.9 (99.9)	99.8 (100)	99.4 (97.0)
Unique reflections	45138 (3289)	41312 (3022)	48596 (7639)
Redundancy	8.4 (7.5)	5.4 (5.1)	5.3 (5.1)
R_{sym} (%)	12.6 (116.5)	12.7 (105.4)	26.0 (120.5)
I/σI	16.85 (1.85)	13.74 (1.62)	7.42 (1.43)
CC(1/2)	99.8* (63.9*)	99.7* (57.9*)	98.4* (46.5*)
Refinement			
PDB code	not deposited	not deposited	not deposited
R_{work}/R_{free}	19.3/25.4	20.3/23.6	20.6/21.8
Reflections (working set)	42865	45679	24213
Reflections (test set)	2273	2434	1274
Number of Atoms			
Protein	11715	11627	11753
DNA	0	0	0
Water	348	252	0
Ligand	20	20	22
R.m.s. deviations			
Bond lengths (Å)	0.01	0.01	0.009
Bond Angles (deg)	1.45	1.40	1.32
Ramachandran			
favoured	96.64	94.99	96
disallowed	3.36	5.01	4
Avg. B-factor (Å²)	84.8	93.2	94.3

Table 1: X-ray data collection and refinement statistics.

Results

DDB2 and CSA are two members of the DCAF family involved in nucleotide excision repair, which our studies have shown to share striking structural similarity between these WD40 β-propeller substrate receptors. While a majority of DCAFs identified by proteomic studies (Angers et al., 2006; Groisman et al., 2006; He et al., 2006; Jin et al., 2006; Bennett et al., 2010) are predicted to contain a WD40 repeat domain, others have been identified as DCAFs that likely do not share these domains. To investigate how a putative non-WD40 DCAF would look like, and how it would bind to DDB1 and recruit it's substrate to the ligase, we determined the structure of DDB1-CRBN.

Overall structure of the DDB1-CRBN complex

To facilitate crystallization, a number of orthologues (*homo sapiens*, *danio rerio*, *gallus gallus*) previously known to bind thalidomide (Ito et al., 2010) were cloned, expressed in "*Hi-Five*" insect cells and screened for crystallization conditions in the presence or absence of the two drugs, thalidomide and lenalidomide. Only a chimeric complex of *homo sapiens* DDB1 and *gallus gallus* CRBN yielded crystals of sufficient quality for structure determination. hsDDB1-ggCRBN in complex with thalidomide and lenalidomide crystallized in space group P 3_2 2 1 (154), and structures were determined at 3.07 Å and 3.16 Å resolution, respectively. A 3.7 Å refined structure of hsDDB1-ggCRBN bound to pomalidomide was obtained under similar conditions (**see Table 1** for a summary of data collection and refinement statistics). The overall sequence conservation of chicken CRBN *versus* human CRBN (91% similarity and 84% sequence identity), make it likely that the results observed will also hold true for the human CRBN orthologue. DDB1 is a highly conserved protein with an overall sequence conservation between chicken and human DDB1 of 98% similarity (97% identity), moreover all residues involved in CRBN interaction are conserved from chicken to human.

The DDB1 subunit predominantly consists of three seven-bladed WD40 β-propellers arranged in a triangle-like shape (BPA, BPB and BPC), and a

helical C-terminal domain (CTD) (Li et al., 2006; Scrima et al., 2008) (**see Figure 4.2a**). The structure of CRBN consists of three domains, a 9 β-sheet containing N-terminal domain (NTD, residues 1-185), a 7 *α*-helices containing helical insertion domain (HID, residues 186-317) that mediates the interaction with DDB1, and another 9 β-sheet containing C-terminal domain (CTD, residues 318-445) that harbors the thalidomide binding pocket and a zinc coordination site (**Figure 4.2a**). The region preceding Asn46 and following Arg427 are not well defined in the electron density map and were omitted from model building. In addition, a segment spanning from Arg205 to Phe222 could not be assigned with sufficient confidence and was omitted from the model.

Comparison of the CRBN structure with other known structures reveals that the region aa46-aa317 (NTD and HID) largely resembles the structure of a bacterial Lon protease N-terminal domain (PDB: 3LJC), while the CTD (residues aa318-aa427) displays similarity to a methionine sulfoxide reductase fold (PDB: 3MAO). Structural comparison using DALI server (Holm and Rosenström, 2010) reported a Z-score of 16.2 with an RMSD of 2.7 Å for CRBN(46-317) with 3LJC over 178 residues aligned. The structure alignment of CRBN(318-427) with 3MAO also reported a Z-score of 9.5 with an RMSD of 2.0 Å over 79 residues.

Although NTD and HID generally align well with the Lon protease (3LJC), a significant difference arises from the DDB1-interacting motif located C-terminal to the NTD. The NTD consists mainly of β-strands and aligns with an overall C-α RMSD of 2.06 Å (SSM superposition, Coot) (Emsley and Cowtan, 2004) to the N-terminal subdomain of 3LJC. While the helices H4, H5, H6 and H7 again show striking similarity with the helices in the Lon protease fold, a 63 amino acid insertion after residue 185 and before H4 (aa252-aa263) forms the DDB1-interacting motif and does not show recognizable similarity with any known structures. It is also different to the canonical HLH motif seen, such as in DDB2 or CSA.

The interaction with DDB1 is mediated through a long loop (aa189-aa223), followed by a helix-loop-helix (aa223-249). This CRBN region occupies a cavity between the DDB1-BPC and BPA domains similar to that seen in other

known DCAFs. DDB2 in contrast employs, in addition to the HLH motif engulfed in the DDB1 cavity, also a large hydrophobic patch to interact with DDB1. The buried surface area of the CRBN-DDB1 complex is 2194 Å^2 (EPPIC Server, Duarte et al., 2012), with major binding contributions made by the loop region spanning CRBN residues Glu188 to Phe222, and a helical arrangement including helices H3 and H4 (residues Arg223 to Tyr250) (**Figure 4.2a**). Additional contacts are formed by residues within helix H7 (aa 306-319), with Gln308 and Arg311 being involved in hydrogen-bonding interactions.

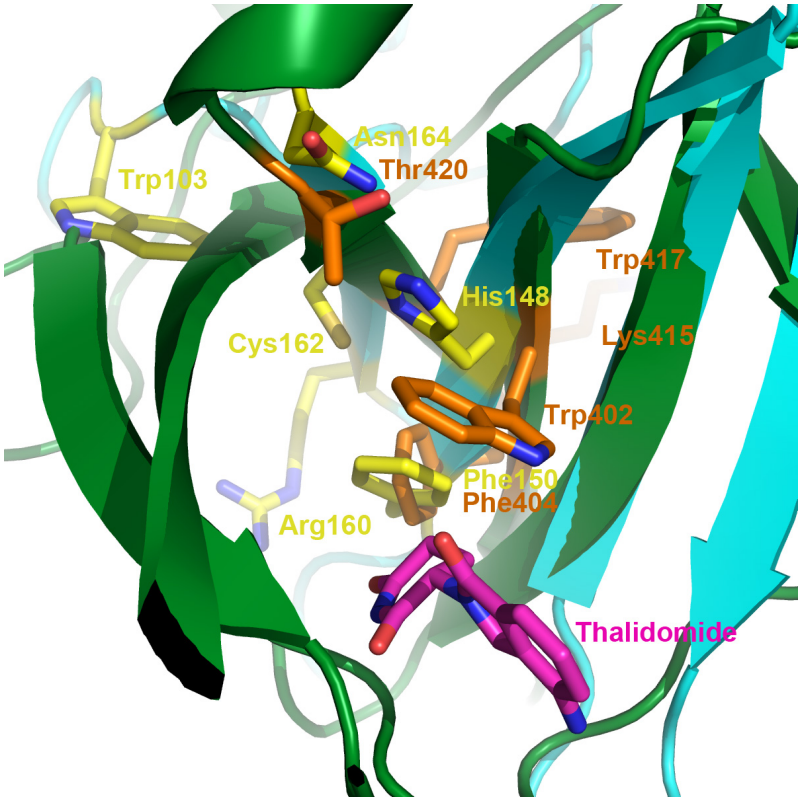

Figure 4.1: Superposition of chicken CRBN with mouse MsrB2 active site. The CTD of CRBN and MsrB2 are depicted as cartoon representation in green and cyan, respectively. Thalidomide bound to CRBN is depicted as sticks representation in magenta. Catalytic residues of MsrB2 and corresponding residues in CRBN are highlighted in yellow and orange, respectively.

The CTD of CRBN is defined by an overall β-strand and globular arrangement, consisting of nine all antiparallel β-sheets. Comparison with two published structures of Methionine-R-Sulfoxide reductases (human MsrB1, PDB: 3MAO and mouse MsrB2, PDB: 2L1U) revealed superimposable structures (rmsd of 2.1 Å over 78 residues and rmsd of 3.1 Å over 62 residues for 3MAO and 2L1U, respectively) (**Figure 4.1**). While a iron ion is coordinated in MsrB1, a zink ion is found in the structures of CRBN and

MsrB2, within the structurally conserved coordination site provided by four cysteins (Cys325, 328, 393 and 396 in ggCRBN). The residues involved in the catalytic activity of MsrB2 (Trp103, His148, Phe150, Arg160, Cys162 and Arg162), and the catalytic cysteine 162, in particular, are not conserved in CRBN. The corresponding residues in CRBN include (Trp402, Phe404, Lys415, Trp417 and Thr420) (**Figure 4.1**), of which residues Trp402 and Phe404 localize to the thalidomide binding pocket.

Thalidomide is the ancestor of a class of molecules called IMiDs (Cellgene, Summit NJ, USA), which exhibit different pharmacological properties despite being highly similar in structure. In order to understand the molecular basis of IMiD binding to CRBN, we determined the structures of DDB1-CRBN bound to all three clinical relevant IMiD compounds, thalidomide (*Thalomid*), lenalidomide (*Revlimid*) and pomalidomide.

Thalidomide occupies a pocket in the C-terminal domain of CRBN

The small molecule inhibitor thalidomide binds to a hydrophobic pocket mainly composed of Tryptophan W382, W388 and W402 in conjunction with residues N353, P354, H355 and F404 (**Figure 4.2a, c**). The presented X-ray structures revealed that lenalidomide and pomalidomide bind to the same pocket of CRBN in a comparable fashion (**Figure 4.2b**).

The glutarimide group of thalidomide (**Figure 4.3a**) faces inwards toward the hydrophobic pocket and is buried within a *hydrophobic cage* provided by W382, W388 and W402 (**Figure 4.2c**), while the phtalimide group is oriented towards the outside in a solvent exposed manner. This binding mode is compatible with the reported linkage of a carboxyl-derivative of thalidomide (**Figure 1.8**) to magnetic beads used in the affinity-based identification of CRBN as target to thalidomide (Ito et al., 2010). The binding of thalidomide to CRBN is mainly mediated through van der Waals forces and two hydrogen bonds formed by the glutarimide oxygens of CRBN and His380 and Trp382. The overall shape of the binding pocket suggests that the S-enantiomer of thalidomide is preferentially bound (**Figure 4.2d**). This is in line with the observation that it is the S- as opposed to R-enantiomer of pomalidomide that shows pharmacologic activity (Lopez-Girona et al., 2012).

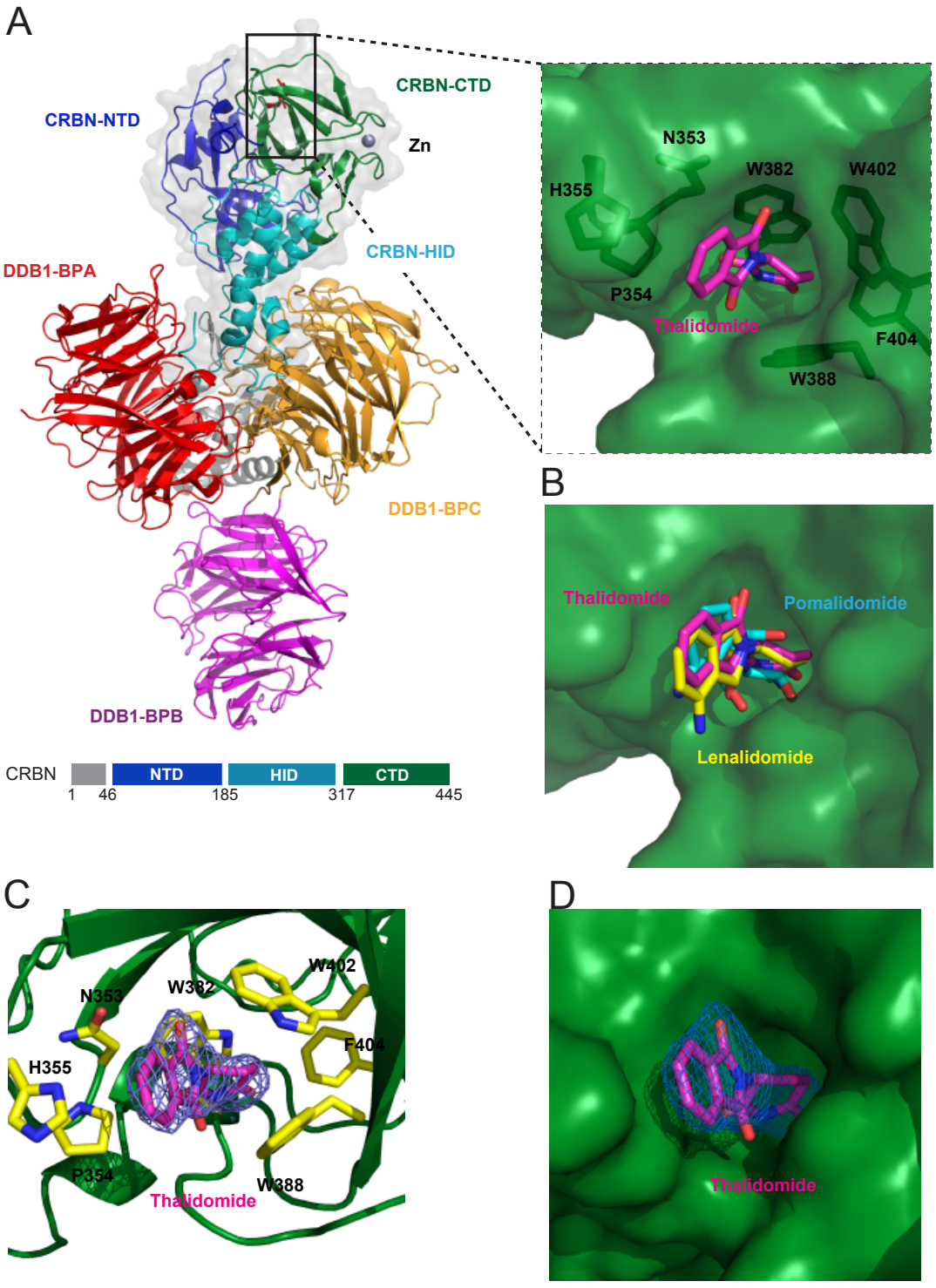

Figure 4.2: Structure of DDB1-CRBN bound to thalidomide. (A) Overall structure of the DDB1-CRBN complex. CRBN (NTD): blue, CRBN (HID): cyan, CRBN (CTD): green, DDB1 (BPA): red, DDB1 (BPB): magenta, DDB1 (BPC): orange, DDB1 (CTD): grey. Schematic overview of the CRBN organization. Thalidomide, in magenta, and the residues involved in thalidomide binding are highlighted. (B) Overlay of Thalidomide, Lenalidomide and Pomalidomide bound to CRBN, with CRBN depicted as surface representation in green. (C) Close-up view of the Thalidomide interacting residues, depicted as yellow sticks. Thalidomide is shown as sticks in magenta, together with its positive Fo-Fc electron density calculated and contoured at 2.5 σ before it was build into the complex. (D) Close-up view on the thalidomide binding pocket in CRBN shown as green surface.

The differences between the three derivatives thalidomide, lenalidomide and pomalidomide are minor (**Figure 4.3a-c**) and, in consequence, the overall binding mode is very similar (**Figure 4.2b**). Minor differences are observed for the aniline of lenalidomide and pomalidomide, absent in thalidomide, which potentially forms a hydrogen bond with the Glu379 side chain (**Figure 4.3e**). This is interaction is not predicted to significantly contribute to binding due to its solvent exposed binding mode. In thalidomide, one of the phthalimide carbonyl oxygens lies within 4 Å of the backbone carbonyl oxygen of Glu379 or may be lodged against the electron-rich face of the indole of the Trp388. In lenalidomide, the lactam analog, the carbonyl is absent. This would relieve these potential, unfavorable interactions.

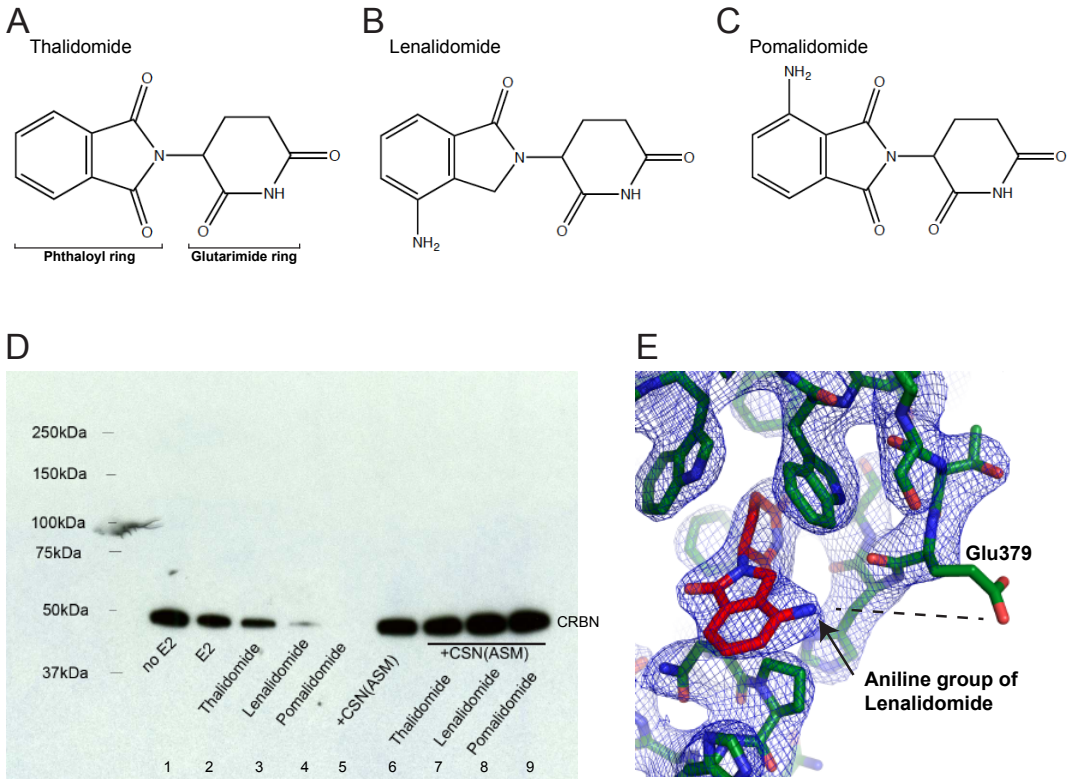

Figure 4.3: Autoubiquitination of CRBN. Skeletal formula of (A) Thalidomide, (B) Lenalidomide and (C) Pomalidomide. Stereisomers are not drawn in this representation. (D) *In vitro* ubiquitination assays were performed with FLAG-CRBN containing CRL4CRBN complex and subjected to anti-FLAG immunoblot analysis. The decrease in signal for CRBN corresponds to increasing amounts of ubiquitinated CRBN. CSN inhibition was achieved with 100nM of CSN5 active site mutant containing CSN complex (CSN(ASM)), compounds were used 10µM final concentration. (E) CRBN and Thalidomide are depicted as sticks in green and red, respectively. 2mFo-Fc electron density is shown in blue calculated and contoured at 1.5 σ.

Ito and colleagues have found that thalidomide inhibits the ubiquitin ligase activity of $CRL4^{CRBN}$ *in vivo* and *in vitro* (Ito et al., 2010), moreover, it has been reported that thalidomide, lenalidomide and pomalidomide exhibit different pharmacological properties that could not be anticipated by our structural studies. In order to better understand the effect of thalidomide on CRBN and the $CRL4^{CRBN}$ ubiquitin ligase, we set out to characterize the effect of thalidomide to $CRL4^{CRBN}$ in a fully recombinant system.

Autoubiquitination of $CRL4^{CRBN}$ is inhibited by CSN *in vitro*

The CRBN subunit of the $CRL4^{CRBN}$ ubiquitin ligase undergoes autoubiquitination *in vivo* and *in vitro* (Ito et al., 2010). This autoubiquitination activity depends on the DDB1 interaction and thereby on $CRL4^{CRBN}$ assembly. Ito and colleagues were further able to demonstrate that CRBN autoubiquitination *in vivo* is inhibited by thalidomide and that a Y384A and W386A mutant abolishes thalidomide binding but not $CRL4^{CRBN}$ assembly. As a consequence, the mutant also resists the inhibitory effect of thalidomide. We focused on characterizing the effect of thalidomide on $CRL4^{CRBN}$ function *in vitro* and the role of CSN in regulating $CRL4^{CRBN}$.

We examined whether recombinant $CRL4^{CRBN}$ complex exhibits E3 ubiquitin ligase activity, *in vitro* ubiquitination assays were performed using recombinant $CRL4^{CRBN}$ comprising a CRBN as N-terminal FLAG fusion protein. Likely due to the promiscuity of the ubiquitination reaction, we were unable to detect poly-ubiquitinated CRBN in anti-FLAG immunoblots. Instead, we observed a decrease of the signal for unmodified FLAG-tag CRBN that we anticipate to be due to polyubiquitination of CRBN including the lysines of the FLAG-tag (**Figure 4.3d** lane 1 and 2). CRBN is autoubiquitinated *in vitro*, irrespective of the presence or absence of thalidomide, lenalidomide or pomalidomide (**Figure 4.3d, lanes** 1-5), while *in vivo* CRBN ubiquitination is sensitive to thalidomide treatment (Ito et al., 2010). We have previously demonstrated that CSN inhibits DDB2 and CSA autoubiquitination (Fischer et al., 2011) and we thus examined the effect of CSN on CRBN autoubiquitination *in vitro*. Within a $CRL4^{CRBN}$ complex, CRBN was ubiquitinated in the presence of an E1 (Uba1) and E2 (UbcH5a), as previously

observed (Ito et al., 2010). CRBN autoubiquitination, however, was inhibited in the presence of CSN (**Figure 4.3d,** lane 6). Moreover, the CSN mediated inhibition of $CRL4^{CRBN}$ was not relieved upon addition of either thalidomide, lenalidomide or pomalidomide (**Figure 4.3d** lanes 7-9).

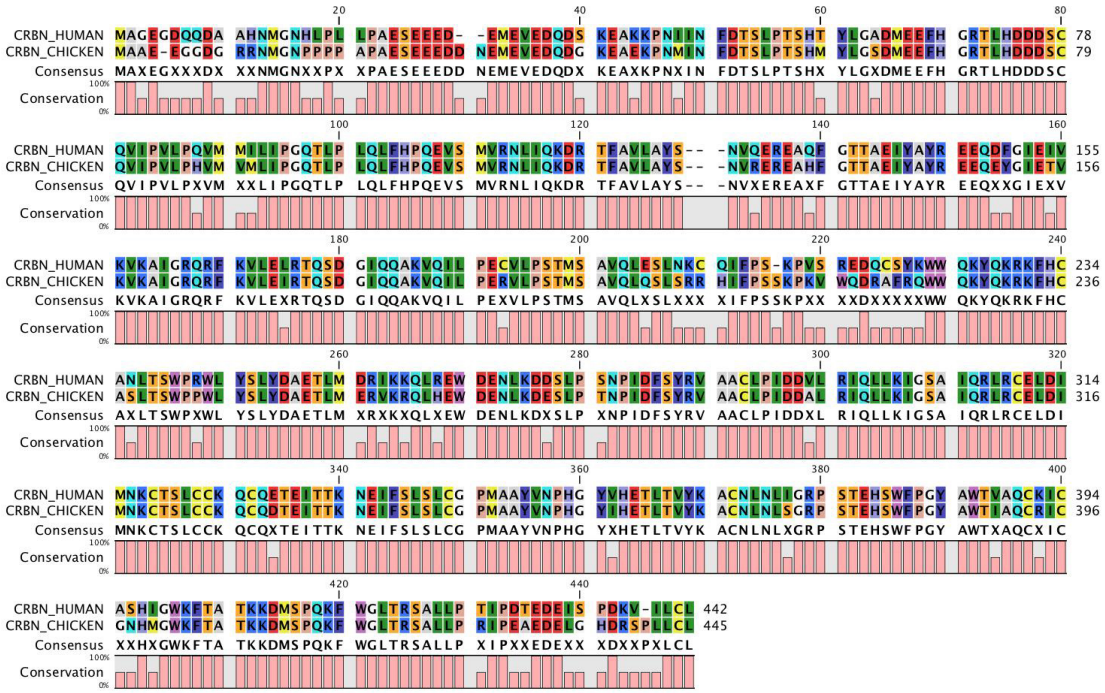

Figure 4.4: **Alignment of human CRBN versus chicken CRBN.** The alignment was generated with CLCbio (clcbio inc, Aarhus, DK) using the ClustalW algorithm (Larkin et al., 2007).

Discussion and outlook

Structure of DDB1-CRBN; New diversity in the CRL4 ligase family

Cullin4-type CRL E3 ubiquitin ligases are assembled in a modular fashion consisting of the scaffolding cullin subunit, which binds the globular Rbx1 protein at the C-terminus, thereby assembling the active center. On the N-terminus, the cullin is anchored to the BPB domain of DDB1, where DDB1 forms the adaptor that binds the substrate recruiting DCAFs. Previous structures of DDB1-DCAF complexes (Scrima et al., 2008; Li. et al. 2006; Angers et al. 2006; Fischer et al., 2011) have highlighted the importance of a conserved helix-loop-helix motif (HLH) that anchors the DCAF to DDB1. Similar helical binding motifs have been identified for viral proteins SV5v (Li et al., 2006) and the HBx protein (Li et al., 2010). Based on these structures, a bipartite binding mode has been established as the canonical form of DDB1-

DCAF interaction, where the HLH motif (DDB2, CSA) in conjunction with hydrophobic patches, on the surface of the WD40 repeat domain, contribute to DDB1 binding.

Here we present the structure of hsDDB1-ggCRBN, the first structure of an endogenous non-WD40 β-propeller DCAF found to bind DDB1 in a way that differs significantly from the previously observed binding modes. CRBN forms a tripartite structure (**Figure 4.2**a) in which the NTD and HID share structural similarities to the N-terminal domain of a bacterial Lon protease (PDB: 3LJC) and in which the CTD largely resembles the structure of the mammalian Methionine-R-Sulfoxide reductase (MsrB1, PDB: 3MAO). The DDB1 interacting region consists of two helices with long interconnecting loop regions, and has evolved at the junction between the NTD and HID domains. The overall buried surface area of the DDB1-CRBN interaction is 2194 Å^2, calculated using the Eppic web server (Duarte et al., 2012) and comparable to the buried surface area of 1895 Å^2 seen for the DDB1-DDB2 interaction.

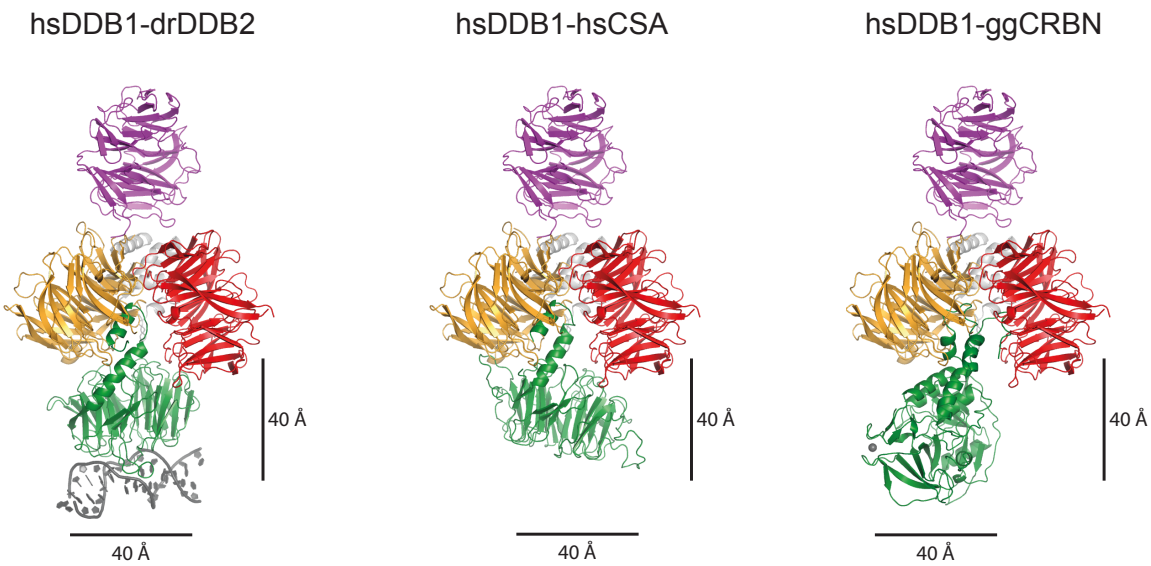

Figure 4.5: comparison of DDB1-DDB2, DDB1-CSA and DDB1-CRBN structures.

Despite the lack of structural conservation between known WD40 DCAF receptors and the structure presented for CRBN, the overall spatial dimensions of the CRL4^{CRBN} arrangement are likely to be similar to that of CRL4^{DDB2} (Fischer et al., 2011) (**Figure 4.5**). CRBN binds to DDB1 in a similar position and the overall arrangement is, to some extent, similar to what has been observed for DDB2 and CSA. It is therefore likely that CRBN binds

its (as yet unknown) substrate through the surface opposing the DDB1 binding site and thereby allows for ubiquitination through the Cul4/Rbx1 ligase arm (**see General discussion and perspectives** for a more detailed discussion of CRL4 architectural constraints).

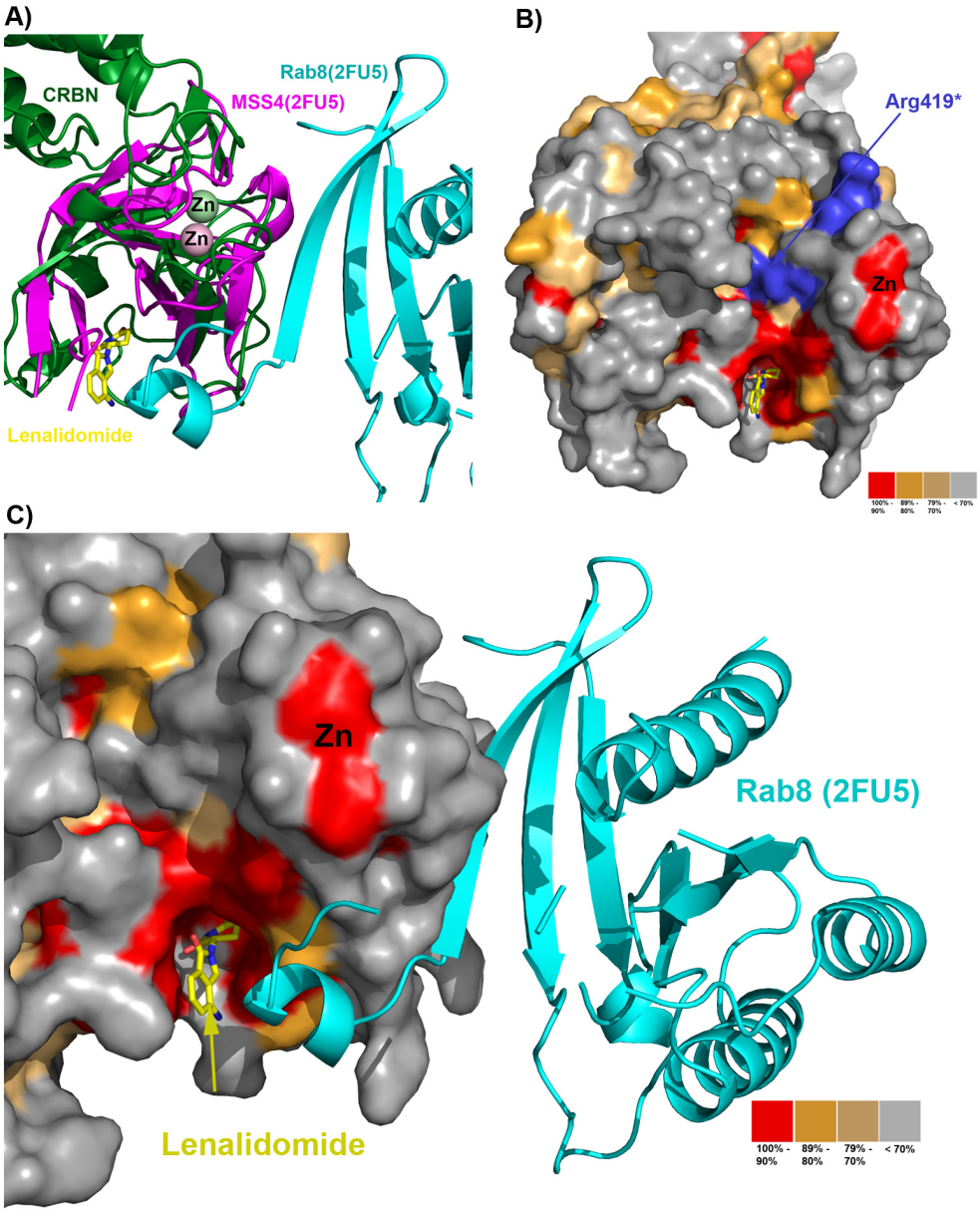

Figure 4.6: Superposition of CRBN with a MSS4-Rab8 complex. (A) A superposition of the CRBN-CTD with MSS4 of 2FU5 in complex with Rab8 is depicted as cartoon representation in green, magenta and cyan, respectively. (B) Surface conservation of CRBN, highlighting the residues absent in the Arg419* mental retardation patient mutation. (C) Surface conservation of CRBN together with Rab8 from the MSS4-Rab8 complex aligned via MSS4 to the CTD of CRBN. The N-terminal helix of Rab8 occupies a surface in MSS4 that is equivalent to a conserved patch in CRBN in proximity to the thalidomide binding pocket.

The CTD of CRBN aligns with MSS4 in the published X-ray structure of a MSS4-Rab8 complex (PDB: 2FU5), CRBN-CTD and MSS4 superimpose with a rmsd of 3.47 Å over 107 residues (Itzen et al., 2006) (**Figure 4.6a**). Moreover, evolutionary conservation of surface residues is a common determinant of functional protein surface residues. We note that the highly conserved areas on the CRBN surface correlate with the position of the thalidomide binding pocket (**Figure 4.6b**), suggesting a functional role of these residues in addition to thalidomide binding. Strikingly, residues in CRBN, equivalent to those involved in protein-protein interactions between MSS4 and Rab8, contribute to the thalidomide binding site or are in close proximity (**Figure 4.6c**). These observations suggest that the thalidomide binding pocket might also be involved in substrate binding and that thalidomide could act as a substrate competitive inhibitor.

Thalidomide binding and activity

Since general inhibitors of the proteasome (*bortezomib*) and the Nedd8 E1 enzyme (*MLN4924*) (Adams et al., 1998; Soucy et al., 2009) have shown promise in clinical trials, approaches to develop drugs with potentially higher efficacy and safety for specific indications have been initiated. In the sequential ubiquitin proteasome system, in which the proteasome represents the most general target, the E3 ligases and therefore also the cullin-RING E3 ligases are the most selective targets. While CRLs have long been considered “undruggable”, recent studies have identified a number of tool compounds, including inhibitors to the *S. cerevisae* CRLs SCF^{Cdc4} (Orlicky et al., 2010) and SCF^{Met30} (Aghajan et al., 2010). And to other targets in the UPS, such as the E2 enzyme Cdc34 (Ceccarelli et al., 2011). More recently thalidomide and the closely related lenalidomide and pomalidomide have been identified as a compound targeting specifically the $CRL4^{CRBN}$ E3 ubiquitin ligase (Ito et al., 2010), thereby being the first in class FDA approved inhibitor of a CRL. The identification of CRBN as the primary cellular target of thalidomide (Ito et al., 2010) and moreover the finding that CRBN is also mediating the anti-myeloma effects of thalidomide and lenalidomide (Lopez-Girona et al., 2012) have shed light on the cellular action of thalidomide. However, without

knowledge of downstream targets, and without ruling out other off-target effects, the precise “mode of action” remains elusive (**see also Chapter 5 General discussion**).

The derivatives of thalidomide, lenalidomide and pomalidomide, have been shown to be more potent and have also been proposed to harbor less severe side effects (Quach et al., 2010). Potency, in this case, has mainly been addressed based on the degree of TNFα inhibition. Structurally, the three analogs are closely related. Lenalidomide has an additional amino group on the forth carbon of the phthaloyl ring, but lacks the carbonyl oxygen at position three. Pomalidomide, the latest derivative to have gone into clinical trials, is essentially a combination of both (**Figure 4.3a to c**). The additional amino group in lenalidomide and pomalidomide is expected to contribute to hydrogen-bonding with Glu379 without adding significant binding energy due to being solvent exposed. In order to fully address the differences in CRBN binding, precise binding studies will be required.

Our structural and biochemical data demonstrates that thalidomide directly binds to a hydrophobic pocket within the CRBN subunit of $CRL4^{CRBN}$ without abolishing the interaction with DDB1. It also does not impair the overall structural integrity of the multi-protein CRL complex; and does not inhibit the ubiquitin ligase activity *per se* (**Figure 4.3d**). Rather, our data suggests that thalidomide binding to CRBN impairs substrate recruitment to the ligase and thereby the CSN mediated activation of the $CRL4^{CRBN}$ ubiquitin ligase. This is in line with the observation that thalidomide treatment inhibits CRBN autoubiquitination *in vivo* (Ito et al., 2010) but not *in vitro* (**see General discussion and perspectives** for a more detailed discussion of CRL4 inhibition). However, to fully understand the mode of action and to confirm the proposed mechanism of inhibition, knowledge of a cellular target of the $CRL4^{CRBN}$ ligase will be required.

Conservation in chicken versus human CRBN

In order to obtain a high resolution structure of DDB1-CRBN bound to thalidomide and its derivatives, a large number of different deletion constructs of zebrafish, chicken and human CRBN were tested for solubility and, if

applicable, were pursued in presence or absence of thalidomide and lenalidomide in crystallization trials.

Diffraction grade crystals were only obtained for the chicken CRBN construct in a chimeric assembly with human DDB1. The overall conservation of chicken CRBN *versus* its human orthologue are 91% (similarity) / 84% (sequence identity) for the full-length constructs used; and 95% (similarity) / 88% (sequence identity) for the boundaries that were modeled according to the electron density (**see Figure 4.4**). All of the residues involved in interactions with thalidomide, lenalidomide and pomalidomide are conserved between chicken and human CRBN. A region of little conservation is located between ggCRBN residues aa 201-224 corresponding to a loop region absent in the electron density and are therefore likely to be unstructured.

The general high level of sequence conservation between human versus zebrafish CRBN, the identity of residues involved in thalidomide binding and the previously observed CRBN dependent thalidomide teratogenicity in chicken embryos (Ito et al., 2010), indicate that the conclusions drawn from the chicken CRBN structure will apply to the human orthologue.

Mapping of patient mutations on CRBN

CRBN was first identified as a new gene mutated in a mild form of mental retardation (Higgins et al., 2004). The identified nonsense mutation causes a premature stop codon after residue Arg419, resulting in a truncated form of CRBN (**Figure 4.6b**). Arginine 419 is located within the C-terminal domain and in proximity to the thalidomide binding pocket.

In the treatment of multiple myeloma with *revlimid* (lenalidomide), resistance to the drug has been reported in certain patient groups (Lopez-Girona et al., 2012), and cell culture experiments demonstrated that acquired resistance to the drug correlates with a loss of CRBN (Zhu et al., 2011; Lopez-Girona et al., 2012). Another potential source of drug resistance could be acquired mutations of the CRBN gene; the COSMIC database (Forbes et al., 2010) reports a number of somatic patient mutations in the CRBN gene (**see Table 2**), one nonsense mutation (p.E106*), and seven missense substitutions. The structure presented now provides a molecular rationale for

the reported mutations. The premature stop codon after E106 likely leads to an unfolded protein, or at least abolishes the interaction with DDB1, resulting in a phenotype similar to a total loss of CRBN expression. W224L and N236T are surface exposed residues involved in DDB1 binding, likely weakening this interaction. The T119A and D249N mutations affect the core of the protein and likely impair correct folding. Mutations E132K, L168P and T403M are surface mutations and could be involved in substrate binding.

Position	Mutation (Amino Acid)	Location	Expected Effect
106	p.E106*	N-terminal of DDB1 interacting motif	Missfolded protein and deficient in DDB1 binding
119	p.T119A	NTD: Hydrophobic core	Minor: Possibly impaired fold
132	p.E132K	NTD: Surface exposed charged residue	Charge reversal: Possibly substrate binding
168	p.L168P	NTD: Surface exposed	Minor: Possibly substrate binding
224	p.W224L	HID: CRBN-DDB1 interface	Possibly impaired DDB1 binding
236	p.N236T	HID: CRBN-DDB1 interface	Minor: Possibly impaired DDB1 binding
249	p.D249N	HID core	Possibly impaired fold & DDB1 binding
403	p.T403M	CTD: Surface exposed	Minor: Possibly impaired fold

Table 2: **Reported somatic patient mutations in the CRBN gene.** (Forbes et al., 2010)

Chapter 5: General Discussion and Perspectives

The structural, biochemical and *in vivo* data presented here provide (i) the molecular basis of $CRL4^{DDB2}$ architecture, targeting to chromatin and regulation by the COP9 signalosome. (ii) Evidence that similar regulatory principles apply to the remainder of the CRL4 ligase family, and (iii) the structural basis of $CRL4^{CRBN}$ inhibition by the small molecule inhibitors thalidomide, lenalidomide and pomalidomide. Based on the work presented and in light of current knowledge, I will discuss how these findings integrate into the present understanding of CRL4 architecture and regulation, and will propose a model how thalidomide inhibits the $CRL4^{CRBN}$ ligase.

Molecular architecture of CRL4 E3 ubiquitin ligases

The structures of $CRL4A^{DDB2}$ and $CRL4B^{DDB2}$ presented in this work are the first X-ray structures of a fully assembled Cullin RING ligase (CRL) bound to its substrate. The structures reveal that the mobility of the ligase arm creates a ubiquitination hot zone around the site of damage and thereby insulates the substrate receptor from the E2 binding site (see **Chapter 2**). Together with the structures of the DDB1-CSA and DDB1-CRBN complexes (see **Chapter 2** and **3**) and previously available structural information on the CRL4 family (Li et al., 2006; Li et al., 2010; Angers et al., 2006; Scrima et al., 2008), a architectural consensus is now emerging amongst CRL4 ligases.

Structural and functional homology between CUL4A and CUL4B

Mammalian cells express two CUL4 isoforms, CUL4A and CUL4B (Jackson and Xiong, 2009), which are believed to be, to a large extent, functionally redundant. $Cul4a^{-/-}$ mice are viable and show only mild phenotypes, while knockdown of Cul4b in $Cul4a^{-/-}$ MEFs results in a growth arrest, suggesting that the Cul4b gene is able to largely compensate for the loss of Cul4a (Liu et al., 2009). The CUL4A and CUL4B proteins share a high degree of sequence homology (83% sequence identity over 752 residues), and exhibit high structural similarity within the cullin fold (rmsd of 1.54 Å over 677 residues) (see also **Chapter 2** for further details). While, the major

difference between the two isoforms arises from a ≈190 residue N-terminal extension in CUL4B (Ota et al., 2004). Within the crystallized boundaries, CUL4A and CUL4B assemble into $CRL4^{DDB2}$ ligase complexes, which are structurally indistinguishable from each other (Fischer et al., 2011). Biochemical assessment of ligase activity towards DDB2 and XPC ubiquitination, CSN mediated inhibition, and DNA damaged induced release suggests that the CUL4B protein can compensate for CUL4A *in vitro* (Fischer et al., 2011; and data not shown). Therefore, the discussion of CSN mediated CRL4 activation will not address specific differences between the two isoforms.

Despite these similarities, the two isoforms are not entirely redundant, which becomes apparent in a number of human pathologies that are specifically associated with either CUL4A or CUL4B. For example, although having a functional Cul4a, X-linked mental retardation (XLMR) has been associated with several familial mutations in the Cul4b gene (Tarpey et al., 2007). It was proposed that the unique N-terminus of CUL4B may be responsible for recruitment and CUL4B dependent degradation of a number of substrates involved in XLMR (Lee and Zhou, 2012). Accordingly, the CUL4B N-terminal domain has been shown to bind the arylhydrocarbon receptor (AhR), a putative substrate receptor, which recruits estrogen and androgen receptors for degradation (Ohtake et al., 2007). While a specific role of the CUL4B N-terminus can be anticipated, the structure of $CRL4B^{DDB2}$ does not provide a rationale how a substrate could be directly recruited through the N-terminus as a target for ubiquitination *in cis*. However, as dimerization has been described for DCAF substrate receptors (Ahn et al., 2011), more complex CRL4 assemblies resulting in a substrate binding mode that involves the N-terminus and ubiquitination *in trans* can not be ruled out at present.

Further evidence for distinct roles of the two isoforms arises from mouse genetics: $Cul4a^{-/-}$ mice show increased stability in several CRL4 substrates, including components of the NER pathway and p21 (Liu et al., 2009). Whether this is due to functional differences or due to a reduction in available Cul4 protein is currently unresolved. For example in 293T cells, cellular concentrations of DDB1 (323 nM) are below the combined concentrations of CUL4A (158 nM) and CUL4B (307 nM) (Bennett et al., 2010). In turn, in a

Cul4a$^{-/-}$ background DDB1 cellular concentrations would be expected to be equal or above the global pool of available Cul4 proteins and this may result in altered CRL4-DCAF homeostasis. In order to fully understand the differential roles played by Cul4a and Cul4b, further structural characterization of the N-terminal domain of CUL4B, as well as biochemical and functional studies will be required.

Common architectural features emerge for CRL4$^{DCAF(WD40)}$

The CRL4A^{DDB2} ubiquitin ligase is believed to be a "special" ubiquitin ligase, as it does not directly recognize a protein substrate. Instead, the DDB2 substrate receptor binds to damaged DNA and thereby recruits proteins to the vicinity of the ligase arm, targeting them for ubiquitination. It has been shown by Angers and colleagues (Angers et al., 2006) that CUL4A folds into an elongated, largely helical shape, forming the scaffold of the CRL4^{DDB2} ligase complex. The E2 binding protein RBX1 is located at the C-terminus of CUL4, while the N-terminus (aa 39-96), in conjunction with the BPB domain of DDB1, bridges the cullin and the adaptor protein DDB1. DDB1 then recruits the DCAFs (DDB1 CUL4 associated factors), which form the substrate receptors within the CRL4 family and confer substrate specificity to the system (see also **Chapter 2** for more details). The available multitude of DDB1 containing crystal structures showed the BPB domain in a number of distinct conformations, leading to the hypothesis that the mobility inherent in the BPB domain directly translating into rotational freedom of the ligase arm (Scrima et al., 2008). Using the crystal structure of CRL4A^{DDB2} and CRL4B^{DDB2}, we were able to experimentally trap the ligase arm in 3 different conformations, spanning an angle of 60° around an axis defined by the DDB1-BPA/BPC and the DDB2 domains. Moreover, using the information derived from the 11 available medium/high resolution structures of DDB1 (Li et al., 2006; Li et al., 2010; Angers et al., 2006; Scrima et al., 2008; Fischer et al., 2011), we were able to deduce that the ligase arm can rotate around 150°, creating a large "ubiquitination hot zone" around the site of damage. We propose that the overall U-shaped CRL4 assembly together with mobility of the ligase arm observed in the CRL4^{DDB2} structures as well as in the CRL4^{SV5v} structure (Angers at al., 2006), is a common feature for all CRL4^{DCAF} complexes and

that the structural variability within the CRL4 family originates from the DCAFs, which confer substrate specificity to the system.

The structure of DDB1-CSA revealed that despite little sequence homology, the DDB2 and CSA proteins share striking similarities in their overall structural arrangement (backbone rmsd of 3.4 Å for 355 CSA/DDB2 residues) (Fischer et al., 2011). Similar to DDB2, CSA is anchored to the DDB1 protein via its helix-loop-helix (HLH) motif bound to a groove between the BPA/BPC domains of DDB1. The majority of identified DCAFs (Higa et al., 2006; Scrima et al., 2008; Li et al., 2010; Fischer et al., 2011) are predicted to comprise a WD40 propeller domain and for at least 13 of them we were able to identify the putative helix-loop-helix (HLH) motif preceding the propeller (Fischer et al., 2011) and we propose that other WD40-DCAFs will display an overall structural arrangement similar to that of $CRL4^{DDB2}$. A helical binding motif has also been observed in the structure of $CRL4^{SV5v}$ (Angers et al., 2006) and a helical peptide stemming from the hepatitis B protein X (HBx) crystallized in complex with DDB1 (Li et al., 2010). Both DCAF DDB1 binding epitopes attach to the same BPA/BPC groove also used by DDB2 and CSA. This suggests that helical binding motifs are not only common determinants of DCAF proteins, but are also employed by viral proteins to take control of a CRL4 ligase (Li et al., 2005). While the structures of DDB2 and CSA provide a structural rationale for understanding the architecture of WD40-DCAFs, a number of endogenous proteins have been predicted to be DCAFs, which do not fall in the WD40 β-propeller class. In order to examine how other putative DCAFs relate to the WD40-DCAFs DDB2 and CSA, we determined the structure of the DDB1-CRBN complex bound to thalidomide.

Substrate receptor plasticity goes beyond WD40 β-propeller DCAFs

The structure of DDB1-CRBN presented in this work provides the first atomic structure of an endogenous “non-WD40” DCAF, which shares virtually no homology to a WD40 β-propeller (**Figure 4.2a**). The crystal structure of CRBN has revealed significant topological similarities between the N-terminal domain (NTD) and the helical insertion domain (HID) of CRBN and the N-terminal domain of a Lon protease (PDB: 3LJC), as well as between the C-

terminal domain (CTD) of CRBN and the human Methionine-R-Sulfoxide reductase MsrB1 (PDB: 3MAO), despite low amino acid sequence similarity. Although there are structural similarities, the active site of MsrB1 is not conserved and at present there is no evidence for any catalytic activity of the CRBN protein. The DDB1 interacting motif of CRBN, while still comprising two helices, differs from the canonical HLH motif observed for DDB2 or CSA, despite also binding to the cavity between the DDB1 BPA and BPC domains. While the structural hallmark of endogenous DCAF proteins has so far been a WD40 propeller preceded by a HLH motif, with CRBN we find that other folds have evolved to interact with DDB1 and serve as substrate receptors to form functional CRL4 ligases.

These results allow us to refine our view of DCAFs: all structurally characterized DDB1-DCAF complexes employ a helix-containing motif to mediate the DDB1-DCAF interaction (Li et al., 2006; Li et al., 2010; Scrima et al., 2008; Fischer et al., 2011), whether an endogenous WD40 β-propeller containing DCAF, a non-WD40 DCAF, or a viral protein hijacking a CRL4 ligase. We propose the canonical HLH motif to be mainly present in WD40 propeller containing DCAFs and likely preceding the propeller domain. As seen in the case of CRBN, non-canonical helices can occupy the same cavity in the DDB1 protein and mediate a DDB1-DCAF interaction, and further viral proteins can donate a helix similar to helix1 in DDB2 in order to recruit DDB1 for a function beneficial to the virus (Li et al., 2010). The overall shape and form of DCAFs can vary, and while CRBN displays some similarity in size and overall shape to DDB2 and CSA, with dimensions of ≈ 40 Å x 40 Å length (**Figure 4.5**), other endogenous DCAFs have been predicted to be of much smaller size (Ifrg15), or be comprised of extended structures with additional domains (Cdt2, DCAF1).

Despite architectural varieties within the known DCAFs, the overall assembly of the ligase complex likely maintains its U-shaped architecture as Rbx1, Cul4 and DDB1 contribute the scaffold. While the mobility of the ligase arm will help to accommodate the different DCAF architectures and compensate for differences in substrate positioning, it will result in spatial separation of substrate recognition and the ligase “active site” and thereby

does not allow for direct crosstalk between the substrate receptor and the ligase, thus requiring CSN to mediate CRL4 activation.

Substrate dictated CSN release and CRL4 ligase activation

CRL4 ligase complexes are linked to many cellular pathways and tight control of ligase activity is therefore a crucial property. As reported for other cullins (Morimoto et al., 2000; Podust et al., 2000; Read et al., 2000; Wu et al., 2000), neddylation, a modification of cullins with the small ubiquitin-like protein Nedd8 at a conserved lysine residue, serves as activator of CRL4 ligases. The activation is counteracted by the COP9 signalosome (CSN), an 8-subunit isopeptidase complex that specifically removes the Nedd8 modification from cullins, thus rendering them inactive (Deng et al., 2000). As detailed in this study, CSN also inhibits the ligase and protects the substrate receptor from autoubiquitination in a non-enzymatic, CSN5 independent fashion (See **Chapter 2** for more details). With CSN being a key regulator of cullin ligase activity, the question arises how a single complex regulates hundreds of specific CRLs?

Substrate triggered dissociation of CSN relieves CRL4 inhibition

A number of regulatory events have been associated with CSN, including posttranslational modifications and differential gene expression. Phosphorylation of CSN subunits has been reported (Bech-Otschir et al., 2002; Matsuoka et al., 2007), potentially affecting CSN activity or the assembly of the CSN holocomplex. Furthermore, CSN6 is cleaved by caspases during apoptosis, although the precise role of this event remains elusive (da Silva Correia et al., 2007; Hetfeld et al., 2008). Despite these potential effects on CSN activity, the conundrum of the differential regulation of specific CRLs by CSN cannot be explained by a modification or regulation of the global CSN pool, and to our knowledge, no cullin specific CSN modification has been reported. Another route to achieve CRL specific regulation is by modulating the association of CSN with a specific ligase. It has been proposed that the presence of a substrate reduces or circumvents the association of CSN with SCF^{Skp2} and thereby increases the level of

neddylation (Bornstein et al., 2006). Further evidence that substrate binding is involved in regulating CRLs is given by similar findings with $CRL2^{VHL}$ (Chew and Hagen, 2007) and work on SCF ligase complexes (Schmidt et al., 2009). Our work established that for $CRL4^{DDB2}$, the binding of the damaged substrate DNA to the substrate receptor DDB2 leads to the release of CSN and activation of the ligase *in vitro*. We also found CSN to be physically dissociated from the ligase, and hence escape of CSN5 mediated deneddylation, non-enzymatic CRL inhibition, and Ubp12 mediated deubiquitinating activity (Zhou et al., 2003) in the presence of substrate. We were able to observe similar behavior for the $CRL4^{CSA}$ ligase in which the binding of CSB (a protein substrate rather than damaged DNA) induces CSN displacement and ligase activation. Therefore, we propose that this regulatory principle will likely extend to the remainder of the $CRL4^{DCAF}$ family. Supporting our proposition, single particle EM reconstructions of $CRL4^{DDB2}$, $CRL4^{Cdt2}$ and $CRL4^{Ifrg15}$ (data not shown) indicate that substrate binding to the DCAF and CSN binding are mutually exclusive, all of which provides a molecular rationale for the observed substrate induced CSN release and CRL activation.

Do similar principles apply to other CRLs?

CSN not only regulates CRL4 ligases, but also has been associated with the regulation of canonical cullin ligases in general (Cul1, Cul2, Cul3, Cul4, and Cul5). Again, we propose that non-catalytic inhibition in conjunction with substrate induced CSN release is likely also a hallmark of a large number of other cullin ligases. In fact, a detailed kinetic study of the CSN mediated deneddylation of Cul1 ligase complexes SCF^{Fbw7} and SCF^{Skp2} has lead to very similar observations (Emberley et al., 2012). The authors show that the deneddylation of SCF^{Fbw7} and SCF^{Skp2} is inhibited by up to 2.5fold in the presence of an appropriate substrate to the ligase. Further, they provide evidence that CSN inhibits SCF ligases independent of CSN5 mediated deneddylation activity, similar to our findings for CRL4. These findings are underlined by EM and biochemical studies of the CSN-SCF^{Skp2} and CSN-SCF^{Fbw7} complexes (Enchev et al., 2012), which not only show striking similarity to the overall assembly of our CSN-$CRL4^{DDB2}$ EM reconstructions

(data not shown), but also provide additional evidence that the substrate triggered dissociation of CSN expands to the SCF ligase family. Together, these findings support a model in which CSN, employing deneddylation in conjunction with passive protection, inhibits Cullin RING ligases and where the binding of a substrate can trigger relief of this inhibition through physical dissociation of CSN from the ligase. In this model, the substrate dictates the state of CSN mediated inhibition, implying that the presence of a substrate would be necessary and sufficient to specifically activate the appropriate CRL ligase. A frequently observed feature of CRL protein substrates is the necessity of a posttranslational modification in order to be recognized by a CRL for degradation (Hon et al., 2002; Min, 2002; Wu et al., 2003; Mizushima et al., 2004; Hao et al., 2005; Mizushima et al., 2007). This provides another layer of control to the timed activation of a ligase and thereby the degradation of a substrate.

Does CSN play a non-enzymatic role *in vivo*?

While the *in vitro* data presented deepens our mechanistic understanding of CRL regulation, the situation is arguably more complex *in vivo*. More than 200 CRLs have been implicated in a multitude of processes (Cardozo and Pagano, 2004) and their activity is likely affected by binding partners and posttranslational modifications (Goldenberg et al., 2004; Wertz et al., 2004; Matsuoka et al., 2007; Olma et al., 2009). Despite these complexities, genetics have provided evidence for the importance of the observed mechanisms *in vivo*. In the yeast *Schizosaccharomyces pombe*, csn1^{-} and csn2^{-} strains exhibit pronounced sensitivity to ionizing radiation and exhibit slow DNA replication, with csn5^{-} strains having a less severe phenotype (Mundt et al., 1999; 2002), indicating that in addition to deneddylation a CSN "non-enzymatic" role also exists in *S. pombe*. Work in *Neurospora crassa* identified active site mutations in the csn5 JAMM domain, which assemble into a CSN holocomplex deficient in cullin deneddylation activity (Zhou et al., 2012), which exhibit a less severe phenotype than a total loss of csn5. The authors could further demonstrate that the csn5 active site mutant not only rescues the CRL1^{FWD-1} mediated degradation of FRQ but also partially

rescues the stability of a number of substrate receptors, likely through the inhibition of autoubiquitination. These findings from plants and yeast indicate the potential *in vivo* relevance of the observed non-catalytic CSN activity in inhibiting CRL ligase activity.

Can substrate binding trigger CSN release *in vivo*?

We have shown that binding of damaged DNA to the DDB2 subunit of $CRL4^{DDB2}$ triggers the release of CSN and the activation of the ligase *in vitro*. Furthermore, the patient mutation DDB2 (K244E) deficient in DNA binding does not trigger the release of CSN *in vitro* (Fischer et al., 2011) and *in vivo* (Takedachi et al., 2010), indicating that a mutant deficient in DNA substrate binding is, following UV exposure, not activated *in vivo*. Similar evidence for the role of substrate binding in relieving CSN mediated CRL inhibition has been found for CRL1 and CRL2 (Chew and Hagen, 2007). The authors could show that mutants of the substrate receptors Skp2 and VHL are defective in substrate binding and preferentially associate with unneddylated cullin. Our findings together with the *in vivo* results and additional *in vitro* experiments (Emberley et al., 2012; Enchev et al., 2012), support a model in which the binding of a substrate to a CRL ligase complex triggers dissociation of CSN and thereby relieve of deneddylation activity and passive non-enzymatic protection.

Recent advances in proteomics (Bennett et al., 2010; Kim et al., 2011), biophysical and biochemical assays (Kleiger et al., 2009; Emberley et al., 2012), and structural methods (Duda et al., 2011; Fischer et al., 2011; Enchev et al., 2012) have began to shed light on the complexities that govern the CRL ligase networks and the regulatory mechanisms involved. Despite these new and detailed insights, further studies will be needed to elucidate how the complex CRL machinery works on a cellular level and specifically to pinpoint how the multitude of regulatory principles contribute to tight CRL regulation *in vivo,* and how this relates to specific physiological mechanisms.

Thorough mechanistic insights into CRL ligase architecture, function and regulation will also deepen our understanding of their role in human diseases

such as cancer and will enable researchers to ultimately design novel CRL targeting medications.

The UPS and CRL4 as targets for therapeutic intervention

Over the past decades tremendous efforts have been made to understand the critical role that posttranslational modifications (PTM) play in pathways driving neoplastic transformation. PTMs offer a plethora of candidates to pharmacologically impede tumor growth not to mention other human disease. While kinase inhibitors are still the largest group within PTM directed therapeutics, the ubiquitin proteasome system (UPS) has raised interest since the successful clinical evaluations of the proteasome inhibitor *bortezomib* (*velcade*), which was approved by the FDA for the treatment of multiple myeoloma in 2003 (Adams et al., 1998). *Bortezomib* acts at the end of the UPS by non-specifically blocking the degradation of poly-ubiquitinated substrates and thereby sensitizing rapidly dividing cells to apoptosis (Adams, 2004). *MLN4924*, another UPS directed small molecule inhibitor, presently in clinical trials, inhibits the Nedd8 specific E1 enzyme (NAE/UBA3) preventing neddylation and thereby activation of the global Cullin RING ligase pool (Soucy et al., 2009; Bennett et al., 2010). Both compounds have limited specificity for biological pathways; they rather affect the overall protein homeostasis through accumulation of a vast number of ubiquitin ligase substrates. However, more precise targeting of CRLs or other components of the UPS would allow specifically to address a pathway involved in carcinogenesis or other diseases, increase efficacy while providing more control over adverse site effects. While the common protein-protein interactions involved in CRL substrate recognition have long been though to be *undruggable*, a number of groups have recently reported success in finding specific inhibitors to SCF^{Cdc4}, SCF^{Met30} and Cdc34 (Aghajan et al., 2010; Orlicky et al., 2010; Ceccarelli et al., 2011). Although these inhibitors are of still experimental nature and in the case of SCF^{Cdc4} and SCF^{Met30} directed to a yeast protein, they serve as prototypes for specific downstream targeting inhibitors of the UPS. On the other hand, a proven compound in clinical development is thalidomide, another specific CRL inhibitor that has been

around for decades and was recently rediscovered as anti-cancer agent resulting in FDA approval for the treatment of multiple myeloma in 2006. Through the discovery that thalidomide targets the $CRL4^{CRBN}$ ligase (Ito et al., 2010), thalidomide and its also FDA approved derivative lenalidomide (*revlimid*) became the prototype of a specific CRL4 ligase inhibitor effective in the treatment of human cancer. In this study we present the first atomic structure of the DDB1-CRBN complex, the cellular target of thalidomide, bound to thalidomide, lenalidomide and pomalidomide (see **Chapter 4** and **Figure 4.2**).

Is Thalidomide the first in class CRL inhibitor used in cancer therapy?

Thalidomide (α-N-phtalimido-glutarimide), is a synthetic derivative of glutamic acid and the ancestor of a class of anti-myeloma compounds termed IMiDs (immunomodulatory drugs) by Cellgene corporation (Summit, NJ, USA) (Shortt et al., 2012) (**Figure 4.3a** to **c**). Thalidomide, despite its adverse side effect in causing multiple birth defects, has been rediscovered for the treatment of multiple myeloma (Galustian et al., 2004) and the amino substituted derivatives lenalidomide (*revlimid*, cc-5013) and pomalidomide (CC-4047, *Actimid*) were synthesized with the aim of optimizing anti-TNF*α* and anti-angiogenic properties. Clinical trials displayed a significant efficacy against multiple myeloma and resulted in FDA approval of thalidomide and lenalidomide. However, both are limited by strict prescription regulations due to the lack of knowledge on the mode of action and the teratogenic nature of IMiDs. The discovery of CRBN as the primary target of thalidomide binding (Ito et al., 2010) has been a milestone in understanding thalidomides teratogenic effects. Further, a comprehensive biophysical, biochemical and cellular study confirmed CRBN as a cellular target of thalidomide in anti-myeloma treatment (Lopez-Girona et al., 2012). These structures now provide a detailed molecular understanding of how these compounds bind with high affinity to the CRBN substrate receptor of $CRL4^{CRBN}$. They also represent the first structure of an FDA approved compound with evident inhibitory function that targets a specific CRL ligase and provide the grounds to explore how this

inhibition is achieved on a molecular basis, and what its underlying cellular mode of action may be.

Structure-function analysis of thalidomide derivatives

Despite minor differences between the compounds thalidomide and its derivatives lenalidomide (one additional amino group at the C4 position of the phtaloyl ring, without the carbonyl oxygen at C3) and pomalidomide (a combination of thalidomide and lenalidomide), cellular and clinical data suggest a significantly increased potency of lenalidomide (Lopez-Girona et al., 2012 and references within) over thalidomide. Pomalidomide has further been assigned a 10-fold increase in potency over lenalidomide through a number of cellular assays (Lopez-Girona et al., 2012). Competition assays of lenalidomide, or pomalidomide, for CRBN binding to thalidomide analog affinity beads (Ito et al., 2010; Lopez-Girona et al., 2012) revealed similar affinities of lenalidomide and pomalidomide to CRBN, but found an increased affinity compared to thalidomide, potentially explaining the efficacy gain for the two derivatives over thalidomide. However, even when incorporating our own structural data we could not find any explanations for the difference in potency between lenalidomide and pomalidomide. To fully resolve the types of chemical interactions and their contributions we require more precise binding studies and higher resolution crystal structures in the future.

Differences in efficacy could also arise from off-target effects; the specific linkage off the affinity beads used by Ito and colleagues (Ito et al., 2010), although compatible with CRBN binding, would not resolve any binding mediated by the phtaloyl ring due to steric clashes. In light of the minor variations among the compounds and the similar overall binding mode, the following discussion will focus on our high resolution structure of DDB1-CRBN bound to thalidomide.

Stereoselectivity of the CRBN-Thalidomide interaction

All three compounds are chiral molecules and although enantioselective synthesis has been achieved, the compounds rapidly racemize *in vivo* (Bosch et al., 2008) preventing stereoselective administration. The thalidomide *R*-

form has often been considered as the “good” enantiomer responsible for sedative effects (Höglund et al., 1998; Eriksson et al., 2000), while the *S*-enantiomer has commonly been associated with teratogenicity (Heger et al., 1994). The presented structures provide a rational of stereoselective thalidomide binding to CRBN, the shape of the binding pocket accommodates the *S*-enantiomer of thalidomide, while binding of a *R*-enantiomer would be disfavored and rather unlikely (**Figure 4.2**). Further evidence for the selectivity is provided by the observation that initial crystallization screens with enantioselective synthesized *S*-thalidomide and *R*-thalidomide only yielded crystals for the *S*-enantiomer and the electron density maps suggest the presence of the S-enantiomer of thalidomide, lenalidomide and pomalidomide, despite the fact that the later were provided as a racemate. Through the use of a non-racemic pomalidomide derivative Lopez-Girona and colleagues (Lopez-Girona et al., 2012), could demonstrate that a *S*-enantiomer of methyl-pomalidomide stimulates Interleukin-2 (IL2) production in activated T cells compared to a *R*-methyl-pomalidomide (IC_{50} values of 0.02 µM compared to >10 µM) and that this corresponds to a similar rank order in binding to CRBN. These results provide strong evidence that only the *S*-enantiomer of thalidomide and derivatives can bind to CRBN and as such, is inducing teratogenicity and anti-myeloma effects.

Does thalidomide employ CSN to inhibit $CRL4^{CRBN}$?

It has been observed that thalidomide inhibits autoubiquitination of CRBN *in vivo* (Ito et al., 2010; Lopez-Girona et al., 2012) and that CRBN autoubiquitination is DDB1 dependent. Despite reported differences in efficacy, our structures, biochemical assays and the published cellular CRBN autoubiquitination assays suggest that thalidomide, lenalidomide and pomalidomide have similar mechanistic effects on CRBN. In this discussion I will therefore be focusing on thalidomide alone. The inhibition of DDB1 dependent CRBN autoubiquitination has been a commonly observed effect of thalidomide administration *in vivo* (Ito et al., 2010; Lopez-Girona et al., 2012). This raises the question, however, how this small molecule effectively inhibits

the activity of a CRL4 ubiquitin ligase when binding to the substrate receptor even though the receptor itself is insulated from the ligase active site?

Our work shows that *in vitro* thalidomide does not inhibit the $CRL4^{CRBN}$ ligase activity *per se.* Accordingly, the structures determined do not provide any evidence for a conformational change induced by thalidomide binding that could translate into ligase inhibition. Instead, we find that $CRL4^{CRBN}$ is, similar to $CRL4^{DDB2/CSA}$, inhibited through binding of the COP9 signalosome (CSN) to $CRL4^{CRBN}$ and that this inhibition is not relieved upon binding of thalidomide. The observed substrate dependent activation of other CRL ligases (Chew and Hagen, 2007; Fischer et al., 2011; Emberley et al., 2012; Enchev et al., 2012) suggests that binding of an as yet unknown substrate to the CRBN substrate receptor could lead to dissociation of CSN from $CRL4^{CRBN}$, thereby activating the ubiquitin ligase. Based on these observations, we propose that thalidomide binding to CRBN, rather then inhibiting the ligase activity *per se*, blocks binding of the unknown substrate to the CRBN substrate receptor and thereby prevents CSN mediated $CRL4^{CRBN}$ activation. This results in a multilayered $CRL4^{CRBN}$ inhibition, where the substrate recruitment to the ligase is inhibited and, in turn, CSN is not dissociated from the ligase. The observed discrepancy between thalidomide-induced $CRL4^{CRBN}$ inhibition *in vivo* (Ito et al., 2010; Lopez-Girona et al., 2012) and the absence of such an effect of thalidomide on ligase activity *in vitro*, is fully anticipated by the proposed model. To validate the proposed mechanism of $CRL4^{CRBN}$ inhibition by thalidomide, lenalidomide and pomalidomide knowledge of the missing cellular substrate will be crucial.

Conclusions and future work

In this thesis I have elucidated the molecular architecture and function of the $CRL4^{DDB2}$ ligase and the mechanism of substrate induced CSN dissociation and CRL ligase activation. Moreover, the crystal structures of DDB1-CSA and DDB1-CRBN expand our architectural understanding of $CRL4^{DCAF}$ ligase complexes beyond WD40 comprising DCAFs, and refine the view on general principles that govern CRL4 architecture. Structural and biochemical studies on the $CRL4^{CRBN}$ inhibitors thalidomide, lenalidomide and pomalidomide, demonstrate how these FDA approved small molecules target a specific CRL4 ubiquitin ligase. On the basis of our findings, we propose the following model for CSN mediated CRL4 ligase activation: the interplay with the substrate and a proposed mode of inhibition by small molecules. We further envision that our model expands to other CRL ligase complexes, which is supported by recent literature and unpublished data.

In complex with CSN (**Figure 5.1**), a CRL4 ubiquitin ligase is held in an inactive state, whereat CSN enzymatically deneddylates the cullin and physically blocks access of Rbx1 to an ubiquitin charged E2 (Fischer et al., 2011; Enchev et al., 2012). Binding of a substrate to the DCAF induces the physical displacement of CSN from the CRL4 ligase (see also **Chapter 3** for more details) and, together with subsequent neddylation of the cullin will result in an active CRL4 ligase complex. The active ligase will in turn readily ubiquitinate substrates recruited to the ubiquitination zone and ultimately the DCAF itself. Thalidomide acts as a substrate competitive inhibitor to the DCAF CRBN and while blocking binding of a putative substrate, will simultaneously inhibit the dissociation of CSN, neddylation and therefore activation of the CRL ligase. The thalidomide bound CRL4 complex will be locked in a CSN bound, inactive state.

The substrate triggered relieve of CSN inhibition has become evident not only for CRL4 but also for cullins in general (Fischer et al., 2011; Emberley et al., 2012; Enchev et al., 2012) and provides an elegant mechanism to explain how a single regulatory enzyme can (differentially) control the multitude of CRL ligase complexes present in a cell. An important question, which goes beyond the scope of my thesis, concerns the contributions of the observed

inhibitory principles and the relevance of substrate triggered CSN release *in vivo*. To better understand how CSN interacts with and acts on specific CRL ligase complexes, detailed kinetic studies on CSN mediated CRL regulation for a large set of CRL complexes are needed. Correlation of CRL-CSN kinetics with cellular concentrations of CRL components (Bennett et al., 2010), would provide insights into the dynamics of CRL regulation by CSN. High resolution structural information on CSN and CSN-CRL complexes of sufficient resolution would further provide insights on how this large multi-protein complex is able to interact with and specifically regulate the large number CRLs.

In order to collect evidence for the proposed model of thalidomide action, it would be necessary to find the substrate of CRBN, which in return could be used to show CSN displacement *in vitro*. A profound knowledge of cellular ligase substrates will also be required to unravel the pleiotropic effects that have been associated with thalidomide in cancer therapy and development. Despite the description of a number of putative substrates or proteins affected by thalidomide treatment, including Fgf8 (Ito et al., 2010), PRKAA1 (Lee et al., 2013), or $BK_{C\alpha}$ (Jo et al., 2005), to our knowledge no evidence for a direct $CRL4^{CRBN}$ ligase substrate has been obtained. Finally, I suggest to use proteome wide screens to discover protein substrates of $CRL4^{CRBN}$ and to decipher the network involved in thalidomide action.

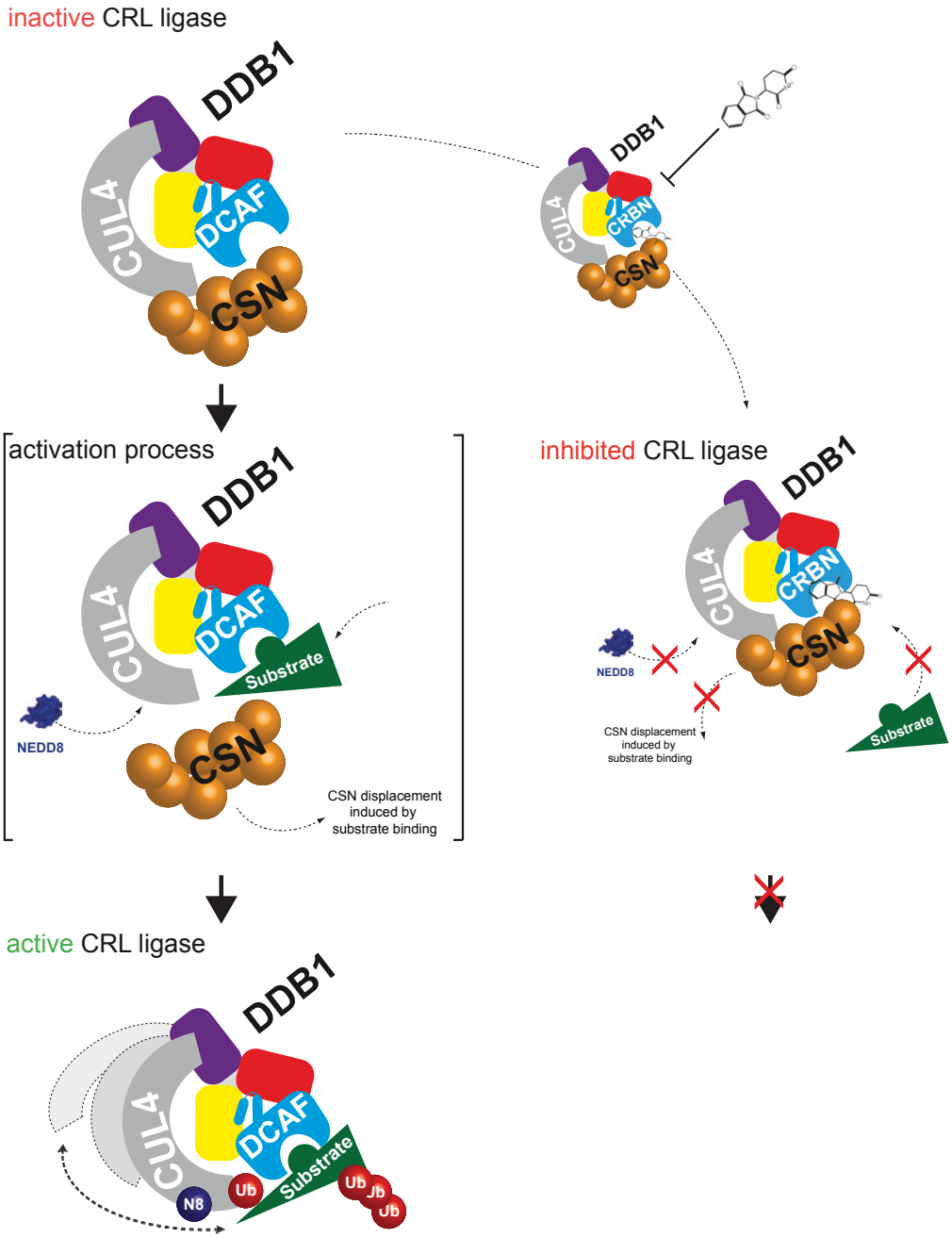

Figure 5.1: Proposed model of CSN mediated CRL4 regulation and thalidomide mediated CRL4^{CRBN} inhibition. CRL4 is held in an CSN bound, inactive state. Binding of a substrate will physically dissociate CSN from the ligase and allow for neddylation of the cullin, which will result in an active CRL4 ligase complex. Thalidomide will bind to CRBN in an substrate competitive manner, thereby blocking the binding of a substrate and subsequent CSN dissociation and ligase activation.

Acknowledgements

With these words, I want to thank all the people who contributed to the success of my PhD project. I would like to thank particularly Nicolas Thomä for providing me the opportunity to conduct my PhD studies in his lab and for his excellent supervision over the past years. He always had an open door for critical and fruitful discussions. I'm especially thankful for the opportunity to develop and pursue my own ideas, and his guidance that combined lots of individual freedom while providing support whenever needed.

I would like to thank Wade Harper for accepting the role as second advisor to my PhD thesis. Discussions with him have always been very encouraging and helpful. I would like to thank Susan Gasser for accepting to serve as my *Fakultätsverantwortlicher* and part of my thesis committee. Susan, thank you for numerous comments and suggestions during committee meetings, GST Meetings and other occasions. I would also like to thank Dirk Schübeler who agreed to chair my PhD defense.

I would like to express my thanks to all, current and past, members of the Thomä lab, I had a great time. Special thanks go to Andrea Scrima for a fantastic collaboration and his advice and guidance throughout the first year of my PhD. I would also like to thank Kerstin Böhm, who worked with me on the project over the past year and substantially contributed to its success.

I would like to thank our collaborators Kaoru Sugasawa and Syota Matsumoto (Kobe University, Japan); Shigenori Iwai (Osaka University, Japan); Hitoshi Kurumizaka (Waseda University, Japan); Wade Harper and John Lydeard (Harvard Medical School, USA); Tsukasa Matsunaga and Mitsuo Wakasugi (Kanazawa University, Japan); Johannes Walther and Courtney Havens (Harvard Medical School, USA); All colleagues at Novartis who provided access to instrumentation or help. Special thanks go to Kaoru Sugasawa, Shigenori Iwai and Hitoshi Kurumizaka for hosting me in Japan.

I acknowledge all the excellent facilities at the FMI. Especially, I thank Heinz Gut, Daniel Hess, Ragna Sack and Iskra Katic for their support and help.

The project would not have been possible without the excellent facilities at the Swiss Light Source (SLS) at Paul Scherrer Institute (PSI) and the support

of the PX beamline staff; I would like to say special thanks to Vincent Olieric, Clemens Schulze-Briese and Takashi Tomizaki.

I acknowledge EMBO for funding my research stay in Japan with a Short Term Fellowship.

I thank my family and friends for supporting me during my PhD studies. I would like to thank Fabio Cortesi for comments on my thesis and corrections. Special thanks go to my wife Lena Kathrin and my daughter Elin for their patience and support despite long hours, continuous work during holidays and weekends, and much more.

References

Abbas, T., Shibata, E., Park, J., Jha, S., Karnani, N., and Dutta, A. (2010). CRL4(Cdt2) regulates cell proliferation and histone gene expression by targeting PR-Set7/Set8 for degradation. Mol Cell *40*, 9–21.

Abbas, T., Sivaprasad, U., Terai, K., Amador, V., Pagano, M., and Dutta, A. (2008). PCNA-dependent regulation of p21 ubiquitylation and degradation via the CRL4Cdt2 ubiquitin ligase complex. Genes Dev *22*, 2496–2506.

Adams, J. (2004). The development of proteasome inhibitors as anticancer drugs. Cancer Cell *5*, 417–421.

Adams, J., Behnke, M., Chen, S., Cruickshank, A.A., Dick, L.R., Grenier, L., Klunder, J.M., Ma, Y.T., Plamondon, L., and Stein, R.L. (1998). Potent and selective inhibitors of the proteasome: dipeptidyl boronic acids. Bioorg. Med. Chem. Lett. *8*, 333–338.

Adams, P.D., Afonine, P.V., BunkÃ³czi, G.B., Chen, V.B., Davis, I.W., Echols, N., Headd, J.J., Hung, L.W., Kapral, G.J., Grosse-Kunstleve, R.W., et al. (2010). PHENIX: a comprehensive Python-based system for macromolecular structure solution. Acta Crystallogr D Biol Crystallogr *66*, 213–221.

Aghajan, M., Jonai, N., Flick, K., Fu, F., Luo, M., Cai, X., Ouni, I., Pierce, N., Tang, X., Lomenick, B., et al. (2010). Chemical genetics screen for enhancers of rapamycin identifies a specific inhibitor of an SCF family E3 ubiquitin ligase. Nature Biotechnology *28*, 738–U1750.

Aghajanian, C., Soignet, S., Dizon, D.S., Pien, C.S., Adams, J., Elliott, P.J., Sabbatini, P., Miller, V., Hensley, M.L., Pezzulli, S., et al. (2002). A phase I trial of the novel proteasome inhibitor PS341 in advanced solid tumor malignancies. Clin. Cancer Res. *8*, 2505–2511.

Ahn, J., Hao, C., Yan, J., Delucia, M., Meherns, J., Wang, C., Gronenborn, A.M., and Skowronski, J. (2012). HIV/SIV accessory virulence factor Vpx loads the host cell restriction factor SAMHD1 onto the E3 ubiquitin ligase complex CRL4DCAF1. J Biol Chem.

Ahn, J., Novince, Z., Concel, J., Byeon, C.-H., Makhov, A.M., Byeon, I.-J.L., Zhang, P., and Gronenborn, A.M. (2011). The Cullin-RING E3 ubiquitin ligase CRL4-DCAF1 complex dimerizes via a short helical region in DCAF1. Biochemistry *50*, 1359–1367.

Ahn, J., Vu, T., Novince, Z., Guerrero-Santoro, J., Rapić-Otrin, V., and Gronenborn, A.M. (2010). HIV-1 Vpr Loads Uracil DNA Glycosylase-2 onto DCAF1, a Substrate Recognition Subunit of a Cullin 4A-RING E3 Ubiquitin Ligase for Proteasome-dependent Degradation. J Biol Chem *285*, 37333–37341.

Ando, Y., Fuse, E., and Figg, W.D. (2002). Thalidomide metabolism by the

CYP2C subfamily. Clin. Cancer Res. *8*, 1964–1973.

Angers, S., Li, T., Yi, X., MacCoss, M.J., Moon, R.T., and Zheng, N. (2006). Molecular architecture and assembly of the DDB1–CUL4A ubiquitin ligase machinery. Nature *443*, 590–593.

Bartlett, J.B., Dredge, K., and Dalgleish, A.G. (2004). The evolution of thalidomide and its IMiD derivatives as anticancer agents. Nat Rev Cancer *4*, 314–322.

Bech-Otschir, D., Seeger, M., and Dubiel, W. (2002). The COP9 signalosome: at the interface between signal transduction and ubiquitin-dependent proteolysis. J Cell Sci *115*, 467–473.

Bennett, E.J., Rush, J., Gygi, S.P., and Harper, J.W. (2010). Dynamics of Cullin-RING Ubiquitin Ligase Network Revealed by Systematic Quantitative Proteomics. Cell *143*, 951–965.

Bornstein, G., Ganoth, D., and Hershko, A. (2006). Regulation of neddylation and deneddylation of cullin1 in SCFSkp2 ubiquitin ligase by F-box protein and substrate. Proc Natl Acad Sci USA *103*, 11515–11520.

Bosch, M.E., Sánchez, A.J.R., Rojas, F.S., and Ojeda, C.B. (2008). Recent advances in analytical determination of thalidomide and its metabolites. J Pharm Biomed Anal *46*, 9–17.

Brownell, J.E., Sintchak, M.D., Gavin, J.M., Liao, H., Bruzzese, F.J., Bump, N.J., Soucy, T.A., Milhollen, M.A., Yang, X., Burkhardt, A.L., et al. (2010). Substrate-assisted inhibition of ubiquitin-like protein-activating enzymes: the NEDD8 E1 inhibitor MLN4924 forms a NEDD8-AMP mimetic in situ. Mol Cell *37*, 102–111.

Canning, P., Cooper, C.D.O., Krojer, T., Murray, J.W., Pike, A.C.W., Chaikuad, A., Keates, T., Thangaratnarajah, C., Hojzan, V., Marsden, B.D., et al. (2013). Structural basis for Cul3 assembly with the BTB-Kelch family of E3 ubiquitin ligases. J Biol Chem.

Cardozo, T., and Pagano, M. (2004). The SCF ubiquitin ligase: insights into a molecular machine. Nat Rev Mol Cell Biol *5*, 739–751.

Ceccarelli, D.F., Tang, X., Pelletier, B., Orlicky, S., Xie, W., Plantevin, V., Neculai, D., Chou, Y.-C., Ogunjimi, A., Al-Hakim, A., et al. (2011). An allosteric inhibitor of the human Cdc34 ubiquitin-conjugating enzyme. Cell *145*, 1075–1087.

Chamovitz, D.A., Wei, N., Osterlund, M.T., Arnim, von, A.G., Staub, J.M., Matsui, M., and Deng, X.W. (1996). The COP9 complex, a novel multisubunit nuclear regulator involved in light control of a plant developmental switch. Cell *86*, 115–121.

Chew, E.-H., and Hagen, T. (2007). Substrate-mediated regulation of cullin neddylation. J Biol Chem *282*, 17032–17040.

Chi, S.-W., Lee, S.-H., Kim, D.-H., Ahn, M.-J., Kim, J.-S., Woo, J.-Y., Torizawa, T., Kainosho, M., and Han, K.-H. (2005). Structural details on mdm2-p53 interaction. J Biol Chem *280*, 38795–38802.

Ciechanover, A., Elias, S., Heller, H., Ferber, S., and Hershko, A. (1980). Characterization of the heat-stable polypeptide of the ATP-dependent proteolytic system from reticulocytes. J Biol Chem *255*, 7525–7528.

Ciechanover, A., Finley, D., and Varshavsky, A. (1984). Ubiquitin dependence of selective protein degradation demonstrated in the mammalian cell cycle mutant ts85. Cell *37*, 57–66.

Ciehanover, A., Hod, Y., and Hershko, A. (1978). A heat-stable polypeptide component of an ATP-dependent proteolytic system from reticulocytes. Biochem Biophys Res Commun *81*, 1100–1105.

Cope, G.A., and Deshaies, R.J. (2006). Targeted silencing of Jab1/Csn5 in human cells downregulates SCF activity through reduction of F-box protein levels. BMC Biochem. *7*, 1.

Cope, G.A., Suh, G.S.B., Aravind, L., Schwarz, S.E., Zipursky, S.L., Koonin, E.V., and Deshaies, R.J. (2002). Role of predicted metalloprotease motif of Jab1/Csn5 in cleavage of Nedd8 from Cul1. Science *298*, 608–611.

D'Amato, R.J., Loughnan, M.S., Flynn, E., and Folkman, J. (1994). Thalidomide is an inhibitor of angiogenesis. Proc Natl Acad Sci USA *91*, 4082–4085.

da Silva Correia, J., Miranda, Y., Leonard, N., and Ulevitch, R.J. (2007). The subunit CSN6 of the COP9 signalosome is cleaved during apoptosis. J Biol Chem *282*, 12557–12565.

de Bie, P., and Ciechanover, A. (2011). Ubiquitination of E3 ligases: self-regulation of the ubiquitin system via proteolytic and non-proteolytic mechanisms. Cell Death Differ. *18*, 1393–1402.

Deng, X., Dubiel, W., Wei, N., Hofmann, K., and Mundt, K. (2000). Unified nomenclature for the COP9 signalosome and its subunits: an essential regulator of development. Trends Genet *16*, 289.

Deshaies, R.J., and Joazeiro, C.A.P. (2009). RING domain E3 ubiquitin ligases. Annu. Rev. Biochem. *78*, 399–434.

Doronkin, S., Djagaeva, I., and Beckendorf, S.K. (2002). CSN5/Jab1 mutations affect axis formation in the Drosophila oocyte by activating a meiotic checkpoint. Development *129*, 5053–5064.

Duarte, J.M., Srebniak, A., Schärer, M.A., and Capitani, G. (2012). Protein interface classification by evolutionary analysis. BMC Bioinformatics *13*, 334.

Duda, D., Borg, L., Scott, D., Hunt, H., Hammel, M., and Schulman, B. (2008). Structural insights into NEDD8 activation of cullin-RING ligases:

conformational control of conjugation. Cell *134*, 995–1006.

Duda, D.M., Olszewski, J.L., Tron, A.E., Hammel, M., Lambert, L.J., Waddell, M.B., Mittag, T., DeCaprio, J.A., and Schulman, B.A. (2012). Structure of a glomulin-RBX1-CUL1 complex: inhibition of a RING E3 ligase through masking of its E2-binding surface. Mol Cell *47*, 371–382.

Duda, D.M., Scott, D.C., Calabrese, M.F., Zimmerman, E.S., Zheng, N., and Schulman, B.A. (2011). Structural regulation of cullin-RING ubiquitin ligase complexes. Current Opinion in Structural Biology *21*, 257–264.

Dye, B.T., and Schulman, B.A. (2007). Structural mechanisms underlying posttranslational modification by ubiquitin-like proteins. Annu Rev Biophys Biomol Struct *36*, 131–150.

Emberley, E.D., Mosadeghi, R., and Deshaies, R.J. (2012). Deconjugation of Nedd8 from Cul1 is directly regulated by Skp1-F-box and substrate, and the COP9 signalosome inhibits deneddylated SCF by a noncatalytic mechanism. J Biol Chem *287*, 29679–29689.

Emsley, P., and Cowtan, K. (2004). Coot: model-building tools for molecular graphics. Acta Crystallogr D Biol Crystallogr *60*, 2126–2132.

Enchev, R.I., Scott, D.C., da Fonseca, P.C.A., Schreiber, A., Monda, J.K., Schulman, B.A., Peter, M., and Morris, E.P. (2012). Structural Basis for a Reciprocal Regulation between SCF and CSN. Cell Reports 1–23.

Eriksson, T., Björkman, S., Roth, B., and Höglund, P. (2000). Intravenous formulations of the enantiomers of thalidomide: pharmacokinetic and initial pharmacodynamic characterization in man. J. Pharm. Pharmacol. *52*, 807–817.

Fang, L., Wang, X., Yamoah, K., Chen, P.-L., Pan, Z.-Q., and Huang, L. (2008). Characterization of the human COP9 signalosome complex using affinity purification and mass spectrometry. J. Proteome Res. *7*, 4914–4925.

Finley, D., Ciechanover, A., and Varshavsky, A. (1984). Thermolability of ubiquitin-activating enzyme from the mammalian cell cycle mutant ts85. Cell *37*, 43–55.

Fischer, E.S., Scrima, A., Böhm, K., Matsumoto, S., Lingaraju, G.M., Faty, M., Yasuda, T., Cavadini, S., Wakasugi, M., Hanaoka, F., et al. (2011). The Molecular Basis of CRL4DDB2/CSA Ubiquitin Ligase Architecture, Targeting, and Activation. Cell *147*, 1024–1039.

Forbes, S.A.S., Bindal, N.N., Bamford, S.S., Cole, C.C., Kok, C.Y.C., Beare, D.D., Jia, M.M., Shepherd, R.R., Leung, K.K., Menzies, A.A., et al. (2010). COSMIC: mining complete cancer genomes in the Catalogue of Somatic Mutations in Cancer. Nucleic Acids Res *39*, D945–D950.

Furukawa, M., Zhang, Y., McCarville, J., Ohta, T., and Xiong, Y. (2000). The CUL1 C-terminal sequence and ROC1 are required for efficient nuclear

accumulation, NEDD8 modification, and ubiquitin ligase activity of CUL1. Mol Cell Biol *20*, 8185–8197.

Galustian, C., Labarthe, M.-C., Bartlett, J.B., and Dalgleish, A.G. (2004). Thalidomide-derived immunomodulatory drugs as therapeutic agents. Expert Opin Biol Ther *4*, 1963–1970.

Goldenberg, S.J., Cascio, T.C., Shumway, S.D., Garbutt, K.C., Liu, J., Xiong, Y., and Zheng, N. (2004). Structure of the Cand1-Cul1-Roc1 complex reveals regulatory mechanisms for the assembly of the multisubunit cullin-dependent ubiquitin ligases. Cell *119*, 517–528.

Goldknopf, I.L., Taylor, C.W., Baum, R.M., Yeoman, L.C., Olson, M.O., Prestayko, A.W., and Busch, H. (1975). Isolation and characterization of protein A24, a “histone-like” non-histone chromosomal protein. J Biol Chem *250*, 7182–7187.

Groisman, R., Kuraoka, I., Chevallier, O., Gaye, N., Magnaldo, T., Tanaka, K., Kisselev, A.F., Harel-Bellan, A., and Nakatani, Y. (2006). CSA-dependent degradation of CSB by the ubiquitin-proteasome pathway establishes a link between complementation factors of the Cockayne syndrome. Genes Dev *20*, 1429–1434.

Groisman, R., Polanowska, J., Kuraoka, I., Sawada, J., Saijo, M., Drapkin, R., Kisselev, A., Tanaka, K., and Nakatani, Y. (2003). The ubiquitin ligase activity in the DDB2 and CSA complexes is differentially regulated by the COP9 signalosome in response to DNA damage. Cell *113*, 357–367.

Gutiérrez-Rodríguez, O. (1984). Thalidomide. A promising new treatment for rheumatoid arthritis. Arthritis Rheum. *27*, 1118–1121.

Hansen, J.M., Harris, K.K., Philbert, M.A., and Harris, C. (2002). Thalidomide modulates nuclear redox status and preferentially depletes glutathione in rabbit limb versus rat limb. J. Pharmacol. Exp. Ther. *300*, 768–776.

Hao, B., Oehlmann, S., Sowa, M.E., Harper, J.W., and Pavletich, N.P. (2007). Structure of a Fbw7-Skp1-cyclin E complex: multisite-phosphorylated substrate recognition by SCF ubiquitin ligases. Mol Cell *26*, 131–143.

Hao, B., Zheng, N., Schulman, B.A., Wu, G., Miller, J.J., Pagano, M., and Pavletich, N.P. (2005). Structural basis of the Cks1-dependent recognition of p27(Kip1) by the SCF(Skp2) ubiquitin ligase. Mol Cell *20*, 9–19.

Havens, C.G., and Walter, J.C. (2011). Mechanism of CRL4(Cdt2), a PCNA-dependent E3 ubiquitin ligase. Genes Dev *25*, 1568–1582.

He, Q., Cheng, P., He, Q., and Liu, Y. (2005). The COP9 signalosome regulates the Neurospora circadian clock by controlling the stability of the SCFFWD-1 complex. Genes Dev *19*, 1518–1531.

He, Y.J., McCall, C.M., Hu, J., Zeng, Y., and Xiong, Y. (2006). DDB1 functions as a linker to recruit receptor WD40 proteins to CUL4-ROC1 ubiquitin ligases.

Genes Dev *20*, 2949–2954.

Heger, W., Schmahl, H.J., Klug, S., Felies, A., Nau, H., Merker, H.J., and Neubert, D. (1994). Embryotoxic effects of thalidomide derivatives in the non-human primate callithrix jacchus. IV. Teratogenicity of micrograms/kg doses of the EM12 enantiomers. Teratog., Carcinog. Mutagen. *14*, 115–122.

Hershko, A., and Ciechanover, A. (1998). The ubiquitin system. Annu. Rev. Biochem. *67*, 425–479.

Hershko, A., Heller, H., Elias, S., and Ciechanover, A. (1983). Components of ubiquitin-protein ligase system. Resolution, affinity purification, and role in protein breakdown. J Biol Chem *258*, 8206–8214.

Hershko, A.A., Ciechanover, A.A., Heller, H.H., Haas, A.L.A., and Rose, I.A.I. (1980). Proposed role of ATP in protein breakdown: conjugation of protein with multiple chains of the polypeptide of ATP-dependent proteolysis. Proc Natl Acad Sci USA *77*, 1783–1786.

Hetfeld, B.K.J., Peth, A., Sun, X.-M., Henklein, P., Cohen, G.M., and Dubiel, W. (2008). The COP9 signalosome-mediated deneddylation is stimulated by caspases during apoptosis. Apoptosis *13*, 187–195.

Higa, L.A., Wu, M., Ye, T., Kobayashi, R., Sun, H., and Zhang, H. (2006). CUL4-DDB1 ubiquitin ligase interacts with multiple WD40-repeat proteins and regulates histone methylation. Nat Cell Biol *8*, 1277–1283.

Higgins, J.J., Pucilowska, J., Lombardi, R.Q., and Rooney, J.P. (2004). A mutation in a novel ATP-dependent Lon protease gene in a kindred with mild mental retardation. Neurology *63*, 1927–1931.

Hohberger, B., and Enz, R. (2009). Cereblon is expressed in the retina and binds to voltage-gated chloride channels. FEBS Lett *583*, 633–637.

Holm, L., and Rosenström, P. (2010). Dali server: conservation mapping in 3D. Nucleic Acids Res *38 Suppl*, W545–W549.

Hon, W.-C., Wilson, M.I., Harlos, K., Claridge, T.D.W., Schofield, C.J., Pugh, C.W., Maxwell, P.H., Ratcliffe, P.J., Stuart, D.I., and Jones, E.Y. (2002). Structural basis for the recognition of hydroxyproline in HIF-1 alpha by pVHL. Nature *417*, 975–978.

Horvath, C.M. (2004). Weapons of STAT destruction. Interferon evasion by paramyxovirus V protein. Eur J Biochem *271*, 4621–4628.

Höglund, P., Eriksson, T., and Björkman, S. (1998). A double-blind study of the sedative effects of the thalidomide enantiomers in humans. J Pharmacokinet Biopharm *26*, 363–383.

Huang, D.T., Ayrault, O., Hunt, H.W., Taherbhoy, A.M., Duda, D.M., Scott, D.C., Borg, L.A., Neale, G., Murray, P.J., Roussel, M.F., et al. (2009). E2-RING expansion of the NEDD8 cascade confers specificity to cullin

modification. Mol Cell *33*, 483–495.

Huang, J., and Chen, J. (2008). VprBP targets Merlin to the Roc1-Cul4A-DDB1 E3 ligase complex for degradation. Oncogene *27*, 4056–4064.

Huang, L., Kinnucan, E., Wang, G., Beaudenon, S., Howley, P.M., Huibregtse, J.M., and Pavletich, N.P. (1999). Structure of an E6AP-UbcH7 complex: insights into ubiquitination by the E2-E3 enzyme cascade. Science *286*, 1321–1326.

Ito, T., Ando, H., and Handa, H. (2011). Teratogenic effects of thalidomide: molecular mechanisms. Cell Mol Life Sci *68*, 1569–1579.

Ito, T., Ando, H., Suzuki, T., Ogura, T., Hotta, K., Imamura, Y., Yamaguchi, Y., and Handa, H. (2010). Identification of a primary target of thalidomide teratogenicity. Science *327*, 1345–1350.

Itzen, A., Bleimling, N., Ignatev, A., Pylypenko, O., and Rak, A. (2006). Purification, crystallization and preliminary X-ray crystallographic analysis of mammalian MSS4-Rab8 GTPase protein complex. Acta Crystallogr Sect F Struct Biol Cryst Commun *62*, 113–116.

Jackson, S., and Xiong, Y. (2009). CRL4s: the CUL4-RING E3 ubiquitin ligases. Trends Biochem Sci *34*, 562–570.

Jin, J., Arias, E., Chen, J., Harper, J., and Walter, J. (2006). A family of diverse Cul4-Ddb1-interacting proteins includes Cdt2, which is required for S phase destruction of the replication factor Cdt1. Mol Cell *23*, 709–721.

Jin, L., Williamson, A., Banerjee, S., Philipp, I., and Rape, M. (2008). Mechanism of ubiquitin-chain formation by the human anaphase-promoting complex. Cell *133*, 653–665.

Jo, S., Lee, K.-H., Song, S., Jung, Y.-K., and Park, C.-S. (2005). Identification and functional characterization of cereblon as a binding protein for large-conductance calcium-activated potassium channel in rat brain. J. Neurochem. *94*, 1212–1224.

Joazeiro, C.A., Wing, S.S., Huang, H., Leverson, J.D., Hunter, T., and Liu, Y.C. (1999). The tyrosine kinase negative regulator c-Cbl as a RING-type, E2-dependent ubiquitin-protein ligase. Science *286*, 309–312.

Kabsch, W. (1993). Automatic Processing of Rotation Diffraction Data from Crystals of Initially Unknown Symmetry and Cell Constants. Journal of Applied Crystallography *26*, 795–800.

Kamura, T., Koepp, D.M., Conrad, M.N., Skowyra, D., Moreland, R.J., Iliopoulos, O., Lane, W.S., Kaelin, W.G., Elledge, S.J., Conaway, R.C., et al. (1999). Rbx1, a component of the VHL tumor suppressor complex and SCF ubiquitin ligase. Science *284*, 657–661.

Kapelari, B., Bech-Otschir, D., Hegerl, R., Schade, R., Dumdey, R., and

Dubiel, W. (2000). Electron microscopy and subunit-subunit interaction studies reveal a first architecture of COP9 signalosome. J Mol Biol *300*, 1169–1178.

Kim, W., Bennett, E.J., Huttlin, E.L., Guo, A., Li, J., Possemato, A., Sowa, M.E., Rad, R., Rush, J., Comb, M.J., et al. (2011). Systematic and quantitative assessment of the ubiquitin-modified proteome. Mol Cell *44*, 325–340.

Kimura, Y., and Tanaka, K. (2010). Regulatory mechanisms involved in the control of ubiquitin homeostasis. J. Biochem. *147*, 793–798.

Kleiger, G., Saha, A., Lewis, S., Kuhlman, B., and Deshaies, R.J. (2009). Rapid E2-E3 assembly and disassembly enable processive ubiquitylation of cullin-RING ubiquitin ligase substrates. Cell *139*, 957–968.

Knobloch, J., and Rüther, U. (2008). Shedding light on an old mystery: thalidomide suppresses survival pathways to induce limb defects. Cell Cycle *7*, 1121–1127.

Komander, D., and Rape, M. (2012). The ubiquitin code. Annu. Rev. Biochem. *81*, 203–229.

Kussie, P.H., Gorina, S., Marechal, V., Elenbaas, B., Moreau, J., Levine, A.J., and Pavletich, N.P. (1996). Structure of the MDM2 oncoprotein bound to the p53 tumor suppressor transactivation domain. Science *274*, 948–953.

Kwok, S.F., Piekos, B., Misera, S., and Deng, X.W. (1996). A complement of ten essential and pleiotropic arabidopsis COP/DET/FUS genes is necessary for repression of photomorphogenesis in darkness. Plant Physiol. *110*, 731–742.

Larkin, M.A., Blackshields, G., Brown, N.P., Chenna, R., McGettigan, P.A., McWilliam, H., Valentin, F., Wallace, I.M., Wilm, A., Lopez, R., et al. (2007). Clustal W and Clustal X version 2.0. Bioinformatics *23*, 2947–2948.

Lee, I., and Schindelin, H. (2008). Structural insights into E1-catalyzed ubiquitin activation and transfer to conjugating enzymes. Cell *134*, 268–278.

Lee, J., and Zhou, P. (2012). Pathogenic Role of the CRL4 Ubiquitin Ligase in Human Disease. Front Oncol *2*, 21.

Lee, J.M., Lee, J.S., Kim, H., Kim, K., Park, H., Kim, J.-Y., Lee, S.H., Kim, I.S., Kim, J., Lee, M., et al. (2012a). EZH2 Generates a Methyl Degron that Is Recognized by the DCAF1/DDB1/CUL4 E3 Ubiquitin Ligase Complex. Mol Cell *48*, 572–586.

Lee, K.M., Jo, S., Kim, H., Lee, J., and Park, C.-S. (2011). Functional Modulation of AMP-activated Protein Kinase by Cereblon. Acta-Bioenerg –.

Lee, K.M., Lee, J., and Park, C.-S. (2012b). Cereblon inhibits proteasome activity by binding to the 20S core proteasome subunit beta type 4. Biochem Biophys Res Commun.

Lee, K.M., Yang, S.-J., Kim, Y.D., Choi, Y.D., Nam, J.H., Choi, C.S., Choi, H.-S., and Park, C.-S. (2013). Disruption of the cereblon gene enhances hepatic AMPK activity and prevents high fat diet-induced obesity and insulin resistance in mice. Diabetes.

Leung-Pineda, V., Huh, J., and Piwnica-Worms, H. (2009). DDB1 targets Chk1 to the Cul4 E3 ligase complex in normal cycling cells and in cells experiencing replication stress. Cancer Res. *69*, 2630–2637.

Li, T., Chen, X., Garbutt, K.C., Zhou, P., and Zheng, N. (2006). Structure of DDB1 in Complex with a Paramyxovirus V Protein: Viral Hijack of a Propeller Cluster in Ubiquitin Ligase. Cell *124*, 105–117.

Li, T., Robert, E.I., van Breugel, P.C., Strubin, M., and Zheng, N. (2010). A promiscuous alpha-helical motif anchors viral hijackers and substrate receptors to the CUL4-DDB1 ubiquitin ligase machinery. Nat Struct Mol Biol *17*, 105–111.

Liu, L., Lee, S., Zhang, J., Peters, S.B., Hannah, J., Zhang, Y., Yin, Y., Koff, A., Ma, L., and Zhou, P. (2009). CUL4A abrogation augments DNA damage response and protection against skin carcinogenesis. Mol Cell *34*, 451–460.

Lopez-Girona, A., Mendy, D., Ito, T., Miller, K., Gandhi, A.K., Kang, J., Karasawa, S., Carmel, G., Jackson, P., Abbasian, M., et al. (2012). Cereblon is a direct protein target for immunomodulatory and antiproliferative activities of lenalidomide and pomalidomide. Leukemia.

Lyapina, S. (2001). Promotion of NEDD8-CUL1 Conjugate Cleavage by COP9 Signalosome. Science *292*, 1382–1385.

Makonkawkeyoon, S., Limson-Pobre, R.N., Moreira, A.L., Schauf, V., and Kaplan, G. (1993). Thalidomide inhibits the replication of human immunodeficiency virus type 1. Proc Natl Acad Sci USA *90*, 5974–5978.

Martin-Lluesma, S., Schaeffer, C., Robert, E.I., van Breugel, P.C., Leupin, O., Hantz, O., and Strubin, M. (2008). Hepatitis B virus X protein affects S phase progression leading to chromosome segregation defects by binding to damaged DNA binding protein 1. Hepatology *48*, 1467–1476.

Marunouchi, T., Yasuda, H., Matsumoto, Y., and Yamada, M. (1980). Disappearance of a basic chromosomal protein from cells of a mouse temperature-sensitive mutant defective in histone phosphorylation. Biochem Biophys Res Commun *95*, 126–131.

Matsuoka, S., Ballif, B.A., Smogorzewska, A., McDonald, E.R., Hurov, K.E., Luo, J., Bakalarski, C.E., Zhao, Z., Solimini, N., Lerenthal, Y., et al. (2007). ATM and ATR substrate analysis reveals extensive protein networks responsive to DNA damage. Science *316*, 1160–1166.

McCarthy, D.M., Kanfer, E.J., and Barrett, A.J. (1989). Thalidomide for the therapy of graft-versus-host disease following allogeneic bone marrow transplantation. Biomed. Pharmacother. *43*, 693–697.

Mccoy, A., Grosse-Kunstleve, R., Adams, P., Winn, M., Storoni, L., and Read, R. (2007). Phaser crystallographic software. Journal of Applied Crystallography *40*, 658–674.

Min, J.H. (2002). Structure of an HIF-1alpha -pVHL Complex: Hydroxyproline Recognition in Signaling. Science *296*, 1886–1889.

Mizushima, T., Hirao, T., Yoshida, Y., Lee, S.J., Chiba, T., Iwai, K., Yamaguchi, Y., Kato, K., Tsukihara, T., and Tanaka, K. (2004). Structural basis of sugar-recognizing ubiquitin ligase. Nat Struct Mol Biol *11*, 365–370.

Mizushima, T., Yoshida, Y., Kumanomidou, T., Hasegawa, Y., Suzuki, A., Yamane, T., and Tanaka, K. (2007). Structural basis for the selection of glycosylated substrates by SCF(Fbs1) ubiquitin ligase. Proc Natl Acad Sci USA *104*, 5777–5781.

Morimoto, M., Nishida, T., Honda, R., and Yasuda, H. (2000). Modification of cullin-1 by ubiquitin-like protein Nedd8 enhances the activity of SCF(skp2) toward p27(kip1). Biochem Biophys Res Commun *270*, 1093–1096.

Mundt, K.E., Liu, C., and Carr, A.M. (2002). Deletion mutants in COP9/signalosome subunits in fission yeast Schizosaccharomyces pombe display distinct phenotypes. Mol Biol Cell *13*, 493–502.

Mundt, K.E., Porte, J., Murray, J.M., Brikos, C., Christensen, P.U., Caspari, T., Hagan, I.M., Millar, J.B., Simanis, V., Hofmann, K., et al. (1999). The COP9/signalosome complex is conserved in fission yeast and has a role in S phase. Curr. Biol. *9*, 1427–1430.

Nishitani, H., Shiomi, Y., Iida, H., Michishita, M., Takami, T., and Tsurimoto, T. (2008). CDK inhibitor p21 is degraded by a proliferating cell nuclear antigen-coupled Cul4-DDB1Cdt2 pathway during S phase and after UV irradiation. J Biol Chem *283*, 29045–29052.

Ohta, T., Michel, J.J., Schottelius, A.J., and Xiong, Y. (1999). ROC1, a homolog of APC11, represents a family of cullin partners with an associated ubiquitin ligase activity. Mol Cell *3*, 535–541.

Ohtake, F., Baba, A., Takada, I., Okada, M., Iwasaki, K., Miki, H., Takahashi, S., Kouzmenko, A., Nohara, K., Chiba, T., et al. (2007). Dioxin receptor is a ligand-dependent E3 ubiquitin ligase. Nature *446*, 562–566.

Olma, M.H., Roy, M., Le Bihan, T., Sumara, I., Maerki, S., Larsen, B., Quadroni, M., Peter, M., Tyers, M., and Pintard, L. (2009). An interaction network of the mammalian COP9 signalosome identifies Dda1 as a core subunit of multiple Cul4-based E3 ligases. J Cell Sci *122*, 1035–1044.

Orlicky, S., Tang, X., Neduva, V., Elowe, N., Brown, E.D., Sicheri, F., and Tyers, M. (2010). An allosteric inhibitor of substrate recognition by the SCF(Cdc4) ubiquitin ligase. Nature Biotechnology *28*, 733–737.

Orlowski, R.Z., and Dees, E.C. (2003). The role of the ubiquitination-

proteasome pathway in breast cancer: applying drugs that affect the ubiquitin-proteasome pathway to the therapy of breast cancer. Breast Cancer Res. *5*, 1–7.

Osterlund, M.T., Ang, L.H., and Deng, X.W. (1999). The role of COP1 in repression of Arabidopsis photomorphogenic development. Trends Cell Biol. *9*, 113–118.

Ota, T., Suzuki, Y., Nishikawa, T., Otsuki, T., Sugiyama, T., Irie, R., Wakamatsu, A., Hayashi, K., Sato, H., Nagai, K., et al. (2004). Complete sequencing and characterization of 21,243 full-length human cDNAs. Nat Genet *36*, 40–45.

Ozkaynak, E., Finley, D., and Varshavsky, A. (1984). The yeast ubiquitin gene: head-to-tail repeats encoding a polyubiquitin precursor protein. Nature *312*, 663–666.

Pan, Z.-Q., Kentsis, A., Dias, D.C., Yamoah, K., and Wu, K. (2004). Nedd8 on cullin: building an expressway to protein destruction. Oncogene *23*, 1985–1997.

Parman, T., Wiley, M.J., and Wells, P.G. (1999). Free radical-mediated oxidative DNA damage in the mechanism of thalidomide teratogenicity. Nat. Med. *5*, 582–585.

Petroski, M., and Deshaies, R. (2005). Function and regulation of cullin-RING ubiquitin ligases. Nat Rev Mol Cell Biol *6*, 9–20.

Pick, E., Hofmann, K., and Glickman, M.H. (2009). PCI complexes: Beyond the proteasome, CSN, and eIF3 Troika. Mol Cell *35*, 260–264.

Pick, E., Lau, O.-S., Tsuge, T., Menon, S., Tong, Y., Dohmae, N., Plafker, S.M., Deng, X.W., and Wei, N. (2007). Mammalian DET1 regulates Cul4A activity and forms stable complexes with E2 ubiquitin-conjugating enzymes. Mol Cell Biol *27*, 4708–4719.

Podust, V.N., Brownell, J.E., Gladysheva, T.B., Luo, R.S., Wang, C., Coggins, M.B., Pierce, J.W., Lightcap, E.S., and Chau, V. (2000). A Nedd8 conjugation pathway is essential for proteolytic targeting of p27Kip1 by ubiquitination. Proc Natl Acad Sci USA *97*, 4579–4584.

Quach, H., Ritchie, D., Stewart, A.K., Neeson, P., Harrison, S., Smyth, M.J., and Prince, H.M. (2010). Mechanism of action of immunomodulatory drugs (IMiDS) in multiple myeloma. Leukemia *24*, 22–32.

Read, M.A., Brownell, J.E., Gladysheva, T.B., Hottelet, M., Parent, L.A., Coggins, M.B., Pierce, J.W., Podust, V.N., Luo, R.S., Chau, V., et al. (2000). Nedd8 modification of cul-1 activates SCF(beta(TrCP))-dependent ubiquitination of IkappaBalpha. Mol Cell Biol *20*, 2326–2333.

Sampaio, E.P., Sarno, E.N., Galilly, R., Cohn, Z.A., and Kaplan, G. (1991). Thalidomide selectively inhibits tumor necrosis factor alpha production by

stimulated human monocytes. J. Exp. Med. *173*, 699–703.

Schmidt, M.W., McQuary, P.R., Wee, S., Hofmann, K., and Wolf, D.A. (2009). F-box-directed CRL complex assembly and regulation by the CSN and CAND1. Mol Cell *35*, 586–597.

Schulman, B.A., Carrano, A.C., Jeffrey, P.D., Bowen, Z., Kinnucan, E.R., Finnin, M.S., Elledge, S.J., Harper, J.W., Pagano, M., and Pavletich, N.P. (2000). Insights into SCF ubiquitin ligases from the structure of the Skp1-Skp2 complex. Nature *408*, 381–386.

Schwechheimer, C., Serino, G., Callis, J., Crosby, W.L., Lyapina, S., Deshaies, R.J., Gray, W.M., Estelle, M., and Deng, X.W. (2001). Interactions of the COP9 signalosome with the E3 ubiquitin ligase SCFTIRI in mediating auxin response. Science *292*, 1379–1382.

Scott, D.C., Monda, J.K., Grace, C.R.R., Duda, D.M., Kriwacki, R.W., Kurz, T., and Schulman, B.A. (2010). A Dual E3 Mechanism for Rub1 Ligation to Cdc53. Mol Cell *39*, 13–13.

Scrima, A., Konícková, R., Czyzewski, B.K., Kawasaki, Y., Jeffrey, P.D., Groisman, R., Nakatani, Y., Iwai, S., Pavletich, N.P., and Thomä, N.H. (2008). Structural Basis of UV DNA-Damage Recognition by the DDB1–DDB2 Complex. Cell *135*, 1213–1223.

Seol, J.H., Feldman, R.M., Zachariae, W., Shevchenko, A., Correll, C.C., Lyapina, S., Chi, Y., Galova, M., Claypool, J., Sandmeyer, S., et al. (1999). Cdc53/cullin and the essential Hrt1 RING-H2 subunit of SCF define a ubiquitin ligase module that activates the E2 enzyme Cdc34. Genes Dev *13*, 1614–1626.

Sharifi, H.J., Furuya, A.M., and de Noronha, C.M.C. (2012). The role of HIV-1 Vpr in promoting the infection of nondividing cells and in cell cycle arrest. Curr Opin HIV AIDS *7*, 187–194.

Sharon, M., Mao, H., Boeri Erba, E., Stephens, E., Zheng, N., and Robinson, C.V. (2009). Symmetrical Modularity of the COP9 Signalosome Complex Suggests its Multifunctionality. Structure *17*, 31–40.

SHESKIN, J. (1965). THALIDOMIDE IN THE TREATMENT OF LEPRA REACTIONS. Clin. Pharmacol. Ther. *6*, 303–306.

Singhal, S., Mehta, J., Desikan, R., Ayers, D., Roberson, P., Eddlemon, P., Munshi, N., Anaissie, E., Wilson, C., Dhodapkar, M., et al. (1999). Antitumor activity of thalidomide in refractory multiple myeloma. N Engl J Med *341*, 1565–1571.

Skaar, J.R., Florens, L., Tsutsumi, T., Arai, T., Tron, A., Swanson, S.K., Washburn, M.P., and DeCaprio, J.A. (2007). PARC and CUL7 form atypical cullin RING ligase complexes. Cancer Res. *67*, 2006–2014.

Smart, O.S., Womack, T.O., Flensburg, C., Keller, P., Paciorek, W., Sharff, A.,

Vonrhein, C., and Bricogne, G. (2012). Exploiting structure similarity in refinement: automated NCS and target-structure restraints in BUSTER. Acta Crystallogr D Biol Crystallogr *68*, 368–380.

Soucy, T.A.T., Smith, P.G.P., Milhollen, M.A.M., Berger, A.J.A., Gavin, J.M.J., Adhikari, S.S., Brownell, J.E.J., Burke, K.E.K., Cardin, D.P.D., Critchley, S.S., et al. (2009). An inhibitor of NEDD8-activating enzyme as a new approach to treat cancer. CORD Conference Proceedings *458*, 732–736.

Stephens, T.D. (1988). Proposed mechanisms of action in thalidomide embryopathy. Teratology *38*, 229–239.

Sugasawa, K. (2006). The xeroderma pigmentosum group C protein complex and ultraviolet-damaged DNA-binding protein: functional assays for damage recognition factors involved in global genome repair. Methods Enzymol *408*, 171–188.

Sugasawa, K., Okuda, Y., Saijo, M., Nishi, R., Matsuda, N., Chu, G., Mori, T., Iwai, S., Tanaka, K., Tanaka, K., et al. (2005). UV-Induced Ubiquitylation of XPC Protein Mediated by UV-DDB-Ubiquitin Ligase Complex. Cell *121*, 387–400.

Takedachi, A., Saijo, M., and Tanaka, K. (2010). DDB2 complex-mediated ubiquitylation around DNA damage is oppositely regulated by XPC and Ku and contributes to the recruitment of XPA. Mol Cell Biol *30*, 2708–2723.

Tan, P., Fuchs, S.Y., Chen, A., Wu, K., Gomez, C., Ronai, Z., and Pan, Z.Q. (1999). Recruitment of a ROC1-CUL1 ubiquitin ligase by Skp1 and HOS to catalyze the ubiquitination of I kappa B alpha. Mol Cell *3*, 527–533.

Tarpey, P.S., Raymond, F.L., O'Meara, S., Edkins, S., Teague, J., Butler, A., Dicks, E., Stevens, C., Tofts, C., Avis, T., et al. (2007). Mutations in CUL4B, which encodes a ubiquitin E3 ligase subunit, cause an X-linked mental retardation syndrome associated with aggressive outbursts, seizures, relative macrocephaly, central obesity, hypogonadism, pes cavus, and tremor. Am. J. Hum. Genet. *80*, 345–352.

Therapontos, C., Erskine, L., Gardner, E.R., Figg, W.D., and Vargesson, N. (2009). Thalidomide induces limb defects by preventing angiogenic outgrowth during early limb formation. Proc Natl Acad Sci U S A *106*, 8573–8578.

Thornton, B.R., and Toczyski, D.P. (2006). Precise destruction: an emerging picture of the APC. Genes Dev *20*, 3069–3078.

Vagin, A., and Teplyakov, A. (1997). MOLREP: an automated program for molecular replacement. Journal of Applied Crystallography.

Vassilev, L.T., Vu, B.T., Graves, B., Carvajal, D., Podlaski, F., Filipovic, Z., Kong, N., Kammlott, U., Lukacs, C., Klein, C., et al. (2004). In vivo activation of the p53 pathway by small-molecule antagonists of MDM2. Science *303*, 844–848.

Verma, R., Aravind, L., Oania, R., McDonald, W.H., Yates, J.R., Koonin, E.V., and Deshaies, R.J. (2002). Role of Rpn11 metalloprotease in deubiquitination and degradation by the 26S proteasome. Science *298*, 611–615.

Vogelsang, G.B., Farmer, E.R., Hess, A.D., Altamonte, V., Beschorner, W.E., Jabs, D.A., Corio, R.L., Levin, L.S., Colvin, O.M., and Wingard, J.R. (1992). Thalidomide for the treatment of chronic graft-versus-host disease. N Engl J Med *326*, 1055–1058.

Walczak, H., Iwai, K., and Dikic, I. (2012). Generation and physiological roles of linear ubiquitin chains. BMC Biol. *10*, 23.

Wang, J., Hu, Q., Chen, H., Zhou, Z., Li, W., Wang, Y., Li, S., and He, Q. (2010). Role of individual subunits of the Neurospora crassa CSN complex in regulation of deneddylation and stability of cullin proteins. PLoS Genet. *6*, e1001232.

Wee, S., Geyer, R.K., Toda, T., and Wolf, D.A. (2005). CSN facilitates Cullin-RING ubiquitin ligase function by counteracting autocatalytic adapter instability. Nat Cell Biol *7*, 387–391.

Wei, N., and Deng, X.W. (1992). COP9: a new genetic locus involved in light-regulated development and gene expression in arabidopsis. Plant Cell *4*, 1507–1518.

Wei, N., and Deng, X.W. (1999). Making sense of the COP9 signalosome. A regulatory protein complex conserved from Arabidopsis to human. Trends Genet *15*, 98–103.

Wei, N., Chamovitz, D.A., and Deng, X.W. (1994). Arabidopsis COP9 is a component of a novel signaling complex mediating light control of development. Cell *78*, 117–124.

Wells, P.G., Kim, P.M., Laposa, R.R., Nicol, C.J., Parman, T., and Winn, L.M. (1997). Oxidative damage in chemical teratogenesis. Mutat Res *396*, 65–78.

Wertz, I.E.I., O'Rourke, K.M.K., Zhang, Z.Z., Dornan, D.D., Arnott, D.D., Deshaies, R.J.R., and Dixit, V.M.V. (2004). Human De-etiolated-1 regulates c-Jun by assembling a CUL4A ubiquitin ligase. Science *303*, 1371–1374.

Wolfenden, R., and Snider, M.J. (2001). The depth of chemical time and the power of enzymes as catalysts. Acc. Chem. Res. *34*, 938–945.

Wu, G., Xu, G., Schulman, B.A., Jeffrey, P.D., Harper, J.W., and Pavletich, N.P. (2003). Structure of a beta-TrCP1-Skp1-beta-catenin complex: destruction motif binding and lysine specificity of the SCF(beta-TrCP1) ubiquitin ligase. Mol Cell *11*, 1445–1456.

Wu, K., Chen, A., and Pan, Z.Q. (2000). Conjugation of Nedd8 to CUL1 enhances the ability of the ROC1-CUL1 complex to promote ubiquitin polymerization. J Biol Chem *275*, 32317–32324.

Zachariae, W., Shevchenko, A., Andrews, P.D., Ciosk, R., Galova, M., Stark, M.J., Mann, M., and Nasmyth, K. (1998). Mass spectrometric analysis of the anaphase-promoting complex from yeast: identification of a subunit related to cullins. Science *279*, 1216–1219.

Zheng, N., Schulman, B.A., Song, L., Miller, J.J., Jeffrey, P.D., Wang, P., Chu, C., Koepp, D.M., Elledge, S.J., Pagano, M., et al. (2002). Structure of the Cul1–Rbx1–Skp1–F boxSkp2 SCF ubiquitin ligase complex. Nature *416*, 703–709.

Zheng, N., Wang, P., Jeffrey, P.D., and Pavletich, N.P. (2000). Structure of a c-Cbl-UbcH7 complex: RING domain function in ubiquitin-protein ligases. Cell *102*, 533–539.

Zhou, C., Wee, S., Rhee, E., Naumann, M., Dubiel, W., and Wolf, D.A. (2003). Fission yeast COP9/signalosome suppresses cullin activity through recruitment of the deubiquitylating enzyme Ubp12p. Mol Cell *11*, 927–938.

Zhou, Z., Wang, Y., Cai, G., and He, Q. (2012). Neurospora COP9 signalosome integrity plays major roles for hyphal growth, conidial development, and circadian function. PLoS Genet. *8*, e1002712.

Zhu, Y.X., Braggio, E., Shi, C.-X., Bruins, L.A., Schmidt, J.E., Van Wier, S., Chang, X.-B., Bjorklund, C.C., Fonseca, R., Bergsagel, P.L., et al. (2011). Cereblon expression is required for the antimyeloma activity of lenalidomide and pomalidomide. Blood *118*, 4771–4779.

Zhuang, M., Calabrese, M.F., Liu, J., Waddell, M.B., Nourse, A., Hammel, M., Miller, D.J., Walden, H., Duda, D.M., Seyedin, S.N., et al. (2009). Structures of SPOP-substrate complexes: insights into molecular architectures of BTB-Cul3 ubiquitin ligases. Mol Cell *36*, 39–50.

Zimmerman, E.S.E., Schulman, B.A.B., and Zheng, N.N. (2010). Structural assembly of cullin-RING ubiquitin ligase complexes. Current Opinion in Structural Biology *20*, 8–8.